NBSIR 80-2054

The Burning of Wood and Plastic Cribs in an Enclosure: Volume I

James G. Quintiere, Bernard J. McCaffrey

Center for Fire Research
National Engineering Laboratory
National Bureau of Standards
U.S. Department of Commerce
Washington, DC 20234

November 1980

Final Report

NBSIR 80-2054
، ۱ ،

THE BURNING OF WOOD AND PLASTIC CRIBS IN AN ENCLOSURE: VOLUME I

James G. Quintiere, Bernard J. McCaffrey

Center for Fire Research
National Engineering Laboratory
National Bureau of Standards
U.S. Department of Commerce
Washington, DC 20234

November 1980

Final Report

U.S. DEPARTMENT OF COMMERCE, Philip M. Klutznick, *Secretary*

Jordan J. Baruch, *Assistant Secretary for Productivity, Technology, and Innovation*

NATIONAL BUREAU OF STANDARDS, Ernest Ambler, *Director*

TABLE OF CONTENTS

Page

Volume II, appendices A, B, and C are in microfiche form
in the back of this volume.

LIST OF FIGURES

Page

LIST OF FIGURES (continued)

Page

vii

LIST OF TABLES

TABLE OF NOMENCLATURE

a — side dimension of ceiling quadrant, figures 6-15 and 6-17

A — crib exposed surface area, eq. 6-45

A_f — flame area (treated as a cylinder)

A_F — room floor area, WL

A_i — crib interior surface area, eq. 6-55

A_o — door area

$A_{o,\ell}$ — door area below neutral plane

$A_{o,S}$ — side projected area of crib assembly, eq. 6-51e

$A_{o,T}$ — top projected area of crib assembly, eq. 6-57d

$A_{o,u}$ — door area above neutral plane

$A_{w,\ell}$ — room surface area below hot layer

$A_{w,u}$ — room surface area above hot layer

A_v — cross-sectional area of crib vertical shafts, $4s^2$

$A_{v,s}$ — cross-sectional area of a single shaft, s^2

APV — average peak values corresponding to the burn period of 95% to 45% of crib initial mass

b — crib square stick thickness

b — side dimension of ceiling quadrant, figures 6-15 and 6-17

B — Spalding B-number, eq. 6-61b

$c_v\cdot$ — specific heat at constant volume (gas-phase)

c_p — specific heat at constant pressure

c_w — specific heat of room "wall" material

C — constant parameter in eq. 6-50 and in eq. A-3

D — layer (thermal discontinuity) distance floor to hot layer

e — energy per unit mass of fluid

E — heat of combustion (appendix A)

$\dot{E}$ — rate of energy transport

f — fraction of total energy release radiated by flame

f — crib friction factor (appendix A)

F_{ij} — radiation exchange shape factor between i and j

F_1, F_2, F_3 — shape factor between cylindrical flame and elemental area oriented normal to coordinate vectors i, j, and k respectively

g   -   gravitational acceleration

$G_s(n_c)$ -   number of side gaps for n_c cribs, eq. 6-57e

$G_T(n_c)$ -   number of top gaps for n_c cribs, eq. 6-57d

h   -   crib height (appendix A)

h   -   convective heat transfer coefficient

H   -   room height, or flame height including crib eq. 6-36

H_c -   crib height

H_f -   flame height measured from top of crib, eq. 6-44

H_i -   vertical distance between target element and layer, figure 6-15

H_2 -   vertical distance between target element and ceiling, figure 6-15

i   -   enthalpy per unit mass

i,j,k -   unit coordinate vectors

I   -   Bessel function

k_f -   flame absorption coefficient

k_g -   hot upper absorption coefficient

k_m -   mixing coefficient, eq. 6-17 and 6-18

k_w -   room "wall" material thermal conductivity

ℓ -   length of crib side

L   -   room length, or distance between flame and target, figure 6-12

L_m -   main beam length, $\dfrac{4 \text{ (enclosed gas volume)}}{\text{(surface area)}}$

L_1 -   struve function

L_{vap} -   effective heat of vaporization

$\dot{m}$ -   mass flow rate

$\dot{m}''$ -   mass flow rate per unit area

$\dot{m}''_{v,o}$ -   free burn pyrolysis rate per unit area

M   -   molecular weight

M_c -   mass of crib assembly

n   -   number of sticks per layer

n_c -   number of cribs

N   -   number of stick layers, and neutral plane height

p	-	pressure
P_s	-	crib shaft perimeter (appendix A)
$\dot{q}$	-	rate of heat transfer
$\dot{q}''$	-	rate of heat transfer per unit area (heat flux)
$\dot{q}''_r$	-	radiant heat flux
$\dot{q}''_c$	-	convective heat flux
$\dot{q}''_k$	-	conductive heat flux
Q	-	rate of energy release by fire
$Q*$	-	dimensionless energy release, eq. 6-50c
r	-	radial distance
r	-	stoichiometric air to fuel mass ratio
r_{ox}	-	stoichiometric oxygen to fuel mass ratio
r_c	-	equivalent crib fire radius
S	-	control volume surface
$S(n_c)$	-	number of crib sides facing the surroundings
t	-	time
$t*$	-	nominal burning time, eq. 6-52b
T	-	temperature
T_{ad}	-	adiabatic wall temperature
T_f	-	effective flame temperature
$\bar{T}$	-	average of top three thermocouples in upper gas layer
u	-	internal energy per unit mass
u,v,w	-	direction cosiness
V	-	fluid velocity
v	-	control volume
W	-	control volume surface velocity
W	-	room width
W_o	-	doorway width
x	-	ratio of excess air after combustion to air required by combustion
Y_i	-	mass concentration of specie i

TABLE OF NOMENCLATURE (continued)

α — "wall" conductance parameter, eq. 6-52b

$\alpha_1, \alpha_2, \alpha_3$ — cylindrical flame emissivity, eq. 6-35

β — mean flame intercept angle, figure 6-12

γ — stoichiometric fuel to air ratio (appendix A)

γ_i — mass production of specie i

γ_ℓ — lower area ratio, $A_f/A_{w,\ell}$

γ_u — upper area ratio, $A_f/A_{w,u}$

Γ — normalizing velocity factor, eq. 6-20

δ — "boundary-layer" factor, eq. 6-20

ϵ — heat of vaporization (appendix A)

ϵ_g — upper layer gas emissivity

ϵ_{gc} — emissivity of upper layer gas quadrant, eq. 6-59F

Θ_o — flame intercept angle, figure 6-12

μ — radiation parameter, eq. 6-35d

ν — stoichiometric coefficient

π — 3.1416

ρ — density

σ — Stefan-Boltzmann constant

ϕ — dimensionless crib drag coefficient (appendix A)

χ_i — mole fraction for specie i

ψ — dimensionless crib pyrolysis rate, $\dot{m}_v''/Cb^{-1/2}$ (appendix A)

ω — ratio of char remaining to initial mass of fuel

SUBSCRIPTS

a — ambient air

b — burned within the enclosure

c — convective

c — crib

e — entrained

f — fuel

f   -   flame

F   -   room floor

g   -   gas-phase

i   -   specie

in   -   inflow

k   -   conductive

ℓ -   lower layer

M   -   mass transport

o   -   door opening

O_2 -   oxygen

0   -   outside surface of crib

r   -   radiative

R   -   energy release

s   -   heat flux sensor

S   -   side of crib

T   -   top of crib

u   -   upper layer

v   -   volatiles

w   -   room (wall) surfaces

SUMMARY

This study was motivated by the desire to achieve three objectives.
The first relates to the general objective of the Products Research Committee
(PRC) to provide a measure of the behavior of cellular plastics in burning
conditions related to real life. Specifically, the burning characteristics
of a structural (high density) polyurethane foam were compared with those of
wood. This comparison was made for uniformly ignited crib fires in a room.
For those experiments the relative fire risk of cellular structural plastics
in furniture items might be inferred.

The second objective was to experimentally determine the effects of fire
size, fuel type, and natural ventilation conditions on the resulting room
fire variables, such as temperature, heat flux, burning rate, and air flow
rate. This was accomplished by burning up to four cribs made of wood (sugar
pine) or polyurethane foam of nearly the same density as the wood. This
range of fire sizes was intended to simulate fires representative of small
furnishings to chairs of moderate size. In addition to variations in fuel
type and quantity, the room door width was varied.

The data from these experiments were analyzed in terms of quantities
averaged over the peak burning period defined as that time corresponding to
the interval from 5 to 55 percent crib mass loss. Thus, for each fuel, fire
size, and door opening, a set of "average peak values (APV)" could be defined
and recorded. These values tend to represent the most severe conditions
for that extent of fire involvement and door opening. By visualizing fire
growth as a succession of such "average peak values" together with tenability
criteria, a risk assessment can be made for various categories of fire hazard.
For example, flashover may be defined as having occurred when an incident
radiant flux of 2 W/cm^2 is exceeded for a point on the floor. Through this
analysis, the data can yield the conditions for flashover in terms of fuel
type, amount, and doorway width.

The <u>third objective</u> was to develop a mathematical model to predict the room fire conditions as a function of fuel type, amount, and room geometry. The data collected were to serve as a basis for assessing the accuracy of the model. The extent of this validation process would provide confidence limits for model extrapolations to other conditions.

Experimental Results

The design of the experiments is discussed in section 2. A code was used to label each run and its corresponding results. The code notation is:

$$\text{PRC} - \underset{1}{\square} - \underset{2}{\square} - \underset{3}{\square} - \underset{4}{\square}$$

where   box 1 = experiment number

box 2 = W for wood or P for plastic crib

box 3 = number of cribs

box 4 = ventilation factor $\begin{cases} 1 = 0.79 \text{ m,} \\ 1/2 = 0.39 \text{ m, or} \\ 1/4 = 0.19 \text{ m, the width of the doorway} \end{cases}$

A complete set of results for the full period of each experiment is tabulated in volume II along with graphical plots over time for many of the measured variables. Also a set of the data are available on magnetic tape. The average peak values for the room fire series and free burn experiments are given in sections 3 and 4, respectively.

The average peak results were analyzed and are discussed in section 5. Except for the plastic cribs burning at the 0.79 m doorway condition, the mass loss rate ($\dot{m}_v$) was found to generally correlate as

$$\dot{m}_v/n_c^{5/4} = \text{function of } A_o\sqrt{H_o} \qquad \text{(figure 5-3)}$$

for each fuel type,

where n_c is the number of cribs

A_o is the area of the doorway

and H_o is the height of the doorway.

The 5/4-power dependence reflects the enhancement in pyrolysis due to radiation from adjacent cribs. The ratio of crib mass loss rate in the enclosure to its free burn value varies from 0.8 for small openings to 1.3 for large door openings (figure 5-4). This displays the extent of the enclosure radiative feedback and ventilation effects on the pyrolysis of the cribs in this series of experiments. The enhancement by the room of incident radiative heat flux to the floor ranged from 2 to 4 for the largest door (0.79 m) (figure 5-21).

Two potentially useful correlations were developed but their generality has not been determined. The air-flow rate $(\dot{m}_a)$ through the doorway was found to behave as

$$\dot{m}_a = \dot{m}_v''^{1/4} \ (A_o\sqrt{H_o})^{1/2} \text{ in kg/s} \qquad \text{(figure 5-7)}$$

where $\dot{m}_v$ is the pyrolysis rate in kg/s and $A_o\sqrt{H_o}$ is the ventilation factor in $m^{5/2}$.

The temperature increase ΔT (°C) in the upper gas layer in the room due to a fire energy release rate $\dot{Q}$ in kW for a room height H (m) and doorway dimensions, H_o (m) and W_o was found to correlate as:

$$\Delta T = 24.2 \left(\frac{\dot{Q}^{2/3}}{H^{5/3}}\right) \left(\frac{H_o}{W_o}\right)^{1/5} \qquad (5-19)$$

The first term in brackets was motivated by plume theory while the second term in brackets represents the flow effect by the doorway. An alternative dimensionless form of this correlation follows from an approximate form of the equations in section 6.

$$\frac{T-T_a}{T_a} \propto \left(\frac{\dot{m}_b \ \Delta H}{\dot{m}_* c_p T_a}\right)^{2/3} \left(\frac{h_k \ A_w}{\dot{m}_* cp}\right)^{-1/2}$$

where $\dot{m}_b$ is the burning rate

    ΔH is an effective heat of combustion

    $\dot{m}_*$ is the maximum possible doorway flow rate, $\frac{2}{3}\sqrt{2g} \ \ \rho_a \ A_o\sqrt{H_o}$

    A_w is the heated internal surface area,

and h_k is an effective heat conductance factor, e.g., $\sqrt{\dfrac{4k\rho c}{\pi t_*}}$ from equation 6-52. The limit of applicability of this correlation has not yet been determined.

Doorway mass flow rates were determined from a limited number of velocity and temperature measurements over a vertical centerline in the doorway. The results yielded a mass balance to within $\pm$ 20 percent for the largest opening and agreed to within $\pm$ 10 percent for the smaller doorways. A flow coefficient was calculated for the inflow and outflow at the doorway and was found to be

$$C_{out} = 0.68$$

and

$$C_{in} = 0.58 - 0.31 W_o$$

where

$$0.2 \text{ m} \leq W_o \leq 0.8 \text{ m}.$$

The position of flow reversal in the doorway, N_v, (as measured from the floor), was found to vary from $N_v/H_o = 0.5$ to 0.7 for a corresponding mean upper gas temperature $\bar{T}$ of 100°C to 800°C (figure 5-9). However, the elevation (N_p) of zero pressure difference between the room and its ambience was always less than or equal to the doorway neutral plane, N_v (figures 5-8a and b). This suggested a downward sloping stagnation streamline from the doorway into the room. The effective hot gas thermal layer (D_T) was found to generally agree with the height of the smoke layer (D_s) (figure 5-10). However, for large fires with the smallest door, D_s was much less than D_T and is indicative of mixing between the upper and lower regions of the room. This phenomenon was also confirmed by temperatures near the room floor as high as 87°C (for PRC-16-P-3-1/4). Finally a hydrostatic pressure calculation, based on measured room temperatures, reasonably predicted horizontal pressure differences between the room and its ambience (figures 5-13 and 5-14). This is significant because these pressure differences are responsible for flow through room openings and a hydrostatic pressure assumption is used in current theoretical flow models.

Estimates made on measured chemical species, CO_2 and O_2, indicated good consistency between relevant measured variables and assumed chemical reaction models for the sugar pine ($CH_{1.74}O_{0.704} \cdot 0.0966H_2O$) and polyurethane

xviii

(PRC material GM-37, $CH_{1.27}N_{0.0823}O_{0.215}$) going to complete combustion
(figures 5-23 and 5-24). Also these calculations yielded a range of excess
air (i.e., the ratio of air flow rate into the room minus the rate of stoichio-
metric air required for combustion divided by the combustion air required) of
0.1 to 10. Although restricted ventilation effects for the smallest door
opening did reduce the fuel pyrolysis, there always appears to have been more
than sufficient air for complete combustion.

The relative risk of these fires can be considered with respect to their
flashover potential and their impact on the surroundings. The former aspect
was emphasized in this study, but some results can be applied to the latter
consideration. The thermal consumption of a filter-paper target sheet sus-
pended in air (by either non-piloted ignition or thermal degradation under
radiant heating) was used as a criterion for flashover. Complete thermal
decomposition of the filter paper occurred under room conditions resulting
from the burning of three or more polyurethane cribs ($\dot{m}_v \geq$ 22 g/s) for all
door openings, and appeared to require more than four wood cribs ($\dot{m}_v$ > 27 g/s)
for complete destruction. If flashover by the remote ignition or pyrolysis
of other non-contiguous room furnishings is considered, then the filter paper
results suggest maximum tolerable burning rates for wood and plastic solid
fuels. A generalization of these results will be addressed later through
mathematical analysis. Measurements indicated that the filter paper was
completely consumed at an incident radiant flux of at least 1.77 W/cm^2.

An assessment of the relative risk of the surroundings with respect to
life safety might be considered based on an estimation of CO concentration
in the combustion product gases exiting from the room. A high of 0.8 percent CO
(by volume) was estimated when three plastic cribs burned in a room with a
0.79 m door width (figure 5-25). CO was only directly measured in the
corridor adjoining the fire room for a limited number of experiments
(all at W_o = 0.79 m). In these cases, the CO/CO_2 ratios ranged from 0.70 to
0.95 for the polyurethane fires and 0.017 to 0.021 for the wood fires. These
ratios might be used to estimate CO levels for other conditions considered
in these experiments.   xix

Theoretical Results

The basis of the mathematical model is a zone (control volume) analysis applied to distinct homogeneous regions of the fire enclosure. The gas-phase is divided into a lower layer (region) and an upper layer which includes the fire plume. Conservation of mass, energy, and species equations are written for each zone along with mass and energy equations governing processes at the boundaries, i.e., wall, ceiling, and floor surfaces and the doorway. Transient effects were not included in this analysis since it is reasonable to ignore the time rate of change of mass and energy within a gas zone, and since the model will address the average peak values derived from the experimental results. Thus, a quasi-steady fire is being modeled. A weakness of this approach is that the conduction into solid boundaries, a true transient, must be approximated as constant. The inaccuracies attributable to this approximation limit the applicability of a steady-state model to a transient fire growth process. However, it can easily be remedied by resorting to an accurate transient conduction calculation along with the other equations given in section 6. This was not done in the present study since the emphasis is placed on "what will happen" under given initial conditions of fuel burning in a room, as opposed to "when a critical event (such as flashover) will occur."

The equations are developed in section 6 and were solved numerically. Complete convergence over all ranges of interest has not been achieved, but the theoretical results do span the range of experimental conditions in this study. Also in section 6, derived relationships for a particular phenomenon are tested against the experimental results by using other experimental data as input. This process provides some assessment of the accuracy of sub-model equations used in the full fire growth simulation model. A summary of the nature of the simulation model is given below. Its distinguishing features include a lower layer that is allowed to be heated through a mixing process between the upper and lower layer (see figures 6-1 and 6-10). Oxygen concentration in the lower layer can therefore be reduced, and this along with radiation feedback from the enclosure affects the pyrolysis rate of the

crib. Thus, a model for fuel pyrolysis in an enclosure contains the effect of radiation for potential enhancement, and the counter-effect of reduced oxygen. Indeed, results show that, as the rate of burning is increased and the door opening is reduced, the mechanisms of radiant feedback and reduced oxygen concentration due to mixing tend to cancel each other, resulting in undramatic changes in crib mass loss rate. However, for other fuel configurations these effects could be more pronounced.

The model can be reduced to seven nonlinear algebraic equations in seven unknowns. Each equation constitutes a conservation law applied to a flow region (control volume) or interface between regions (boundary condition). The input parameters, governing independent equations and dependent relationships, are summarized below.

Model Summary

INPUT PARAMETERS

Physical properties:

g - gravitational acceleration

σ - Stefan-Boltzmann constant

ρ_a, T_a - reference (air) density, temperature

c_p - specific heat (air)

Room Geometry:

H, W, L - room height, width, length

H_o, W_o - doorway height, width

Crib Geometry:

n_c - number of cribs

$\dot{m}''_{v,o}$ - free burn pyrolysis rate per unit area

ℓ, b - stick length and thickness (square cross section)

n - number of sticks per layer

N - number of layers

Fuel Properties:

r - stoichiometric mass air to fuel ratio

ΔH - effective heat of combustion

xxi

f - fraction of energy radiated from flame

L_{vap} - effective heat of vaporization

ω - char fraction

k_f - flame absorption coefficient

T_f - effective flame temperature

M_c - mass of (single) crib

Model Parameters:

C_{in}, C_{out} - in and out doorway flow coefficients

k_m - layer mixing coefficient (eq. 6-17)

C - heat transfer factor (eq. 6-50b)

x_a - excess air factor (eq. 6-41b)

α - wall conduction time factor (eq. 6-52)

$h_{c,\ell}$ - lower layer surface heat transfer coefficient

INDEPENDENT VARIABLES

N, D - hot upper layer height in doorway (neutral plane), in room (thermal discontinuity)

$T_{g,u}$, $T_{g,\ell}$ - upper, lower layer gas temperatures

$T_{w,u}$, $T_{w,\ell}$ - upper, lower layer surface temperatures

$\dot{m}_v$ - fuel pyrolysis rate

GOVERNING EQUATIONS

$f_1 = 0$: Conservation of mass - plume and upper layer

$f_2 = 0$: Conservation of mass - lower layer

$f_3 = 0$: Conservation of energy - plume and upper layer

$f_4 = 0$: Conservation of energy - lower layer

$f_5 = 0$: Conservation of energy - upper solid/gas interface

$f_6 = 0$: Conservation of energy - lower solid/gas interface

$f_7 = 0$: Fuel pyrolysis model

DEPENDENT VARIABLES - Subroutines

$\dot{m}_a$ - air flow rate

$\dot{m}_e$ - rate of entrainment between layers

ε_g - upper layer gas emissivity

$\dot{q}''_{r,u}$ - radiant flux to upper surfaces

$\dot{q}''_{r,o}$ - radiant flux out of doorway

$\dot{q}''_{r,d}$ - radiant flux between upper and lower layers

$\dot{q}''_{c,u}$ - convective flux to upper surfaces

$\dot{q}''_{r,\ell}$ - radiant flux to lower surfaces

$Y_{0_2,u}$ - oxygen mass concentration, upper layer

$Y_{0_2,\ell}$ - oxygen mass concentration, lower layer

$\dot{q}''_{r,s}$ - incident radiant flux to crib sides

$\dot{q}''_{r,T}$ - incident radiant flux to crib top

$\dot{q}''_{r,\text{floor target}}$ - incident radiant flux to floor target

Results of the model are compared to experimental values in figures 6-23 through 6-30. The agreement may be considered fair to good. One problem in making this type of comparison is that room gas properties do not behave as upper and lower homogeneous zones as portrayed in the model. This fact is underscored from measurements of lateral variations in gas temperatures between the center of the room and doorway by as much as 25 percent (figures 6-26a and b). Finally, theoretical results are presented (figure 6-31) that predict the minimum fuel mass loss required to achieve "flashover" (equivalent to an incident floor flux of 2 W/cm^2) as a function of sugar pine and rigid polyurethane, room size, and doorway size. These results appear to be in accord with results from furnishing item fires in rooms (figure 6-32).

Based on the theoretical and experimental results, an approximate quantitative comparison of the relative risk of room flashover between these two materials (sugar pine and structural polyurethane of comparable density) is that roughly twice as much area involvement is required for wood over the plastic. Although this conclusion may apply to other woods and plastics of comparable properties as those examined in this study, it applies only to non-spreading fires with a flashover criterion based on remote ignition.

THE BURNING OF WOOD AND PLASTIC CRIBS IN AN ENCLOSURE: VOLUME I

James G. Quintiere and Bernard J. McCaffrey

Abstract

This study was designed to assess the fire hazard of a cellular plastic material which has comparable structural characteristics to wood. The study attempts to determine the relative fire risk of such materials in furniture. Rigid (high density) structural polyurethane foam and sugar pine were selected for fuels and burned in the form of cribs in a room. The crib loading and door width were parameters experimentally varied. Twenty-one room fire experiments and eight free burn experiments were conducted. Measurements of mass loss, temperature, heat flux, CO_2 and O_2 concentration were recorded. These data were analyzed and empirical correlations were developed for air flow rate and upper gas temperature. A theoretical fire simulation model was developed and yielded results in fair to good agreement with the data. An extrapolation with the theoretical model was used to predict the critical (or minimum) fuel pyrolysis rate to cause flashover (as implied by 2 W/cm^2 of incident radiation to the room floor). This was done for various size rooms and door openings. It appears that to cause flashover, for a given room and door size, about twice as much wood must be involved in fire as the rigid polyurethane material.

Key words: Crib fires; experiments; mathematical model; plastic; polyurethane; room fires; wood.

1. INTRODUCTION

Understanding the developing fire in a room is a major objective of fire research. The use of new materials in room furnishings and building construction raises questions concerning their potential role in fire spread. It is not a simple matter to assess the potential fire hazard of a room and its contents. The growth of a fire within a room will depend on the nature of its combustible contents, their arrangement, and the construction and geometry of the room and its openings. Moreover, the concept of "fire hazard" is subjective and multi-faceted. For example, the obscuration due to smoke, the toxic effects of the combustion products, the rate of fire spread, and their combination can all be indicators of hazard. In this study the concept of hazard will be limited to the potential for fire growth.

In recent years mathematical models have been used to predict the dynamics of a developing room fire [1-6][1]. The basis of these models is an idealized room fire concept which consists of a fire plume and upper and lower homogeneous gas zones (layers). A rate of energy release expression is formulated for the fire and the conservation equations are solved for the zones. In reality, the term flashover is used by observers of fire to describe the phenomena of rapid transition in a developing room fire from a small fire to full room involvement. Although the occurrence of flashover is usually apparent its cause may be attributed to one of several mechanisms. Moreover, these mechanisms have not been fully understood. Mathematical models currently assess this transition by evaluating the rate of fire spread, the ignition of objects remote from the primary fire, or the excess of a room temperature or heat flux. Thus, models can be very specific in adopting operational definitions of flashover, but they may not be complete. The application of modeling results to the prediction of flashover will be applied in this context.

---

[1] Numbers in brackets refer to the literature references listed at the end of this report.

2

In this study the effects of flame spread over objects and combustible room linings will not be considered. The simpler case of a discrete fire centrally located and burning at a nearly steady rate will be considered. This relates to the real case of a furniture fire in a room with noncombustible linings. Conditions at the peak fuel gasification rate will be determined from the experimental results, and the potential for room flashover will be evaluated based on the potential for ignition of a floor target. This evaluation could lead to the determination of a critical (or minimum) fuel mass loss rate that is just sufficient to cause remote ignition (or flashover) in a room of given geometry and construction. Moreover, the results would apply to the developing fire in which the increase in the rate of fuel gasification is relatively slow. This is usually the case for furniture items before the onset of flashover. Hence, this process yields a result that can determine whether flashover will occur, but not when it will occur. Consequently, it will be sufficient to use a steady-state mathematical model for this application. In general, for slowly developing room fires in residential-size rooms, the transient fluid dynamic effects are insignificant, but the solid conductive heat transfer transient effects could be important. This latter effect will be accounted for by approximately evaluating heat transfer into solid boundaries at a time characteristic of the peak fire size; the time history of the solid will not be computed. Ultimately, the intent is to use the mathematical model to extrapolate to conditions beyond the range of the experiment. The validity of this extrapolation can be judged from the accuracy of the theoretical results relative to the experimental data. This summarizes the intent and nature of this study.

In particular, the objectives of the investigation are listed below:

(1) To conduct room fire experiments in which fuel representative of a discrete furniture item will be burned; (In order to investigate the performance of cellular plastics, a structural cellular plastic with a density comparable to wood, and a wood material are selected as fuels. A series of experiments is conducted in which the quantity

3

and type of fuel are varied under natural ventilation conditions of various doorway widths.)

(2) To determine and evaluate the peak average burning condition with respect to a potential for remote ignition of a floor target;

(3) To develop mathematical models of relevant phenomena within the framework of a two-layer room fire model, and attempt to verify these models (or sub-models) by comparison with experimental results;

(4) To predict results using a steady-state two-layer mathematical room fire model, and compare these predictions with the experimental results; and

(5) To make a quantitative statement on the factors influencing flashover for discrete room fires.

2. EXPERIMENTAL DESIGN OF ENCLOSURE FIRES

In this section the experimental facility will be described. The process selecting the fuel configuration will be discussed. The type of instrumentatio and measurements will be presented. And finally the experimental procedure and scope of experiments will be listed.

2.1 Fire Test Room

The experiments were conducted in the NBS Fire Test Building (205) in a test room which adjoined a corridor. A plan view of the facility is shown in figure 2-1. The combustion products from the room fire would exit at the open end of the corridor into an exhaust hood. To avoid the influence of the corridor on burn room flow, the height of the room doorway was selected such that the layer of hot combustion products in the corridor did not fall below the top of the doorway. The doorway of the room was located at a corner and had a channel-like door frame with a depth of 0.5 m approximately. These were facility constraints and could not be easily modified. The width of the room doorway was varied over the series of experiments in three sizes: 0.79, 0.39, and 0.19 $\pm$ 0.01 m.

4

Not to scale

TEST ROOM
2.18x2.18x2.41 high

~3

CORRIDOR

EXHAUST HOOD

All dimensions in meters
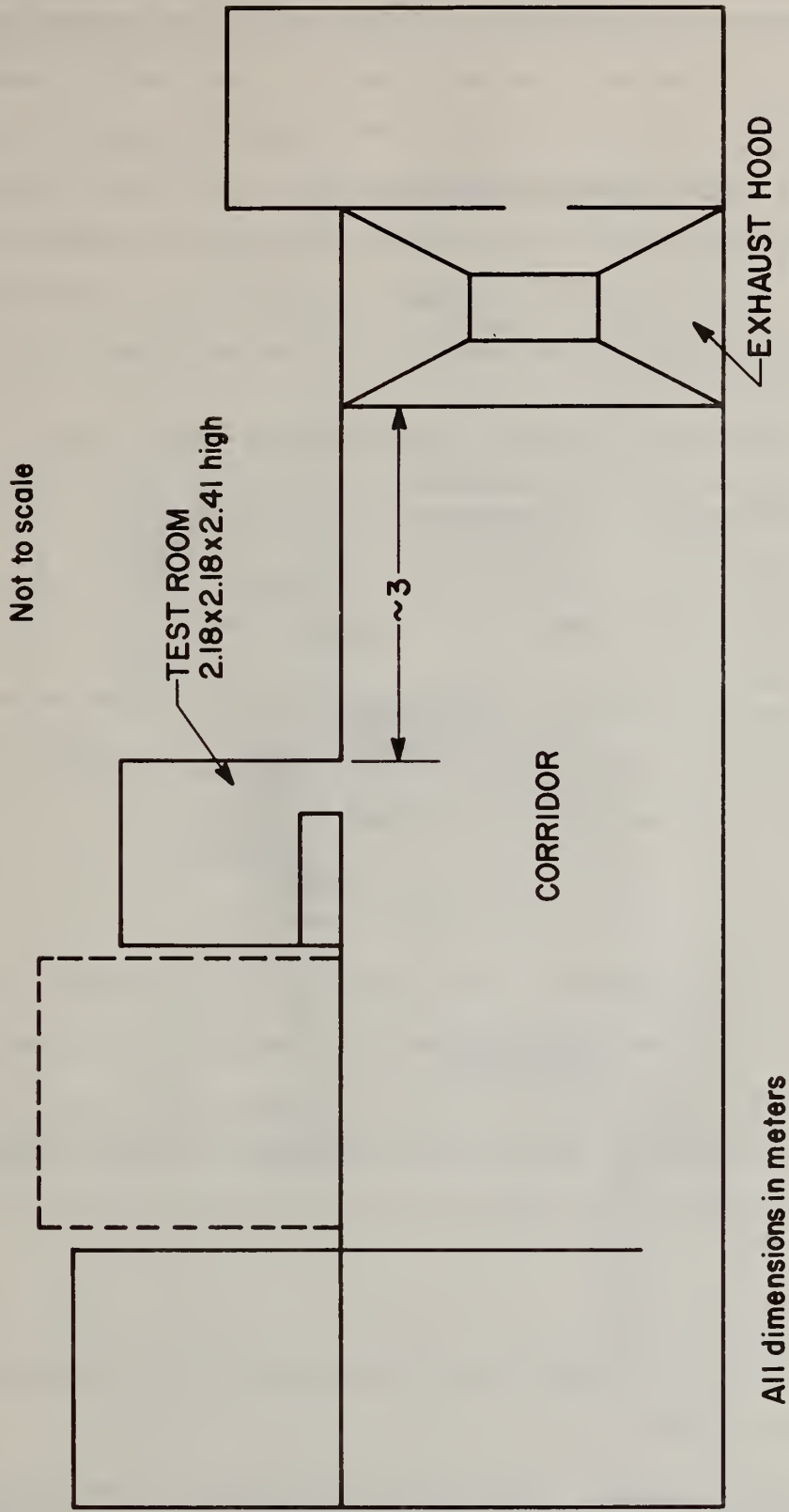
Figure 2-1. Plan view of experimental facility

A plan view of the room is shown in figure 2-2. Its dimensions of 2.18 x 2.18 x 2.41 m high are relatively small by residential standards but not uncommon for a minor bedroom or study in new housing. The room was lined with a calcium silicate board (Johns-Manville, Marinite XL[2]) with a thickness of 1.9 cm. This material has physical properties similar to gypsum board as shown in table 2-1. Also it should respond thermally as a semi-infinitely thick wall over the anticipated burning duration of the experiment (10 minutes).

Table 2-1. Physical properties at 22°C

	Density (kg/m^3)	Thermal Conductivity (W/m-K)	Specific Heat (kJ/kg-K)	Moisture Content (%)
Marinite XL	700	0.11-0.14	1.12	<5
Gypsum board	960	0.17	1.1	<5

During the period of the experiments the ambient laboratory conditions were roughly 22°C and 30-40 percent relative humidity.

2.2 Fuel

A wood and rigid polyurethane foam material were selected. The source of the polyurethane was the Products Research Committee (PRC) materials bank and is GM-37 by their designation. Often throughout the text, the materials will be referred to commonly as "wood" and "plastic". Both leave a char residue when burned. A description of fuel materials is given in table 2-2.

---

[2]Certain commercial equipment, instruments, or materials are identified in this paper in order to adequately specify the experimental procedure. In no case does such identification imply recommendation or endorsement by the National Bureau of Standards, nor does it imply that the material or equipment identified is necessarily the best available for the purpose.
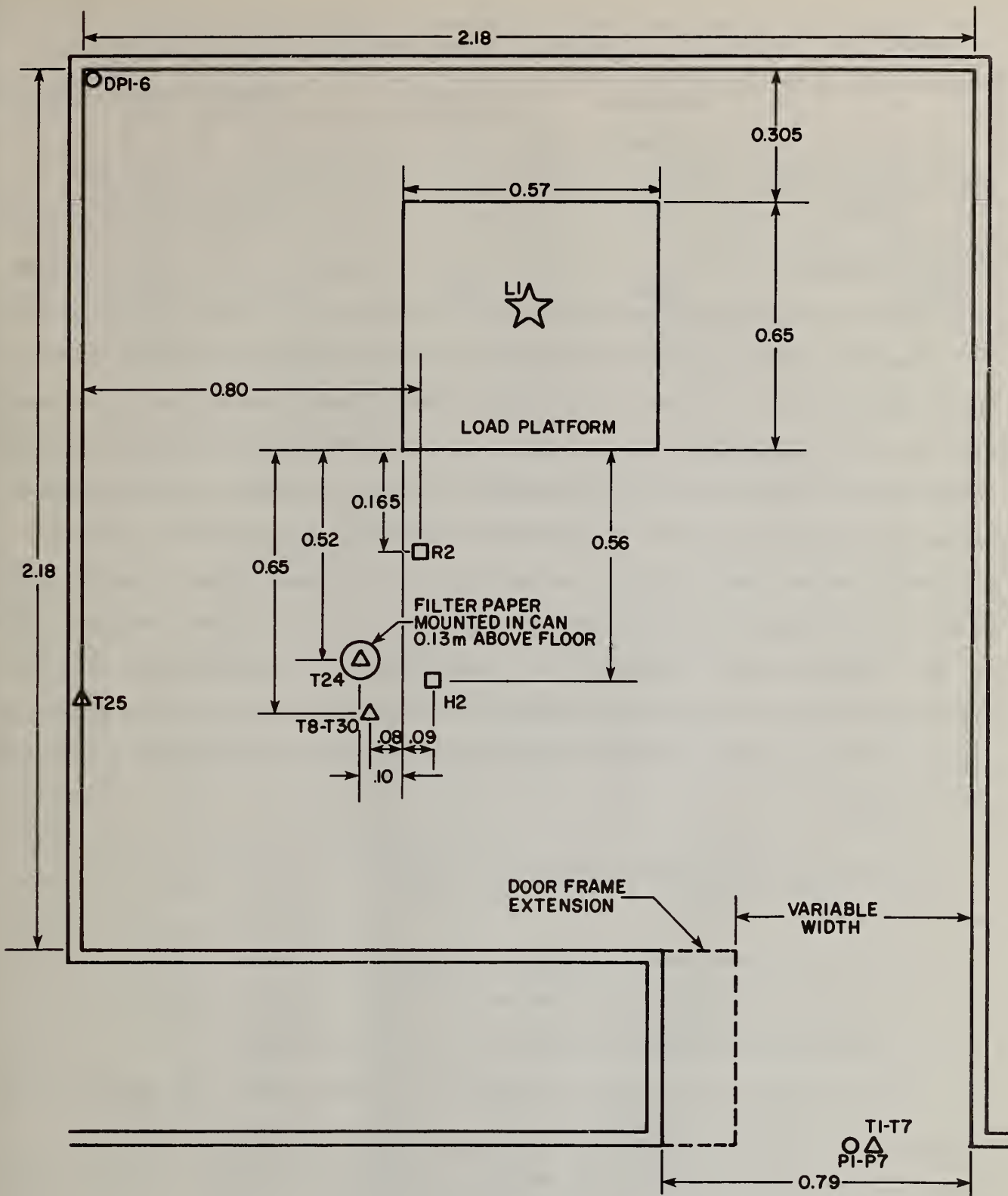
Figure 2-2. Plan view of test room

Table 2-2. Chemical and physical description of the fuel materials

	Density kg/m^3	Moisture Content %	Element composition (dry) C %	H %	O %	N %
Wood: Sugar pine, clear	370	6.5	47.6	6.4	44.7	0.07
Plastic: Rigid polyurethane, GM-37	340	nil	66.5	7.0	19.0	6.4

A more difficult task than selecting the fuel materials was to select their configuration. Perhaps the simplest fuel configuration is a horizontal slab covering a portion of the room floor. This configuration burning in an enclosure can sense a significant amount of energy feedback from the heated enclosure. As a result of this feedback, its burning rate can be greatly enhanced. Such a configuration is a relatively "simple" case to model. Unfortunately, both wood and high density rigid polyurethane do not sustain combustion in this configuration. Moreover, vertical slabs of these materials are also difficult to burn unless some preheating or long duration ignition source is applied. Consequently, the configuration of a "crib" (ordered array of sticks) was selected.

The design of the crib configuration was subject to the following specifications:

(1) The burning rates should be over a relevant range. It was thought that 5 to 20 g/s would be satisfactory. This represents small wastebasket fires to moderate size chair fires.

(2) The duration of the fires should be sufficiently long to provide a realistic simulation of furniture-like fires, and should be reasonably steady over several minutes of burning. A nominal fire of 10 minutes was considered acceptable.

(3) The crib fires should be surface controlled and sufficiently open in porosity to permit some room energy feedback.

(4) The ratio of the projected horizontal cross-sectional area of the fuel to floor area should be small. Also the height of the fuel

element should be, if possible, below the thermal (or smoke) layer
in the room. These constraints should insure unrestricted ambient
air flow to the fuel.

The theory of free burning wood crib fires is well developed [7,8] and
was used to design the crib configuration subject to these specifications.
However, empirical parameters needed to be determined in order to apply the
theory polyurethane. A series of preliminary experiments burning wood and
plastic cribs of various sizes and arrangements was conducted. The theoret-
ical and experimental results that led to a wood and plastic crib design are
given in appendix A. Insufficient data and uncertainty of empirical parameters
for polyurethane cribs do not fully insure that our design for polyurethane
is in the stick surface area-controlled burning regime. Also during burning the
polyurethane sticks swelled up to 50 percent of their original thickness, and
this phenomenon affects the certainty of a surface area-controlled crib design.
Observations showed that the plastic cribs would fissure and cause jets
of flame in spots whereas for wood the velocity of the volatiles leaving the
surface appears more uniform. For both materials there appears to be a
distinctly greater fuel gasification rate per unit area for internal stick
surfaces than for outside surfaces of the crib. The results from appendix A
yield an average peak gasification rate per unit of exposed area, $\dot{m}_v''$, for
the area-controlled regime as

$$\dot{m}_v'' = C \ b^{-1/2} \tag{2-1}$$

where b is the thickness of a square stick in cm and C is 1.2 mg/cm$^{1.5}$-s for
polyurethane and 0.88 mg/cm$^{1.5}$-s for sugar pine.

For our limited data over a range of crib sizes, equation (2-1) predicts
the mass loss rate to within $\pm$ 20 percent for sugar pine and $\pm$ 20 percent for
polyurethane. It should be emphasized that equation (2-1) corresponds to the
average peak gasification rate[3], and that the reproducibility for our crib data
is about $\pm$ 20 percent.

_____
[3]The average peak gasification rate is defined in section 3, and is generally
the "best" slope of the fuel mass loss curve over the most active flaming period.

Based on these results, a crib was designed and it is presented in table 2-3.

Table 2-3. Geometry design of crib

Square stick thickness	b	3.5 cm
Stick length	ℓ	24.5 cm
Spacing between sticks	s	7.0 cm
Number of sticks per layer	n	3
Number of layers	N	10

This design, for the wood and plastic materials, has a nominal peak average mass loss rate of 5 g/s, a nominal burning duration of 12 minutes, and a duration during the peak burning period of 200-400 s. In order to vary the fire size, the cribs were burned in arrangements of one to four cribs. The cribs were arranged on a platform, 0.18 m above the floor of the room, as shown in figure 2-3. Heat flux sensor H2 is included for orientation. The combined height of the platform and crib was slightly under 30 percent of the doorway height, and the area of the platform was about 10 percent of the room floor area. Thus, the last specification on crib design appears to have been met

2.3 Instrumentation

The instrumentation was designed to characterize the thermal and flow aspects of the compartment fire. The number of probes was chosen to avoid an excessive amount of data to analyze and yet give a sufficient set of data to, hopefully, fully characterize the phenomena. A vertical temperature profile was measured in the room outside the flame zone. Wall and ceiling surface temperatures were measured, as well as the surface temperature of a filter paper target at the floor level. The rate of fuel gasification was recorded,
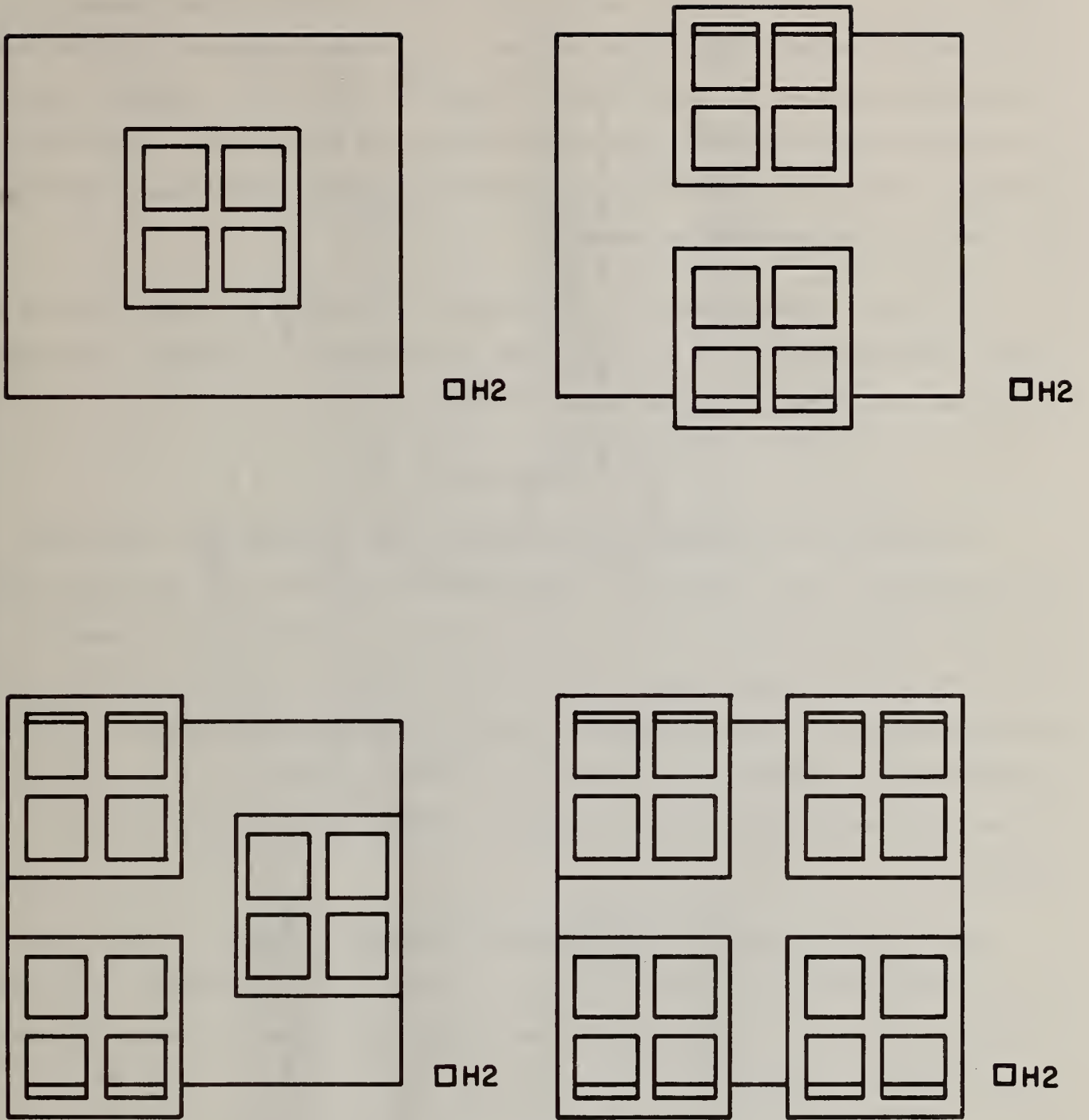
Figure 2-3. Crib configuration on the load platform for room fire experiments

11

along with the oxygen and carbon dioxide concentration of the combustion product flow. Velocities and temperatures were measured in the doorway so that a mass flow rate could be determined. Total and radiative incident heat fluxes were measured at significant locations in the room. (However, all of our radiometer data is suspected to be invalid due to soot fouling of the radiometer window.) Also static pressure differences were measured between the room and the surrounding ambience.

The type of instrumentation is described in table 2-4. Also given is a symbol and letter key that has been used to designate each sensor. The sensor locations are shown in figures 2-2, 2-4, and 2-5.

2.3.1 Temperature

In figure 2-5 the number associated with the thermocouples gives the bead diameter in mm. This set of thermocouples was installed after test PRC 8 and they were used through PRC 20 except for some individual replacement. Also after PRC 8 temperature sensors T26-T30 were added in order to determine a "true" gas temperature in the lower layer. The smaller bead thermocouples and the aspirated probe would be less affected by radiant heating and thus yield a more correct gas temperature. An assessment of radiation effects is given in appendix B.

The surface monitoring thermocouples were held in place by their own spring force, and half of their bead was pressed into the surface. The leads from the bead were in contact with the surface for a short distance to minimize wire conduction losses.

2.3.2 Heat Flux

The primary results of interest are the total incident heat flux measurement at the ceiling (H1) and at the floor (H2). The floor sensor primarily represents the sum of the radiative heat flux from the flame and the enclosure, plus a small convective component. This is essentially the flux seen by the lower space thermocouples and the filter paper target. Unfortunately, the

12

Table 2-4. Type of Instrumentation

Measurement	Label	Symbol	Probes	Description
Temperature	T	△	T1-T27,29,30	Chromel alumel thermocouple (∼0.5 mm bead diam. generally)
Temperature	T	△	T28	Aspirated thermocouple probe (United Sensor)
Total heat flux	H	□	H1,2	Thermopile-type water cooled with 0.98 absorptivity sensing face (Medtherm)
Radiative flux	R	□	R1,2	Thermopile-type water cooled with (Kodak) ITRAN 2 window (Medtherm)
Oxygen volume concentration	G	⬡	G1	Electrolytic cell, dry basis
CO_2 volume concentration	G	⬡	G2	Infra-red absorption, dry basis (Beckman)
Weight	L	☆	L1	Strain-gage load platform, water cooled (BLH Electronics)
Static pressure difference	DP	○	DP1-6	Variable reluctance pressure transducer and signal processor (Dynascience, Natel)
Velocity pressure	P	○	P1-7	Bidirectional velocity probe, capacitance type pressure transducer and electronic manometer (Datametrics)

13
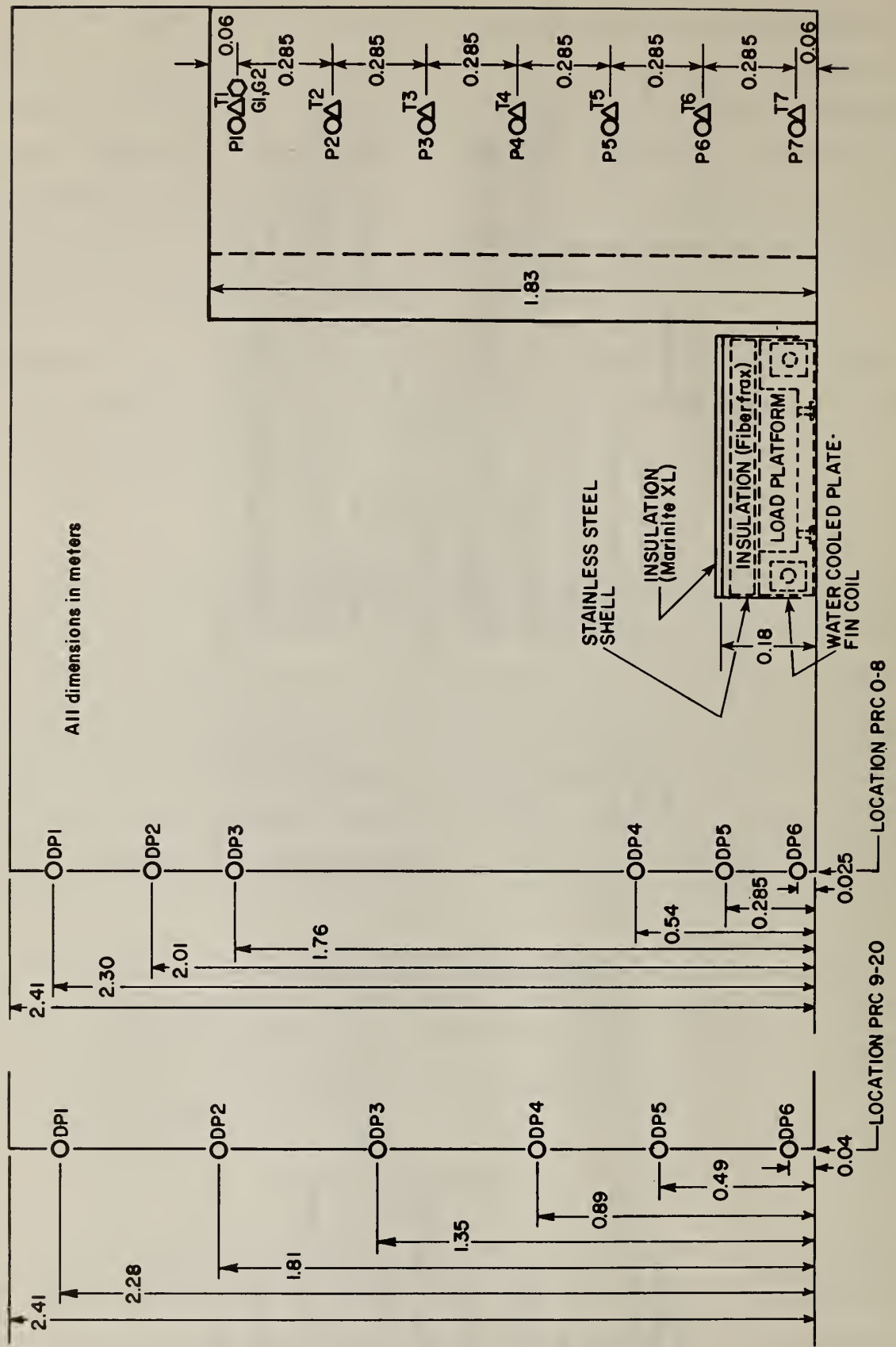
Figure 2-4. Room instrumentation – side view

14
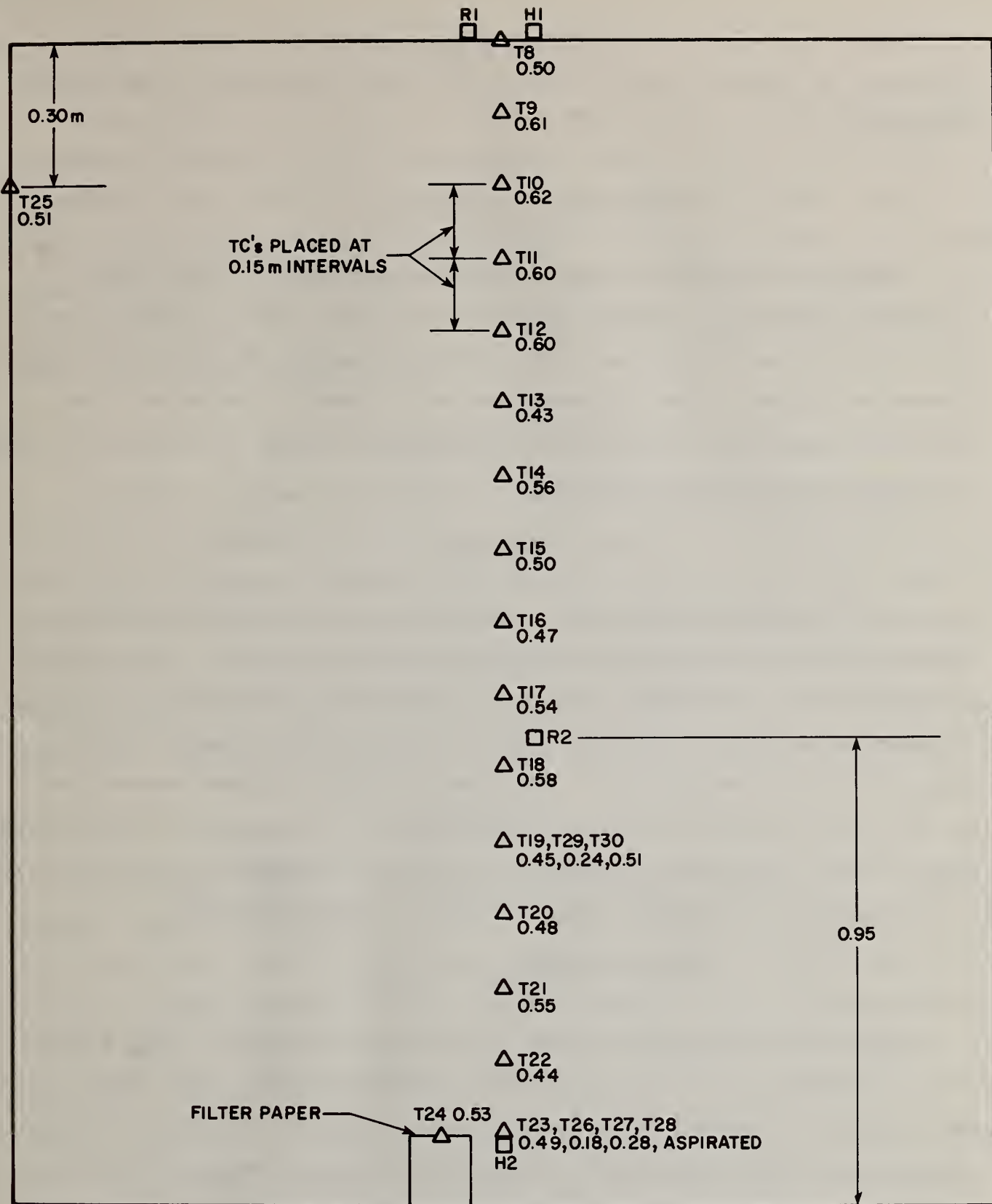
Figure 2-5.   Room instrumentation - thermocouple section with bead
diameter in mm

15

windows on the radiometers could not be kept clean during a room fire experiment so radiative and convective flux components could not be reliably determined.

2.3.3   Gas Concentrations

Oxygen and CO_2 volume concentrations were measured on a dry basis (H_2O was condensed out in the sampling line) in the exhaust products flowing out of the doorway. Both measurements give information on the nature of the combustion process. Also CO_2 concentration is needed to determine a gas emissivity, and the O_2 concentration is required in order to estimate the rate of energy release within the room.

2.3.4   Mass Loss

A 45 kg capacity strain gage load platform, insensitive to eccentric loads, was used to monitor the mass loss of the burning cribs. The platform was contained in a stainless steel box surrounded by water-cooled fin tubing as shown in figure 2-4. The top cover of the box was insulated and was supported by the load platform. Sufficient clearance existed between the top and bottom sides of the box. The accuracy of the system and fluctuations under a static load were ±50 g approximately; this suggests an error of up to ± 3 percent during the peak average period in these experiments.

2.3.5   Room Static Pressure

Six pressure taps were located vertically in the corner of the room as shown in figures 2-2 and 2-4. After PRC 8 their positions were changed to a more optimum configuration for displaying the pressure distribution. These pressure taps measured the static differential pressure across the wall of the room. In general, it is this pressure difference which drives the flow through any room openings during a fire. An assumption in developing a theory for fire induced flows is that the pressure distribution is hydrostatic in a room. These measurements, along with the room temperature distribution, would allow a check on this assumption.

16

2.3.6 Doorway Velocity

The velocity in the doorway was measured with seven bidirectional probes as shown in figure 2-4. Their pressure differentials were sensed by seven transducers whose output was sequenced by a multiplexer through a single electronic manometer. Each transducer signal was integrated over 1 s intervals (after PRC 8) and recorded every seventh data scan or every 35 seconds. This arrangement proved to be satisfactory in determining the doorway mass flow rate over the peak burning period.

2.3.7 Filter Paper Target

In order to assess the hazard of remote ignition of other objects, a filter paper target was used. A 15 cm diameter sheet of Whatman Qualitative[2] No. 1 filter paper was suspended over the open face of a metal can. This was located on the floor of the room as shown in figures 2-2 and 2-5. The paper was not preconditioned, and a thermocouple (T24) monitored its temperature. The position of the target in the room did not enable us to view it during an experiment, but the condition of the paper following the test was recorded.

2.4 Data Recording

Up to fifty channels of data were recorded by a high-speed data acquisition system. The set of channels was scanned every 5 seconds at a maximum rate of 40 channels per second. The raw data were processed by a computer to yield values in appropriate units for each channel number. A key for interpreting the raw data (as given in volume II) is given in table 2-5. It should be noted that channel 30 identifies the probe position corresponding to the velocity recorded in channel 35. The number in channel 30 corresponds approximately to 10 times n where n is the digit on the bidirectional probe coding label Pn. (See figure 2-4 or table 2-5).

Continuous color video recordings were made for each experiment. The television camera viewed through the lower half of the room doorway. The visible portions of the room walls were marked by labeled horizontal lines

defining the height. This enabled the smoke layer height to be determined by a study of the video tape for each test.

Table 2-5. Correlation key for raw data

	Instrumentation	Monitored Variable	Channel Number	Units
L1	Load Cell Platform	Burning mass loss	31	g
H2	Floor Heat Flux Meter	Total heat flux incident on floor	32	W/cm^2
T24	Thermocouple (TC) on Target Filter Paper	Incidents ignition of target filter paper	23	°C
T8-T23	Room TC Rake 16 TC's including Ceiling	Representative room gas gradient	7-22	°C
T25	Wall TC	Representative upper wall temperature	24	°C
T1-T7	Doorway TC Rake 7 TC's	Gas temperature distribution in doorway	0-6	°C
P1-P7	Bidirectional Velocity Probes (7)	Gas outflow and inflow velocity	35 (30,probe ID)	m/s
G1, G2	Doorway Gas Sampling	O_2 and CO_2 concentration of exhaust gas	40 and 47	o/o
DP1-DP6	Static Pressure	Room static pressure distribution (differential-room to ambient)	41-46	N/m^2
R1	Ceiling Radiant Energy Meter	Incident radiant heat flux to ceiling	33	W/cm^2
H1	Ceiling Heat Flux Meter	Total incident heat flux to ceiling	34	W/cm^2
R2	Radiometer	Heat flux from upper region of room located 0.95 m above floor[a]	39	W/cm^2
T26-T30	Small Wire Thermocouples An Aspirated Thermocouple (T28)	Room gas temperature[b]	25-29	°C

[a] Added for PRC 13 - PRC 18

[b] Added for PRC 9 - PRC 20

18

2.5 Experimental Procedure

Before each experiment the test room was cleaned of excess soot deposits, and cracks in the lining were patched with a furnace cement. The probes were cleaned and their positions checked and realigned if necessary. An instrumentation checklist (figure 2-6) was followed and calibrations of the load platform and heat flux sensors were performed.

The heat flux sensors were calibrated in place by a reflecting sphere apparatus shown in figure 2-7. A reference sensor was mounted flush to the inside of the sphere. On the side opposite, a collar accommodated the sensor to be checked so that its face was also flush with the inside of the sphere. The heat source was a lamp mounted at the center of the sphere. The flux was varied by varying the lamp voltage. A calibration constant had to be applied to relate the test sensor to the standard reference sensor. This factor depended on the orientation of the system and the radiometer window. This procedure provided a quick and convenient check of the heat flux sensors. If a sensor deviated from its initial calibration it would then be removed and recalibrated under laboratory conditions.

After the instrumentation was prepared, then the preparation for ignition commenced. The wood cribs were kept in a conditioning room (20°C, 50% RH) for several days prior to a test. Their moisture content ranged from 5 to 8 percent. The cribs were arranged on the load platform (figure 2-3) and the spacing between cribs was equal to the stick spacing, 7 cm. Each crib was placed on a 30 cm square metal pan with a 1 cm high lip and was supported by two Marinite strips 2 cm high. Forty ml of heptane was poured into each pan to promote rapid and uniform ignition of the cribs. Ignition of all the pans was virtually simultaneous. On ignition the data and video systems began recording.

PRC Checklist

Date _____
Test _____

Blue Instrument Rack
(from top)

MULTIPLEXER ENCODER   On   ☐

MULTIPLEXER   On (plug in rear cable)
Scan rate	Ext	Manual operation: Single scan	☐
Channel	Auto	Manual	☐
Switch	1	Desired Channel	☐

MANOMETER   On   ☐
NULLING VALVES   On
Set valves in Null position; turn manometer range switch to x.1(3 or 4) cribs - x.03(1 or 2)cribs; zero each channel with screwdriver on multiplexer face. Multiplexer will be required to be in manual operation. Return multiplexer to Ext-Auto-1 positions; set nulling valves to run position (it is advisable to set manometer range switch to zero position when shifting valves from Null to Run); make certain manometer range switch is in correct position, i.e. x.1 or x.03.

DELTA P TRANSDUCERS   Power switch in (indicator light is not working)   ☐

CO_2 Power should be on continuously
CH47
Set zero output with zero pot.
Set 10.00 mv output with gain pot while pressing calibrate button.   ☐
Pump should be drawing air through sensor during this procedure

Blue Instrument Rack
(rear)

LOAD CELL POWER SUPPLY   Turn on Sorenson power supply   ☐

GAS SAMPLING MANIFOLD   Connect O_2 cell (alligator clip connectors)   ☐
Fill dewar with ice water   ☐
Replace millipore filters   ☐
Clean, and replace cotton wool, cold trap   ☐
Turn motor on (plug cord in bus bar)   ☐
Observe flow - should be about 2+ SCFH   ☐

Clean HF & RD sensors   ☐
Press ceiling ☐ and wall ☐ TC in place
Spring load TC to filter paper
Turn on cooling water
Set heater & water temperature
Turn on N_2 purge

CALIBRATIONS

Time _____
Temperature _____
Humidity _____
Manometer constant x _____
Cribs: MC _____   Initial mass _____   Load cell tare _____ mv
(CH31)

Weight (kg)	Load cell (mv)
_____	_____
_____	_____
_____	_____
_____	_____
_____	_____
_____	_____

Heat Flux Sensors ("standard" lamp)
R1	mv	H1	mv	H2	mv
(33)		(34)		(32)	

Check Vidar operation of each channel (Note overloads or shorts)   ☐
Scan Vidar to bring multiplexer to channel 1   ☐
Run seven zero scans   ☐
Observations:

Figure 2-6.   Experimental checklist

HOLDER FOR REFERENCE HEAT FLUX SENSOR

7cm R REFLECTING SPHERE

LAMP

COLLAR FOR TEST SENSOR
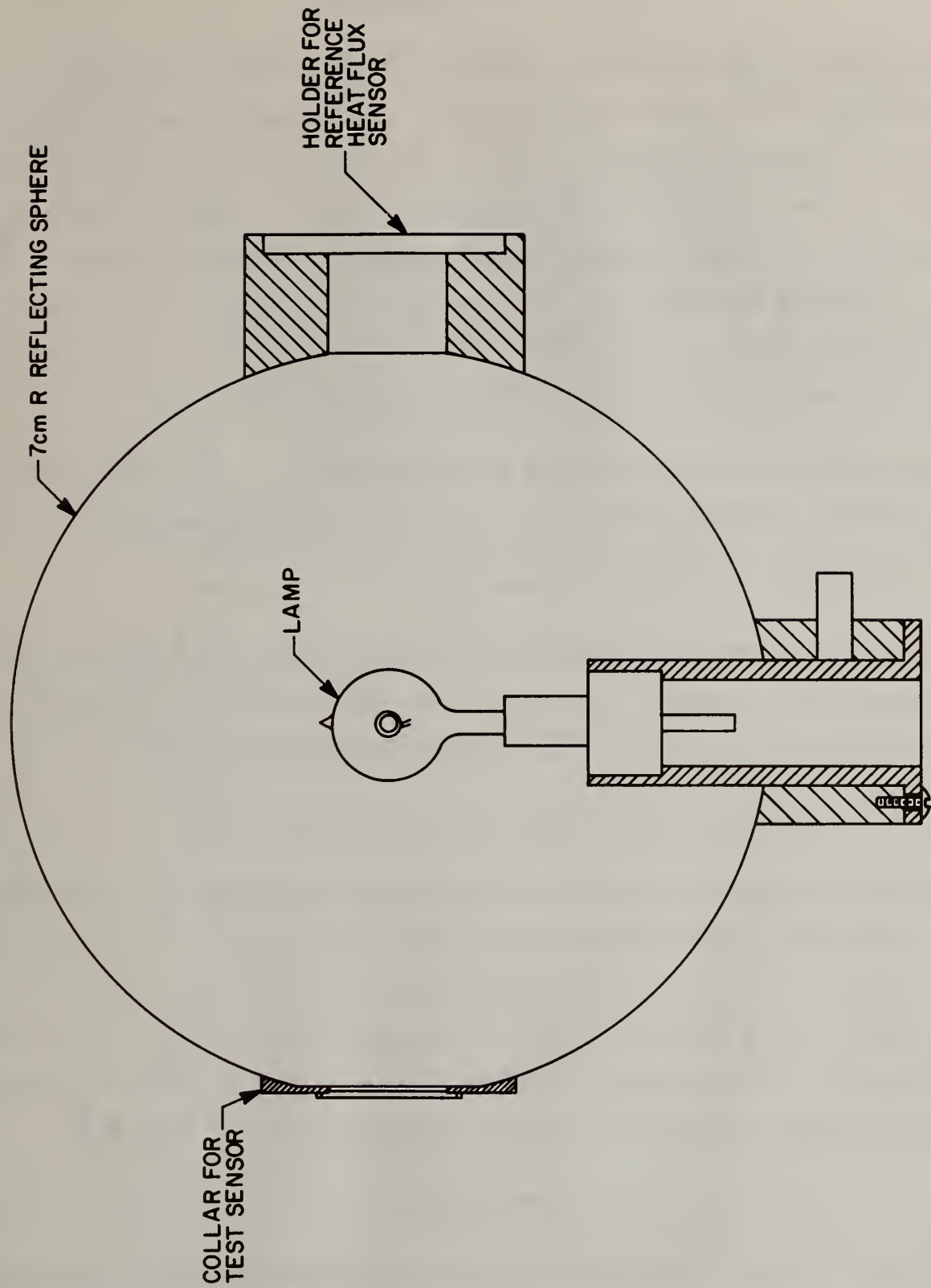
Figure 2-7. Reflecting globe for calibration of heat flux sensors

2.6 Scope of the Experiments

The scope of experiments was designed to range over fire sizes representative of discrete furniture fires, the biggest comparable to a chair fire. The ventilation conditions were to reflect typical door openings (although our variable width doorway does not exactly simulate a door in various open positions) including doorways small enough to be possibly ventilation limited. A range of door sizes and crib loadings was selected in order to span these conditions, and to provide a basis for comparison with theoretical results and their extrapolation to other realistic conditions.

The sequence of experiments is given in table 2-6. The second through fourth columns provide a descriptive code used for each experiment.

Test Number - Fuel Type - Number of Cribs - Door Factor

The code will be used throughout the text, and as a label on the figures for identification purposes. Also given are some comments for each experiment and the condition of the filter paper target following the test.

3. RESULTS OF ROOM FIRE EXPERIMENTS

In this section some observations made during the room fire experiments will be presented along with the average peak burning data. A complete set of the transient raw data, in the format given in table 2-5, is available on magnetic tape, and a printed listing of the data is tabulated in volume II of this report. Also included in volume II, are numerous computer generated plots which display the behavior of each measured variable over time.

3.1 Observations

Typical of room fire experiments, an immense amount of data was collected. By design, we have chosen to examine, for the most part, the quasi-steady results during the peak burning period. This minimizes an analysis for each experiment, and directs our analysis to the effects of the initial conditions on the "peak" fire conditions. Some observations made over the period of each

Table 2-6. Sequence of room fire experiments

Date	Exp. No. PRC	Fuel W-Sugar Pine P-Polyurethane	No. of Cribs	Doorway Width Factor 1 = 0.79 m ½ = 0.39 m ¼ = 0.19 m	Filter Paper Target 0-no effect 1-charred 2-consumed	Comments
3-07-77	0	W	1	1	0	Shakedown
3-11-77	1	P	1	1	0	
3-15-77	2	W	3	1	0	
3-17-77	3	W	1	1	0	
3-17-77	4	P	2	1	0	
3-22-77	5	W	2	1	0	Slow crib ignition
3-22-77	6	P	3	1	2	Walls & ceiling cracked
3-24-77	7	W	4	1	1	
3-25-77	8	P	4	1	2	
4-21-77	9	W	2	½	0	Wall & ceiling replaced
4-22-77	10	P	2	½	1-	T23 shorted
4-27-77	11	W	3	½	0	
4-30-77	12	P	1	¼	0	
5-04-77	13	W	2	¼	0	
5-04-77	14	P	2	¼	1	Initial ceiling temp. ~50°C
5-06-77	15	W	4	½	1	Possible load cell problem
5-06-77	16	P	3	¼	2	Possible load cell problem
5-11-77	17	W	4	¼	1+	Possible load cell problem
5-11-77	18	P	3	½	2	Possible load cell problem
5-26-77	19	W	4	¼	1+	Repeat of PRC 17
5-26-77	20	P	3	¼	2	Repeat of PRC 16

experiment are useful to consider here in order to give the reader some impressions of these experiments. Complete color video records are available for each test.

Some features of the experiments will be given: The wood cribs would generally collapse at about 10 minutes after ignition whereas the plastic cribs would swell and char but maintain a structure similar to its original form. Figures 3-1 through 3-3 from PRC 7 (PRC 7-W-4-1) display conditions prior to ignition, full involvement of the cribs, and the glowing char remains at the end of the test. The residue after combustion of the plastic cribs in PRC 14 (PRC-14-P-2-1/4) is shown in figure 3-4. The char residue after the flames extinguished was about 10 percent for wood and 13 percent for plastic.

Although no quantitative measure of the smoke was made, the general character of the smoke was observed. The wood smoke tended to be light to dark grey in color, while the smoke from the plastic cribs was black with large visible flakes of soot. The smoke did tend to produce a distinct interface within the room, but in the small doorway cases the smoke did stratify more and its interface did nearly fall to the floor. A plot of the smoke layer interface with the room for PRC 7 is plotted in figure 3-5. This was obtained by a study of the video record of the experiment. A photograph of the smoke layer in the room doorway and corridor for PRC 14 is shown in figure 3-6. It should be noted that the corridor smoke layer is above the room door as desired in the experimental design.

3.2 Average Peak Values

Since a true steady burning period is not achievable, some arbitrary determination of the peak values must be made. An average peak value (APV) was determined for each measured variable and derived experimental parameter. This was done in the following manner. The time interval was identified which corresponded to the crib mass changing from 95 to 45 percent of its initial mass. All parameters were numerically averaged over this time interval to the average peak mass loss rate. This procedure, for the most part, yields

24

Figure 3-1. Cribs prior to ignition-PRC 7

Figure 3-2. Full involvement of cribs-PRC 7

Figure 3-3. Glowing char residue-PRC 7

Figure 3-4. Char residue of polyurethane cribs-PRC 14

Figure 3-6. Smoke laden hot gases flowing from room into corridor-PRC 14

25

PRC-7-W-4-1
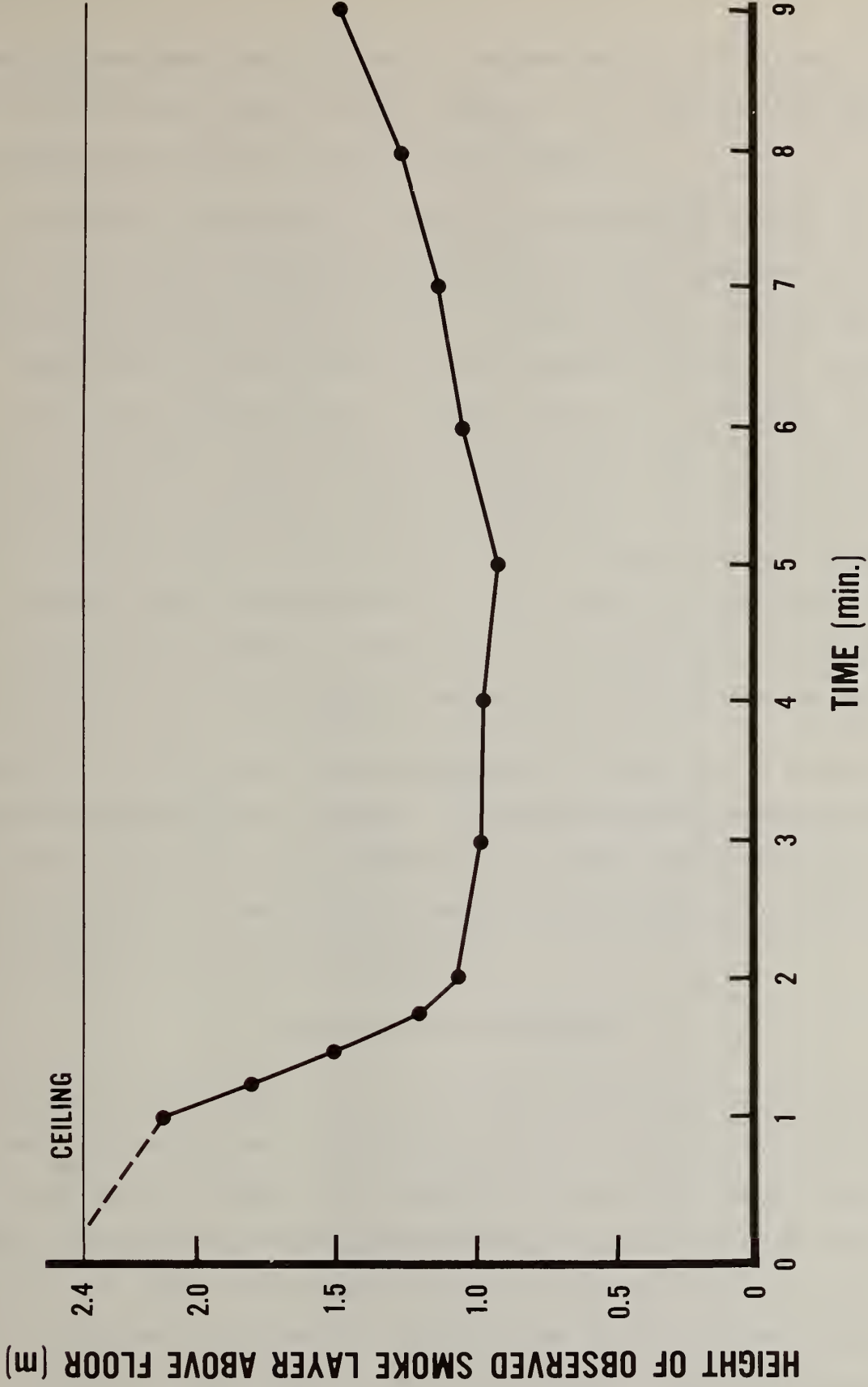
Figure 3-5. Height of smoke layer interface above floor - PRC 7

26
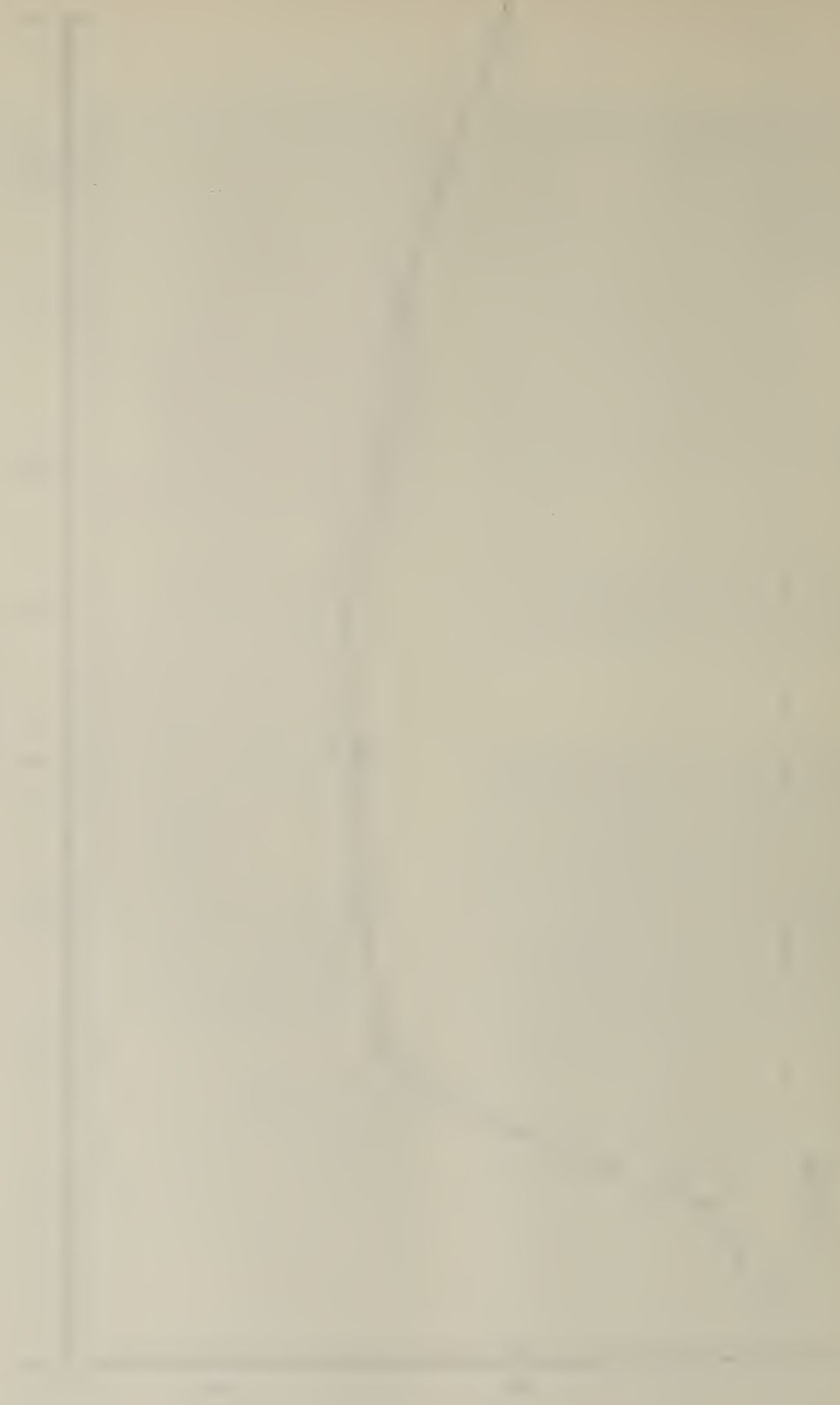
an average peak mass loss rate that is approximately $\pm$ 15 percent of the rate
of mass loss in that time-averaging interval. The time-averaged peak values of
the raw data are listed for each run in volume II.

In table 3-1, significant average peak experimental results are given.
Listed are the time interval defined for peak "steady" burning and the
corresponding peak mass loss rate ($\dot{m}_v$). Arbitrarily an average room upper
layer temperature ($\bar{T}$) was defined as the arithmetic average of thermocouples
9, 10, and 11 near the ceiling. Also the ceiling (T_8) and upper wall tempera-
ture (T_{25}) are given. The calculated doorway flow rates, $\dot{m}_{in}$ and $\dot{m}_{out}$ are
listed along with the doorway average velocities. The location of the zero
velocity (neutral plane height, N) position, the observed smoke height (D_s),
and a defined thermal layer height (D_T) are given in dimensionless variables
normalized with the doorway height (H_o). The thermal layer height was defined
as the height (z) at which $\dfrac{d^2 T}{dz^2}$ is a maximum for the vertical gas temperature
distribution in the room. This is generally the same as, or slightly below,
the position where $\dfrac{dT}{dz}$ is a maximum. The average volume concentrations
(dry basis) for CO_2 and O_2 are given for the upper doorway position. Other
values listed are the room static pressure differential (ΔP), and the ceiling
(H2) and floor (H1) total heat fluxes.

4. FREE BURN CRIB EXPERIMENTS

Following completion of the room fire experiments a series of free or
open burn experiments was conducted for each of the room crib arrangements.
Eight burns were performed - one through four wood and plastic cribs each.
Basically the same or similar instrumentation was used in these experiments
as used in the room. The experiments were conducted directly under the large
exhaust hood shown in figure 2-1. The purpose of this series of experiments
was to establish a basis for the rate of crib mass loss uninfluenced by a
heated enclosure. Also, the direct radiation heat transfer from the crib
fires needed to be determined, and a means of computing the rate entrained
air into the crib fire had to be developed.

27

Table 3-1. Average peak values for significant results

	APV Times (s)	$\dot{m}_v$ (g/s)	$\dot{m}_{in}$ (kg/s)	$\dot{m}_{out}$ (kg/s)	$\bar{T}_{9-10-11}$ (°C)	T_8 (°C) Ceiling Temp. (°C)	T_{21} (°C) Wall Temp. (°C)	H_2 (w/cm^2)	H_1 (w/cm^2)	% O_2	% CO_2	N/H$_o$	Thermal D/H$_o$	Video Tapes D/H$_o$
$W_o = 0.79m$ ($A_o\sqrt{H_o} = 1.96 m^{5/2}$)														
PRC 0-W-1-1	105-440	5.08	.237	.371	157	85	--	.153	--	19.1	2.43	.633	.66	
PRC 3-W-1-1	120-460	5.10	.242	.380	151	137	81	.148	.336	19.0	2.37	.653	.66	.73-.86
PRC 5-W-2-1	175-455	11.86	.445	.470	243	158	124	.248	.774	18.2	3.80	.651	.57	.88
PRC 2-W-3-1	130-375	20.14	.410	.631	328	211	193	.543	1.21	16.7	5.10	.665	.49	.60
PRC 7-W-4-1	85-320	28.64	.503	.685	416	319	293	1.01	2.54	15.6	6.94	.590	.53	.55
PRC 1-P-1-1	70-290	6.98	.517	.598	212	122	119	.381	.655	18.6	2.52	.634	.57	.46
PRC 4-P-2-1	65-215	20.19	.450	.667	366	286	240	1.04	2.06	15.1	5.86	.634	.49	.49
PRC 6-P-3-1	50-185	33.02	.516	.650	682	607	543	2.39	7.78	10.7	11.8	.566	.49	.50
PRC 8-P-4-1	60-230	35.29	.489	.697	794	754	716	2.86	10.4	9.57	11.4	.534	.37	.44
$W_o = 0.39m$ ($A_o\sqrt{H_o} = 0.98$)														
PRC 9-W-2-1/2	95-385	11.94	.259	.370	288	145	139	0.42	0.81	16.7	3.21	.574	.57	.57
PRC 11-W-3-1/2	105-370	18.73	.354	.385	356	231	200	0.58	1.30	15.3	5.99	.587	.49	.52
PRC 15-W-4-1/2	70-310	28.28	.389	.422	424	314	316	1.01	2.25	13.7	6.86	.561	.41	.37
PRC 10-P-2-1/2	60-255	15.42	.341	.421	386	245	254	1.00	1.90	14.2	5.31	.557	.29	.33
PRC 18-P-3-1/2	70-260	25.02	.400	.492	680	644	639	2.39	6.65	7.81	10.4	.532	.25	.42
$W_o = 0.19m$ ($A_o\sqrt{H_o} = 0.49$)														
PRC 13-W-2-1/4	130-425	11.27	.173	.225	319	185	174	0.43	0.90	14.8	5.36	.557	.45	.45
PRC 17-W-4-1/4	85-365	24.48	.224	.272	488	415	376	1.45	3.12	8.01	12.5	.530	.29	.30
PRC 19-W-4-1/4	85-345	26.41	.196	.283	478	386	352	1.40	1.95	9.67	10.9	.530	.25	
PRC 12-P-1-1/4	85-350	5.90	.203	.207	238	151	129	0.39	0.71	16.4	2.67	.564	.41	.04
PRC 14-P-2-1/4	55-265	14.55	.213	.251	403	324	292	0.98	2.11	11.8	7.05	.542	.29	.02
PRC 16-P-3-1/4	85-300	21.97	.242	.297	632	576	564	1.77	5.70	9.50	9.69	.516	.25	.02
PRC 20-P-3-1/4	60-260	22.93	.214	.283	642	600	554	1.79	5.94	8.43	10.4	.508	.25	

Table 3-1 (continued)

	v_1 (m/s)	v_2 (m/s)	v_3 (m/s)	v_4 (m/s)	v_5 (m/s)	v_6 (m/s)	v_7 (m/s)	Δp_1 (N/m^2)	Δp_2 (N/m^2)	Δp_3 (N/m^2)	Δp_4 (N/m^2)	Δp_5 (N/m^2)	Δp_6 (N/m^2)
$W_o = 0.79$m ($A_o\sqrt{H_o} = 1.96$m$^{5/2}$)													
PRC 0-W-1-1	1.95	0.595	0.064	-.241	-.170	-.380	-.329	3.46	3.14	2.19	-0.649	-0.075	--
PRC 3-W-1-1	1.80	0.744	0.0035	-.205	-.150	-.342	-.301	4.81	2.78	2.00	-0.049	-0.082	-0.477
PRC 5-W-2-1	2.46	1.30	.0115	-.400	-.428	-.525	-.561	7.03	5.43	3.45	-0.461	-0.225	-0.513
PRC 2-W-3-1	3.36	2.40	-.156	-.133	-.504	-.377	-.642	7.00	7.125	4.47	-0.811	-0.371	-0.141
PRC 7-W-4-1	3.68	2.58	.225	-.311	-.460	-.776	-.727	10.58	7.97	5.02	-0.704	-0.192	-0.062
PRC 1-P-1-1	2.29	1.75	.0567	-.356	-.477	-.724	-.658	6.22	5.22	3.67	-0.761	-0.224	-0.723
PRC 4-P-2-1	3.34	2.52	.0996	-.623	-.732	-.278	-.176	9.64	7.64	4.92	-0.079	--	--
PRC 6-P-3-1	4.65	2.92	.510	-.373	-.502	-.829	-.878	10.78	9.71	6.20	-0.214	-0.320	-1.474
PRC 8-P-4-1	4.93	2.98	.593	-.166	-.747	-.617	-.969	11.67	9.34	5.73	-0.172	-0.791	-0.722
$W_o = 0.39$m ($A_o\sqrt{H_o} = 0.98$)								$H = 2.28$m	1.81	1.35	0.89	0.49	0.04
PRC 9-W-2-1/2	3.21	2.46	.529	-.487	-.586	-.707	-.685	7.86	4.68	2.42	-0.455	-1.13	-0.198
PRC 11-W-3-1/2	3.81	2.94	.522	-.702	-.779	-.864	-.871	10.69	6.15	1.41	0.655	-1.25	-0.322
PRC 15-W-4-1/2	4.31	3.38	1.15	-.748	-8.75	-1.09	-.969	11.37	6.81	2.72	0.471	-1.68	-0.66
PRC 10-P-2-1/2	3.82	3.07	1.073	-.623	-.816	-.926	-.929	10.06	5.20	3.40	-0.511	-0.917	-0.364
PRC 18-P-3-1/2	5.42	4.17	2.23	-.643	-.971	-1.13	-1.13	11.89	8.13	3.31	-0.039	-1.20	-1.98
$W_o = 0.19$m ($A_o\sqrt{H_o} = 0.49$)													
PRC 13-W-2-1/4	3.82	3.02	1.12	-.638	-.863	-.835	-.992	9.26	5.68	2.04	0.446	-1.305	-1.197
PRC 17-W-4-1/4	5.05	4.12	2.86	-.695	-1.06	-1.24	-1.24	12.33	8.10	3.36	0.331	-1.458	-2.48
PRC 19-W-4-1/4	5.10	4.26	2.86	-.672	-.925	-1.11	-1.10	12.01	9.25	4.00	0.194	-1.03	-1.68
PRC 12-P-1-1/4	2.97	2.55	1.09	-.753	-.986	-1.06	-1.04	7.063	5.13	2.18	-0.306	-1.25	-1.34
PRC 14-P-2-1/4	4.09	3.46	1.90	-.694	-1.05	-1.19	-1.19	10.13	6.91	3.58	0.148	-1.447	-2.26
PRC 16-P-3-1/4	5.17	4.46	2.98	-.340	-1.22	-1.55	-1.37	--	9.35	4.32	-0.94	-0.486	--
PRC 20-P-3-1/4	5.07	4.24	2.90	-1.63	-1.10	-1.34	-1.33	11.57	9.38	3.60	-0.02	-1.63	-2.45

In addition to these experiments a single wood crib and a single plastic crib were burned in the open in order to determine the effective heat of combustion for each crib. This was done by measuring the rate of oxygen consumption in the captured plume from the crib fire.

4.1   Instrumentation

The instrumentation for the set of eight experiments was more elaborate and will be discussed first. Then the oxygen consumption experiments will be described.

4.1.1   Free Burn Basis

The velocity and temperature fields were measured within, around, and above the cribs. Thirteen bidirectional velocity probes and bare chromel-alumel thermocouples were used. Seven of the bidirectional signals were processed through a single electronic manometer with each probe read every 35 seconds. Two radiometers (with IRTRAN 2 windows) and two total heat flux sensors were used to measure the radiation field. The same load platform as used in the room fire experiment monitored the crib weight. Also O_2 and CO_2 concentrations were measured at the top of one of the crib channels. A list of the instruments and their identification is shown in table 4-1.

Figure 4-1 shows the distribution of the probes for the first experiment with one wood crib (designated as PRC 21-W-1). This instrumentation arrangement was basically used for each subsequent experiment, except for the changes in probe positions as given in table 4-2. The crib configuration for each burn is shown in figure 4-2 relative to sensor H1.

Table 4-1. Identification code for free burn instrumentation

Channel Number	Symbol	Sensor Function
0	T1	Temperature at bidirectional probe P6-V
1	T2	Temperature at bidirectional probe P5-V
2	T3	Temperature at bidirectional probe P6-D
3	T4	Temperature at bidirectional probe P2-V
4	T5	Temperature at bidirectional probe P4-V
5	T6	Temperature at bidirectional probe P3-V
6	T7	Temperature at bidirectional probe P7-D
7	T8	Temperature at bidirectional probe P1-V
8	T9	Temperature at bidirectional probe P5-D
9	T10	Temperature at bidirectional probe P4-D
10	T11	Temperature at bidirectional probe P3-D
11	T12	Temperature at bidirectional probe P2-D
12	T13	Temperature at bidirectional probe P1-D
13	G1	Oxygen concentration (dry basis)
14	L1	Mass
15	H1	Floor heat flux, horizontal element
16	H2	Flame plume heat flux, horizontal element
17	R1	Heat flux, vertical element
18	ID	Sensor identification x 10 ± 0.5
19	P1-D to P7-D	Bidirection probe velocity pressure
20	P1-V	Bidirection probe velocity pressure
21	P2-V	Bidirection probe velocity pressure
22	P3-V	Bidirection probe velocity pressure
23	P4-V	Bidirection probe velocity pressure
24	P5-V	Bidirection probe velocity pressure
25	P6-V	Bidirection probe velocity pressure
26	R2	Heat flux, vertical element
27	G2	CO_2 concentration (dry basis)

31

Table 4-2. Change in probe positions for free burns
with respect to locations shown in figure 4-1

Exp.	Distance from vertical centerline of load platform	Distance from edge of crib	Distance from edge of load platform
PRC 21-W-1	–	–	–
PRC 22-W-2	P6-D to 31 cm P7-D to 32 cm	P4-D to 1 cm	–
PRC 23-W-3	"	"	–
PRC 24-W-4	"	"	R2 to 57.5 cm
PRC 25-P-4	"	"	R2 to 62 cm
PRC 26-P-3	"	"	R2 to 60 cm
PRC 27-P-2	P6-D to 21.5 cm P2-V to 9 cm P7-D to 24.5 cm	" P3-D to 3 cm	R2 to 59.5 cm H1 to 54.5 cm
PRC 28-P-1	"	P3-D to 5 cm	R2 to 50 cm

Note: For PRC 22 through PRC 26 P3-D/T11 was placed at the top of a vertical
internal crib channel, and P1-V/T28 was centered in the gap between two
adjacent cribs.
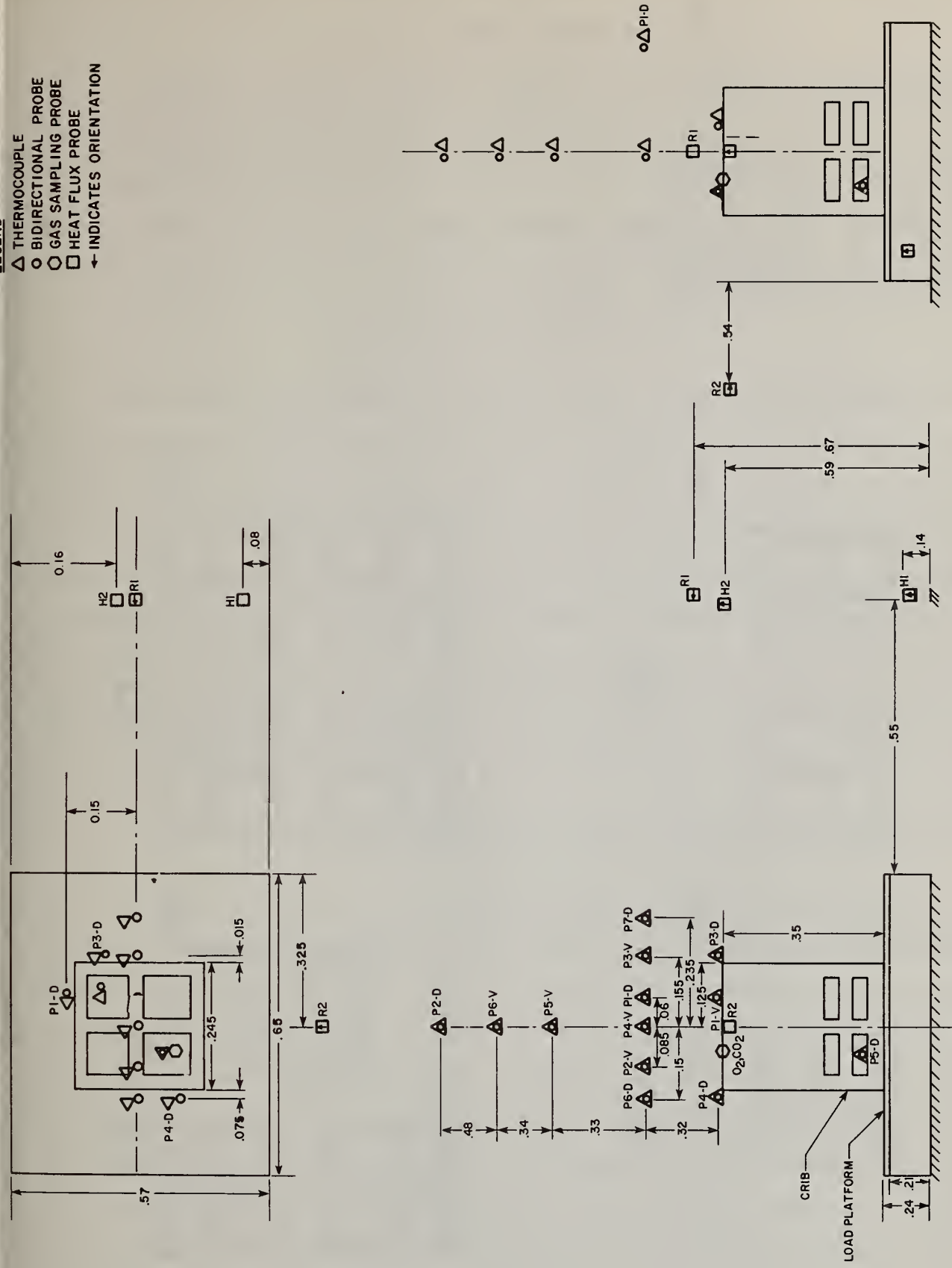
Figure 4-1. Basic layout of free burn instrumentation (dimensions in m)

33

CRIB ARRANGEMENT

P-2

W-2

W-4, P-4

W1, PI

W-3, P-3
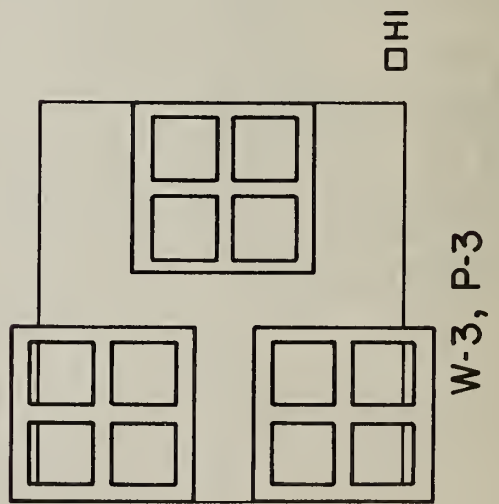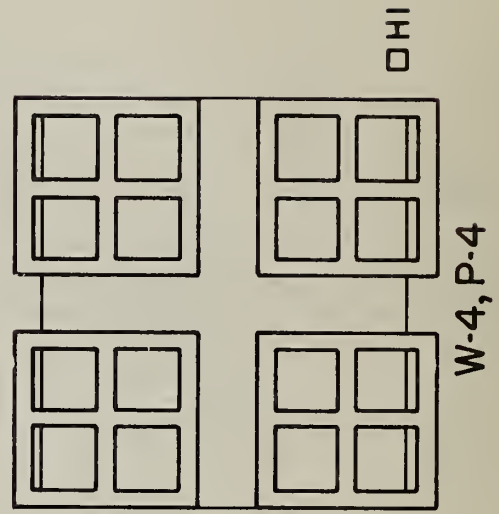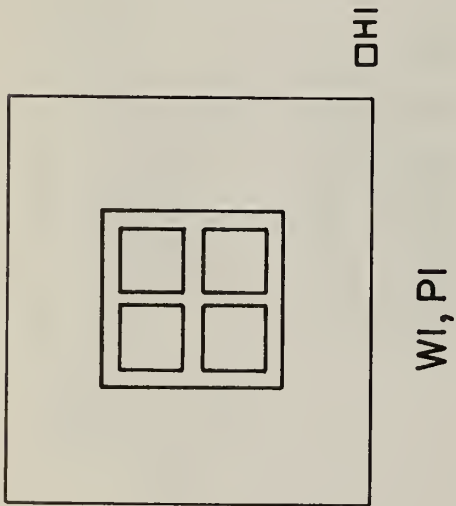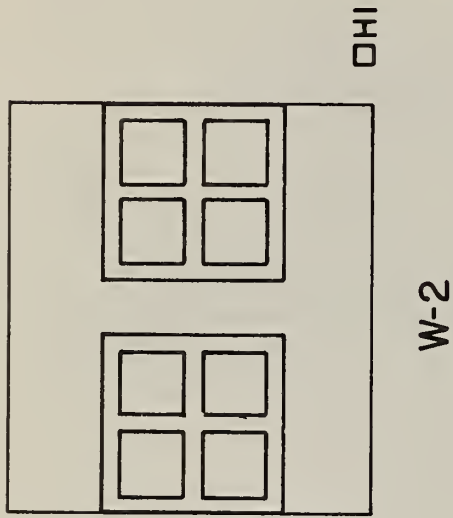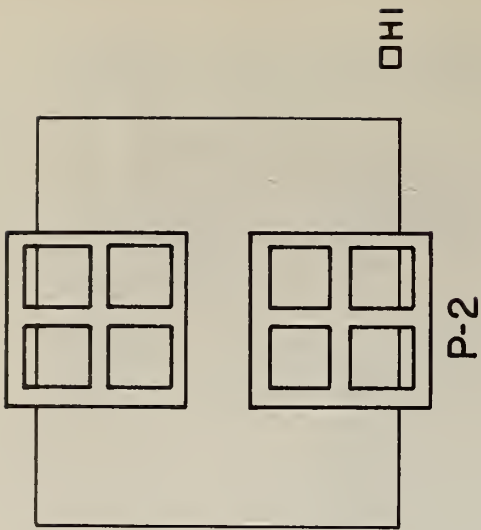
Figure 4-2. Configuration of cribs for free burn experiments

4.1.2 Oxygen Consumption

A schematic of the oxygen consumption experiments is shown in figure 4-3. It utilized the apparatus and procedure developed by Sensenig [9] for estimating the energy release rate of burning items comparable in size to our cribs. A single wood and plastic crib were studied. The significant results are the rate of mass loss and the rate of oxygen mass flow in the exhaust gases.

4.2 Results of Free Burns

The results from these two sets of experiments will be summarized here. The procedures for processing the data are similar to the room fire data analysis, and only the average peak results will be presented and utilized in this work. Table 4-3 gives the significant average peak values for the set of eight free burn experiments. Also listed here are the average peak flame heights based on observation of the video recordings of the experiments.

The oxygen consumption experimental results are summarized in table 4-4. The single crib mass loss rates differ in tables 4-3 and 4-4, and this indicates the degree of reproducibility as further discussed in appendix A.

5. ANALYSIS OF RESULTS

In this section the experimental average peak values will be analyzed in order to evaluate experimental consistency, general trends and mathematical correlations for these data, and to gain further phenomenological understanding of fire phenomena. Separate sections will include the following topics: mass rate, airflow rate, pressure, temperature, heat transfer, and finally, a section on chemistry. In the following figures open symbols will signify - a wood burn; filled symbols - a plastic burn; squares - 1 crib; triangles - 2 cribs; hexagons - 3 cribs; circles - 4 cribs; large symbols - widest door; intermediate size symbols - intermediate size door; small symbols - smallest door (see figure 5-1).
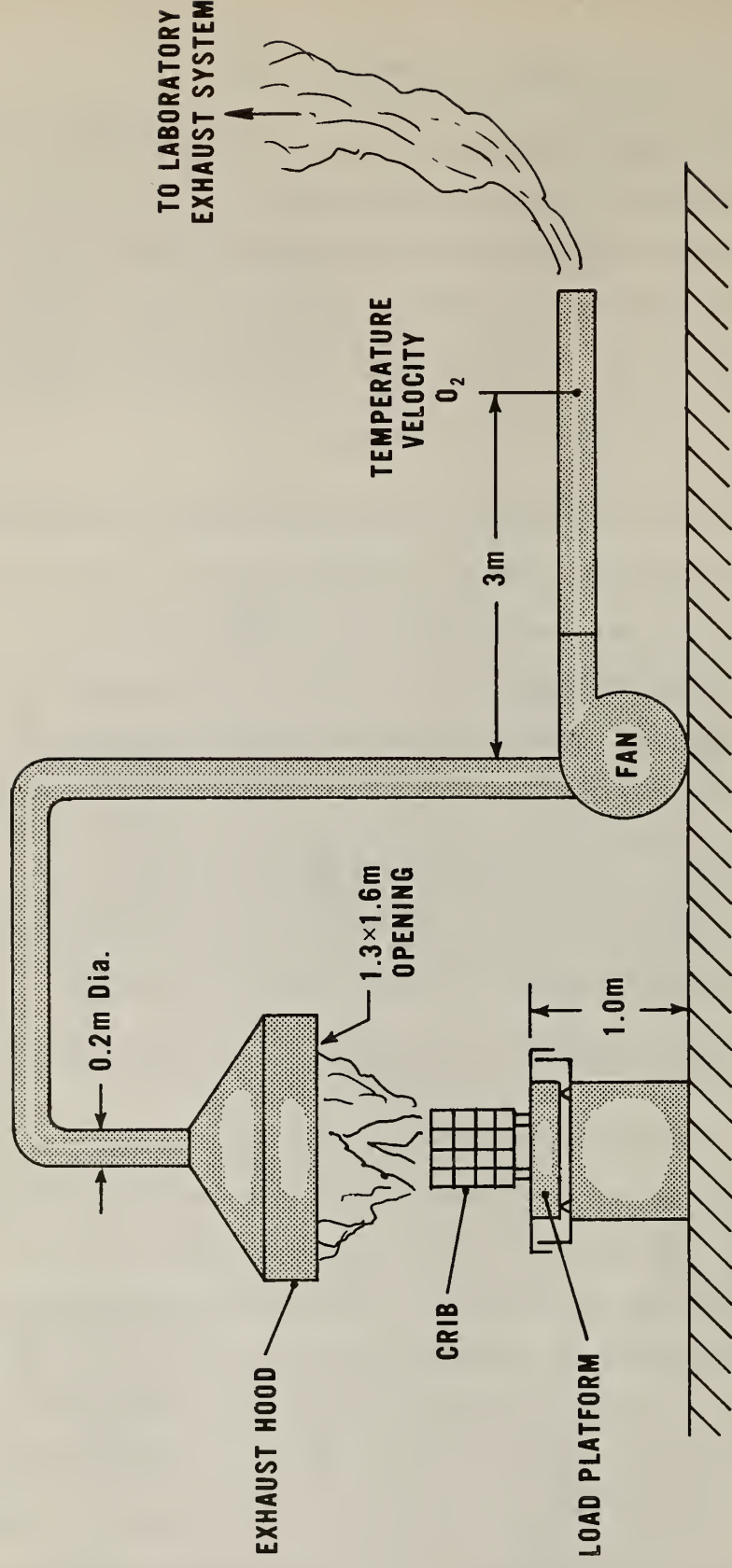
Figure 4-3. O_2 consumption apparatus (by Sensenig [9])

Table 4-3. Average peak values - free burn experiments

| Exp. | Mass Loss Rate $\dot{m}_v$ (g/s) | Flame Height above Crib H_f m | Incident Radiant Heat Flux | | | | Volume Concentration (dry) | | Corresponding Velocity and Temperature | | | | | | | |
| | | | H1 (W/cm²) | H2 (W/cm²) | R1 (W/cm²) | R2 (W/cm²) | O_2 (%) | CO_2 (%) | Crib Channel Bottom | | Crib Channel Top | | Crib Edge | | | |
									V9 (P5-D) (m/s)	T9 (°C)	V8 (P1-V) (m/s)	T8 (°C)	V10 (P4-D) (m/s)	T10 (°C)	V11 (P3-D) (m/s)	T11 (°C)
PRC 21-W-1	4.40	0.51	0.077	0.029	0.258	--	8.28	12.6	1.33	521	2.12	849	1.49	250	1.69	261
PRC 22-W-2	9.20	0.53	0.131	0.070	0.379	0.645	3.42	15.9	-5.3	553	0.670	400	1.11	127	3.59	746
PRC 23-W-3	17.6	0.60	0.209	0.114	0.652	1.03	4.29	14.7	-4.5	533	1.16	695	1.22	122	3.25	965
PRC 24-W-4	25.6	0.74	0.414	0.261	1.29	1.52	0.685	16.7	-6.4	856	1.60	777	1.01	96.7	3.64	936
PRC 25-P-4	36.4	1.0	0.826	0.715	2.32	2.75	6.49	12.1	1.33	786	-37.1	943	1.89	514	2.54	737
PRC 26-P-3 (1)	26.1	0.96	0.667	0.502	1.68	2.26	8.49	12.3	--	836	2.80	930	--	380	--	739
PRC 27-P-2	15.6	0.82	0.606	0.447	1.58	1.37	5.75	13.5	1.24	686	2.83	745	2.09	464	2.22	548
PRC 28-P-1	6.05	0.72	0.233	0.155	0.652	0.746	13,0	7.73	1.76	713	0.89	743	1.57	524	1.90	470

NOTE: 1. Signal processor inadvertently turned off for P1-D through P7-D

Table 4-3 (continued)

Corresponding Velocity and Temperature

	Plume Centerline												Plume off-center					
Exp.	V5 (P4-V) (m/s)	T5 (°C)	V2 (P5-V) (m/s)	T2 (°C)	V1 (P6-V) (m/s)	T1 (°C)	V12 (P2-D) (m/s)	T12 (°C)	V3 (P6-D) (m/s)	T3 (°C)	V4 (P2-V) (m/s)	T4 (°C)	V13 (P1-D) (m/s)	T13 (°C)	V6 (P3-V) (m/s)	T6 (°C)	V7 (P7-D) (m/s)	T7 (°C)
PRC 21-W-1	4.42	1009	5.59	527	5.32	251	3.15	167	1.62	303	4.63	582	0.497	87.4	1.30	200	0.871	76.0
PRC 22-W-2	2.62	427	3.88	328	4.64	214	3.30	164	0.734	195	4.19	755	0.647	100	3.18	891	1.91	315
PRC 23-W-3	2.81	644	4.67	420	5.59	281	3.73	215	0.969	271	4.34	782	0.935	156	2.81	796	1.67	251
PRC 24-W-4	3.51	771	5.81	679	7.45	492	5.56	381	1.43	237	3.97	1050	2.28	529	3.06	847	2.14	345
PRC 25-P-4	4.08	966	6.07	911	8.82	793	6.22	640	2.18	445	4.75	894	2.99	780	2.40	899	2.24	481
PRC 26-P-3 (1)	2.77	915	4.26	888	6.56	557	--	493	--	563	4.21	973	--	747	2.34	786	--	424
PRC 27-P-2	2.73	825	5.03	806	6.87	597	4.94	372	1.46	444	5.02	497	3.69	799	2.44	594	1.94	335
PRC 28-P-1	1.58	613	1.87	408	2.04	165	1.82	109	1.03	305	1.89	515	3.02	524	1.56	392	0.95	214

NOTE: 1. Signal processor inadvertently turned off for P1-D through P7-D

Table 4-4. Average peak values - O_2 consumption

Crib Material	Peak Times Δt (s)	Rate of Mass Loss $\dot{m}_v$ (g/s)	Rate of O_2 Consumption $\dot{m}_{O_2}$ (g/s)
WOOD (Sugar Pine)	65-390	5.3	4.9
PLASTIC (Polyurethane)	60-255	7.0	10.3

LEGEND

$$A_0\sqrt{H_0}\ (m^{5/2})$$

NO. OF CRIBS	1.96	0.98	0.49
1	□	◻	◽
2	△	△	△
3	⬡	⬡	⬡
4	◯	◯	○

OPEN SYMBOLS - WOOD
FILLED SYMBOLS - POLYURETHANE

Figure 5-1.   Symbol legend for figures in sections 5 and 6

5.1   Rate of Mass Loss ($\dot{m}_V$)

The mass loss rates plotted against ventilation factor, $A_o\sqrt{H_o}$ (A_o, area of opening; H_o, height of doorway) is shown in figure 5-2. Besides the data for the three door widths the open or free burn values are also plotted on the right-hand side and designated as $A_o\sqrt{H_o} = \infty$. The mass loss rates for the wood in the open configuration range from 4.4 g/s for one crib to 25.6 g/s for four cribs; and for the plastic cribs, the range is 6.05 g/s to 36.4 g/s. In general the burning rate of plastic cribs is one and a half times that of wood. This order of increase is preserved in the enclosure until the effects of the enclosure (radiation feedback and insufficient airflow) begin to dominate.

The first effect of the enclosure can be seen in figure 5-2 by observing the increase in mass loss rate as one moves from the open configuration, $A_o\sqrt{H_o} = \infty$ to $A_o\sqrt{H_o} = 1.96$, the largest door or the least ventilation constraining of the enclosure runs. Except for one case, the mass loss rates increase over that of the free burn cases. For one crib the increase is about 15% and for two cribs the increase is about 30% for both wood and plastic. Increasing the fuel load further to three and four cribs causes a net decrease in the enhancement which is gradual for the wood and quite dramatic for the plastic which at four cribs exhibits a negative enhancement, i.e., the burning rate for four plastic cribs in the enclosure is actually less than that of the free burn.

Radiation from the hot upper gas layer trapped in the enclosure and from the ceiling and walls, absent in the free burns, is thought to be responsible for the increased $\dot{m}_V$ seen in the enclosure. However, since the effect is non-monotonic (enhancement decreasing after two cribs), and even disappears in the case of four plastic cribs, an additional mechanism appears to be operating. The rate of combustion or burning rate within an enclosure is limited by the airflow rate through the enclosure opening, and it is empirically known that the mass loss rate of wood cribs is limited by the airflow rate, i.e., a ventilation controlled fire. With the consideration that radiation feedback and limiting airflow are operating in opposition, the behavior of the remaining smaller door cases is readily explainable.

41
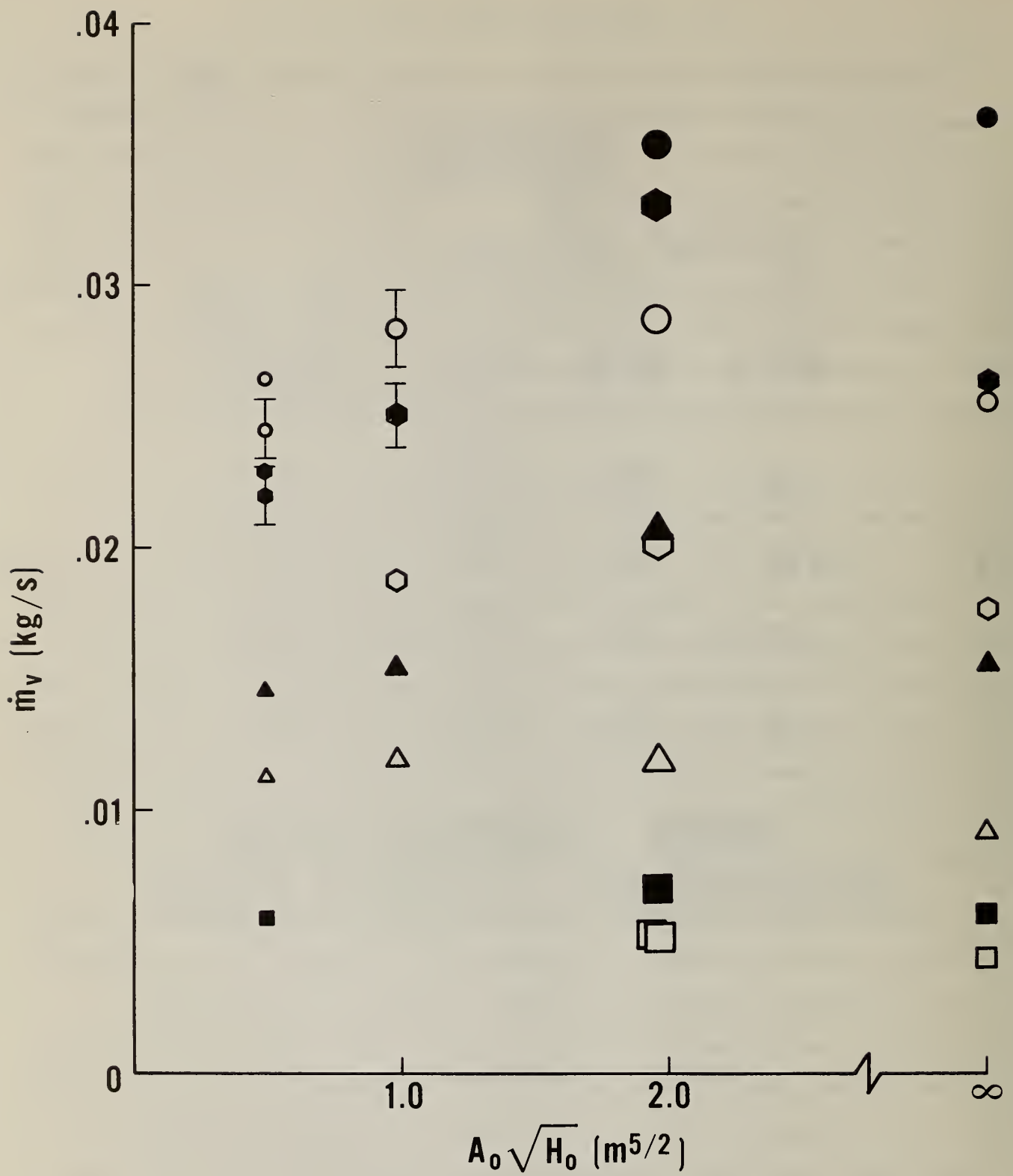
Figure 5-2. Mass loss rate versus ventilation factor

For the open crib burns there is a self-enhancement phenomena operating distinctly from the enclosure enhancement. That is, two cribs burn at a higher $\dot{m}_V$ than the value obtained by multiplying the single rate by two. Three and four cribs likewise follow this fuel loading dependence. A simple explanation involving radiation interaction between the cribs can be forwarded for this self-enhancement. For one crib burning, the sticks making up the four outer sides *see* relatively cool walls. When two cribs are assembled two of the eight outer sides now *see* each other. Those mutually adjacent sides are now going to burn more vigorously (like the internal sticks of a larger crib) than those sides not receiving the high radiative fluxes.

For all four cribs utilized in this work the self-enhancement increases with the number of cribs. The mass loss rate turns out to be a function of the number of cribs (n_c) to approximately the 5/4 power. Without self-enhancement $\dot{m}_V$ would be linear with the fuel loading (n_c). Since for all cribs the enhancement is increasing with the number of cribs , it would appear that inadequate airflow into the central regions of the large configurations is not a major factor in these open burns. Hence any problems with airflow for the enclosure burns are largely due to the enclosure restriction and are not due to the configuration itself (this may not be necessarily true for more than four cribs). Thus the burning appears to be in the fuel surface area controlled regime. Mass loss rate per unit "area" (or simply the number of cribs in this case) is shown in figure 5-3 plotted against ventilation factor. Here the self-enhancement correlation, the 5/4 power, is used for convenience in collapsing the data. The behavior of both the wood and plastic fires described previously is clearly differentiated in this plot. The behavior of the wood fires may be characterized by a single function of the ventilation. Place the cribs in a large-opening enclosure and $\dot{m}_V$ will increase, presumably due to radiation feedback. Start closing the door and nothing very much happens, a further increase in radiation being balanced by lower airflows. Close the door further and the restricted airflow will begin to dominate over radiation, thus lowering the burning rate again (concave downward).

43
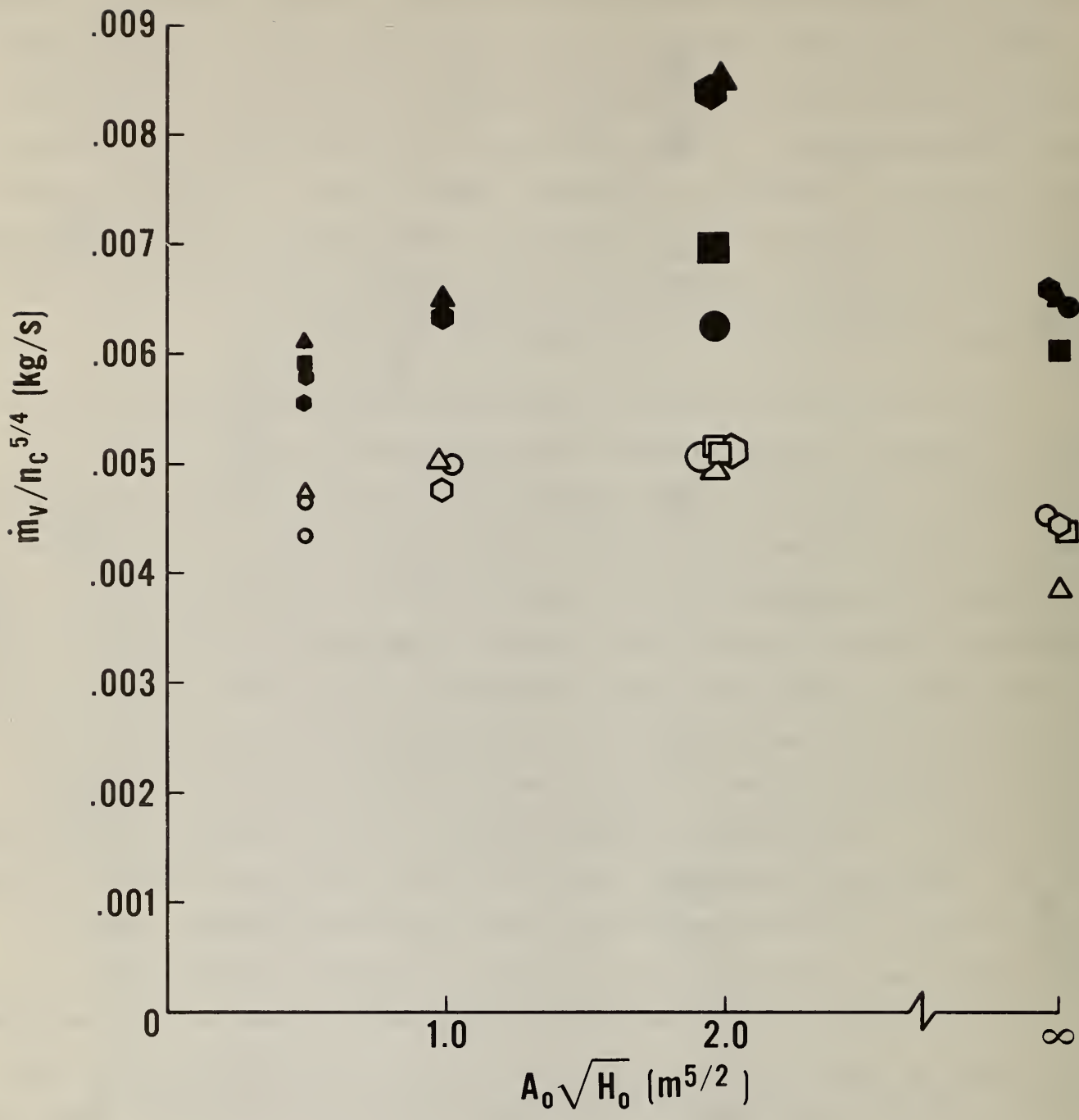
Figure 5-3. Normalized mass loss rate versus ventilation factor

44

The plastic follows this general behavior somewhat except that the $\dot{m}_v$ for smaller door openings is generally lower than that burn rate for large openings. However, the different behavior at $A_o\sqrt{H_o} = 1.96 \text{ m}^{5/2}$ is striking. An explanation of these differences as seen in figure 5-3 is not at all evident.

A further illustration of the complexity of enclosure effects on mass loss rate is shown in figure 5-4. There, the ratio of the enclosure to free burn mass loss rate is plotted against the incident heat flux to an element on the floor. This flux reflects the degree of radiant feedback to the cribs. A clear correlation in terms of heat flux and ventilation factor is not evident. But decreasing door width and increasing fuel load does appear to reduce the enhancement.

A maximum enhancement of 1.3 for the largest door opening is nearly identical with the results of Croce [10] for well ventilated $(A_o\sqrt{H_o}/\dot{m}_v > 40 - \text{m}^{5/2}$ -s/kg) wood crib fires in enclosures and for the same porosity value $(\frac{A_v}{A}s^{1/2}b^{1/2} = 0.8 \text{ mm})$ used in this study.

5.2 Doorway Flow

Figure 5-5 presents the mass balance - a comparison of the mass flow out, $\dot{m}_{out}$, with the sum, $\dot{m}_{in}$ plus the burning rate, $\dot{m}_v$ plus the burning rate, $\dot{m}_v$ ($\dot{m}_v$ accounts for up to 10 percent of the total for large fires in the smaller door cases). The doorway mass flow rates were determined by numerical integration of

$$\dot{m}_{in} = \rho_a T_a W_o \int_0^{N_v} (V/T)\, dz \tag{5-1a}$$

and

$$\dot{m}_{out} = \rho_a T_a W_o \int_{N_v}^{H_o} (V/T)\, dz \tag{5-1b}$$

where V and T are the velocity and temperature respectively, measured along the vertical centerline (z-coordinate) of the doorway. The vertical distances N_v and $H_o - N_v$ are the regions over which the flow is in and out of the room respectively. Implicit is the assumption of uniform velocity and temperature in the horizontal direction over width W_o. In general, as the door width decreases the velocity increases, (even though mass flow decreases) especially

45
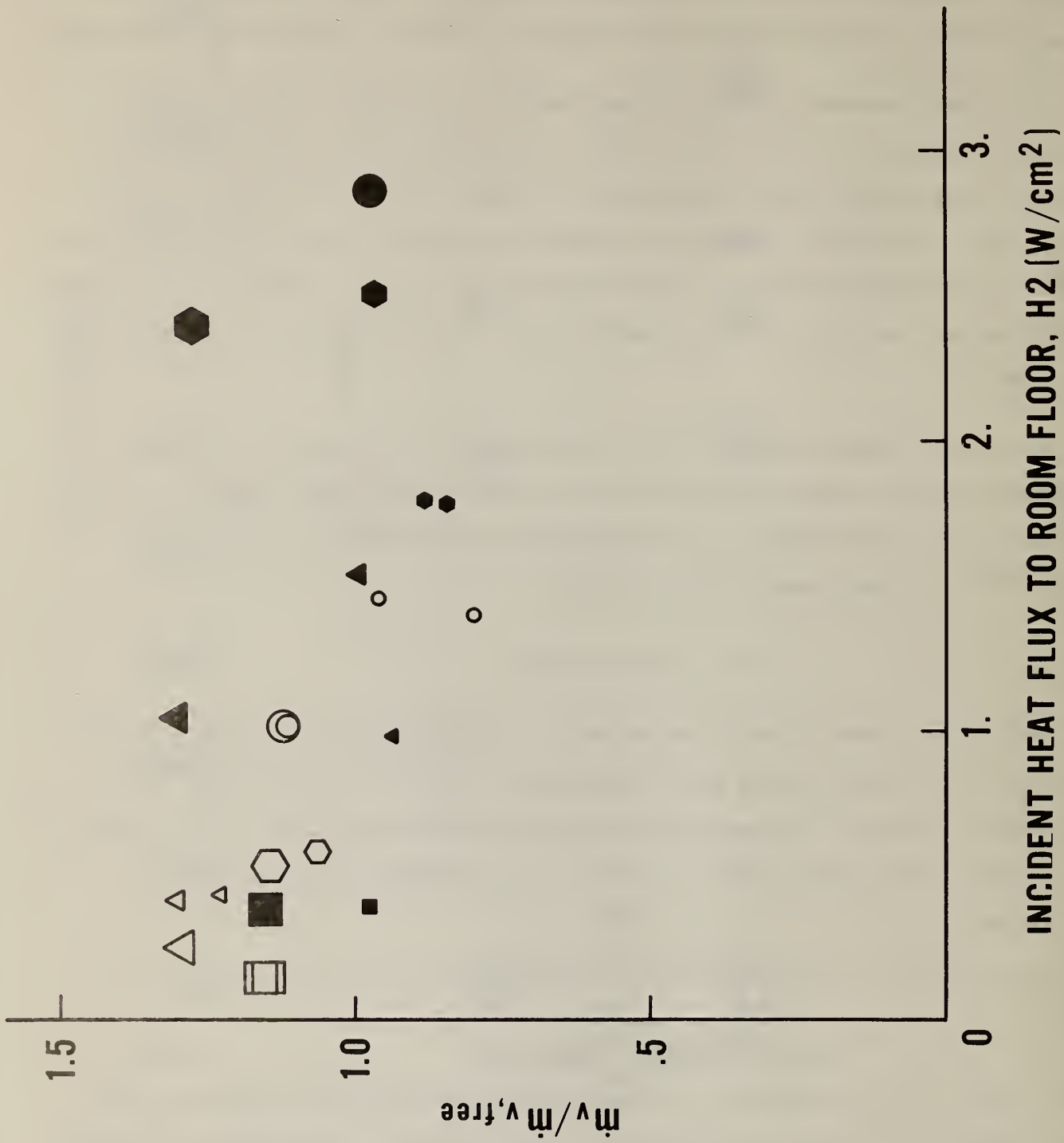
Figure 5-4. Room enhanced mass loss rate
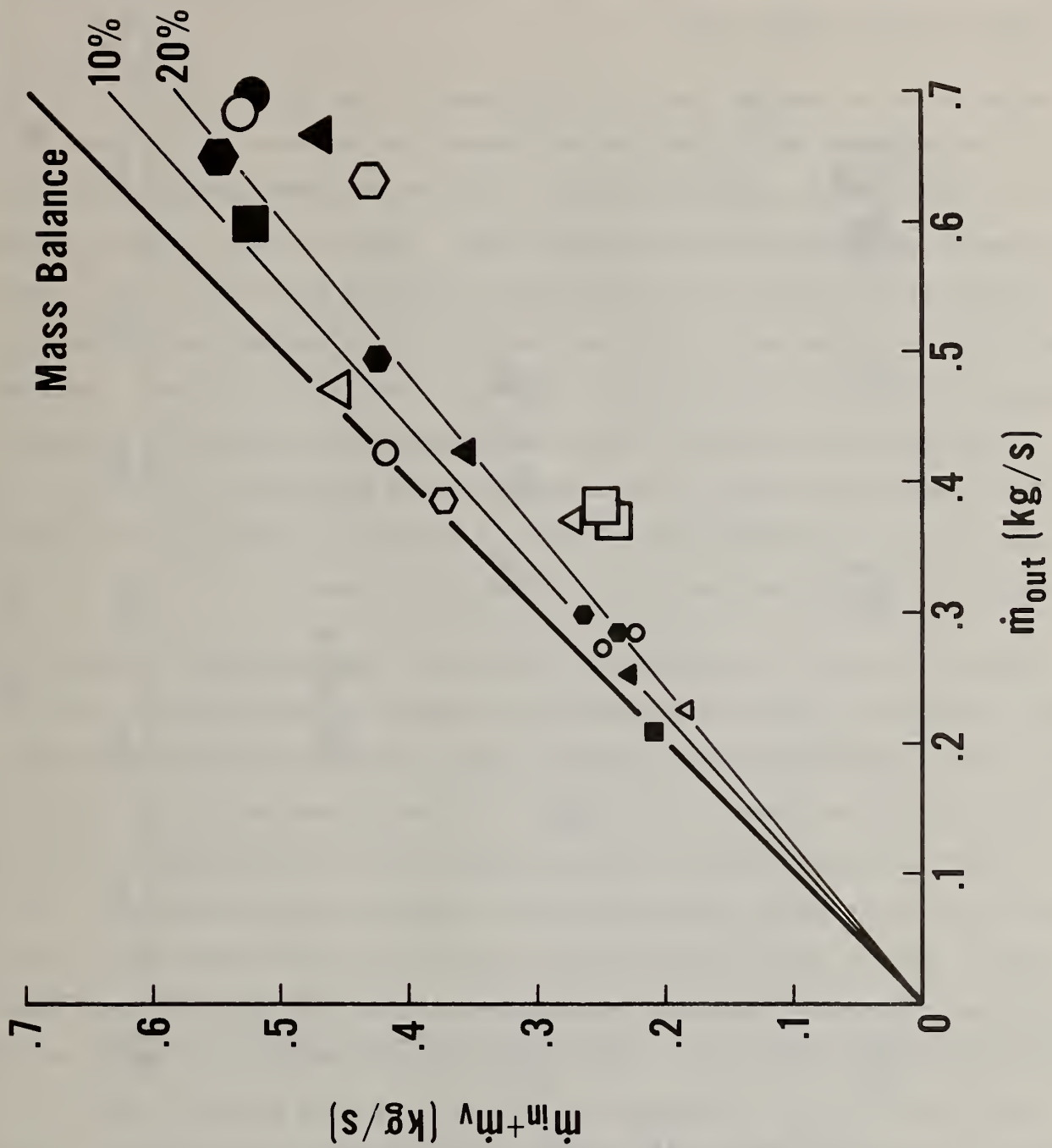
Figure 5-5. Mass balance assessment of doorway flow rates

47

the inflow; and hence, the capability of accurately measuring velocity improves. There is less scatter in the 1/2-door result than in the one-door result and less again in the 1/4-door runs.

Aside from the scatter there is a systematic bias in the results. About 10 to 15 percent more gas appears to be flowing out compared to the rate of air going in plus the fuel gasification rate. This measurement imbalance may be due to the use of centerline velocity values only. There is some evidence available which indicates that the outflow velocities, being on the order of five times target than the inflow velocities, may exhibit a more parabolically-shaped velocity profile across the door as compared to that of the inflow. Measurement of the centerline velocity then would overestimate the outflow relative to inflow. Until this point is resolved by future experiments, the best value for flow rate will be taken as the numerical average of the two quantities, $\dot{m}_{out}$ and $\dot{m}_{in} + \dot{m}_v$, defined here as $\dot{m}_a$, the airflow rate.

Figure 5-6 shows $\dot{m}_a$ plotted as a function of the ventilation factor. For a given loading, $\dot{m}_a$ varies with ventilation factor to approximately the 1/2 power. This compares with the classical result assumed for fully-developed fires that $\dot{m}_a$ varies linearly with $A_o \sqrt{H_o}$. In every case the plastic cribs have a higher airflow rate than the wood cribs, which is consistent with the higher $\dot{m}_v$ for the plastic cribs resulting in higher room temperatures. For the largest opening the $\dot{m}_a$ of all four plastic cribs are grouped more or less together and the proper sequence is preserved, i.e., the four crib case draws more air than three cribs, etc. They do not however exhibit the large variation with fuel size as do the wood cribs in the large opening probably because airflow is insensitive to average compartment temperature above 150°C. Taking advantage of the square root dependence of $\dot{m}_a$ on ventilation, figure 5-7 is drawn to illustrate the dependence of airflow on burning rate or fuel loading. A faired curve through the data yields approximately a 1/4-power dependence with the constant of proportionality being about 1.0 $(kg/s)^{3/4} m^{-5/4}$. That is,

$$\dot{m}_a = (\dot{m}_v)^{1/4} \ (A_o \sqrt{H_o})^{1/2} \text{ in kg/s} \qquad (5-2)$$

48
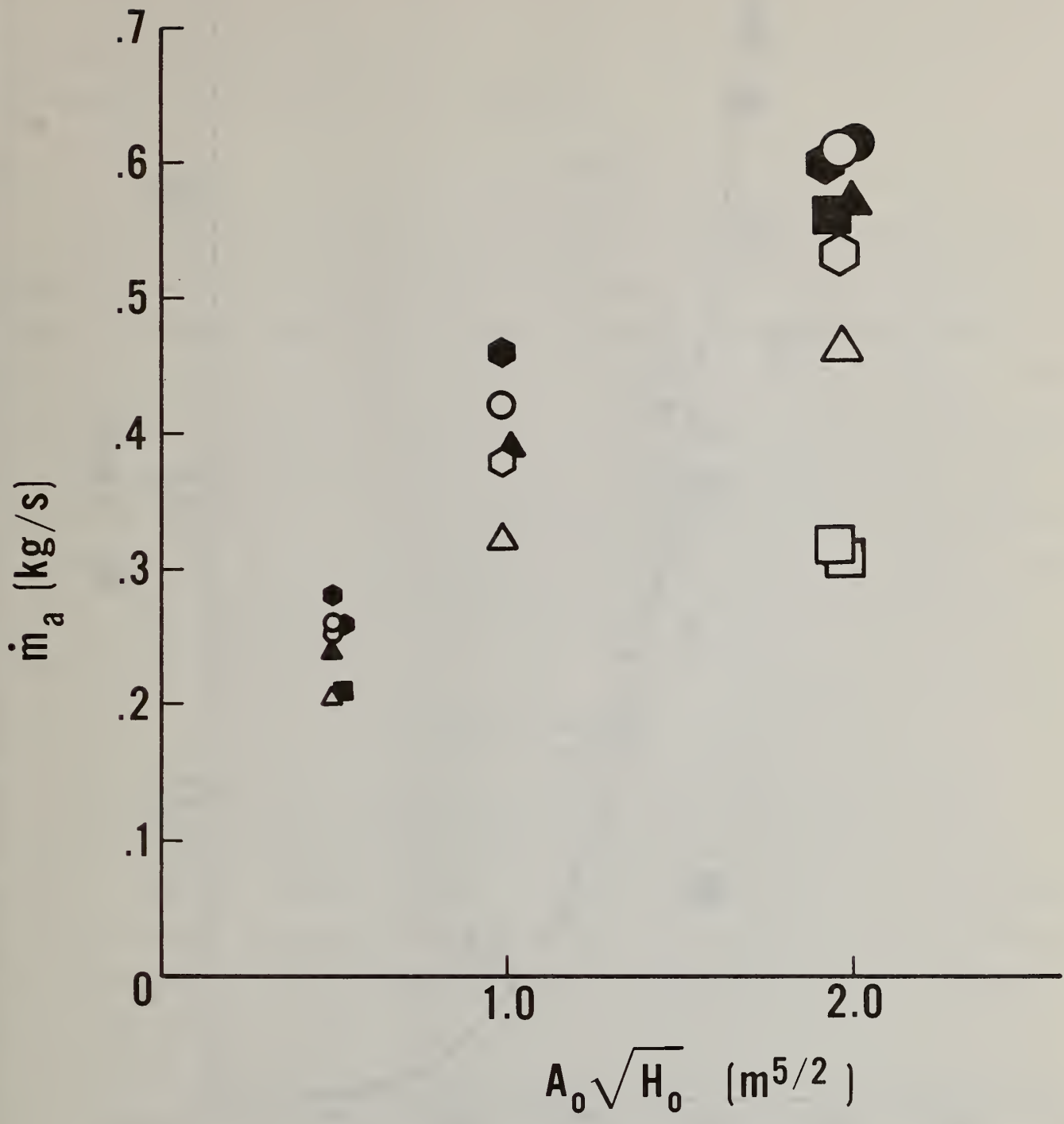
Figure 5-6. Airflow rate versus ventilation factor

49
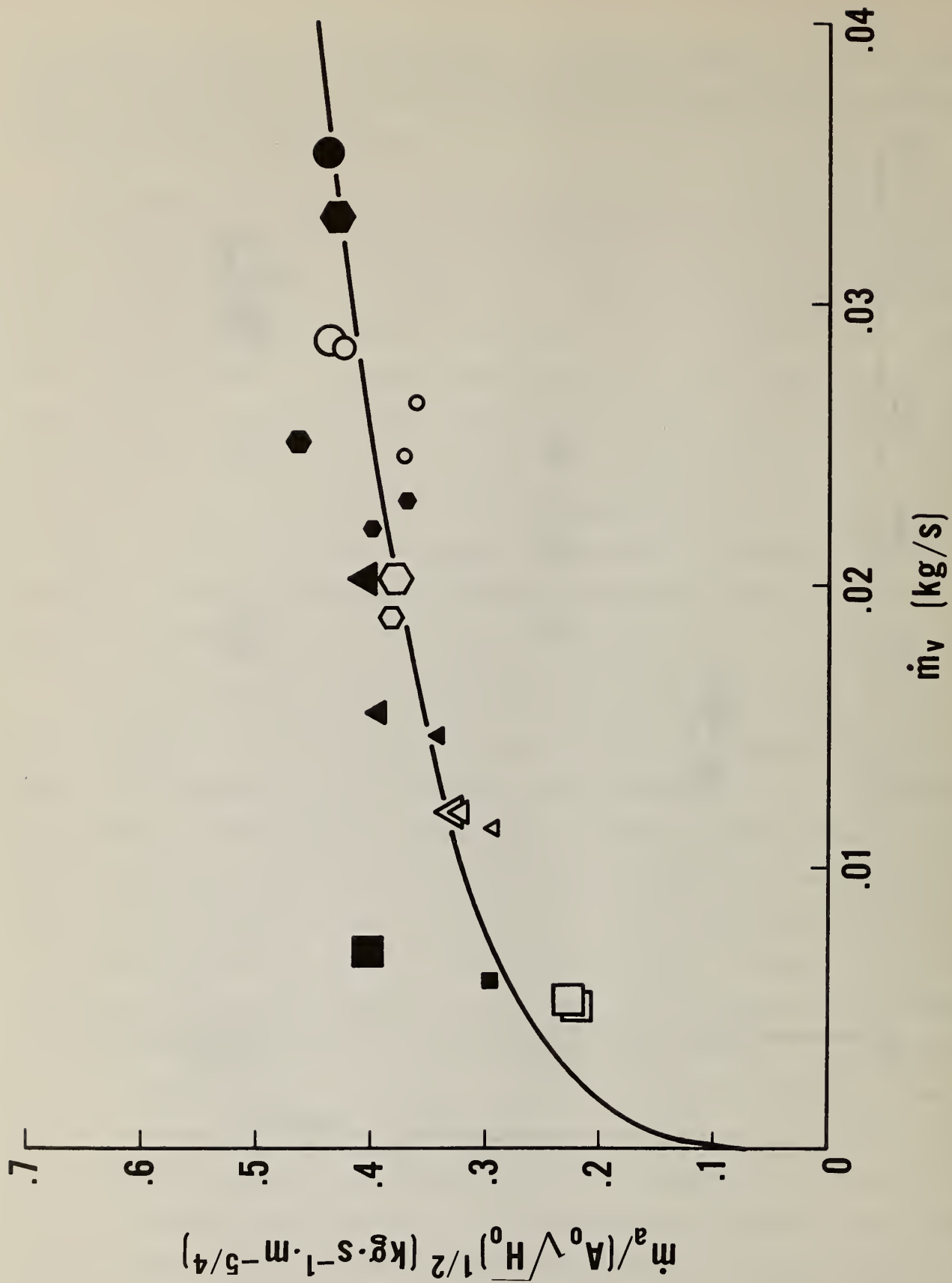
Figure 5-7. Correlation for airflow rate

50

Looking solely at the plastic fires with the largest opening, the small power dependence of $\dot{m}_a$ on $\dot{m}_v$ would sink further such that the flow would be independent of the burning rate. A complete correlation should probably include the effect of compartment gas temperature as well, and this correlation may not be generally applicable to other situations.

5.3 Two Layer Concept

Upon observation of compartment fires, a horizontal interfacial plane is usually discerned between the smoky upper layer and relatively clear lower layer. The smoke displays the primary flow pattern caused by the constraint of the enclosure and buoyancy. Also for a compartment with an open door, the flow enters and leaves as illustrated in our experiments. Hence, the concept of two layers has emerged in understanding and describing room fires. The layers are separated by a surface extending from the flow reversal position at the doorway into the room, separating the hot smoky region from the cool clear region. Some optional definitions will be necessary to discuss this layer height in our experiments.

5.3.1 Neutral Plane (N)

In the doorway the horizontal plane separating the hot outflowing combustion products from the cool incoming fresh air is called the neutral plane, a distance N above the floor. This is usually defined as the position of zero pressure drop across the doorway such that the flow reverses direction at that height. It can be identified as the position (N_v) of zero velocity interpolated from our data. Or it can be identified as the position (N_p) of zero pressure differential in the room. These experimentally derived heights are plotted for PRC 8 in figure 5-8. In all cases, the velocity neutral plane N_v was higher than the pressure neutral plane N_p. This may be a characteristic of our long doorway for in the present setup the door frame was uncommonly wide, i.e., in the order of 30 cm as opposed to a normal door frame of 10 cm. From visual observation the flow in appeared to fall as fluid moved from the front edge of the door frame towards the rear part of the frame and into the room.

51
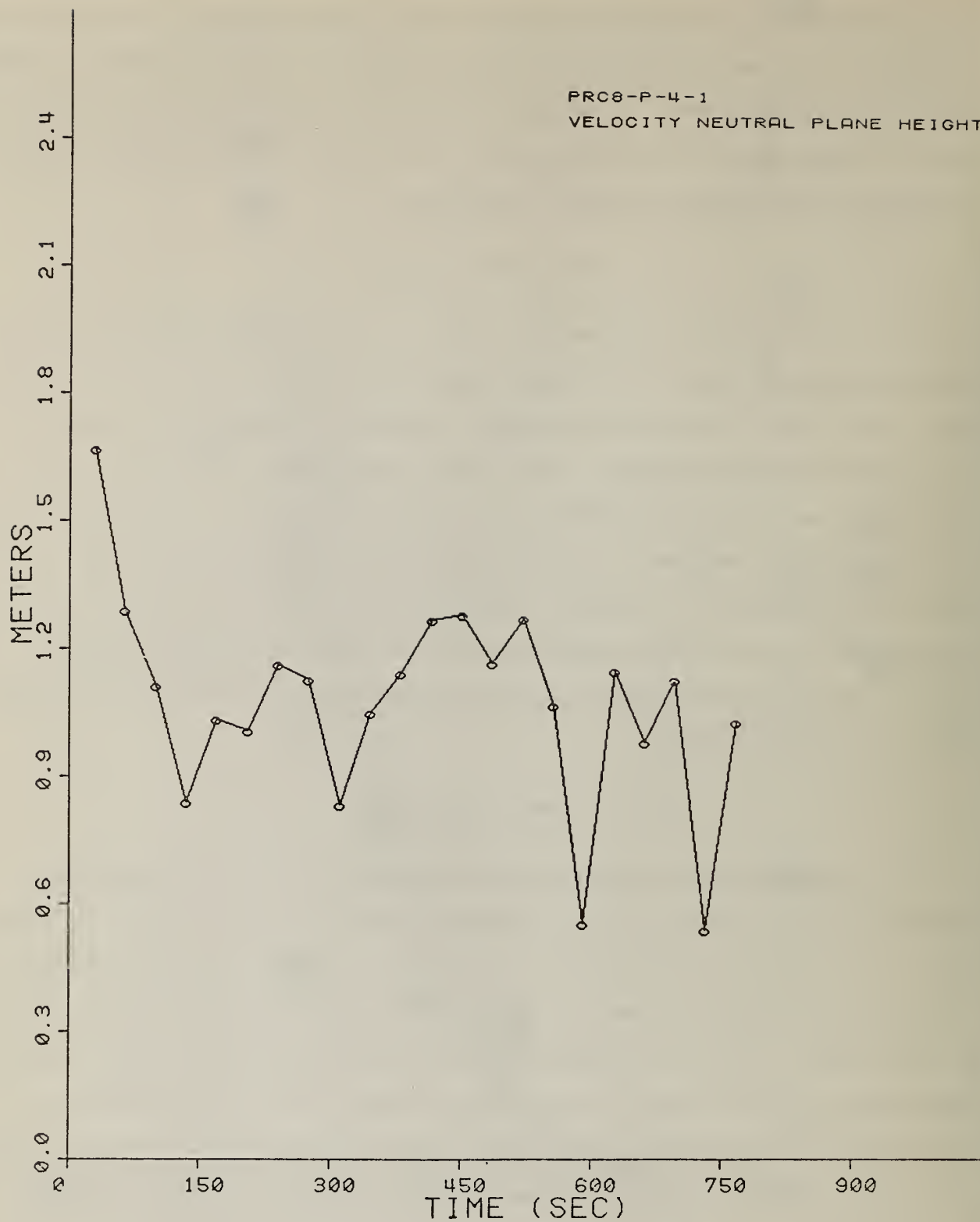
Figure 5-8a. Velocity neutral plane for PRC 8

52
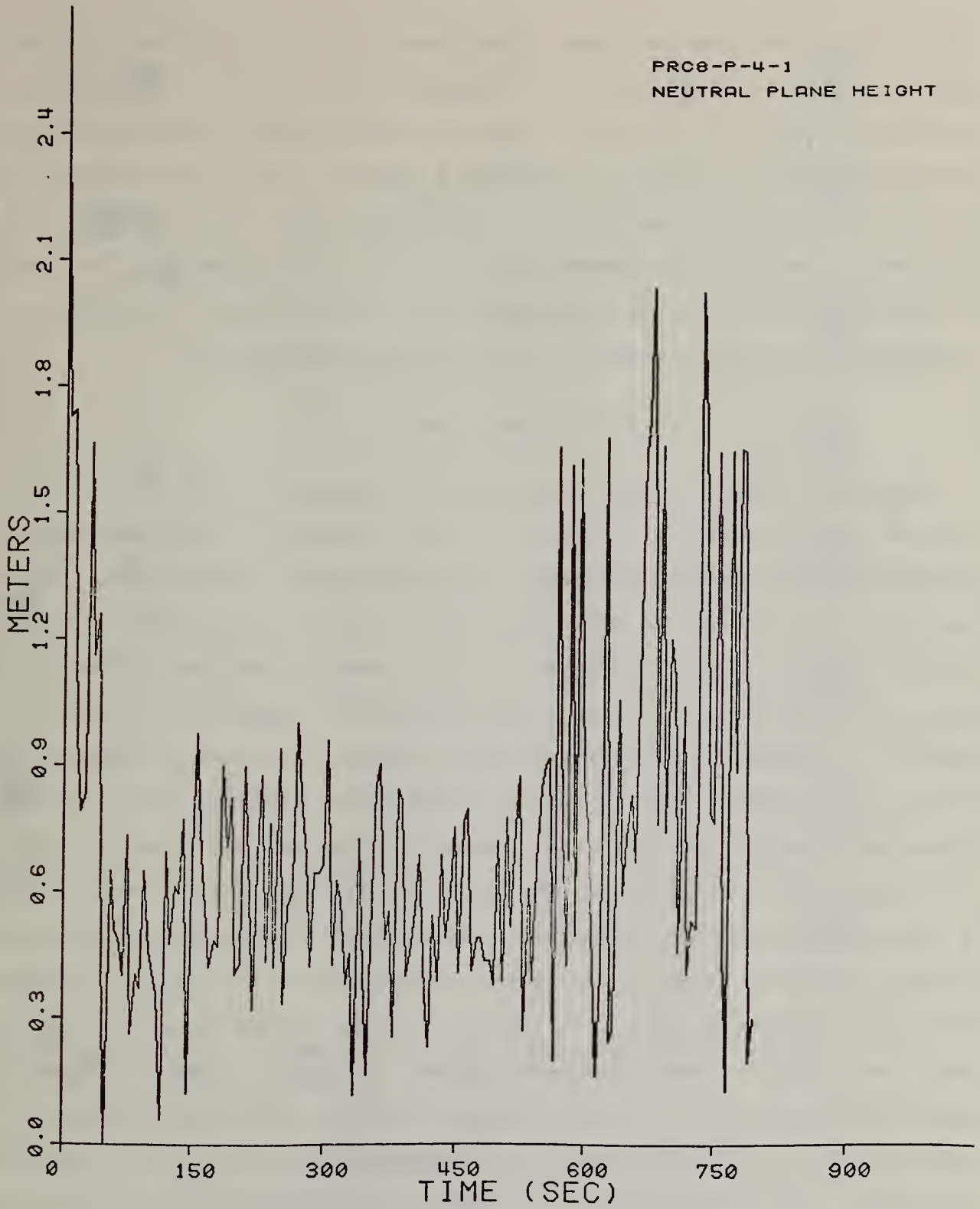
Figure 5-8b. Pressure neutral plane for PRC 8

53

This sinking phenomena has been noted previously but the effect is probably exaggerated by this particular door frame. The interface or 'stagnation' streamline along the distance of the door frame could be sketched from the two measurements, N_v and N_p. Figure 5-9 presents the velocity-defined neutral heights in the doorway normalized by the door height and plotted against the representative upper gas temperature, $\bar{T}$. This illustrates that the position of the neutral plane is fairly stable over a large range of compartment temperatures, dropping slightly with increasing temperature.

5.3.2 Room Layer Height (D)

Another parameter that is required for modeling is the height of the thermal discontinuity in the room, D. This concept of a distinct layer height comes from the idealized two-layer conceptual model of room fires. Unfortunately nature doesn't conform to this idealization and the thermal discontinuity instead of being sharp is rather a gradual, smoothly decreasing temperature function from the more or less uniform upper gas temperature down to a uniform ambient. Defining an effective thermal discontinuity then is somewhat arbitrary. The one chosen here based on the APV temperatures involved finding the height where the greatest change in the temperature gradient was occurring, i.e., $\Delta^2 T/\Delta z^2_{MAX}$. (By differencing, the position of $\left(\frac{\Delta T}{\Delta Z}\right)_{MAX}$ was not defined to within a thermocouple location, therefore a second derivative condition was applied in this region to uniquely locate the layer height). Figure 5-10 compares this definition denoted as D_T/H_o, to the visually determined smoke layer height in the room, D_s/H_o. The agreement in general appears to be good. The one and two wood crib cases in the largest enclosure deviate to the right because of the small amount of smoke generated from the small wood fires, i.e., one cannot see the smoke. The three plastic crib cases in the smallest door deviate to the left for the opposite reason - there is now too much smoke, it has diffused and mixed into the cold layer.

The thermal discontinuity D_T/H_o is shown in figure 5-11 plotted against upper gas temperature. Also shown by the lines are the approximate location

54
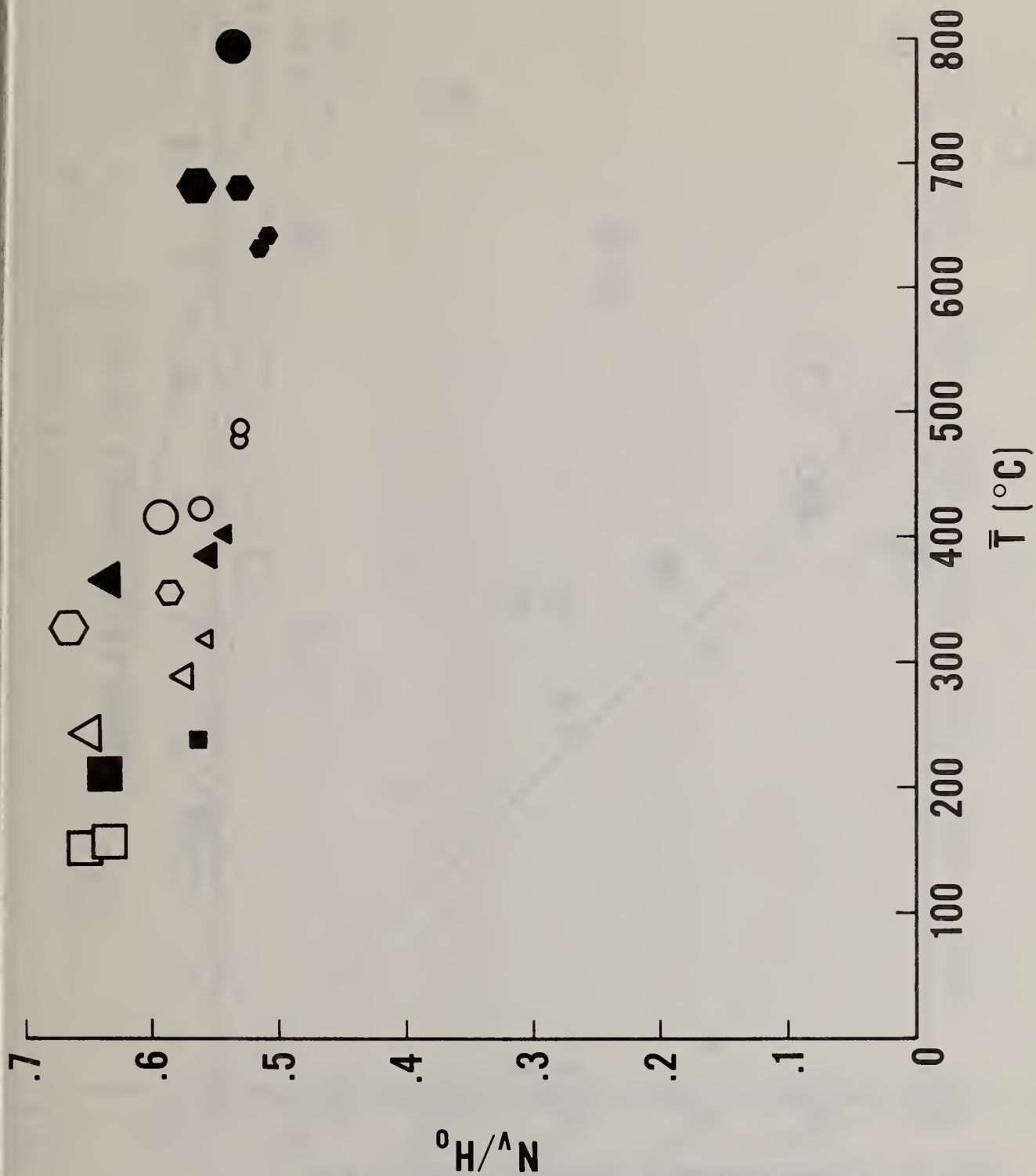
Figure 5-9. Doorway neutral plane versus upper layer temperature

The vertical axis is labeled N_v/H_0 with values .1, .2, .3, .4, .5, .6, .7. The horizontal axis is labeled $\overline{T}$ (°C) with values 0, 100, 200, 300, 400, 500, 600, 700, 800.
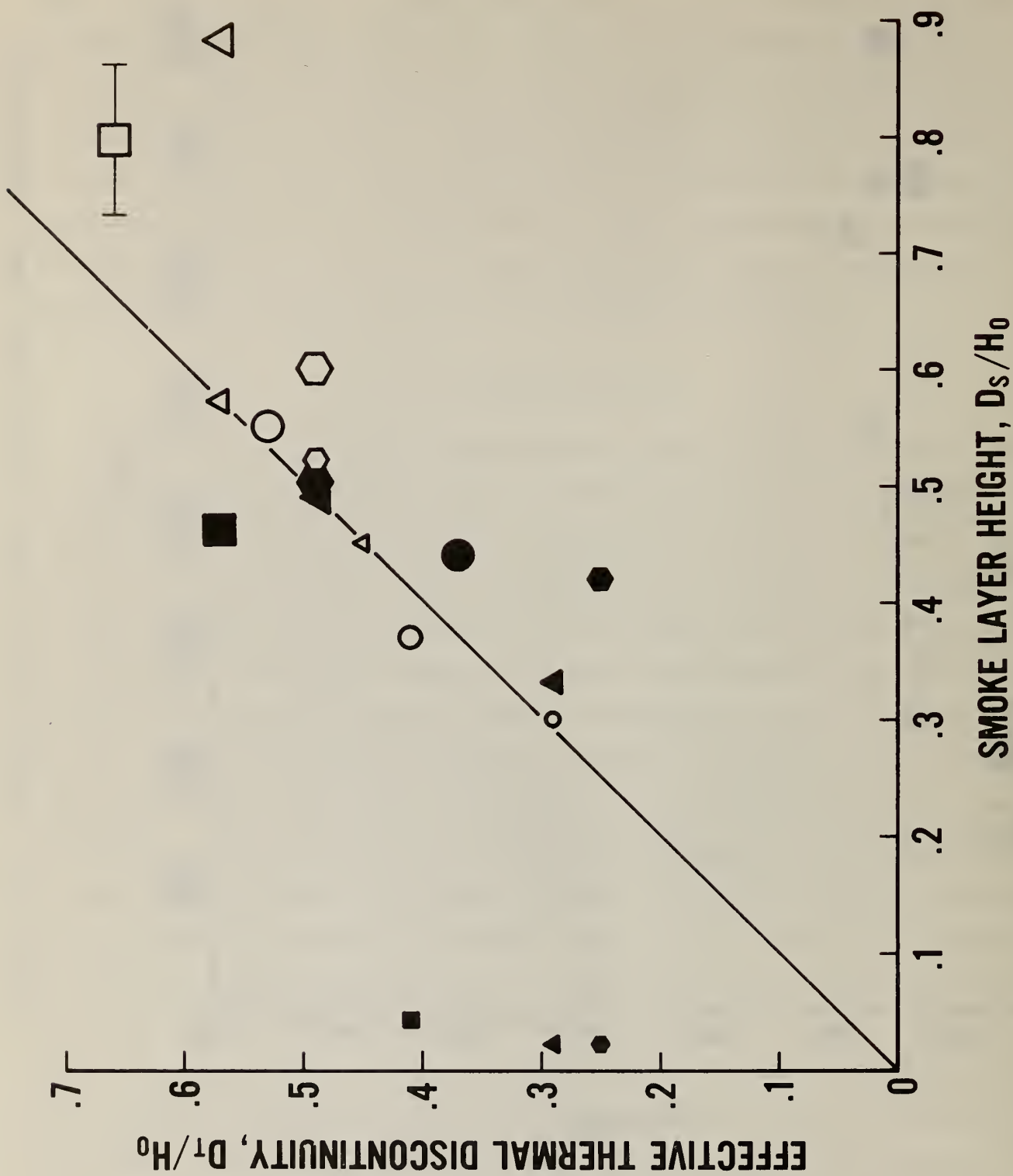
Figure 5-10. Thermal and smoke layer heights

Figure 5-11. Thermal discontinuity versus upper layer gas temperature

57

of the doorway neutral plane taken from figure 5-9, (N-D is an important parameter used in modeling door flow). D_T/H_o can be seen to be a strong function of temperature and also of door width. Theory indicates that the maximum flow is obtained when D_T approaches the floor; this would be a fully-involved compartment fire. The trends here for lower D_T with higher temperatures and smaller door width are consistent with the flow theory.

5.4 Room Static Pressure Differential (Δp)

The airflow rate through the compartment is not only important from the standpoint of limiting O_2 to a large fire but also it can be responsible for convecting away in the order of 50 percent of the total heat release of the fire. Present modeling techniques start with an assumed vertical temperature distribution in the room. This distribution both above and below an assumed neutral plane is integrated to yield the hydrostatic pressure distribution in the enclosure and then the flow through the door is calculated using Bernoulli's equation with an appropriate orifice coefficient. It has been previously shown [11] that the room static pressure relative to ambient pressure is essential hydrostatic. That is, it can be calculated directly from the room and ambient vertical temperature distributions. The extent to which that was true for the current experiments, as well as implications to a two-layer flow model, will be shown.

From hydrostatics, the room pressure differential is given as

$$\Delta p(y) = g \, \rho_a \, T_a \int_N^y \left(\frac{1}{T_a} - \frac{1}{T} \right) dy \qquad (5\text{-}3a)$$

for a uniform ambient air temperature T_a and density ρ_a. T is the room vertical temperature distribution as a function of y measured (+upward) from the floor. For a two-layer concept, the lower portion of the room is filled up to a height D with ambient air at a temperature, T_a and at D the temperature rises abruptly to T where it is uniform up to the ceiling. For this case the hydrostatic

58

pressure differential at height, y, is:

$$\Delta p = \rho_a \, g \left(1 - \frac{T_a}{T}\right) (y-N) \qquad (5-3b)$$

Substituting for y the height of the ceiling and choosing a neutral plane, N, which is assumed here to be independent of temperature, gives the curves in figure 5-12. A neutral plane to door height ratio of 0.39 to 0.53, corresponding to N_p experimental values, yields Δp results that seem to bracket most of the data.

Since the temperature factor, $\rho_a g (1-T_a/T)$ appears to correlate the data in figure 5-12, it can be used to normalize the vertical pressure distribution data using the experimental $\bar{T}$ for each run. Figure 5-13 presents the APV Δp normalized by $\rho_a g (1-T_a/T)$ plotted against height, y in the enclosure for the three separate door widths. The symbols represent the numerical average of the data at each height; the "error" bars indicate the high and low values. The low side scatter seen for the largest opening could be reduced significantly if the one wood crib case were not included. These were very small fires for the large opening, resulting in very small signals. The decreased signal to noise ratios are characteristic of the readings in the lower part of the room. The signals there were approaching the sensitivity limit of these particular instruments. Given a very noisy (acoustical not electrical) background like a fire situation, the scatter in the data will be a large fraction of the signal. The APV averaging will filter out some of the larger fluctuations resulting in the correct algebraic signs and order of magnitude of the results. (The more sensitive pressure transducers available during this work were used exclusively with the bidirectional velocity probes in the doorway, not for these room static pressure measurements.)

The level of fluctuation in the pressure signal is shown in figure 5-14 for the set of pressure taps in PRC 8. Also shown is a calculation (using eq. 5-2a) of hydrostatic pressure difference based on the time varying room temperature distribution and neutral plane height N_p shown in figure 5-8b.
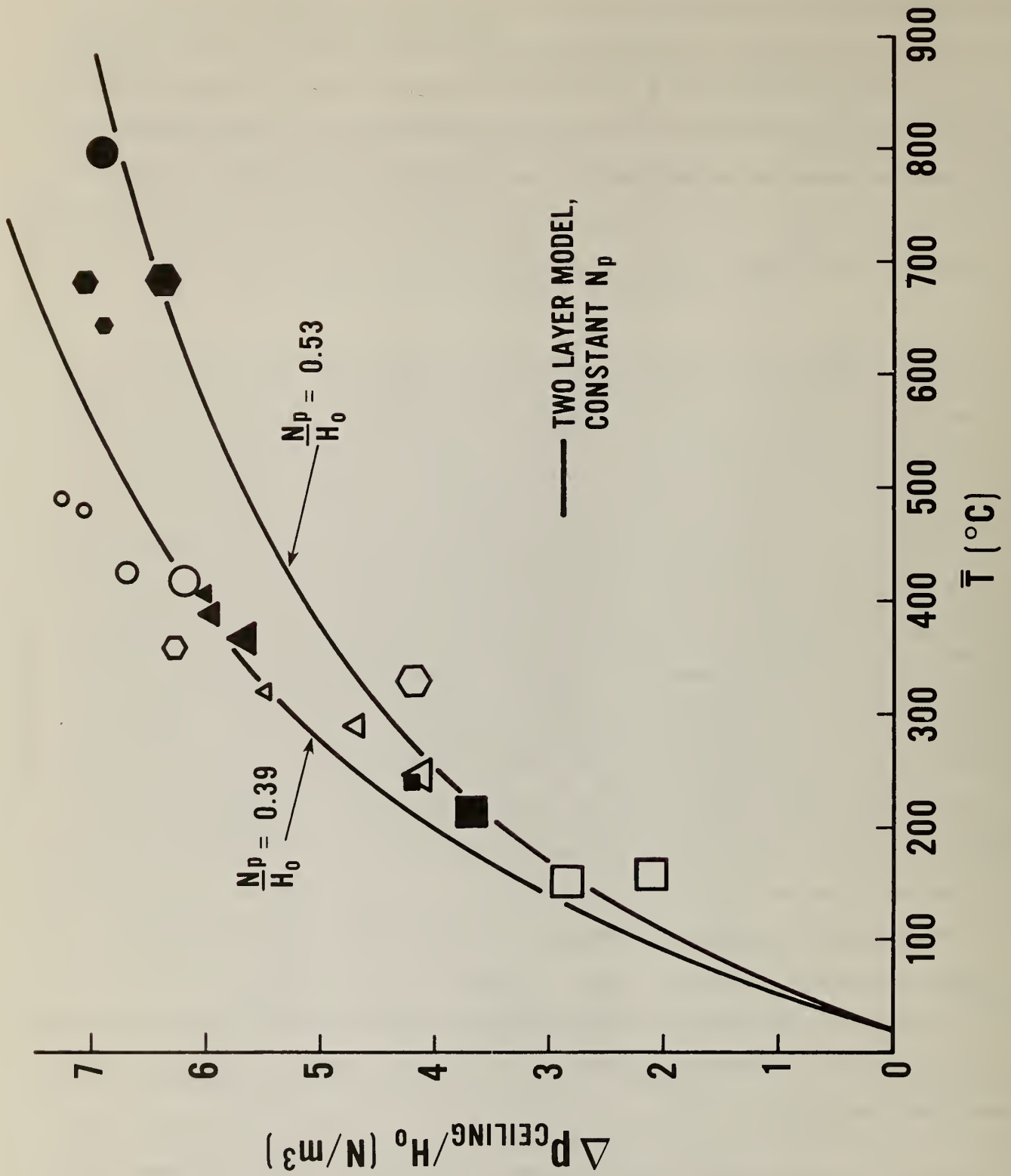
Figure 5-12. Room pressure difference at the ceiling
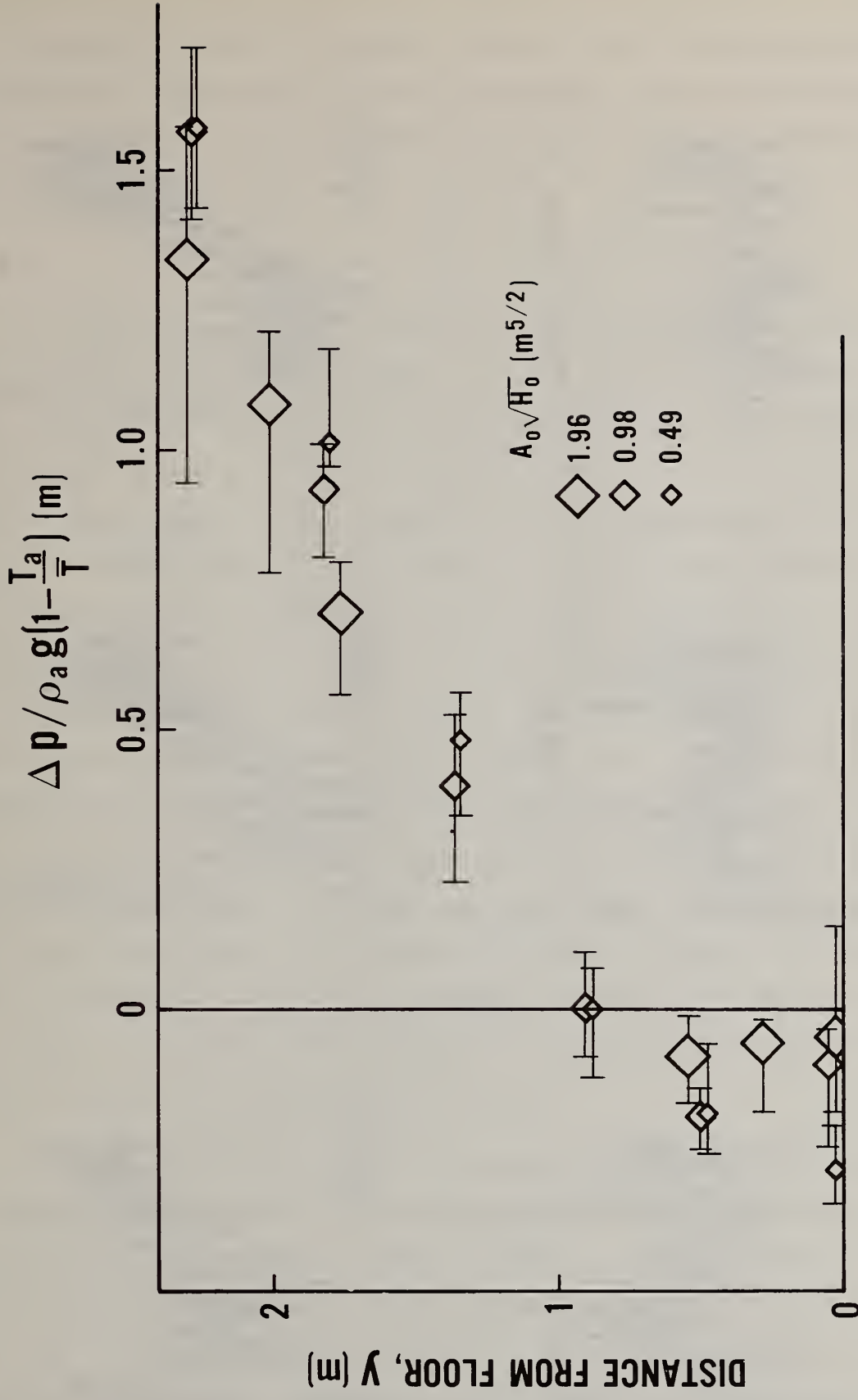
Figure 5-13. Average pressure distributions for each doorway size
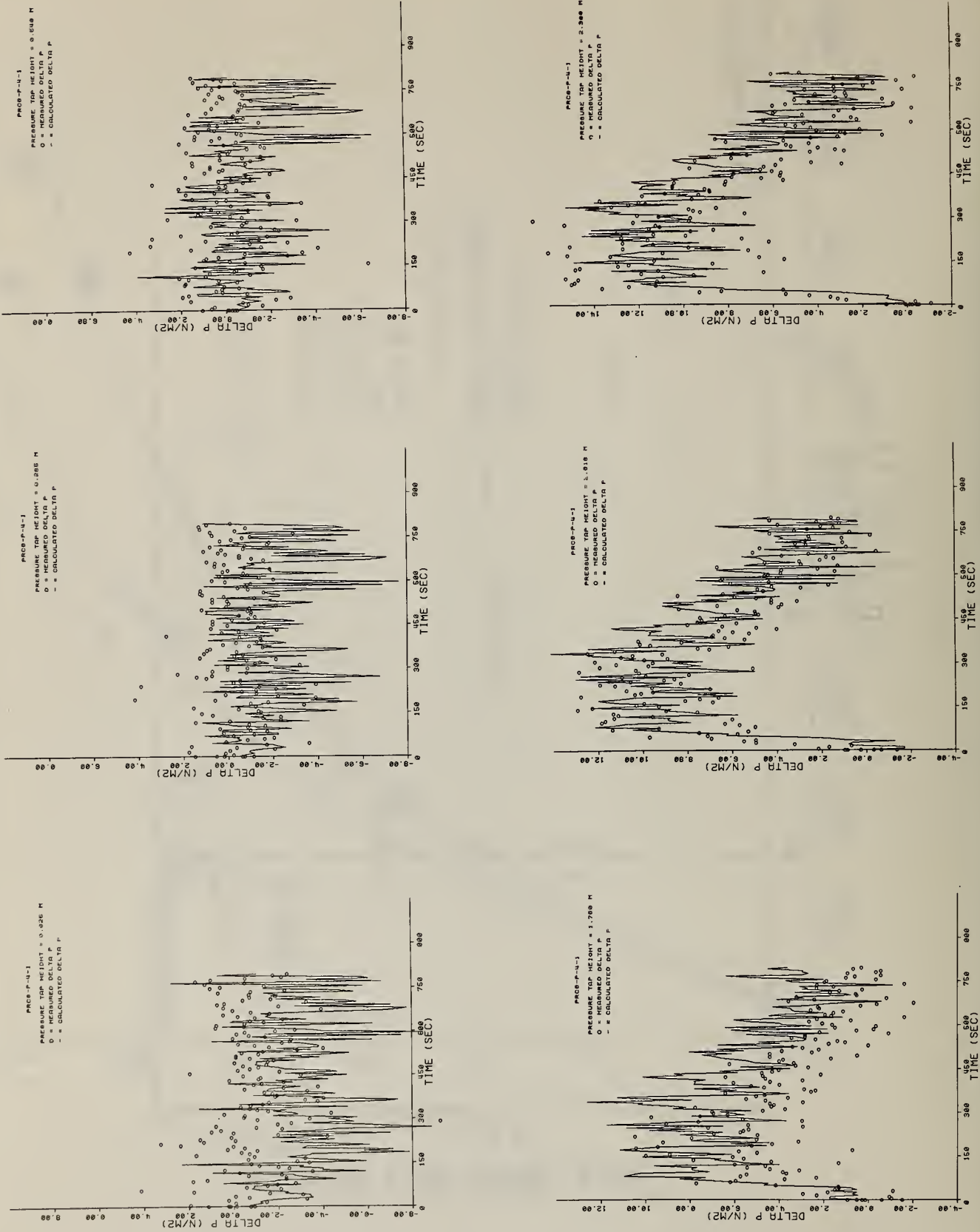
Figure 5-14. Comparison of measured room pressure and calculated hydrostatic pressure for PRC 8

In general it can be concluded that the room differential pressure field is essentially hydrostatic and can be computed from the temperature. Also a two-layer model yields a good approximation for the pressure differential provided the neutral plane height is known.

5.5 Doorway Velocity and Flow Coefficient

The differential static pressure is responsible for the velocity profile in the doorway. The velocity data were used previously to generate the airflow rate. Figure 5-15 shows the door centerline velocity profile range for all the runs normalized by $(2g \, (\bar{T}/T_a - 1))^{1/2}$ and for each door size. The normalization factor comes directly from Bernoulli's equation and the two-layer model for Δp. Like the pressure plot (figure 5-13) the symbols represent the average of the data for that particular height and enclosure and the error bands represent the high and low values. The lines are simply a faired representation of the data to make the figure clearer. The neutral planes (N_v) are higher than those in the corresponding Δp plot in figure 5-13. Note also the correct order in decreasing door width as well as the larger velocities with the smaller doors. For a two-layer model, the upper curves would vary as $(y-N)^{1/2}$ where y is the height above the floor. The data does approximate this parabola somewhat. However, for the incoming flow the two-layer model predicts a uniform velocity below the hot upper layer with a curvature in the region between D and N. It is probably this region where the model is breaking down owing to the lack of a sharp thermal discontinuity in the data.

A measure of how effectively the pressure difference across the opening is converted into velocity can be expressed by a flow coefficient. In an understanding of conventional orifice flows, a flow coefficient depends on viscous and jet contraction effects, and is defined in terms of the entire flow rate. For illustrative purposes, a local flow coefficient can be defined which, on "averaging", is equivalent of a total flow coefficient. This coefficient is defined as

$$C = \frac{V_{measured}}{V_{theoretical}} \tag{5-4a}$$

63
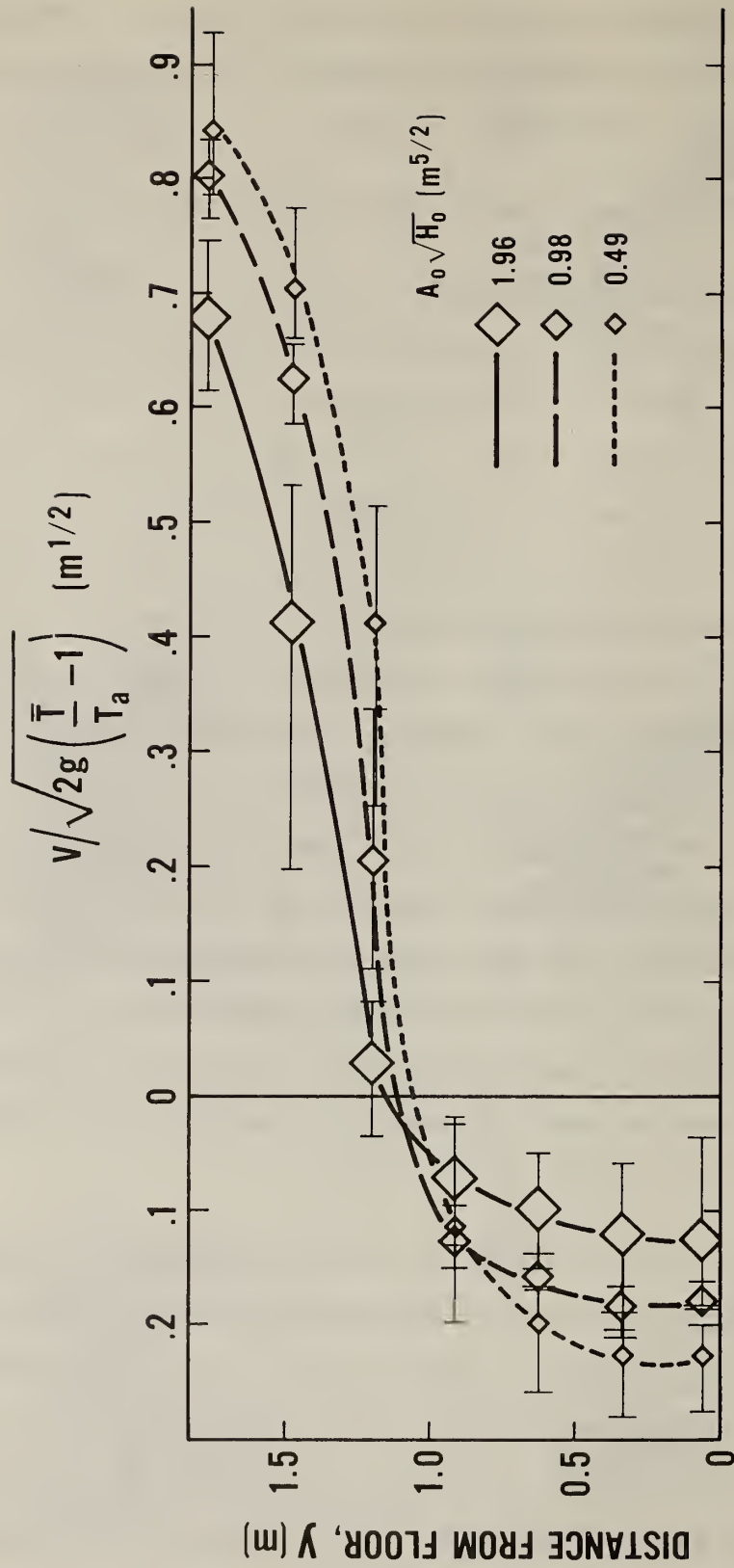
Figure 5-15.   Average normalized velocity distribution for each doorway size
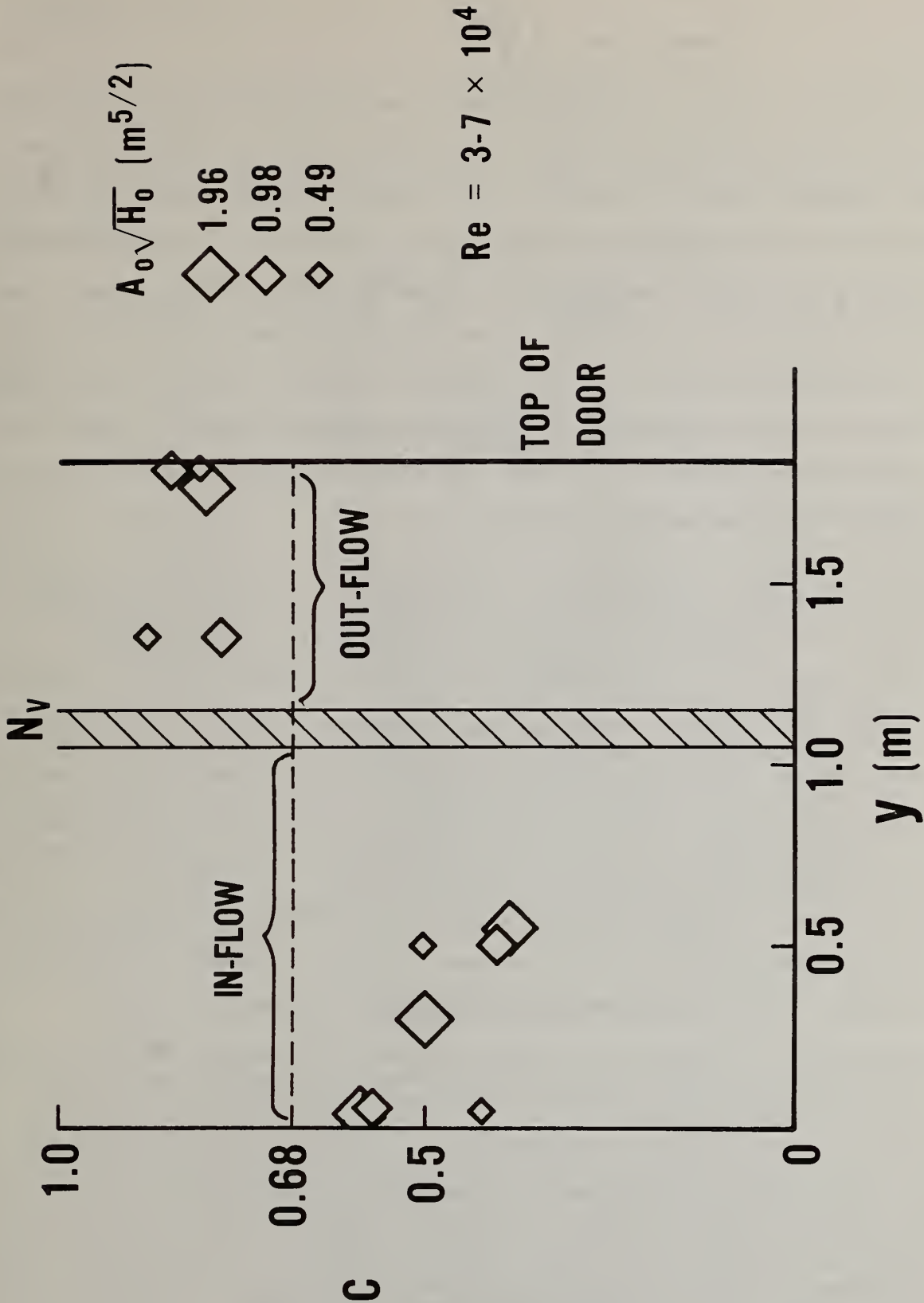
Figure 5-16. Local doorway flow coefficients

where

$$V_{theoretical} = \sqrt{\frac{2\nabla\rho}{\rho}} \qquad (5\text{-}4b)$$

In orifice flow, the actual velocity at the vena contracta would be slightly less, due to viscous effects, than the theoretical velocity predicted from the imposed pressure drop ∇p. Here it is of interest to determine how well the pressure field is responsible for the flow especially since the doorway flow is counter-current. Note the actual pressure distribution is used from figure 5-13 as opposed to one derived from temperature so the result is independent of any assumed model. If the pressure values at the measuring heights are used then the actual measured velocity values can be found at the corresponding height from figure 5-15. Here, it should be noted that mean results are being used from a given door width.

Figure 5-16 shows C spanning the door height for the three enclosures configurations. The amount of averaging for both sets of pressure and velocity data comprising the calculation of C will probably mask any variation among the three door widths. What is clear, however, is that the outflow C is considerably greater than that of the inflow. This is a result which has been obtained previously [12], and it is interesting to observe that the mismatch is in the same direction as the lack of mass balance noted earlier. If instead of using averages, a run by run calculation is performed, the scatter will be greater but the conclusions will be the same - higher discharge coefficients for the outflow. The calculation breaks down near the neutral plane (cross hatched area on figure 5-16) where it was noted earlier that the point of zero pressure difference inside the enclosure falls below the velocity reversal point in the doorway. The familiar C = 0.68 for orifice flow is sketched on figure 5-16 for reference. A Reynolds number based on door width can be defined for these flows as: $Re = \dot{m}_a/W_o\mu$ where μ is the viscosity and W_o is the doorway width. For both the inflow and outflow the above C's apply for Re in the range 3 to 7 x 10^4.

A more conventional or global flow coefficient can be defined for the door flow. This definition is somewhat arbitrary and eventually needs to be

66

developed consistently with a flow model. The definition used in this analysis was

$$C = \frac{\dot{m}_{measured}}{\dot{m}_{theoretical}} \quad (5-5)$$

which applies to the in and out flow. The theoretical flow rate was defined [12] as

$$\dot{m}_{th, out} = W_o \, \rho_a \, T_a \sqrt{2g} \int_o^{H_o} {}^{-N_v} \left(\frac{1}{T_d}\right) \sqrt{T_d \int_o^z \left(\frac{1}{T_a} - \frac{1}{T_i}\right)} \, dz \, dz \quad (5-6a)$$

and

$$\dot{m}_{th, in} = W_o \, \rho_a \, T_a \sqrt{2g} \int_o^{N_v} \sqrt{\left(\frac{1}{T_a}\right) \int_o^z \left(\frac{1}{T_a} - \frac{1}{T_i}\right)} \, dz \, dz \quad (5-6b)$$

where in each equation z is taken as positive away from experimental neutral plane N_v, T_i are the interpolated corresponding room gas temperatures, and T_d are the corresponding doorway gas temperatures at the measured positions. The results of these calculations are shown in figure 5-17. Whereas the trend differs from the "local" results of figure 5-15, the general magnitudes are similar. In both cases the outflow coefficient is higher than the inflow coefficient. While this is consistent with reference [12] it does not necessarily agree with the constant value of 0.68 found by Prahl and Emmons [13]. It appears that a more complete understanding is needed of factors on which the C's depend.

5.6 Room Temperature ($\bar{T}$)

It is the temperature level in the upper portion of the room which promotes the spread and growth of the fire. The vertical and lateral variation of these temperatures preclude assigning a definite unique value, but the averages of T9, T10 and T11 do tend to reflect an average maximum room gas temperature $\bar{T}$ outside of the fire plume. The factors influencing $\bar{T}$ will be considered. Figure 5-18 presents $\bar{T}$, plotted against fuel loading. Similar to previous parameters the gas temperatures for the plastic fires are considerably greater than those corresponding to the wood fires.

67
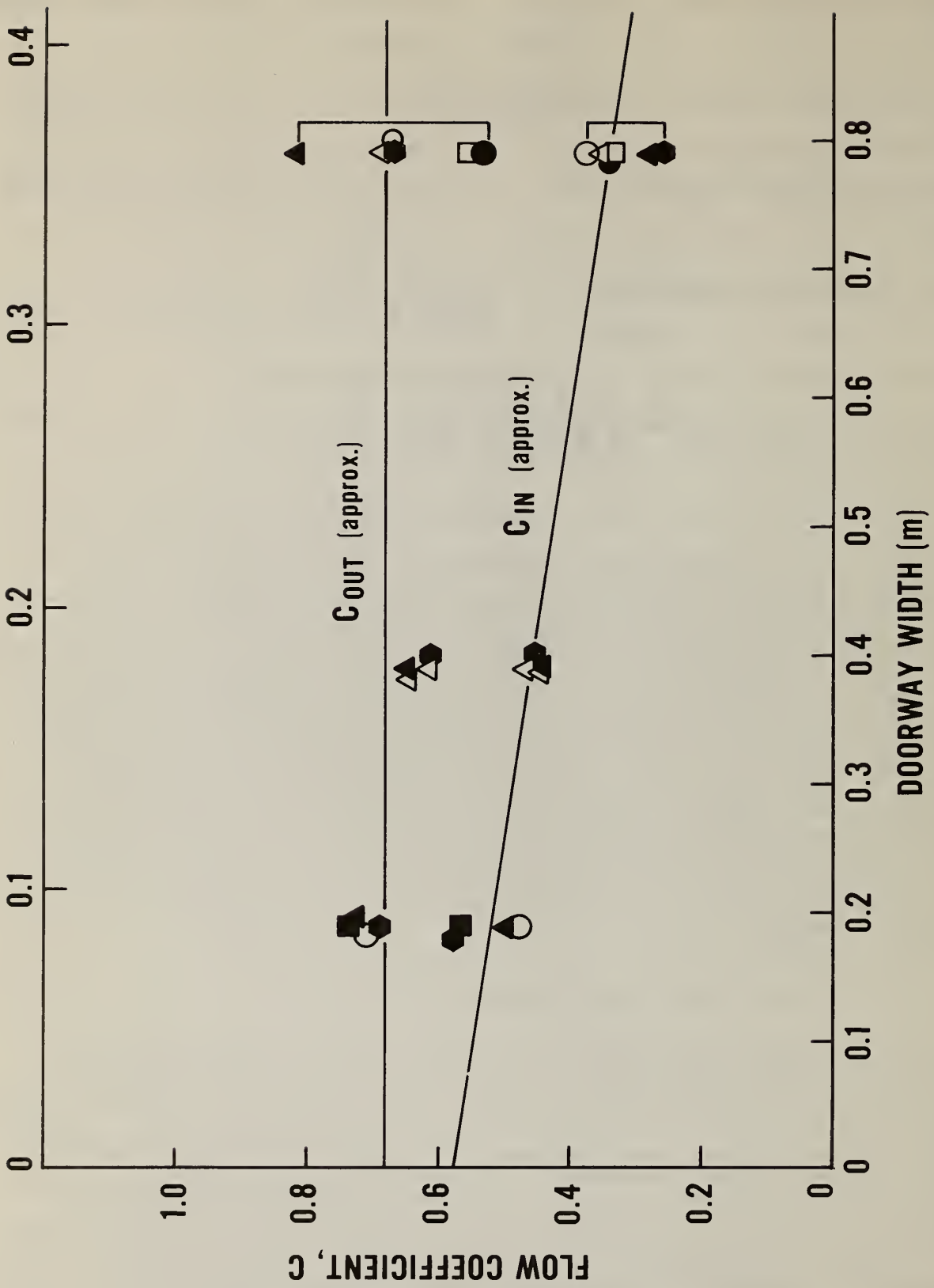
Figure 5-17. Doorway flow coefficients

The concept of "flashover" has often been applied to fires taking place in enclosures. Localized burning continues until the upper gas temperatures reach above about 500 to 700°C, resulting in certain critical values of radiant flux to the floor, or more specifically to uninvolved fuel in the enclosure. This is sufficient to "spontaneously" ignite most of the remaining fuel. This can result in a fully involved fire sufficiently large enough to be deficient with the room oxygen with consequent burning outside the enclosure. From figure 5-18 it can be seen that four and three plastic cribs in all of the enclosure appear to meet this qualitative description of flashover. (Limited fuel in the present work precluded flaming out of the door.) Additional confirmation comes from the fact that the cellulose filter paper tell-tabs for these five cases (one repeat) did indeed ignite or were destroyed during the fires. Those of the other large fires were discolored but remained intact through the experiment. The four wood crib case does not exhibit the same high temperatures in contrast to the three and four plastic crib cases.

The variation of $\bar{T}$ with ventilation can also be seen on figure 5-18. There is a slight inverse relation of $\bar{T}$ with ventilation in all cases except for the flashed-over plastic cribs where the variation, although slight, appears to go directly with ventilation.

In a previous study [11] it was found that the upper gas temperatures for smaller, "non-flashed over" fires could be correlated using plume theory. Figure 5-19 shows $\Delta\bar{T}$, i.e., $\bar{T} - T_a$, plotted against heat release rate, $\dot{Q}$, to the 2/3 power divided by the height of the enclosure, H, to the 5/3 power, all multiplied by an inverse ventilation parameter. The $\dot{Q}^{2/3}/H^{5/3}$ is a scaling relationship from plume theory; $H_o^{5/2}$ is simply a normalizing factor required in order for the ventilation factor, $A_o\sqrt{H_o}$, to scale properly, and 1/5 power was chosen to best fit the data. The ventilation term, $H_o^{5/2}/A_o\sqrt{H_o}$, reduces simply to H_o/W_o. Probably a room aspect ratio as well as the wall thermal properties would also be required to generalize this correlation. But since these parameters were not varied here, they were not included. In converting mass loss rate to heat release rate the following heats of reaction were used:

69
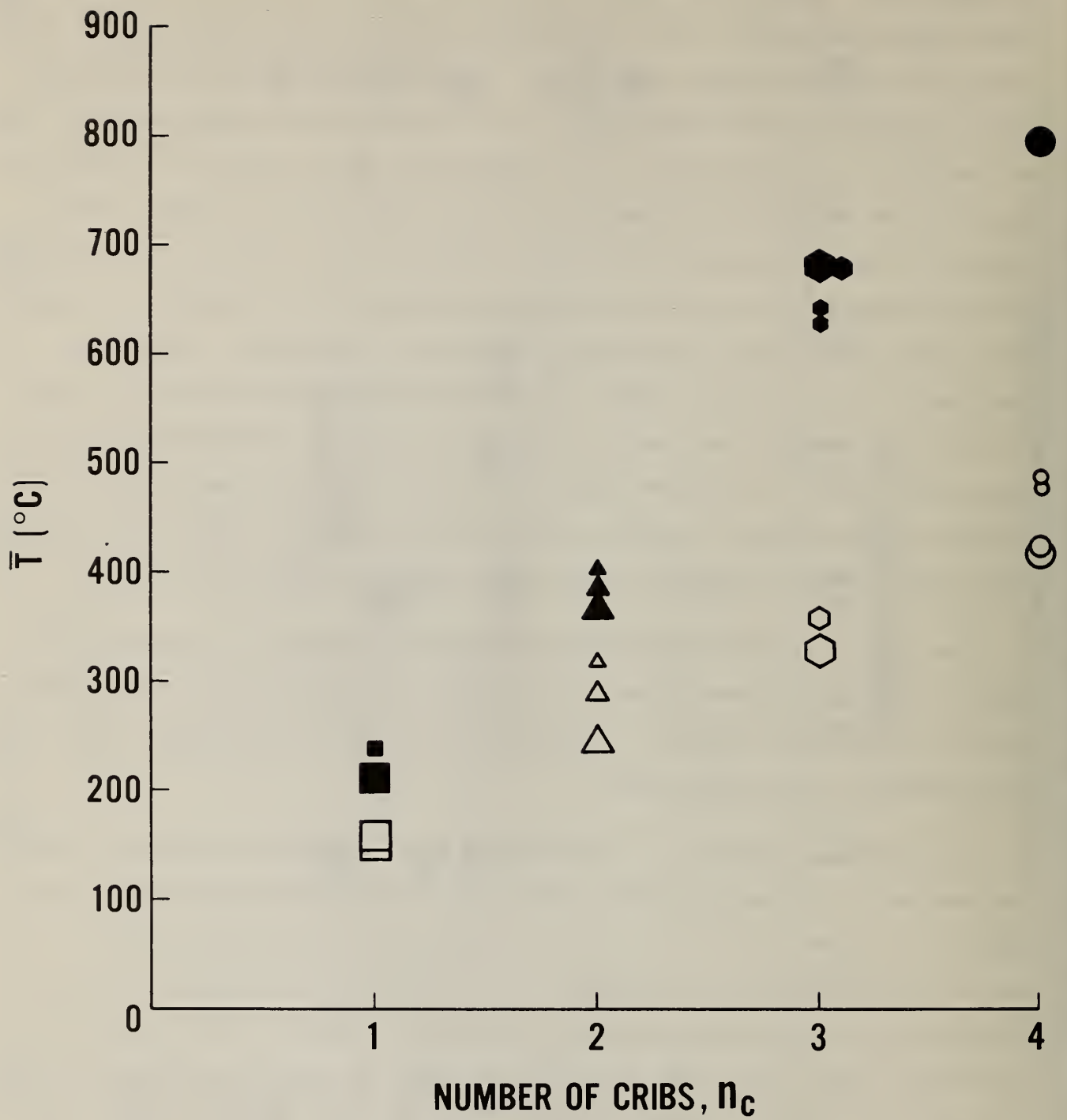
Figure 5-18. Ceiling layer gas temperature versus fuel load

70

wood, 15.6 kJ/g and polyurethane, 22.2 kJ/g. The line shown on figure 5-19 is:

$$\Delta T = 24.2 \frac{\dot{Q}^{2/3}}{H^{5/3}} \left(\frac{H_o}{W_o}\right)^{1/5}$$ (5-6)

The result is within the scatter of the data from other enclosure fires given in reference [11]. Like the results there, it is not obvious why the "flashed-over" data are not following this correlation. It is not yet clear why a plume-like correlation should systematize the low temperature data, but it is interesting to speculate that perhaps with flashover the plume-like burning behavior is lost and an area or volume of burning in the upper part of the room is dominating. Also in figure 5-19 there is a gap between the low temperature (T < 450°C) data and that of the high temperature (T > 600°C). This gap has been observed previously [11] and may be a further clue for modelers trying to understand flashover.

5.7 Room Heat Flux

The variation of incident heat transfer to the floor with upper gas temperature can be seen in figure 5-20, where the APV values of heat flux meter H2 are plotted. This was a total heat flux meter more than a half meter away from the load platform and not directly in the path of the doorway air inflow. It may be assumed that all of the heat transfer will be due to radiation from above; however, the contribution from the crib is also signifi-cant. In fact, the heat flux to the floor target (H1) in the free burns is plotted against the corresponding floor flux (H2) in the room burns (with W_o = 0.79 m) in figure 5-21. The line labeled "no effect" represents equal values of the floor flux; therefore, the horizontal distance from zero to that line represents the flame contribution, and from the "no effect" line to the data represents the enclosure contribution. The measured enclosure flux is seen to be up to 3-1/2 times the free burn flux for the plastic cribs and up to 2-1/2 times for the wood cribs.

The nominal incident floor heat flux value of 2 W/cm_2 may be used as an indicator of the potential onset of flashover. The measured incident floor

71
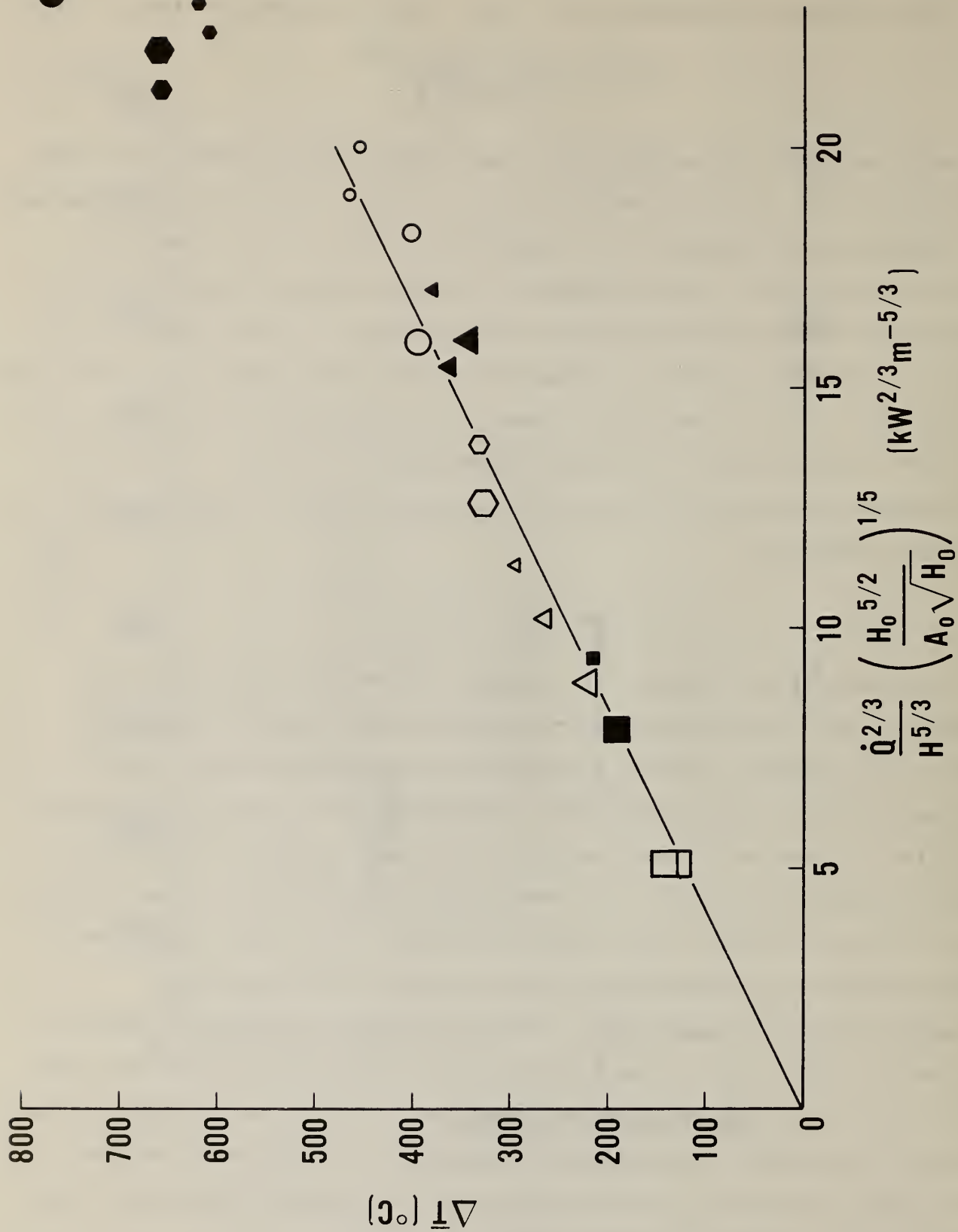
Figure 5-19. Correlation for upper layer gas temperature

72
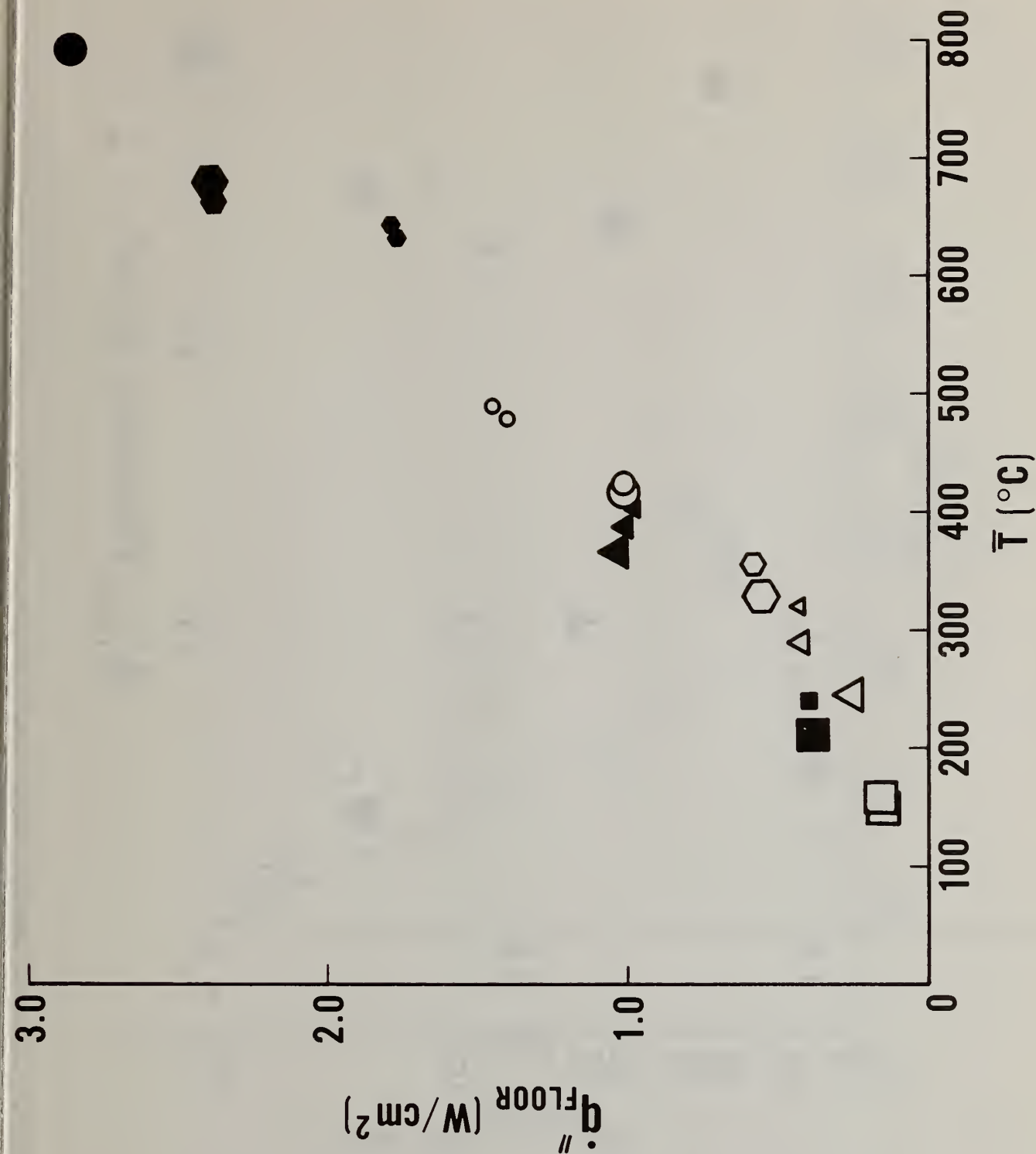
Figure 5-20. Incident floor heat flux (H2) versus upper layer gas temperature

73
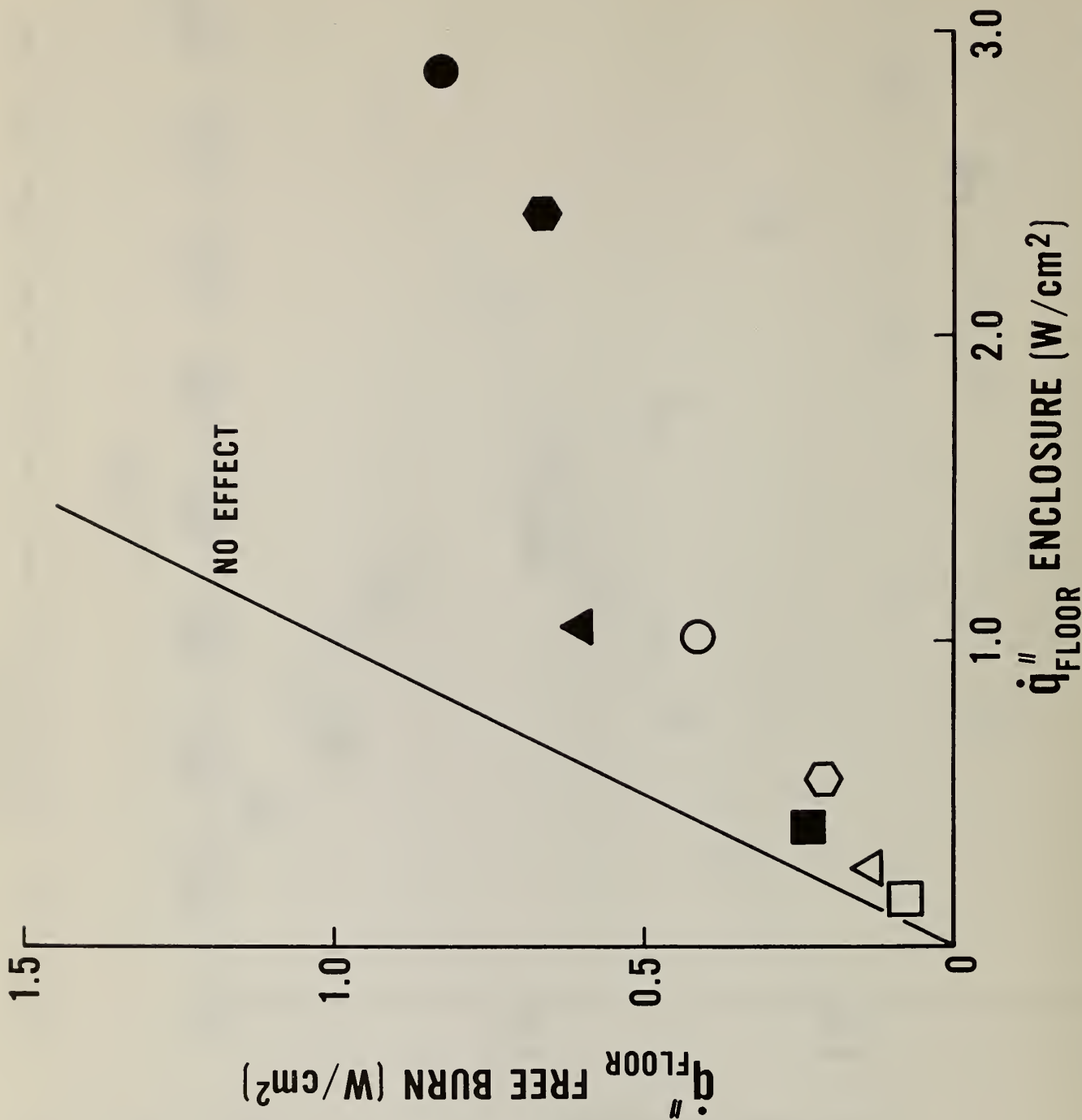
Figure 5-21. A comparison of free burn to room floor flux
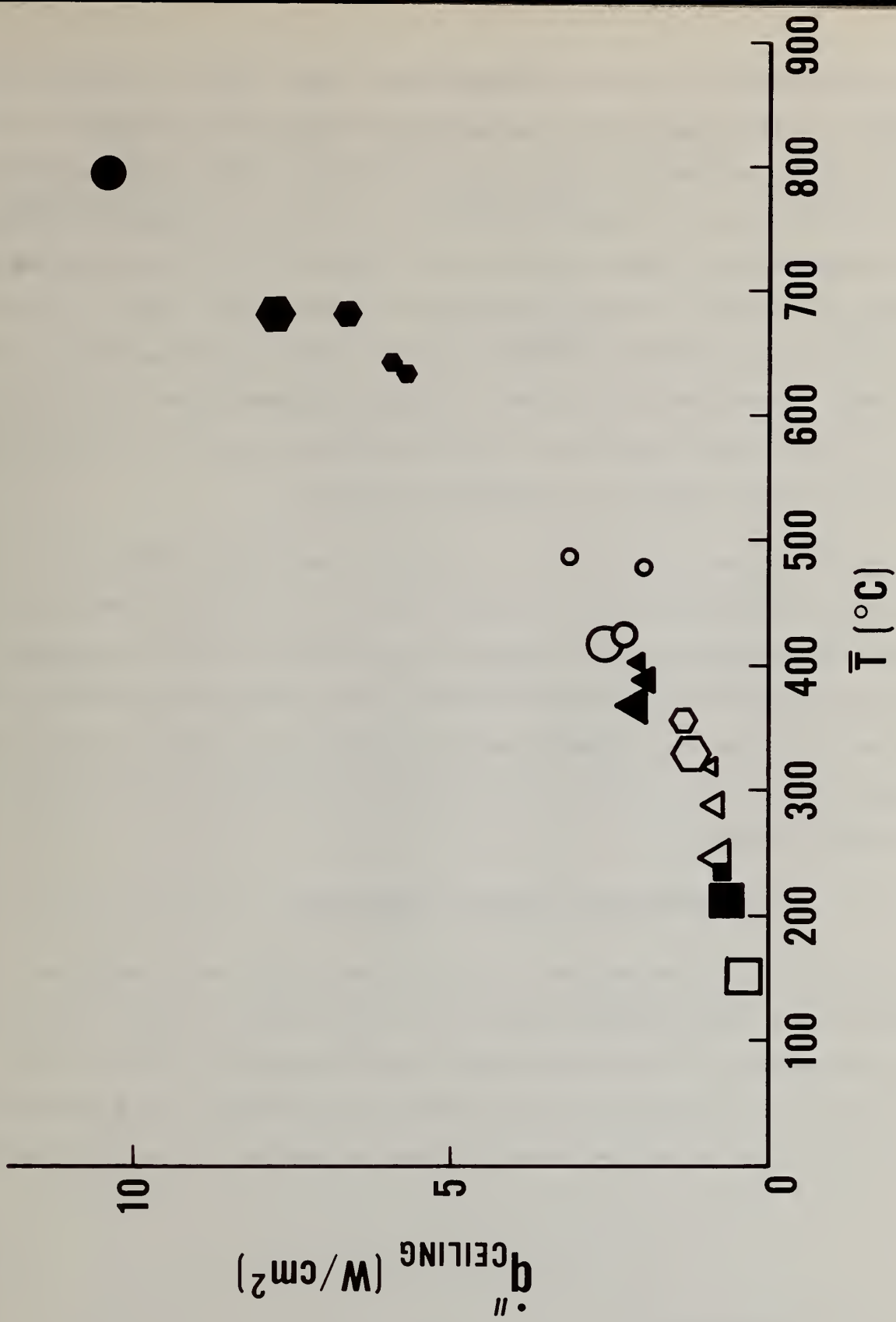
Figure 5-22. Ceiling incident heat flux versus upper layer gas temperature

flux and the disposition of the adjacent filter paper target is given in table 5-1. Hence, filter paper ignition or complete consumption occurred at a minimum of 1.77 W/cm_2 applied for roughly 200 s or more. Under more controlled laboratory conditions, with radiant exposure to the same target configuration, the paper charred black under 2.5 W/cm_2 and ripped at 120 s, but only decomposed to a brown color under 1.5 W/cm_2. Shivadev and Emmons [14] report on experimental ignition critical incident radiant flux for filter paper heated from below as 2.4 W/cm_2. Since the filter paper is only a representative room furnishing material, it would seem sufficient to use the nominal value of 2 W/cm_2 as a criterion for remote ignition or flashover potential.

Figure 5-22 presents the APV total incident heat flux (radiative + convective) to the ceiling plotted as a function of $\bar{T}$. In this figure the extremely high heat fluxes associated with flashover are evident and the gap between the "plume burning behavior" and "flashover" can be seen to be dramatic. An alternative criterion for flashover may be formulated in terms of this ceiling heat flux based on the potential for significant pyrolysis and ignition of ceiling lining material.

5.8 Combustion Product Composition

Dry O_2 and CO_2 concentrations of the effluent gases were monitored continuously by a single sample drawn from a point near the upper velocity probe in the doorway. A correction could have been made to give the true concentrations in the moisture laden products by estimating the H_2O concentration. This correction for the volume concentrations of specie i (O_2 or CO_2) would be

$$x_i = x_{i,DRY} \left(1 - x_{H_2O} \right) \tag{5-7a}$$

where x_{H_2O} is estimated as

$$x_{H_2O} = x_{CO_2} \frac{\nu_{H_2O}}{\nu_{CO_2}} \tag{5-7b}$$

with ν_i = stoichiometric coefficient for the ith specie. The ratio ν_{H_2O}/ν_{CO_2}

76

Table 5-1

Effect of Enclosure Heat Flux on Filter Paper Target

Experiments in Decreasing Order	Disposition of Filter Paper	Average Peak
	1 = charred 2 = consumed	Floor Flux W/cm^2
PRC 8	2	2.86
PRC 6	2	2.39
PRC 18	2	2.39
PRC 16, 20	2	1.77, 1.79
PRC 17	1+	1.45
PRC 19	1+	1.40
PRC 7	1	1.01
PRC 14	1	0.98
PRC 15	1	1.01
PRC 10	1-	1.00

is roughly 0.7 for the polyurethane and 1.2 for the wood (from section 6.3.1). This correction would reduce the reported dry concentration values by no more than 15 percent. A single sample is only reliable if the gases in the upper part of the room are well mixed and that the gas flow out the top of the door is representative of that mixture. In fact, that measurement should be corrected for profile shape to derive a true mixed-mean value. It is likely that simi-larity nearly exists for property profiles at the doorway such that $(0.21 - x_{O_2})$ and x_{CO_2} are equivalent profiles. It can be shown that the profile shape factor relative to the maximum measurement is approximately 0.7 (section 6.3.1) e.g.,

$$x_{CO_2}, \text{ mixed mean } \simeq 0.7 \; x_{CO_2}, \text{ MAX}$$

This correction and the "wet" correction factor will not be applied. Both corrections taken together would yield mixed-mean values for CO_2 and O_2 in the exhaust gases that are correspondingly lower and higher than those measured.

The following discussion will indicate the consistency and characteristics of the O_2 and CO_2 measurements. (It should be noted that the chemical analysis used will differ slightly from that in section 6. The consequences of the differences are not significant so these analyses were not made consistent.) Figure 5-23 gives the APV of O_2 and CO_2 for all the enclosure fires. As a guide the straight lines show an ideal complete combustion prediction for assumed chemical composition of fuel with x being the excess amount of air:

$$\text{fuel} + (1+x) \; O_2 + 3.76(1+x)N_2 \rightarrow CO_2 + H_2O + 3.76(1+x)N_2 \qquad (5-8)$$
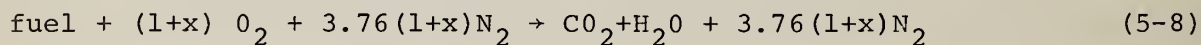
for the wood experiment exceeds that of the urethane consistent with the complete combustion model.

Using the chemical model above, a consistency check of the data presented can be made. The amount of excess air, x, can be determined directly from the CO_2 and O_2 measurements as well as from the burning rate and airflow rates assuming some chemistry. From the CO_2, O_2 measurements $x = x_{O_2}/x_{CO_2}$ for wood and $x = 0.83 \; x_{O_2}/x_{CO_2}$ for the urethane. This measurement is designated $x(O_2, CO_2)$

78
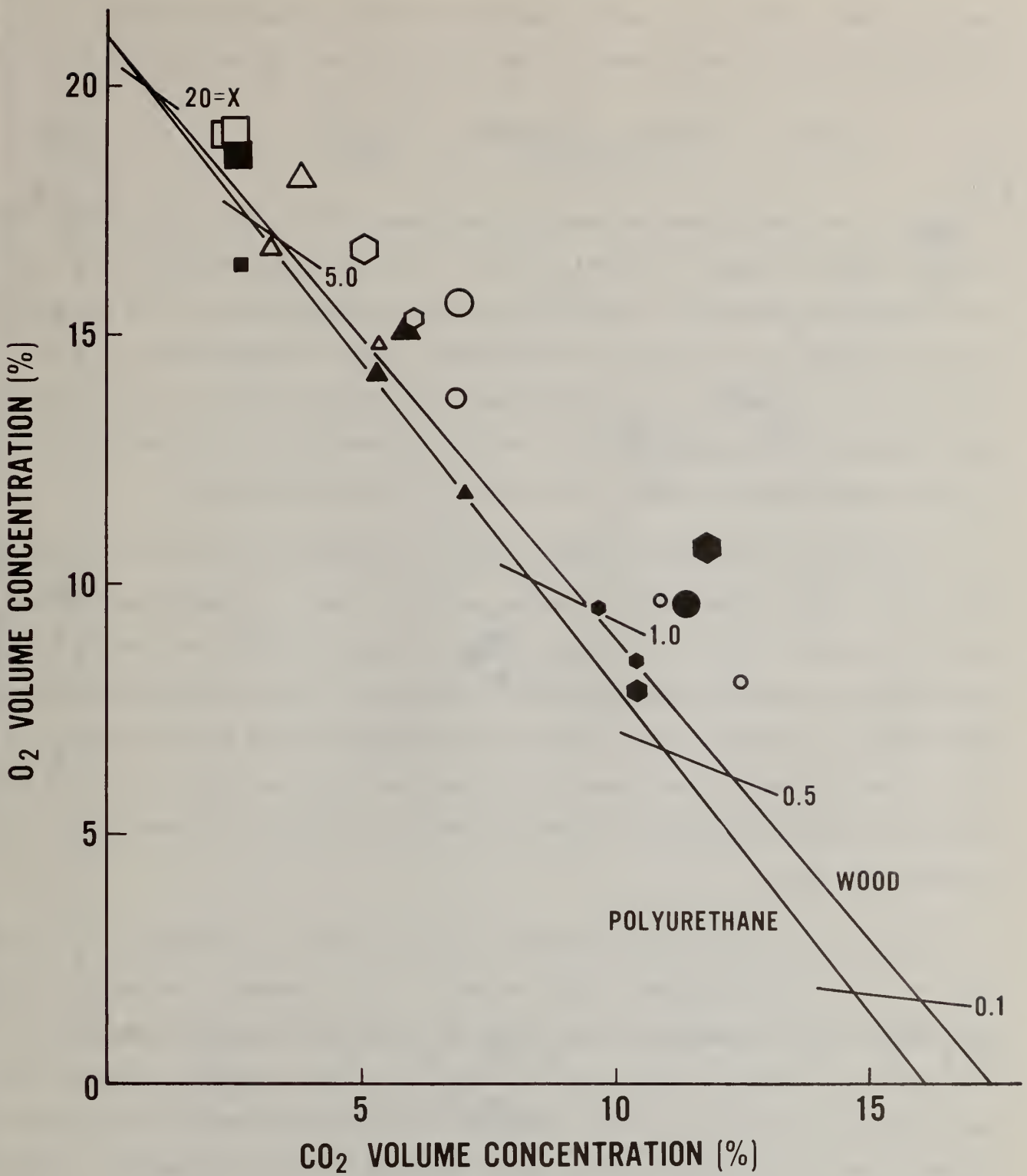
Figure 5-23.   Oxygen and CO_2 concentrations with x = excess air (%) as a parameter

From the definition of x, another calculation of x, designated $x(\dot{m}_b, \dot{m}_a)$, can be derived from the measurement of the burning rate, $\dot{m}_b$ and airflow rate, $\dot{m}_a$:

$$x(\dot{m}_b, \dot{m}_a) \equiv \frac{\dot{m}_{actual} - \dot{m}_{required}}{\dot{m}_{required}} = \frac{\dot{m}_a - r\dot{m}_b}{r\dot{m}_b} \qquad (5\text{-}9)$$

where r is the stoichiometric air to fuel mass ratio. Using the above assumed chemical composition of the fuel, $r_{wood} = 4.64$ gm air/gm volatile and $r_{PU} = 9.42$ gm air/gm volatile. Figure 5-25 shows the comparison of the two methods for determining x. Over nearly two decades (10% to 1000% excess air) of variation the agreement is probably good, the plastic cribs in the smallest door showing the largest deviation which is probably more indicative of a defect in the assumed chemical model rather than in the measurements.

It should be pointed out that ordinary enclosures turn out to be designed very poorly from a combustion chamber point of view. A significant amount of air is swept into the room, entrained at the edge of the plume and the exiting airstream and swept out again without ever taking part in the chemical process. Furthermore, it appears that x does not necessarily have to go to zero for the fire to be air limited and result in lower gasification rates. This is evident from the previous discussion of the effect of radiation and ventilation factor on mass loss rate.

Although doorway CO measurements were not made, an estimate of CO concentration in the room effluent could be made. In a companion toxicology experiment [15] samples of the exhaust gases from the enclosure fires were collected from the adjoining corridor and brought through an animal exposure chamber where measurements of CO and CO_2 were obtained. These measurements can be used to estimate the concentration of CO being produced in the room burns. Provided the location of the sampling line and sample gas flow rate remain approximately fixed a dilution ratio may be obtained by comparing the doorway concentration measurements of CO_2 with those of the animal exposure chamber. That is, a certain constant fraction of what is being exhausted from the room will arrive in the chamber.
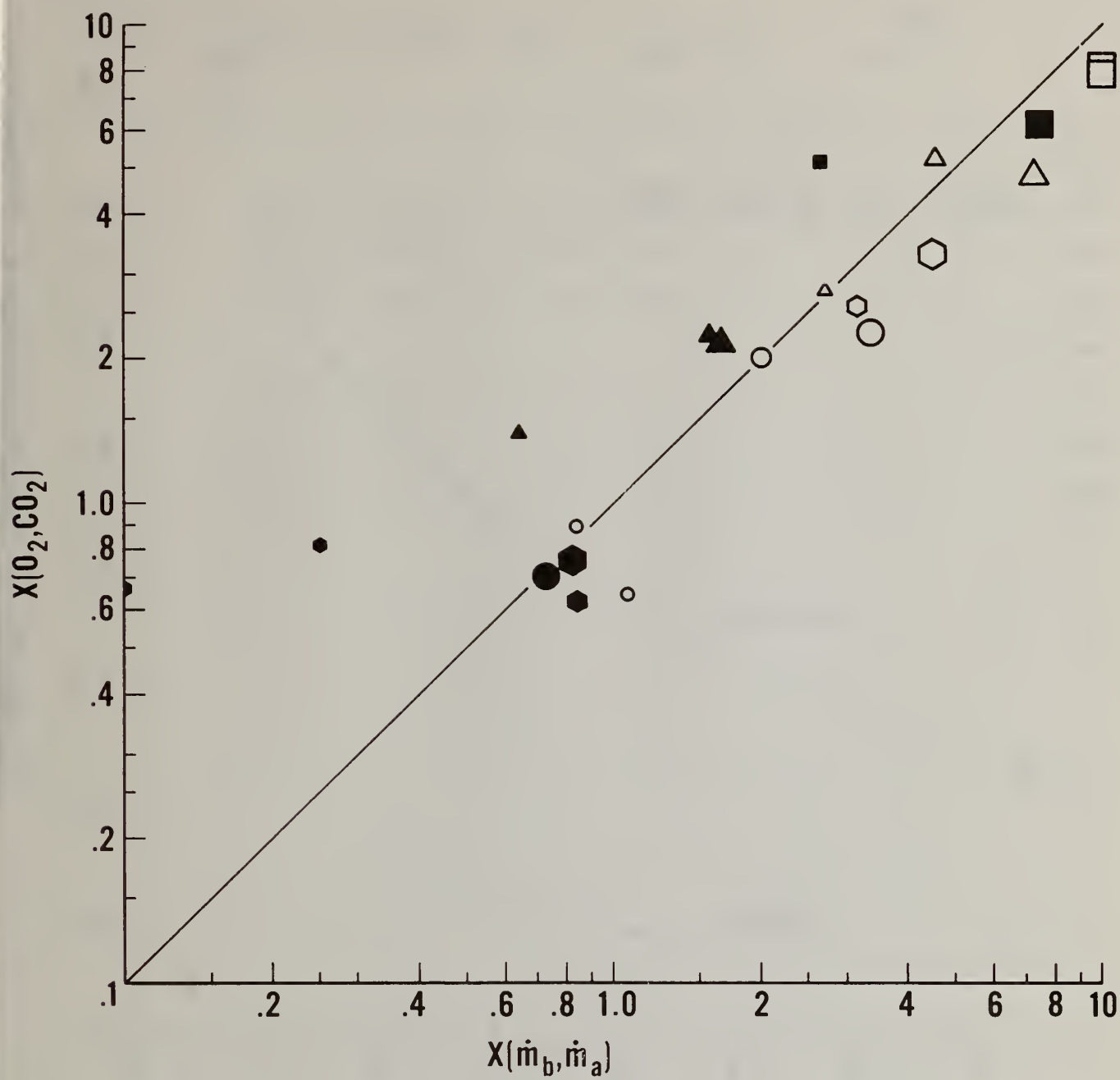
Figure 5-24. A consistency evaluation of the determination of excess air

Table 5-2. Gas Concentrations for Estimating Room CO Production

Run	Number of Cribs	Doorway %O_2	%CO_2	Animal Exposure Chamber %CO_2	%CO	%CO/%CO_2	Estimated Doorway %CO
WOOD							
PRC 5	2	18.2	3.80	0.874	0.018	0.021	0.078
PRC 2	3	16.7	5.10	0.815	0.014	0.017	0.088
PRC 7	4	15.6	6.94	1.23	0.021	0.017	0.12
URETHANE							
PRC 1	1	18.6	2.52	0.201	0.019	0.095	0.24
PRC 4	2	15.1	5.86	1.25	0.122	0.098	0.57
PRC 6	3	10.7	11.8	1.48	0.104	0.070	0.83
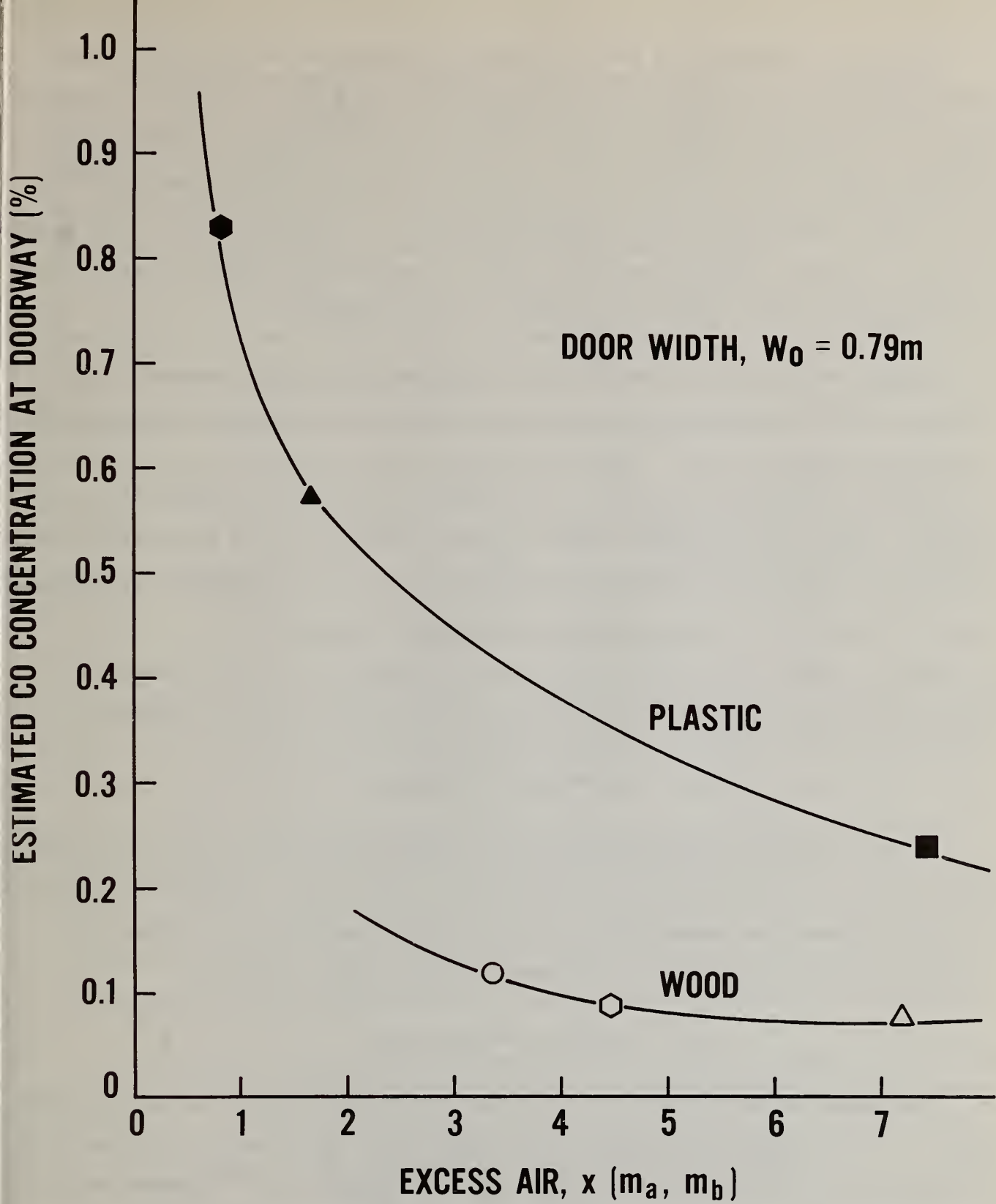
Figure 5-25. Estimation of door CO concentrations

83

Table 5-2 contains the APV's of the concentrations in both the doorway and animal exposure chamber for the widest door, $A_o \sqrt{H_o} = 1.96$ m$^{5/2}$. Looking first at the exposure chamber gases, the ratio of CO and CO_2 is about 0.018 for the wood and about 0.087 for the urethane, a result consistent with the greater air requirements for urethane burning. The temperatures at the sampling location in the corridor were low enough to insure that further CO conversion was frozen and hence the CO/CO_2 ratios will be preserved.

Figure 5-25 shows the estimated CO concentration in the doorway flow plotted against the excess air, $x(\dot{m}_a, \dot{m}_b)$ which is calculated using measured airflow and burning rates. The CO concentration is obtained by multiplying the inverse of doorway CO_2 value by the CO/CO_2 ratio for the animal exposure chamber. Even at 800 percent excess air the amount of CO is significant and the difference in the two fuel types is evident, i.e., $\sim$ 0.25 percent for urethane and 0.08 percent for wood. As expected CO rises dramatically as x $(\dot{m}_a, \dot{m}_b)$ decreases. This will result from decreasing ventilation, by decreasing the doorway width for example, or by increasing the fire load for a fixed door width.

6. MATHEMATICAL MODEL

In this section the mathematical fire simulation model will be developed, and pieces of it will be checked against the average peak experimental results. In this process, the assumptions, limits of applicability, and a sense of accuracy of the ingredients of the model should become apparent.

6.1 Conceptual Formulation

The model follows the basic two-layer approach currently being utilized [1-6]. The enclosure is divided into an upper (u) and lower (ℓ) volume, each of spacially uniform properties with temperature (T_g) and ith specie concentration (Y_i). Also a homogeneous combustion zone is identified in the lower space. The corresponding upper and lower solid boundary surfaces are at uniform temperature, $T_{w,u}$ and $T_{w,\ell}$ respectively. Mass can flow across zone boundaries due to pyrolysis (but not in our application since we neglect combustible linings), pressure differences, and turbulent entrainment. Figure 6-1 depicts the model for our case.

The phenomena to be considered are illustrated also in figure 6-1. Radiative and convective heat exchange is considered and the upper ($T_{w,u}$) and lower ($T_{w,\ell}$) surfaces temperatures will be determined accordingly. Mass flow will be calculated for a doorway configuration based on the hydrostatic pressure difference model corrected for derived flow coefficients. In addition, mixing between the layers due to shear effects of the incoming flow will be considered. Consequently a lower layer oxygen (mass) concentration ($Y_{O_2,\ell}$) and temperature $T_{g,\ell}$ different from the incoming air flow can be found. A new plume and crib entrainment model will also be incorporated in the model.

The details of these sub-models will be discussed in the following sections. It will be useful to preview that development by anticipating the modeling parameters that would be required. These are listed in table 6-1.

6.2 Steady-State Limitation

Perhaps the most questionable aspect of a steady-state mathematical model for our application is the approximate constant treatment of the transient conduction wall loss. Unless the steady-state constraint is relaxed, the effects of this approximation must be accepted in our model. However, the general transient effects of fire growth are always present to some extent, and it would be useful to illustrate the applicability and limitations of a steady-state model. This will be done by considering the conservation of energy applied to the upper spatial zone (control volume) in figure 6-1.

The general conservation of energy (1st law) for a region fixed in space is:

$$\dot{q}_{net,added} - \dot{W}_{by} = \frac{d}{dt} \iiint_V \rho e \, dV + \iint_S \rho e (\overline{V} - \overline{W}) \cdot \hat{n} \, dS \qquad (6\text{-}1)$$

where $\dot{q}_{net,\,added}$ is the net rate of heat added, $\dot{W}_{by}$ is the net work done (just pressure work here) and e is the energy per unit mass in volume, V. In application to the upper layer, the region is defined as bounded by the solid upper surfaces, the plane of the doorway, and a lower surface at height D that
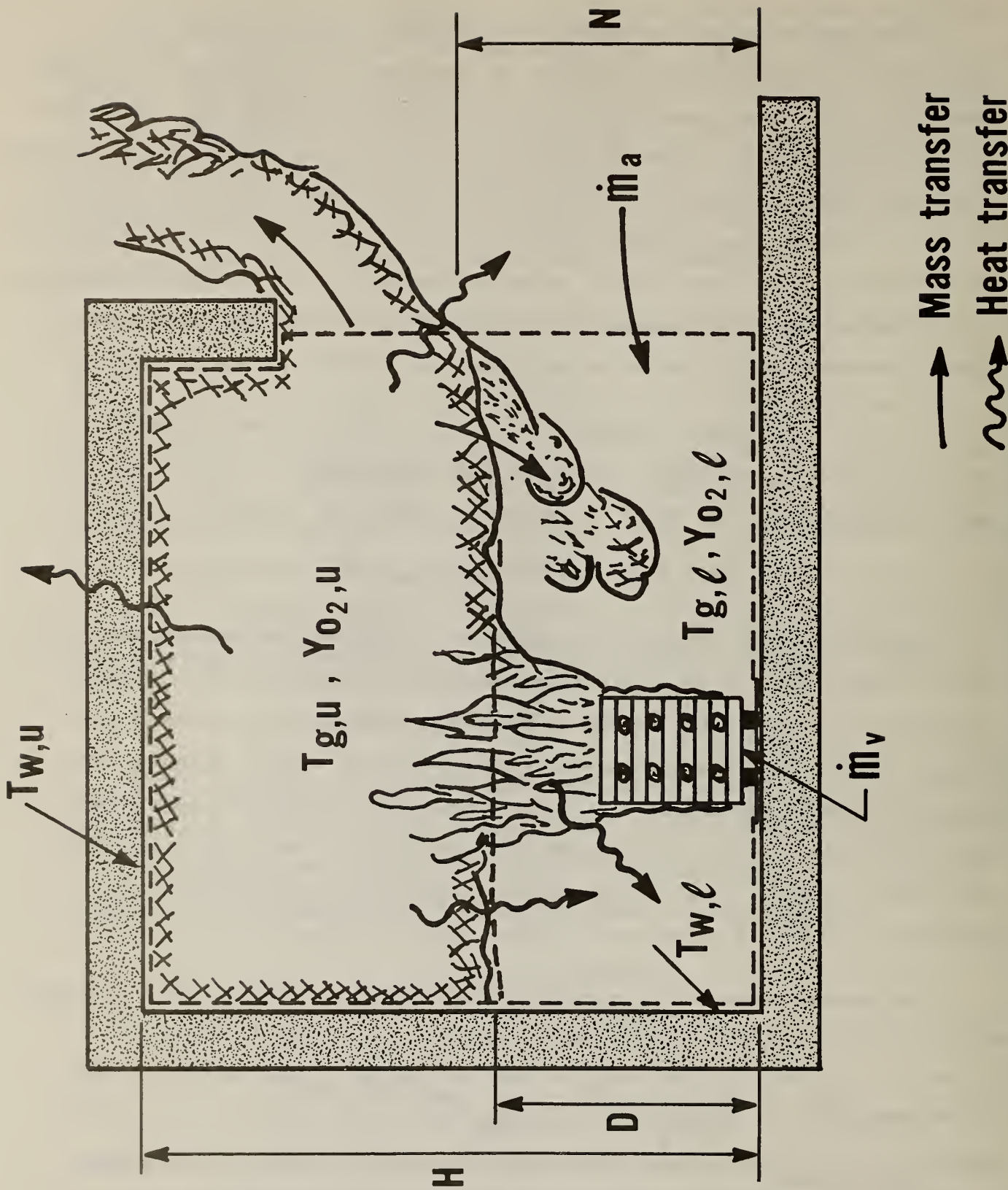
Figure 6-1.   Conceptual model

Table 6-1

Anticipated Modeling Parameters

Pertains to:	Parameter
Fuel	ΔH, effective heat of combustion
	L_{vap}, effective heat of vaporization
	r, stoichiometric air to fuel mass ratio
	f, fraction of energy radiated per total
	ω, fraction of char produced per unit mass
	k_f, flame absorption coefficient
	T_f, effective flame temperature
Crib	Geometry
	$\dot{m}''_{v,o}$, free mass loss rate per unit area
Room	Geometry
	$k\rho c$, wall thermal inertia
	t^*, characteristic time
Flow	C_i, doorway flow coefficents
	k_m, mixing coefficient
Heat Transfer	k_g, upper layer absorption coefficient
	h_g, upper layer convective coefficient

has no relative motion of fluid across it (i.e., $\bar{V}$, the velocity equals $\bar{W}$ the surface velocity, $\frac{dD}{dt}$) except for the transport of the plume gases and possible shear induced mixing across it. Neglecting kinetic and potential energy of the fluid

$$e = u = c_v \ (T-T_a) \tag{6-2}$$

equation (6-1) becomes

$$\dot{q}_{net, \ added} = \frac{d}{dt} \ [m \ c_v \ (T-T_a)] + \sum_{net, \ out} (\dot{m}i) \ flows \tag{6-3}$$

where m is the mass of fluid in the volume at any time

    $\dot{m}$ is the rate of mass efflux

    i is the enthalpy

The left hand side of (6-3) contains the transient conduction heat loss effect. The first term of the right hand side of (6-3) is usually small, but is significant when the room is "filling" with hot gases or when the change in temperature is rapid. A conventional size room would "fill" - layer falls and gases begin to flow out of the door - in less than 30 seconds. Also a flashover transition would raise the gas temperature several hundred degrees Celsius in less than 30 seconds. These two phenomena are not accounted for by a steady-state model. The second sum term of the right primarily contains the fire energy release rate and the doorway rate of enthalpy efflux. The fire energy release rate usually is slowly varying in time up to flashover. Also the doorway flow rate, following the filling phenomena, (and mixing) is very slowly varying in time. Hence the steady-state model can approximate very well all terms except the first on the right, and thus should represent conditions between "filling" and flashover with validity.

6.3   Sub-Model Development and Verification

This section precedes the development of the governing simulation model equations, and establishes a basis for it. Property and necessary model parameters will be determined. Necessary model relationships and subsidiary relationships will be formulated and assessed. Although actual fire conditions

do not perfectly fit a two-layer model, associated experimental parameters, such as N and D, have been derived from the data. These experimental values will provide sets of known independent variables for theoretically calculating other variables, such as airflow rate, $\dot{m}_a$. A theoretical value can then be compared to its experimentally derived value. The extent of agreement would establish the acceptability of the theoretical approach.

6.3.1 Effective Heat of Combustion and Air-Fuel Ratio

A chemical equation, based on the analysis of table 2-2 and a char analysis (except for sugar pine where a pure carbon char was assumed) was developed for each fuel material. Char yields were based on the residue of the crib burns after flaming ceased - approximately 10 percent for wood and 13 percent for the plastic. The combustion reaction for each is then given as sugar pine (6.5% moisture)

$$CH_{1.74}O_{0.704} \cdot 0.0966 H_2O + 0.860 (O_2 + 3.77 N_2)$$
$$\text{(solid)} \qquad\qquad\qquad \text{(air)}$$

$$\longrightarrow 0.777 CO_2 + 0.969 H_2O + 3.24 N_2 + 0.223 C$$
$$\text{(char)}$$

Polyurethane

$$CH_{1.27}N_{0.0823}O_{0.215} + 1.02 (O_2 + 3.77 N_2)$$
$$\text{(solid)} \qquad\qquad\qquad \text{(air)}$$
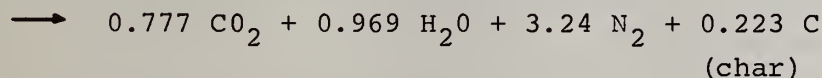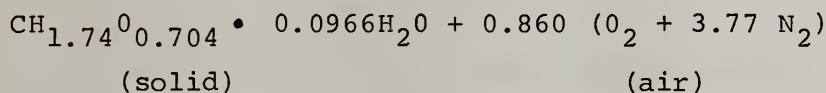
$$\longrightarrow 0.844 CO_2 + 0.565 H_2O + 3.88 N_2$$
$$+ 0.156 CH_{0.874} N_{0.0765} O_{0.0582}$$
$$\text{(char residue)}$$
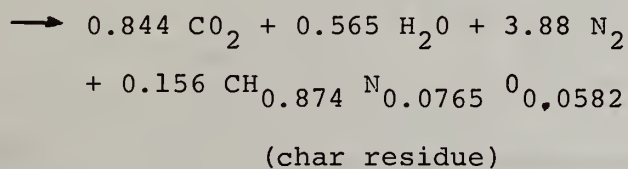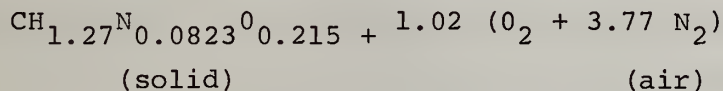
These assumed reactions will establish the stoichiometric relationships required in subsequent modeling. The oxygen and air stoichiometric mass ratio, based on volatile fuel since that relates directly to measured mass loss, is given in table 6-2.

Table 6-2

Air and O_2-Fuel Ratio

	r_{ox} g O_2/g volatile fuel	g air/g volatile fuel
Sugar Pine	1.14	4.92
Polyurethane	2.10	9.03

An effective heat of combustion, ΔH, was derived by considering two analyses. First, from the free burn experiments

$$\Delta H = \frac{\Delta H_{ox} \ \dot{m}_{O_2}}{\dot{m}_V} \tag{6-4}$$

Based on complete combustion of the fuels, ΔH_{ox} was estimated to be 13.7 to 15.3 kJ/gO_2 for the wood and 12.9 kJ/gO_2 for the plastic. In general, ΔH_{ox} is approximately 13 kJ/g O_2 for most fuels under various degrees of combustion completeness. Using these values, substitution into equation (6-4) from table 2-2 yields $\Delta H = 12.7 - 14.1$ kJ/g volatile fuel for sugar pine, and $\Delta H = 19.0$ kJ/g volatile fuel for polyurethane.

A second approach was to analyze the room as a combustion calorimeter utilizing the O_2 consumption method for determining ΔH. Based on the doorway outflow it can be shown that:

$$\Delta H = \frac{W_o \ \Delta H_{ox}}{\dot{m}_V} \int_{O}^{H_o-N} (0.23-Y_{ox}) \ \rho v \ dy \tag{6-5}$$

where the property profiles are assumed similar as

$$\frac{0.23 - Y_{ox}}{0.23 - Y_{ox,min}} = \frac{\rho v}{(\rho v)_{max}} = \left(\frac{y}{H_o - N}\right)^n \tag{6-6}$$

with y measured up from the neutral plane.

Since the outflow rate is

$$\dot{m}_{out} = W_o \int_0^{H_o-N} \rho v \, dy \tag{6-7}$$

it follows from equations (6-5) - (607) that

$$\Delta H = \left(\frac{n+1}{2n+1}\right)\left(0.23 - Y_{ox,min}\right) \frac{\dot{m}_{out}}{\dot{m}_V} \Delta H_{ox} \tag{6-8}$$

Values for $Y_{ox, min}$ (G1), $\dot{m}_{out}$, and $\dot{m}_v$ are derived from table 3-1. The profile factor, $\frac{n+1}{2n+1}$, was taken as 0.7 (which corresponds to n between 1/2 and 1), and a nominal value of $\Delta H_{ox} = 13$ kJ/g O_2 was used. The results are shown in figure 6-2 along with theoretical (complete combustion) values of $\Delta H_{PU} = 28$ kJ/g and $\Delta H_w = 17.7$ to 19.7 kJ/g. Except for the data point of P-3-1/2, the room calorimeter results appear credible.

The heat of combustion results are tabulated in table 6-3. In anticipation of the fact that the simulation model will yield an average upper layer temperature, which would be below actual room temperatures near the ceiling, somewhat maximum values were selected for ΔH in the modeling analysis. This would tend to compensate for the inherent inability of the model to predict the maximum room temperature.

Table 6-3

Effective Heat of Combustion Results

	Theoretical ΔH (kJ/g)	From Free Burns ΔH (kJ/g volatiles)	From Room Exp. ΔH (kJ/g volatiles)	Model ΔH (kK/g)
Sugar Pine	17.7-19.7	12.7 – 14.1	11 – 15.5	15.0
Polyurethane	28.0	19.0	14.5-26.0	23.0

6.3.2 Fire Induced Flow

Three phenomena of fire induced flows need be quantitatively described in the mathematical model. The first is flow due to pressure differences through enclosure openings. The theory of this is well developed; however, the definition and determination of flow coefficients needs to be established. This will be addressed. A second flow phenomena, not well quantified, is the mixing that occurs in the vicinity of openings as jets of fluid entrain on leaving and entering. Finally, flow induced by a fire plume can be predicted by several buoyant plume theories, but none truly predicts the correct fluid entrained near the base of the fire [16]. Moreover, no entrainment theory exists for crib fires. These relationships will be developed.

91
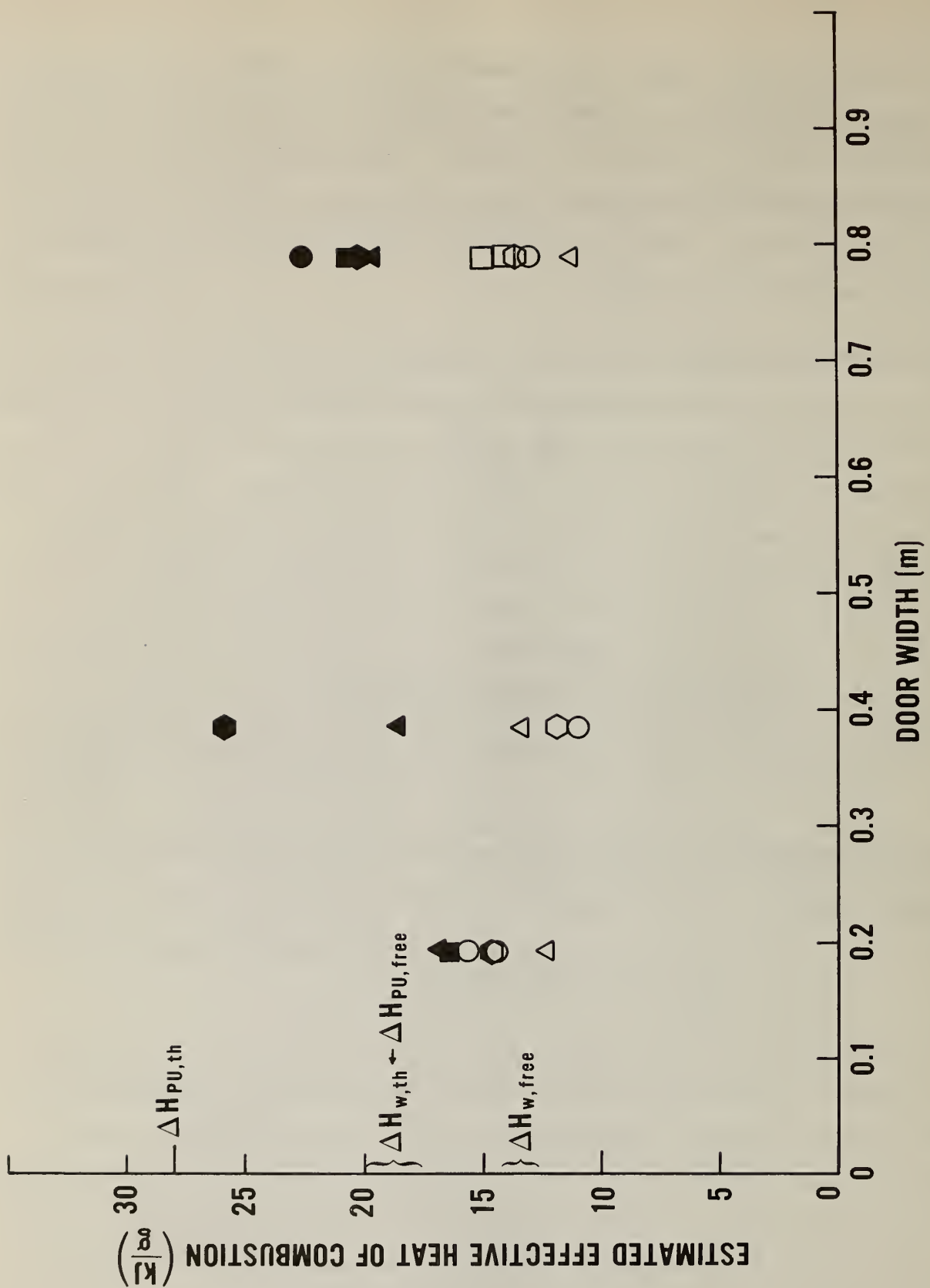
6.3.2.1 Doorway Flows

The doorway flow coefficients were determined in section 5. An average analytic expression was used in the modeling to represent the variation in coefficients with doorway width.

$$C_{out} = 0.68 \tag{6-9a}$$

$$C_{in} = 0.58 - 0.31 \, W_o \, (m) \tag{6-9b}$$

These coefficients were used in a two-layer flow model calculation.

For a two-layer model with a "warm" lower layer as shown in figure 6-1, the doorway flow can be determined by integrating the general equations [12]. The results follow:

$$\dot{m}_{out} = \frac{2}{3} \, C_{out} \, W_o \, \rho_a \sqrt{2g \left(\frac{T_a}{T_{g,u}} \right) \left(1 - \frac{T_a}{T_{g,u}} \right)} \; (H_o - N)^{3/2} \tag{6-10}$$

$$\dot{m}_{in} = \frac{2}{3} \, C_{in} \, W_o \, \rho_a \sqrt{2g} \left\{ \sqrt{1 - \frac{T_a}{T_{g,u}}} \; (N - D)^{3/2} + \frac{(a + bD)^{3/2} - a^{3/2}}{b} \right\} \tag{6-11a}$$

where $a = \left(1 - \dfrac{T_a}{T_{g,u}} \right) (N-D)$

$\quad\quad b = 1 - \dfrac{T_a}{T_{g,\ell}}$

By expanding equation (6-11a) about b = 0 for small b (and N-D not small)

$$\dot{m}_a \cong \frac{2}{3} \, C_{in} \, W_o \, \rho_a \sqrt{2g \left(1 - \frac{T_a}{T_{g,u}} \right)} \left\{ (N-D)^{1/2} (N + D/2) \right. \tag{6-11b}$$

$$\left. + \frac{3 \left(1 - T_a / T_{g,\ell} \right) D^2}{8 \left(1 - T_a / T_{g,u} \right) (N-D)^{1/2}} \right\}$$

The second term in the bracket is of the order of 5 percent of the first term. This second term was dropped in the following analysis, but equation (6-11b) was used in the simulation later.

By using the experimental values of N, D, (=D_T), $T_{g,u}$ (=$\bar{T}$) from table 3-1, and the C's from equation (6-9), the mass flow rates were calculated from equations (6-10) and (6-11a). The results are compared in figures 6-3a and 6-3b. Some anomalous results are derived from eq. (6-11a) in a few cases because measurements indicate that N was less than D. For these cases the computed flow was set equal to zero; also, the same comparison is made for inflow results in figure 6-4 with a constant value of C = 0.68 which is usually assumed. It appears that the variable C values derived for the inflow provide better theoretical results. But a general conclusion here must await a more complete study.

6.3.2.2 Mixing Model

Upon correction of the lower layer thermocouples (appendix B) or by direct reading of the small diameter thermocouple or aspirated probes, it was clear that mixing was occurring between the layers. This would increase the lower layer gas temperature and decrease its oxygen concentration by dilution with combustion products. The nature of this mixing is a turbulent shear entrainment that occurs as the cold air jet enters the doorway and diffuses downward. It has been observed previously [17], and a similar mixing phenomena also takes place, as a hot jet emerges from a doorway into another room impinging upon its ceiling. These entrainment phenomena are illustrated by the sketch in figure 6-5.

A model for this mixing process is proposed as follows:
The net rate of mass entrained $\dot{m}_e$ is given as:

$$\dot{m}_e = \rho_e \, A_e \, V_e \qquad (6\text{-}12)$$

where ρ_e is the density of the fluid entrained

A_e is an effective jet surface area

V_e is the velocity normal to the jet surface.

The entrainment velocity is assumed proportional to an average jet velocity (based on the mean doorway velocity) V:

$$V_e = k_m V \qquad (6\text{-}13)$$
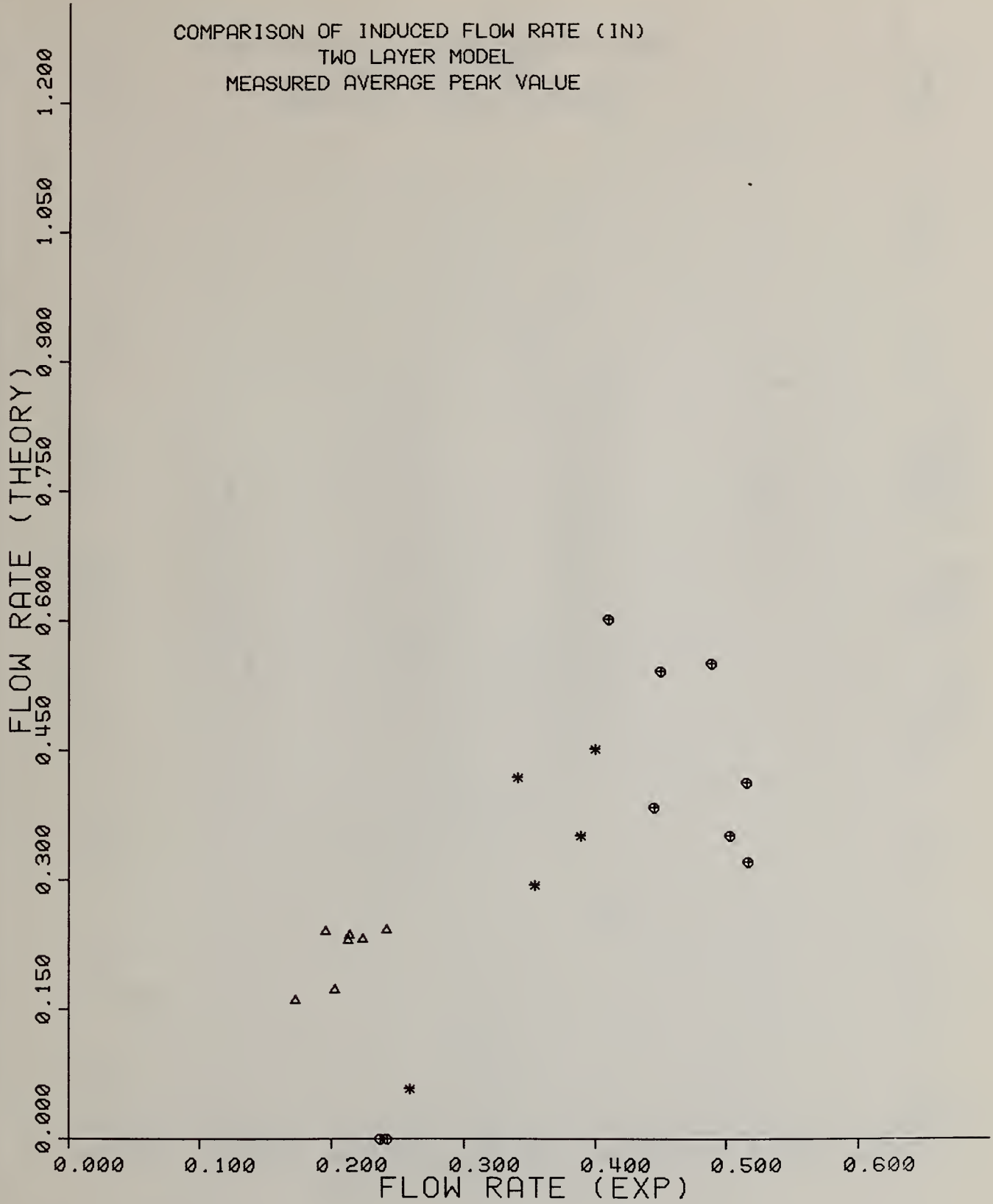
Figure 6-3a. Comparison of calculated and measured doorway inflow rates
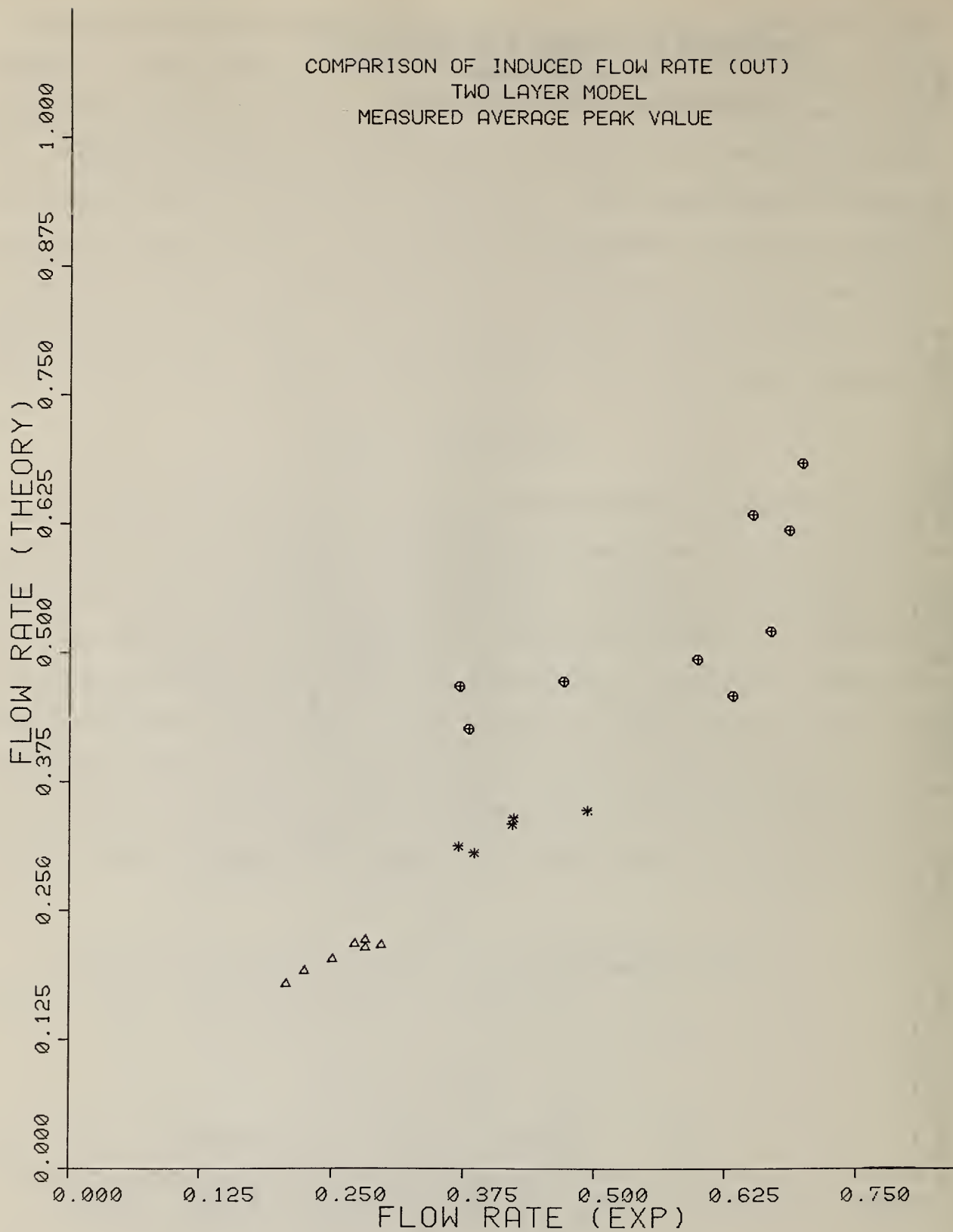
Figure 6-3b.   Comparison of calculated and measured doorway outflow
              rates

96
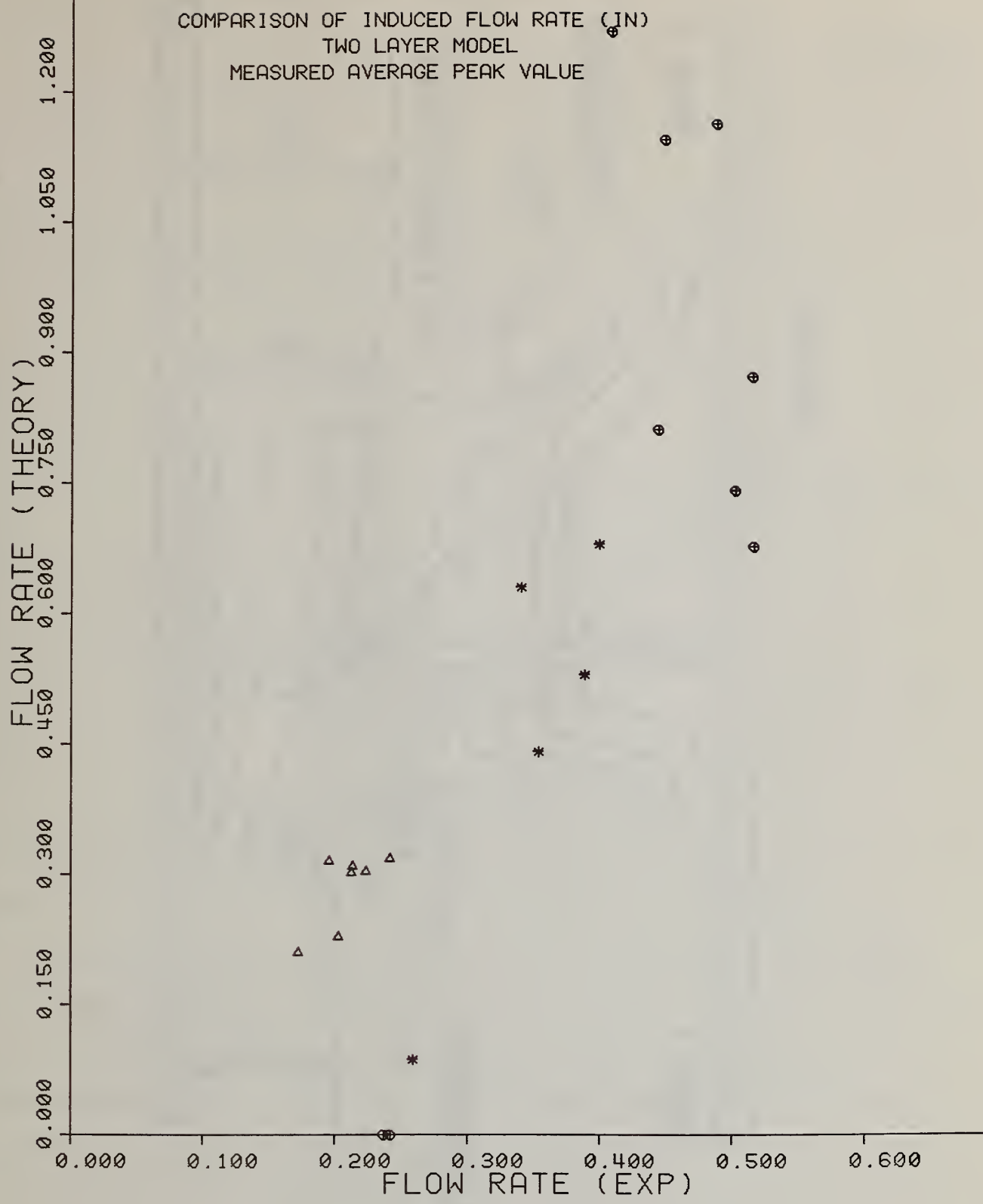
Figure 6-4. Comparison of calculated and measured doorway inflow rates in kg/s C_{in} = 0.68
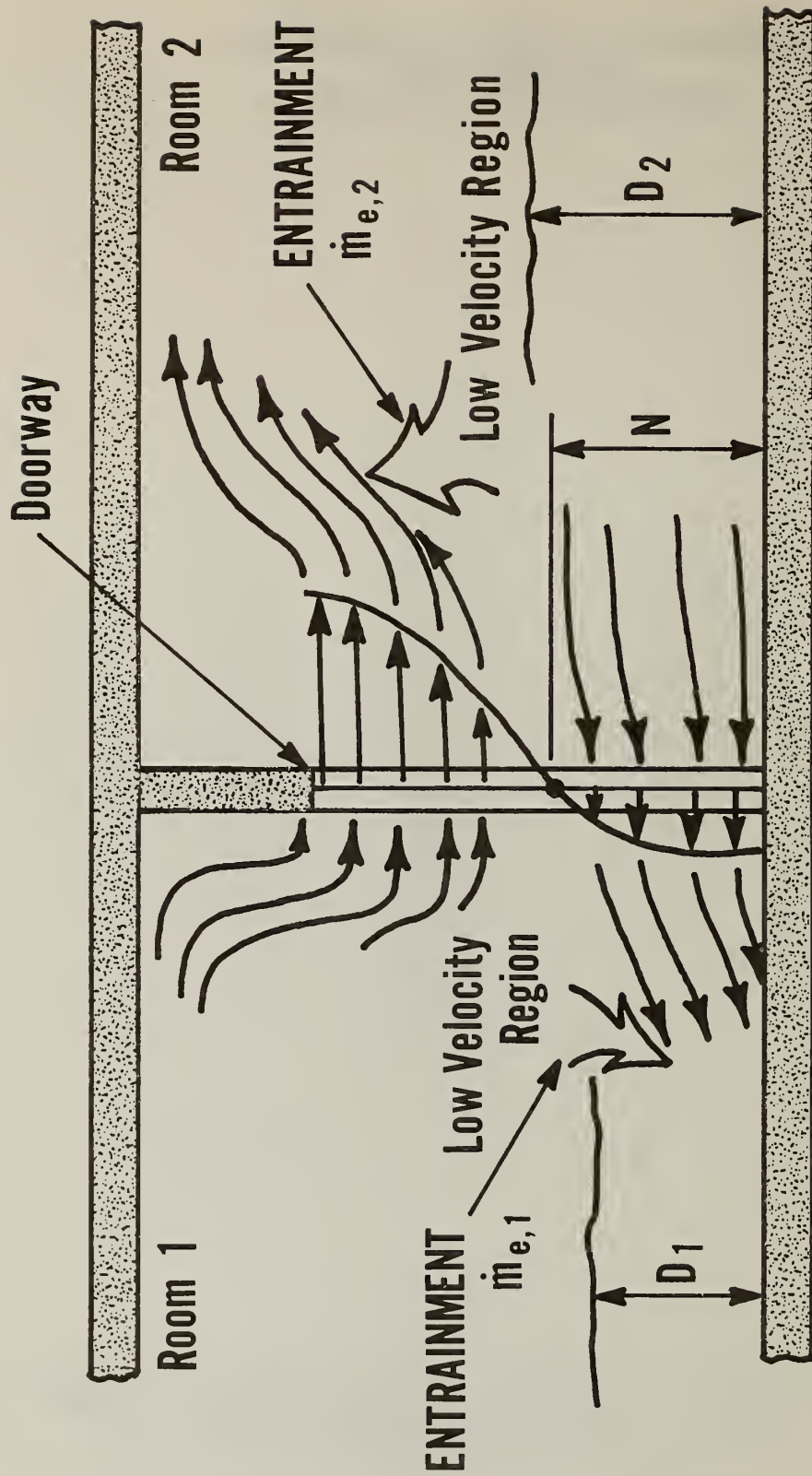
Figure 6-5. Entrainment concept

Also the doorway mass flow rate is given as

$$\dot{m}_{out} = \rho_{g,u} V_{out} W_o (H_o - N) \tag{6-14}$$

and

$$\dot{m}_{in} = \rho_a V_{in} W_o N \tag{6-15}$$

Also the jet surface area is assumed to be

$$A_e = \delta W \left(\frac{W}{W_o}\right)^{n-1} \tag{6-16a}$$

where $\delta = N - D_1$ for the inflow (D_1 and D_2 defined in fig. 6-5) $\tag{6-16b}$

and $\delta = D_2 - N$ for the outflow. $\tag{6-16c}$

$\left(\frac{W}{W_o}\right)^{n-1}$ is an empirical factor included to account for area changes in the

jet as it expands from the doorway into the corridor.

A $\delta \leq 0$ implies $\dot{m}_e = 0$.

Hence for the flow in

$$\dot{m}_{e,1} / \dot{m}_{in} = k_m \left(\frac{T_a}{T_{g,u}}\right) \left(\frac{N-D_1}{N}\right) \left(\frac{W}{W_o}\right)^n \tag{6-17}$$

and for the outflow

$$\dot{m}_{e,2} / \dot{m}_{out} = k_m \left(\frac{T_{g,u,2}}{T_a}\right) \left(\frac{D_2-N}{H_o-N}\right) \left(\frac{W}{W_o}\right)^n \tag{6-18}$$

Results (unpublished) for a room-corridor model indicated $k_m = 2$ and $n = 1/4$.

Equation (6-17) was applied to the current room fire experiments.

In order to apply equation (6-17) to see if it fits the current data, $\dot{m}_e$ had to be determined. It was not measured directly, but could be estimated from an energy balance on the lower layer provided a mean lower (and upper) layer temperature $T_{g,\ell}$ was known. The corrected value T22 was selected for $T_{g,\ell}$ (and $\bar{T}_{9, 10, 11}$ was used for $T_{g,u}$). A conservation of energy equation was written for the control volume shown in figure 6-6. The results yield the mixing ratio

$$\frac{\dot{m}_e}{\dot{m}_a} = \frac{T_{g,\ell} - T_a}{T_{g,u} - T_{g,\ell}} \tag{6-19}$$

99
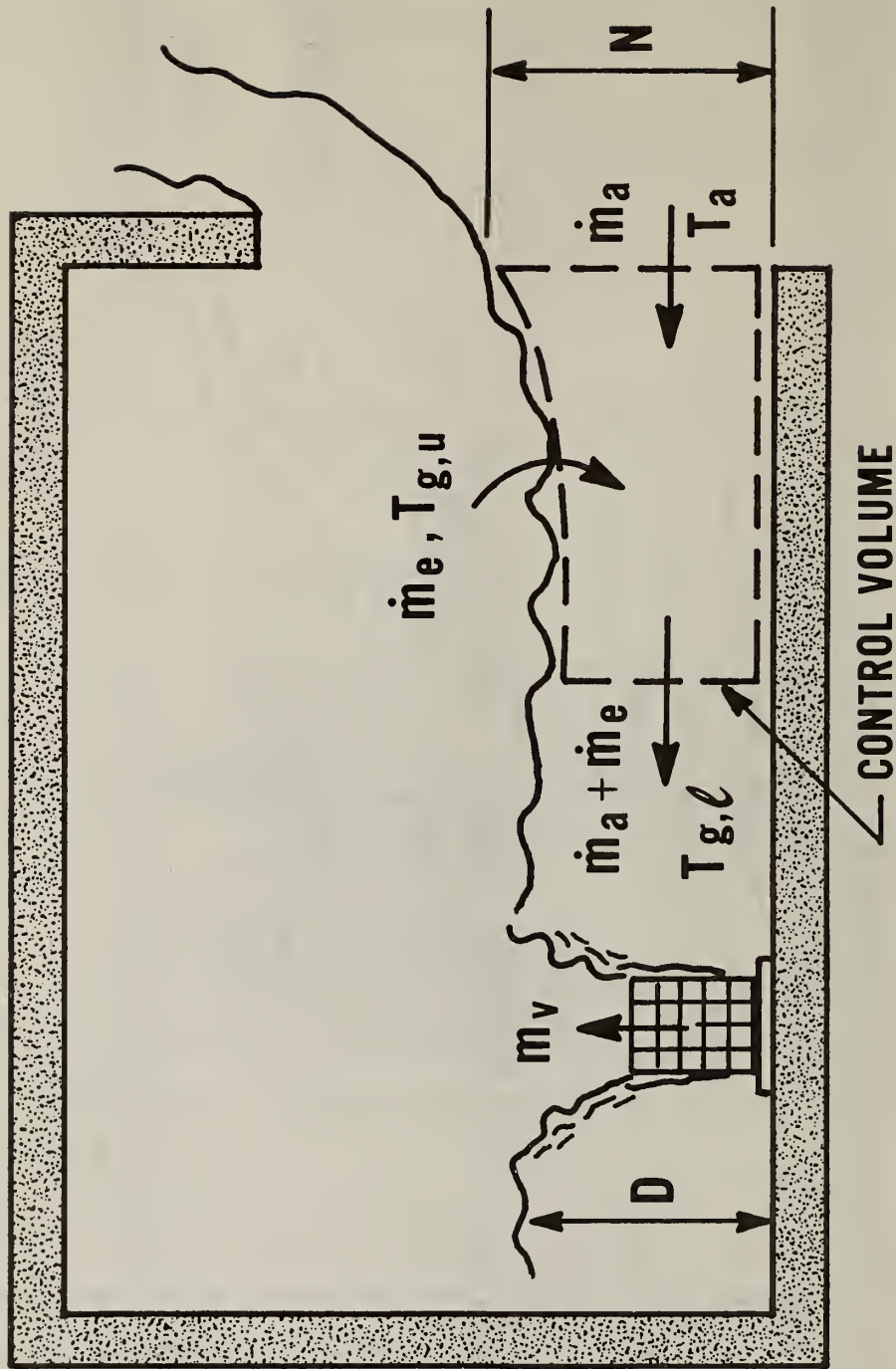
Figure 6-6. Analysis to determine $\dot{m}_e$ and the mixing coefficient, k_m
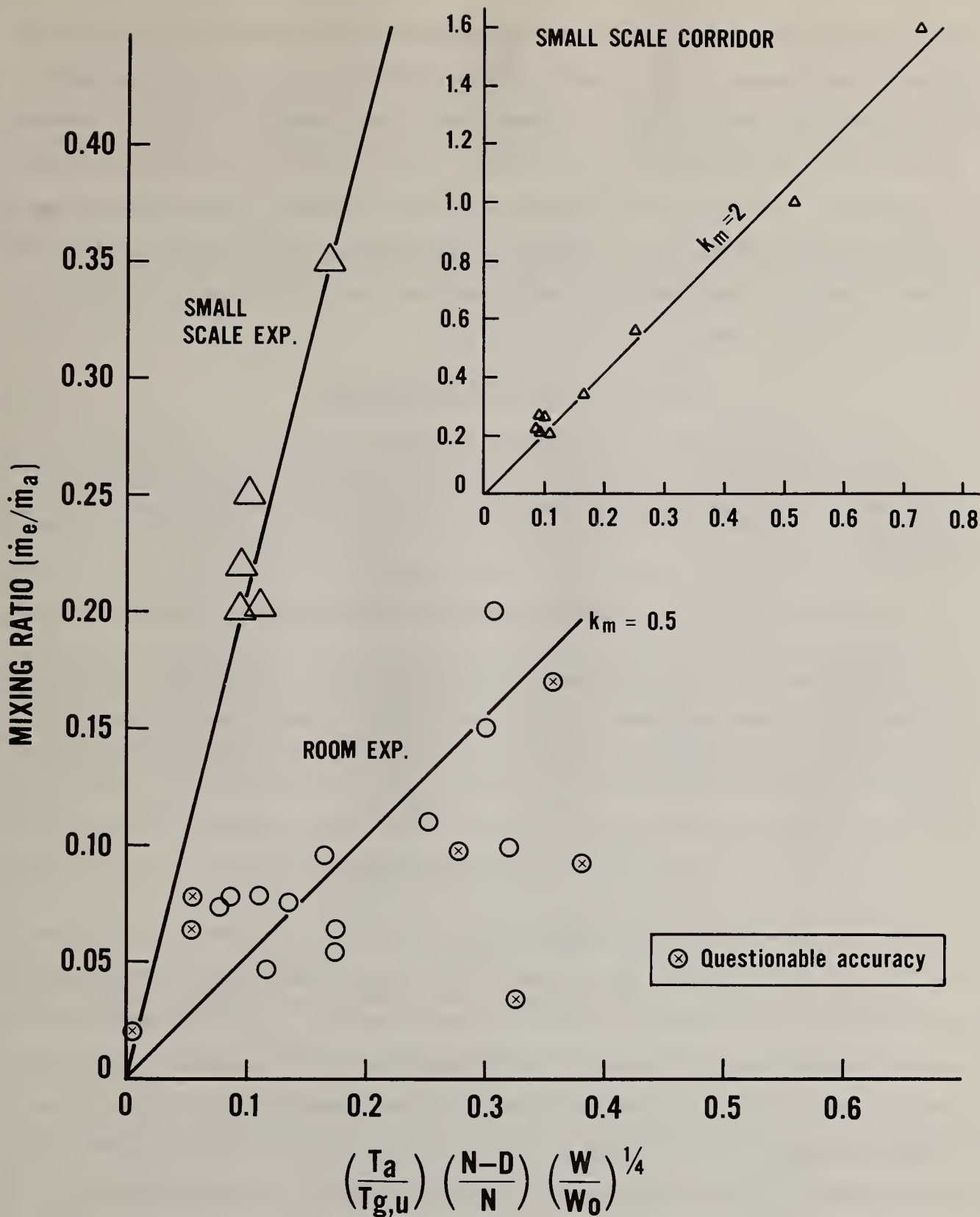
Figure 6-7.   Mixing correlation

101

The accuracy of this estimate for $\dot{m}_e$ could be of the order of $\pm$ 50 percent. Results correlated by equation (6-17) are plotted in figure 6-7 and data points of questionable value are indicated. The k_m was found to be 0.5 on average. It could be as high as one, but is not two as derived in the small-scale results also shown. It is not clear whether this discrepancy is due to inaccuracy in the estimate for $\dot{m}_e$, the offset corner doorway of our room, or an inadequate theory. The simulation model will use the mixing model given by equation (6-17) with k_m = 0.5 and n = 1/4.

6.3.2.3 Crib Fire Entrainment

The entrainment of air into the fire was viewed as being composed of two components: the contribution from the crib(s) plus that from the fire above the crib.

6.3.2.3.1 The Crib

The flow of air and combustion products through and around the crib was divided into three components: that through the four internal channels, the flow up the exterior sides of the crib, and third, the flow between adjacent cribs.

6.3.2.3.1.1 Internal Channels

A pressure probe/thermocouple P1V/T8 or P3D/T11 sensed the flow coming up through the channel. No systematic difference was noted for the temperature and velocity for different numbers of cribs burning. In calculating mass flow, it was assumed that the velocity is representative of an average across the cross section of the channel exit and further, that the flow through the flow monitored channel is the same as the flow through any of the four channels. The results for mean temperature, velocity and mass flow for the four experiments are found to be:

Table 6-4

Crib Channel Flow

	T (°C)	V (m/s)	ṁ/crib (kg/s)
Wood	874	3.15	0.0191
Polyurethane	741	2.72	0.0186

These mass flow rate results are consistent with the theory of Block [8] (appendix A).

6.3.2.3.1.2 Exterior Surfaces of Cribs

The exterior sides are those not adjacent to sides of another crib. For one crib there are four exterior sides, for two cribs there are three exterior sides for each crib, etc. Sensors (P4D/T10 and P3D/T11) were located at the top of the crib at various distances from the sides of the crib with a region where the flow was expected to be upward. The shape of the profile for those cases where more than one probe was present (one wood, one and two plastic) indicated that a laminar-like distribution of flow velocity would be adequate to describe the profile. That is, a two-constant parabolic fit was made for these data. The constants (Γ and δ) were further refined using the data for the remaining runs which had only a single probe in the exterior layer. The distribution is given as

$$V/\Gamma = \frac{y}{\delta} \left(1 - \frac{y}{\delta} \right)^2 \qquad (6-20)$$

with the constants Γ and δ tabulated in table 6-5.

Table 6-5

Crib Flow in Exterior Layer

	Γ (m/s)	δ (m)	$\bar{\bar{T}}$	ṁ/exterior perimeter (kg/s-m)
Wood	8.8	0.038	171	0.024
Polyurethane	18.1	0.074	504	0.051

The mass flow per unit length of exterior side was obtained by integrating the velocity profile assuming an average density from average temperature readings.

The boundary layer thickness, δ, are of the same order as those calculated from natural convection along a vertical hot plate.

6.3.2.3.1.3 Contiguous Surfaces

In a manner similar to 6.3.2.3.1.1, the average velocity and temperature were measured (P1V/T8 when not used in the channel) and flow rate calculated per intersection. One crib has no intersections, two have one, three have two, and four cribs have four intersections. The results are given in table 6-6.

Table 6-6

Flow Between Cribs

	T (°C)	V (m/s)	$\dot{m}$/intersection (kg/s)
Wood	624	1.1	0.0088
Polyurethane	926	2.8	0.014

The calculated flows to the top edge of the crib obtained by summarizing the three components:

$$\dot{m}_{crib} = \dot{m}_{channel} + \dot{m}_{exterior} + \dot{m}_{contiguous} \qquad (6-21)$$

are shown in table 6-7.

Table 6-7

Rate of Air Entrained Over Height of Crib

$\dot{m}_{crib}$ (kg/s)

Number of Cribs	Wood	Polyurethane
1	0.042	0.068
2	0.082	0.12
3	0.012	0.18
4	0.16	0.23

For the wood 45 to 50% of the flow comes through the interior channels, 30 to 55% from the exterior surfaces and the remaining 0 to 20% comes up through the contiguous intersections. For the plastic only 25 to 30% comes from the interior channels and 45 to 75% comes from exterior surfaces while the contiguous

104

surfaces account for about the same percentage as the wood.

The flow was found to be proportional to burning rate

$$\dot{m}_{crib} = 8 \cdot \dot{m}_b \qquad (6\text{-}22)$$

A more exact expression given in terms of potential heat release $\dot{Q}$ (using ΔH of 15.6 kW/g/s for wood and 22 kW/g/s for plastic) is

$$\dot{m}_{crib} = 0.0022 \, \dot{Q}^{0.7} \qquad (6\text{-}23)$$

where $\dot{Q}$ is in kW and $\dot{m}_b$ in kg/s.

6.3.2.3.2 Fire Plume

Pressure probes and thermocouples were located on the centerline above the crib up to a height of four times the crib height. Also, a rake of instruments was located at one crib height above the crib in order to obtain the transverse distribution. Figure 6-8 presents results of centerline velocity and temperature during the steady peak burning period. Velocity is normalized by the nominal heat release rate raised to the 1/5 power and the height above the top surface of the crib, z, is normalized by $\dot{Q}^{2/5}$. This scaling comes from a study [18] of diffusion flames above a gas burner and the results of that study are shown by solid lines. Although exhibiting considerable scatter the trend of the data in general is consistent with the gas burner results. The temperatures are lower than those of the burner, but this will not significantly affect entrainment since its dependence on temperature is weak.

Included on the figure is a dimensionless parameter, $V/\sqrt{2g \, z \, \Delta T/T_o}$, which is the ratio of the measured velocity to a buoyancy generated velocity due solely to a temperature difference. The line is the burner result and again the crib data exhibit similar results to the burner. The fire plume above the crib appears to be consistent with the results of the gas burner even though the behavior at z = 0 is different in the two cases. The velocity of the gases leaving the burner surface is negligible compared to the velocity of the gases through the crib channels and sides.

105
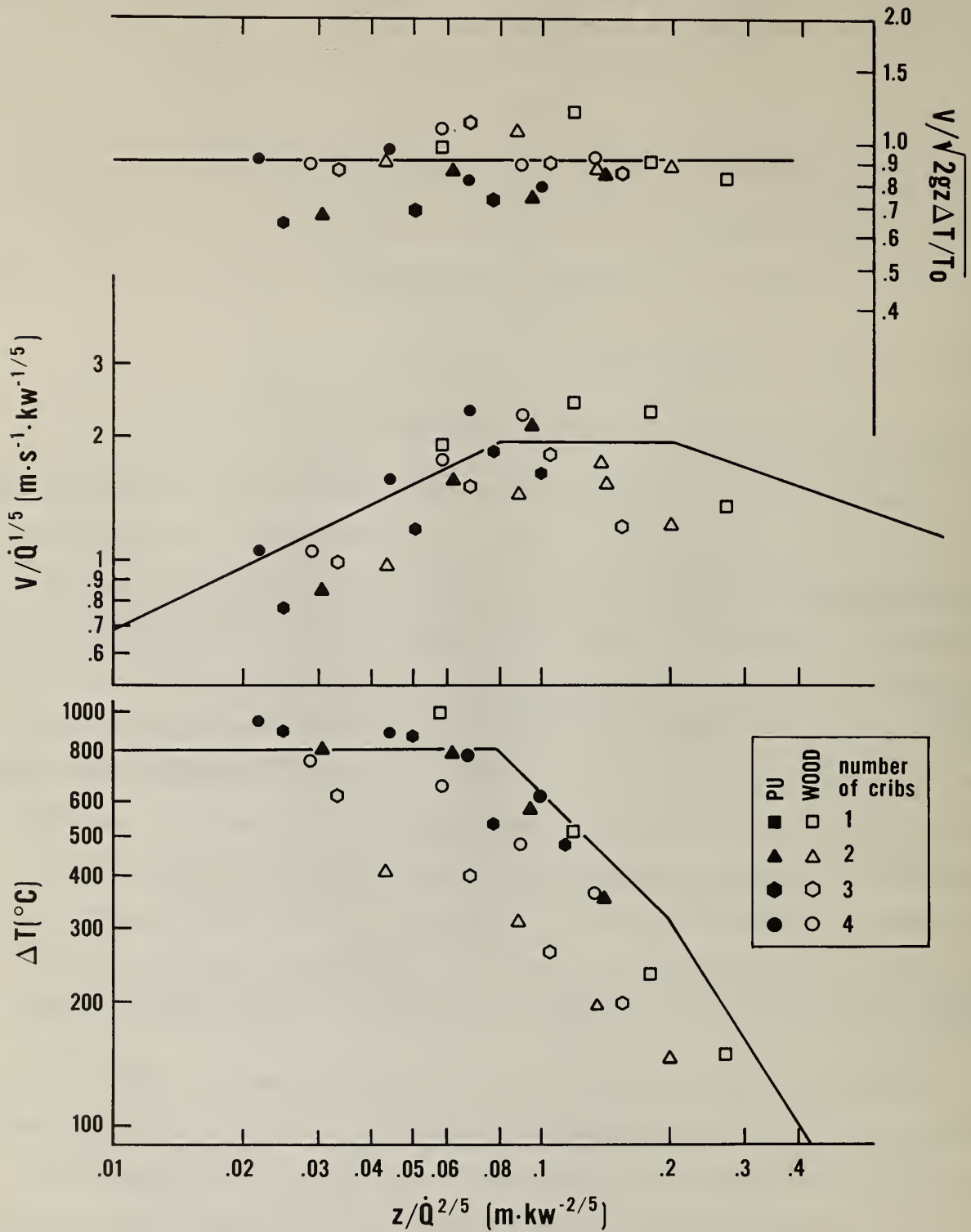
Figure 6-8. Crib fire plume velocity and temperature correlations

106

Results in the radial direction (data not shown) indicate that the transverse scaling developed in the gas burner study was also adequate for predicting the behavior of the fire plume above the cribs. From that report [18] the near field approximation for fire plume entrainment is

$$\dot{m}_{\text{fire plume}} = 0.55 \ z \ \dot{Q}^{1/2} \text{ in kg/s} \tag{6-24}$$

where z is the height above the top of the crib (in m) and $\dot{Q}$ is the nominal heat release rate in kW.

6.3.2.3.3 Results

Combining the two expressions for crib and plume entrainment yields

$$\dot{m}_p = 0.0022 \ \dot{Q}^{0.7} + 0.055 \ \dot{Q}^{0.5} \ [D-0.53] \tag{6-25a}$$

or approximately from eq. (6-22),

$$\dot{m}_p = 8.\dot{m}_b + 0.055 \ \dot{Q}^{0.5} \ [D-0.53] \tag{6-25b}$$

where D (m) is the height of the thermal discontinuity in the room. Also, the crib is 0.35 m high and sits on weighing platform 0.18 m above the floor, hence z = D - 0.53 m. Entrainment by the fire plume is envisioned to occur over the distance from the top of the crib to the thermal discontinuity D.

Figure 6-9 shows the derived entrainment expression, labeled $\dot{m}_{\text{predicted}}$, against the measured flow through the door, $\dot{m}_{\text{measured}}$. The abscissa is the mean of the two flows $\dot{m}_{\text{out}}$ and $\dot{m}_{\text{in}} + \dot{m}_b$. The ordinate requires the heat release rate and the height of the thermal discontinuity. A 45° line is provided for comparing the two results. The agreement is generally within ± 0.25 percent. For those data with D ≤ 0.53 m for large fires and small doors, the agreement as expected is poor. The thermal discontinuity is approaching and falling below the top of the crib thereby cutting off the entrainment of the fire plume. Those points then will show only what the crib contributes to entrainment about one half to somewhat more than one half of the measured flow. In reality the fire plume will entrain from a region around the fire

107

$$\dot{m}_{\text{PREDICTED}} = .0022\,\dot{Q}^{0.7} + .055\,\dot{Q}^{0.5}\,(D-.53)$$

$$\dot{m}_{\text{MEASURED}} = (\dot{m}_b + \dot{m}_{\text{IN}} + \dot{m}_{\text{OUT}})/2$$
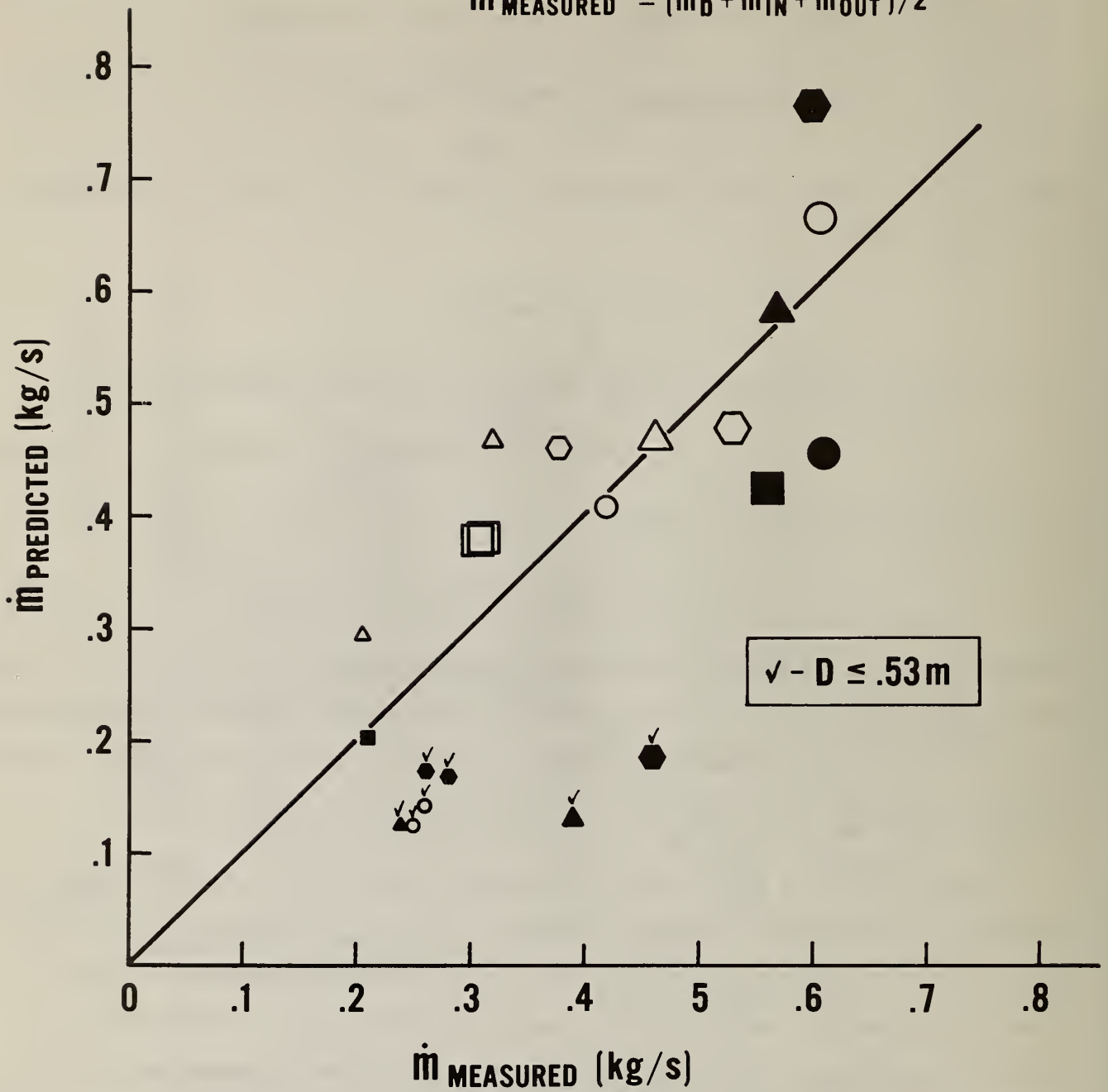
Figure 6-9. Comparison of calculated and measured entrained flow by the fire plume in the room experiments

108

up beyond the thermal discontinuity and an account of this can be incorporated into the model.

6.3.3 Species Concentration

In both the upper and lower layer it is important, for many reasons, to know the concentration of various gaseous and particulate (soot) concentrations. Carbon dioxide, H_2O, and soot are needed to predict the absorption-emission properties of the gases. Oxygen and CO are significant with respect to toxicity, and "smoke" particulate concentration determines obscuration. Some expressions for calculating these concentrations in the upper and lower layer will be derived and applied in the forthcoming analyses.

A conservation of species mass will be made for the upper layer including the combustion plume (CV_I), and the lower layer (CV_{II}). This is shown in figure 6-10. The mass concentrations of species i are assumed uniform in the upper ($Y_{i,u}$) and lower ($Y_{i,\ell}$) layers.

In general, the conservation equation is

$$\frac{d}{dt} \iiint_V \rho Y_i \, dV + \iint_S \rho Y_i (\vec{V} - \vec{W}) \cdot \hat{n} \, dS = Y_i \qquad (6\text{-}26a)$$

where Y_i is the net rate of production of specie i.

For steady-state and Y_i uniform in the control volume,

$$\sum_{j, \text{net out}} (Y_i \dot{m})_j = Y_i \qquad (6\text{-}26b)$$

Specific application to CV_I (fig. 6-10) yields:

$$(\dot{m}_a + \dot{m}_v + \dot{m}_e) Y_{i,u} - (\dot{m}_e + \dot{m}_a) Y_{i,\ell} = (-1)^m \frac{\nu_i}{\nu_f} \frac{M_i}{M_f} \frac{\dot{m}_b}{(1-\omega)} \qquad (6\text{-}27)$$

where ν_i is the stoichiometric coefficient of i (m = 1, i = reactant; m = -2, i = a product)

ν_f is the stoichiometric coefficient of the fuel (solid)

M_i is the molecular weight of i

M_f is the molecular weight of the fuel (solid)

$\dot{m}_b$ is the rate of volatile fuel reacted within CV_I

$1-\omega$ is the ratio of volatile fuel produced to solid fuel burned
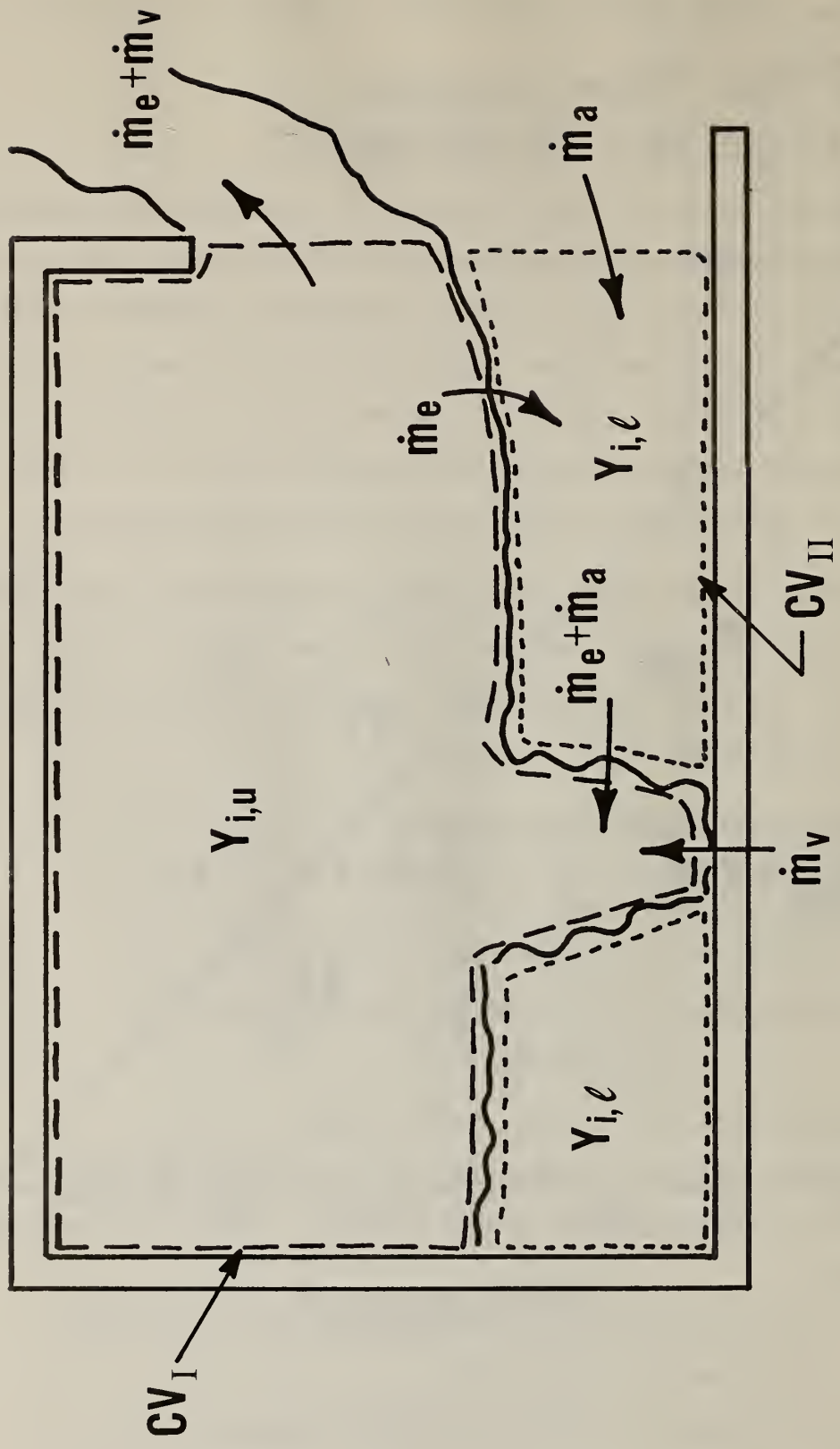
Figure 6-10. Conservation of species in upper and lower layers

and
$$\dot{m}_b = \begin{cases} \dot{m}_v ' & r \leq \dot{m}_a/\dot{m}_v \\ \dfrac{\dot{m}_a}{r} , & r > \dot{m}_a/\dot{m}_v \end{cases} \qquad (6\text{-}28)$$

For the lower layer, where no generation is considered,

$$(\dot{m}_e + \dot{m}_a)\, Y_{i,\ell} - \dot{m}_e\, Y_{i,u} - \dot{m}_a\, Y_{i,u} - \dot{m}_a\, Y_{i,a} = 0 \qquad (6\text{-}29)$$

Also the volume or mole fraction (X_i) can be estimated from

$$X_i = \frac{29\, Y_i}{M_i} \qquad (6\text{-}30)$$

where a mean mixture molecular weight of 29 is used. Some special results will be considered.

For $i = CO_2$ and H_2O, $Y_{i,a} = 0$ and subtracting equation (6-29) from (6-27) yields

$$Y_{i,u} = \left(\frac{\nu_i\, M_i}{\nu_f\, M_f}\right) \left(\frac{\dot{m}_b}{1-\omega}\right) \Big/ \left(\dot{m}_a + \dot{m}_v\right) \qquad (6\text{-}31)$$

Substituting the stoichiometric coefficients from the chemical equations in 6.3.1 and the values in table 3-1 into equation (6-31) for CO_2 yielded the comparison shown in figure 6-11. The corrections discussed in 5.8 were not accounted for in the doorway CO_2 values.

For $i = O_2$, $Y_{i,a} = 0.23$ and similarly

$$Y_{i,u} = \frac{0.23\, \dot{m}_a - \left(\dfrac{\nu_i\, M_i}{\nu_f\, M_f}\right) \left(\dfrac{\dot{m}_b}{1-\omega}\right)}{\dot{m}_a + \dot{m}_v} \qquad (6\text{-}32a)$$

It should be noted that the stoichiometric air to volatile fuel mass ratio

$$r = \frac{\nu_{O_2}\, M_{O_2}/0.23}{\nu_f M_f\,(1-\omega)}$$

Thus

$$Y_{O_2,u} = \frac{0.23\left[1 - r\,\dot{m}_b/\dot{m}_a\right]}{1 + (\dot{m}_v/\dot{m}_a)} \qquad (6\text{-}32b)$$

111

For the lower layer, from equation (6-29)

$$Y_{0_{2,\ell}} = \frac{0.23 + (\dot{m}_e/\dot{m}_a) \; Y_{0_{2,u}}}{1 + (\dot{m}_e/\dot{m}_a)}$$ (6-33)

Similar analysis can be applied to other components of interest for which chemical information exists. The level of accuracy depends on the assumed stoichiometry, the model, and, of course, the interpretation of the measured value. The extent of agreement shown in figure 6-11 is a good measure of the anticipated accuracy for this (sub)model.

6.3.4 Crib Fire Radiation

A comparison of the free burn and room burn radiation field as shown in figure 5-20 suggests that a significant amount of radiant energy is transferred directly from the crib fire in the room experiments. Hence, a model is needed to predict this flux field. Ultimately in the room fire simulation model the incident floor flux will be calculated as the super position of the room upper layer contribution plus the crib fire flux. The crib fire model will not account for distortions in flame shape due to the room geometry. The flame heights did not vary greatly with crib loading and did not impinge on the ceiling in this study.

The mathematical model selected is based on the analysis of Dayan and Tien [19] for a cylindrical grey flame (figure 6-12). The crib and flames above will be represented by an equivalent cylinder of radius

$$r_c = \sqrt{\frac{A_{o,T}}{\pi}}$$ (6-34a)

where $A_{o,T}$ is the projected top surface area of the cribs

$$A_{o,T} = n_c \ell^2 + a_{g,T} \; G_T(n_c)$$ (6-34b)

where $G_T(n_c)$ are the number of gaps for n_c cribs and $a_{g,T}$ the gap area = 0.245 x 0.07 m^2. The height of the cylinder is the sum of the crib height plus flame length above it. The analysis by Dayan and Tien yielded the

112
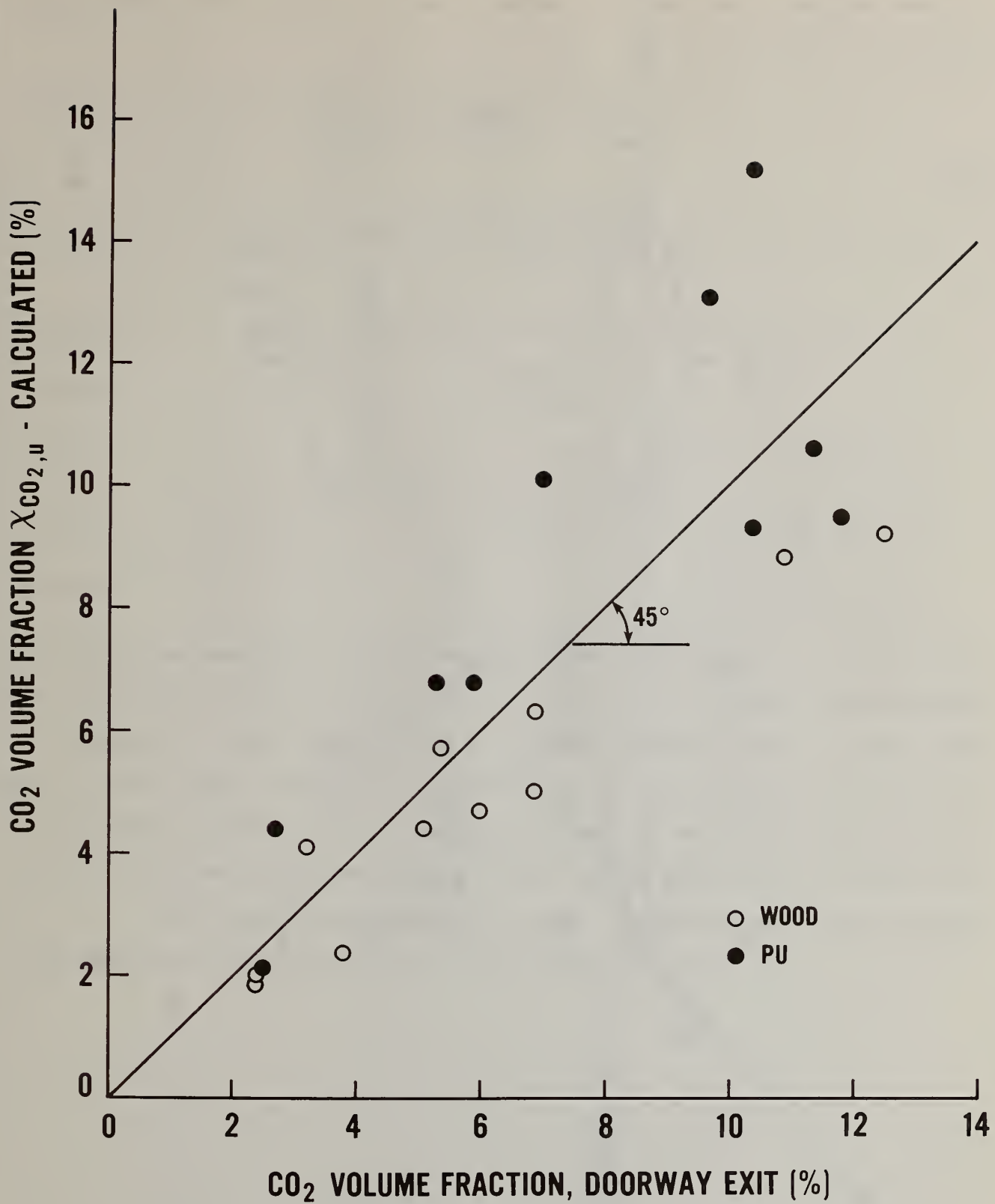
Figure 6-11. Comparison of calculated and measured doorway CO_2 concentrations

113

incident radiant flame flux to a target element dA with a unit normal vector
$\hat{n} = u\hat{i} + v\hat{j} + w\hat{k}$ for $L/r_c \geq 3$

$$\dot{q}'' = \sigma \, T_f^4 \, (\alpha_1 F_1 + \alpha_2 F_2 + \alpha_3 F_3) \qquad (6\text{-}35a)$$

where

$$\alpha_1 = (1 - \frac{2}{\mu^2}) + 2e^{-\mu} \, (\frac{1}{\mu} + \frac{1}{\mu^2}) \cong 1 - e^{-0.7\mu}, \; 0 \leq \mu \leq 1.2 \qquad (6\text{-}35b)$$

$$\alpha_2 = \alpha_3 = \pi \, [I_1(\mu) - L_1(\mu)] \cong 1 - e^{-1.9\mu}, \; 0 = \mu \leq 0.6 \qquad (6\text{-}35c)$$

$$\mu = \frac{2 \, r_c k_f}{\sin \beta} \qquad (6\text{-}35d)$$

$$F_1 = \frac{1}{4\pi} \, (\frac{r_c}{L})^2 \, (\pi - 2\Theta_o + \sin 2\Theta_o) . u \qquad (6\text{-}35e)$$

$$F_2 = \frac{1}{2\pi} \, (\frac{r_c}{L}) \, (\pi - 2\Theta_o + \sin 2\Theta_o) . v \qquad (6\text{-}35f)$$

$$F_3 = \frac{1}{\pi} \, (\frac{r_c}{L}) \, \cos^2 \Theta_o . w \qquad (6\text{-}35g)$$

with k_f and T_f an effective absorption coefficient and flame temperature respectively. Since the crib fire is a hybrid of hot sticks and flame, k_f and T_f are not truly representative of a homogeneous flame. A somewhat arbitrary but suitable process was selected to determine these values. The k_f was selected from the available and appropriate literature results, and the "best" T_f to make the model results agree with measurements R1 for one and four cribs was determined. This is summarized in table 6-8.
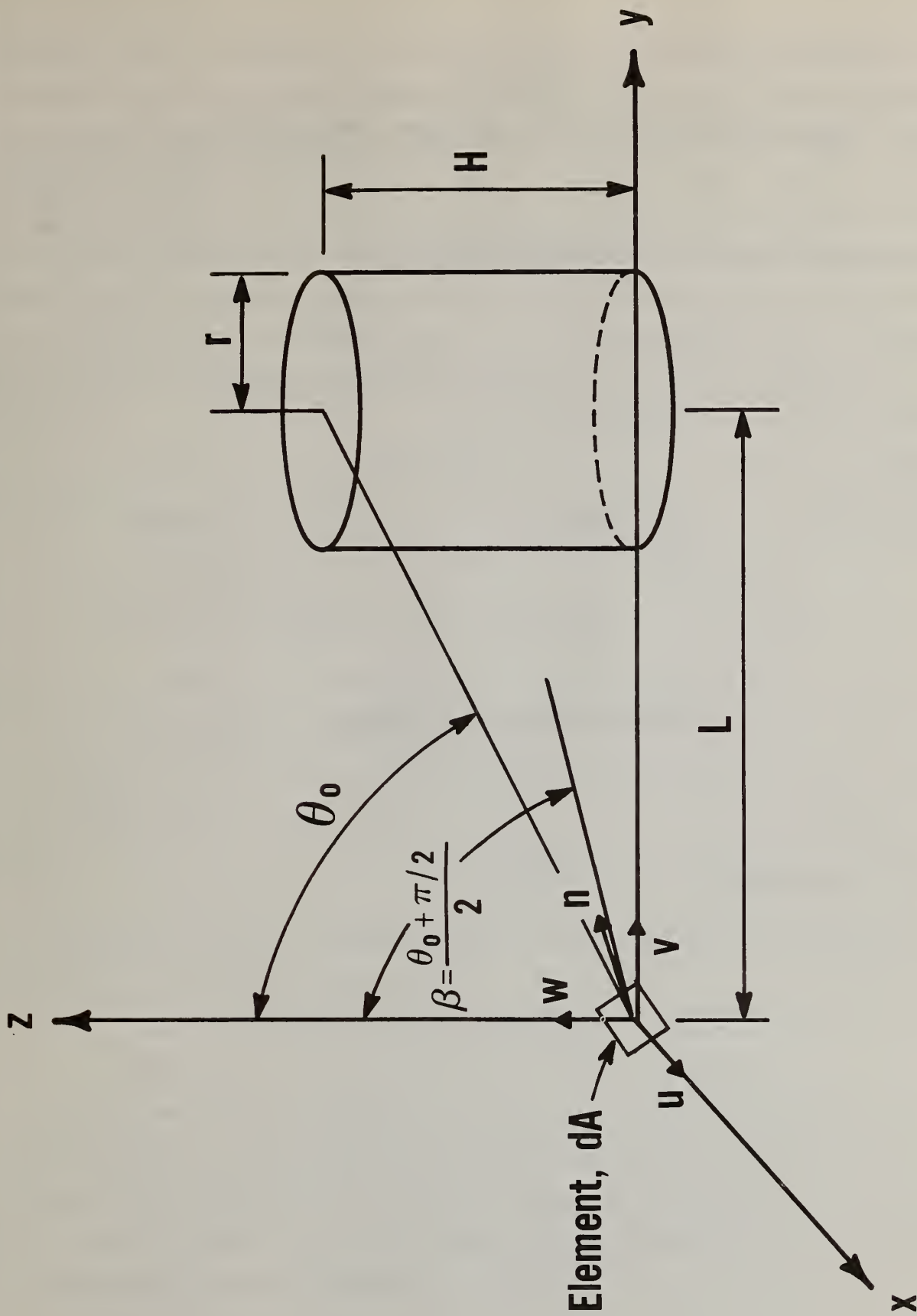
Figure 6-12. Cylindrical flame model of Dayan and Tien [19]

Table 6-8

Absorption Coefficient and Flame Temperature

	Literature Value		
Source	Material	k_f (m^{-1})	T_f (K)
Markstein [20]	Polyurethane foam, pool fire	1.28 ± 0.17	1408 ± 12
Hagglund and Persson [21]	Flames above wood crib fires of thickness 0.2 to 2 m	0.75 - 1.3	873 - 1303

	Modeling Values for Cribs	
Crib Material	k_f (m^{-1})	T_f (K)
Rigid Polyurethane	1.3	1200
Sugar Pine	0.8	1100

Equation (6-35) was applied to the free burn experiments to calculate the incident flux at the sensor locations shown in figure 4-1. The theoretical results are compared to the measured values in figure 6-13. These results indicate the degree of accuracy of this cylindrical flame model.

Another parameter needed in the simulation model is the fraction of total energy release from the fire plume that is radiation. In a room, this energy will be transported to all portions of the room and intermediary absorbing gases. For the model considered, the total radiation energy rate would be

$$\dot{q}_f = A_f \epsilon_f \alpha \ T_f^4 \qquad (6-36)$$

where A_f is the total surface area, $2\pi \ r_c \ (H + r_c)$

$\qquad \epsilon_f$ is the emissivity, $1 - e^{-L_m k_f}$

$\qquad \qquad$ with $L_m = \dfrac{3.6 \ \text{Volume}}{\text{Area}} = 1.8 \ \dfrac{1}{1/r_c + 1/H}$

and

$\qquad \sigma$ is the Stephen-Boltzmann constant.

For the values selected previously for k_f and T_f (table 6-8) and H (table 4-3), it was found that the fraction, f

where $\qquad \qquad \qquad \qquad \qquad \qquad f \equiv \dfrac{\dot{q}_f}{\dot{m}_b \Delta H} \qquad \qquad \qquad (6-37)$

is 0.16 to 0.20 with an average of 0.18 for wood, and 0.20 to 0.27 with an average of 0.22 for the polyurethane.

6.3.5 Room Heat Transfer

In this section the room heat transfer processes will be formulated. The radiative transport and upper layer emissivity will be defined, convection heat transfer to the ceiling will be based on existing correlations, and an approximate wall conductive model will be utilized. These relationships will be verified by comparison with the experimental results.
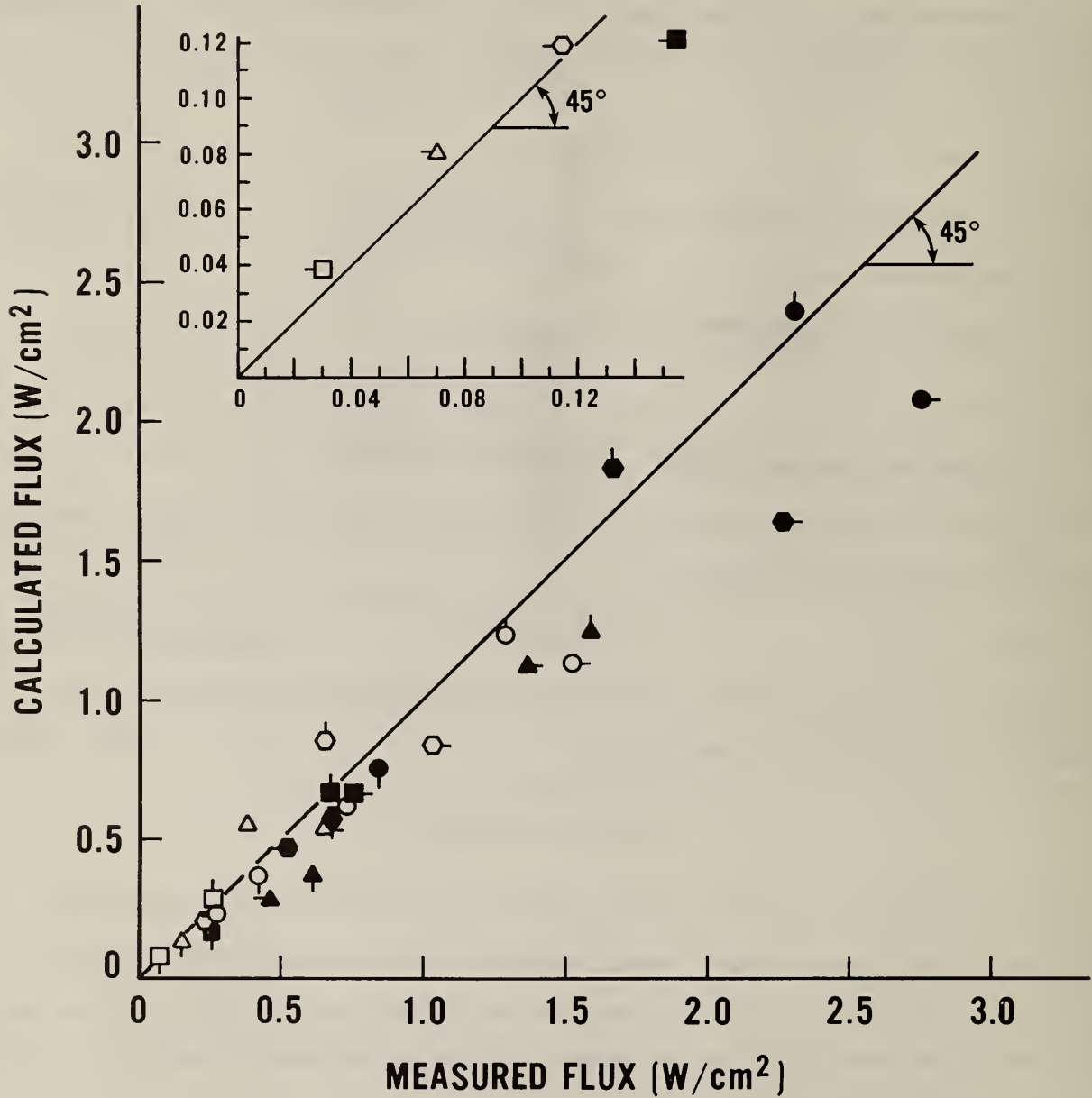
Figure 6-13. Comparison of calculated and measured free burn radiative incident target fluxes

6.3.5.1 Upper Layer Emissivity

Fundamentally the emissivity (absorptivity) of the layer gases can be calculated provided their composition, Y_{H_2O}, Y_{CO_2}, and Y_{soot}, are known. The soot concentration was not measured in these experiments. However, it can be estimated that the fraction of soot produced per mass of fuel decomposed (β) is roughly 0.01 for wood and 0.05 for most plastics. With this estimate and the calculation code developed by Modak [20], the upper layer emissivity was determined. But since this calculation relies on an estimate for β, an empirical approach was taken, for computational convenience, that yielded comparable values.

Modak's calculation is given functionally below

$$\varepsilon_{MODAK} = \varepsilon_{MODAK} \ (X_{H_2O}, \ X_{CO_2}, \ X_{soot}, \ L_m, \ T_g) \qquad (6\text{-}38)$$

The volume fractions were determined from equation (6-31) for H_2O and CO_2, and

$$X_{soot} = \beta \left(\frac{\rho_g}{\rho_{soot}} \right) \left(\frac{\dot{m}_v}{\dot{m}_a + \dot{m}_v} \right) \qquad (6\text{-}39)$$

where ρ_g is the density of the upper layer $= \rho_a T_a / \bar{T}$

and ρ_{soot} is the density of soot, estimated as $2 \ g/cm^3$. The path length L_m was taken for this calculation as 4 (layer volume/surface area) or

$$L_m = \frac{2 \ WL \ (H\text{-}D)}{(H\text{-}D) \ (W+L) \ + \ WL} \qquad (6\text{-}40)$$

and T_g the bulk upper layer temperature was taken as $\bar{T}$ from table 3-1.

The empirical method is based on the assumption of a grey gas with a bulk representative absorbing-emitting specie concentration proportional to $\dot{m}_v / (\dot{m}_a + \dot{m}_v)$. And since the spectral absorption coefficient is proportional to concentration, it is assumed that

$$k_g = \frac{[\dot{m}_v / \ (\dot{m}_v + \dot{m}_a)]}{[\dot{m}_v / (\dot{m}_v + \dot{m}_a)]_{flame}} \ k_f \qquad (6\text{-}41a)$$

119

where the flame specie concentration factor is

$$\left(\frac{\dot{m}_v}{\dot{m}_v + \dot{m}_a}\right)_{flame} = \frac{1}{x_a r + 1} \tag{6-41b}$$

with x_a the fraction of stoichiometric air required by the flame. Literature results suggest that x_a may be as high as 20. It seemed that $x_a = 1$, i.e., a stoichiometric flame, yielded satisfactory agreement between ε_{MODAK} and

$$\varepsilon_{APPROX} = 1 - e^{-k_g L_m} \tag{6-42}$$

This comparison is shown in figure 6-14. Although a better fit could have been achieved by a slightly larger value of x_a, it was not done since the certainty of β is questionable in the alternative analysis. Equation (6-41) and (6-42) will be used in the simulation model.

6.3.5.2 Radiative Flux to Floor Target

The incident radiative flux to the floor sensor H2 is the sum of the flame and upper layer contribution.

$$\dot{q}''_{r,2} = \dot{q}''_{r,\, layer} + \dot{q}''_{r,\, flame} \tag{6-43}$$

From section 6.3.4 the flame flux is given as

$$\dot{q}''_{r,\, flame} = \alpha_3 F_3 \sigma T_f^4 \tag{6-44a}$$

with $L = 0.906$ m and $H = H_f + H_c$. H_c is the crib height, 0.35 m, and H_f is an average flame height above the crib based on the free burns.

$$H_f = \begin{cases} 0.63 \text{ m, wood} \\ 0.87 \text{ m, polyurethane} \end{cases} \tag{6-44b}$$

The layer contribution is based on the analysis of Modak and Matthews [23]. It is given as the sum of contributions from four layer sectors shown in figure 6-15.

$$\dot{q}''_{r,\, layer} = \sum_{i=1}^{4} \dot{q}''_i \tag{6-45a}$$

120
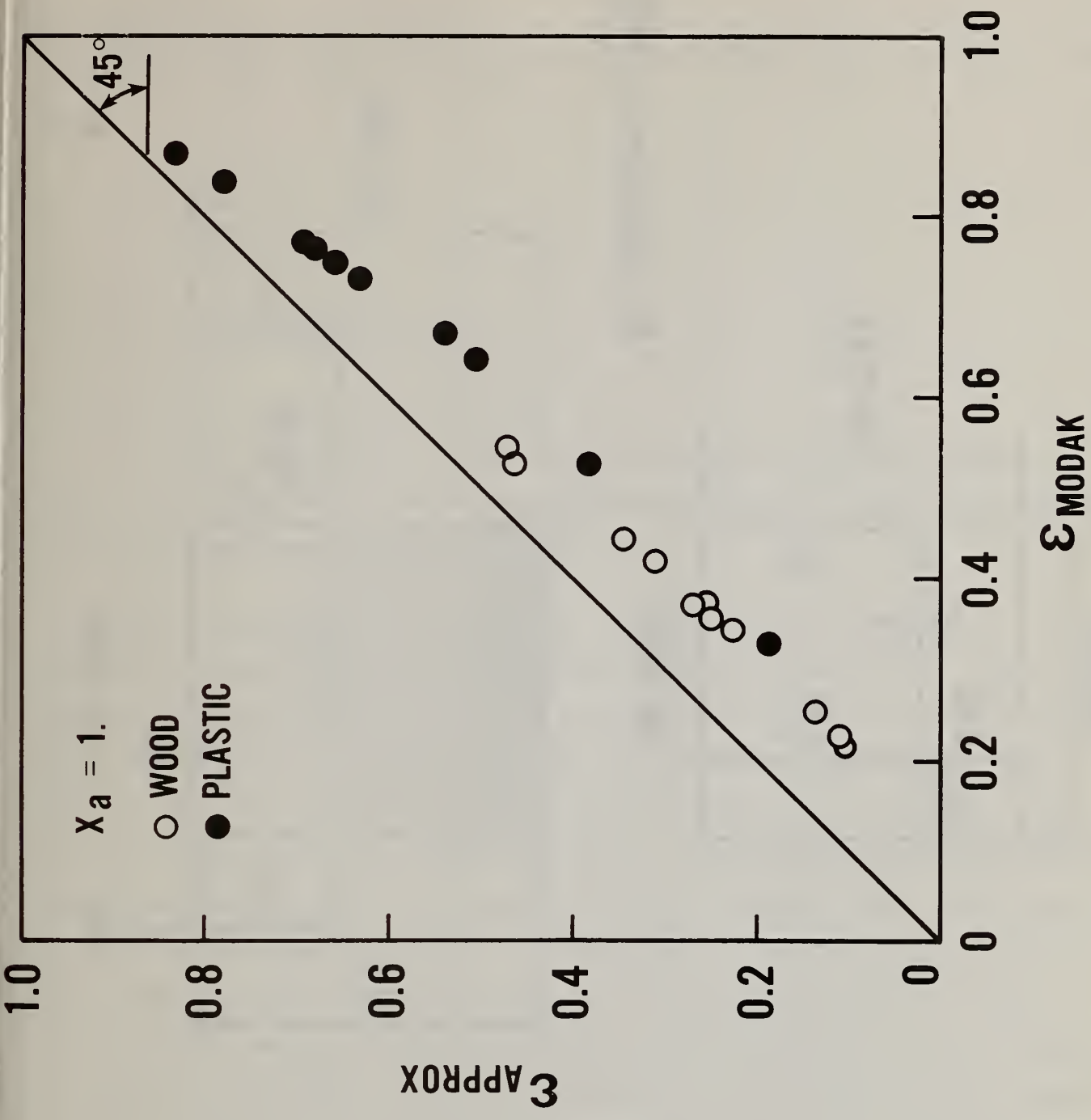
Figure 6-14. Comparison of empirically calculated layer emissivity with Modak's [22] method

121
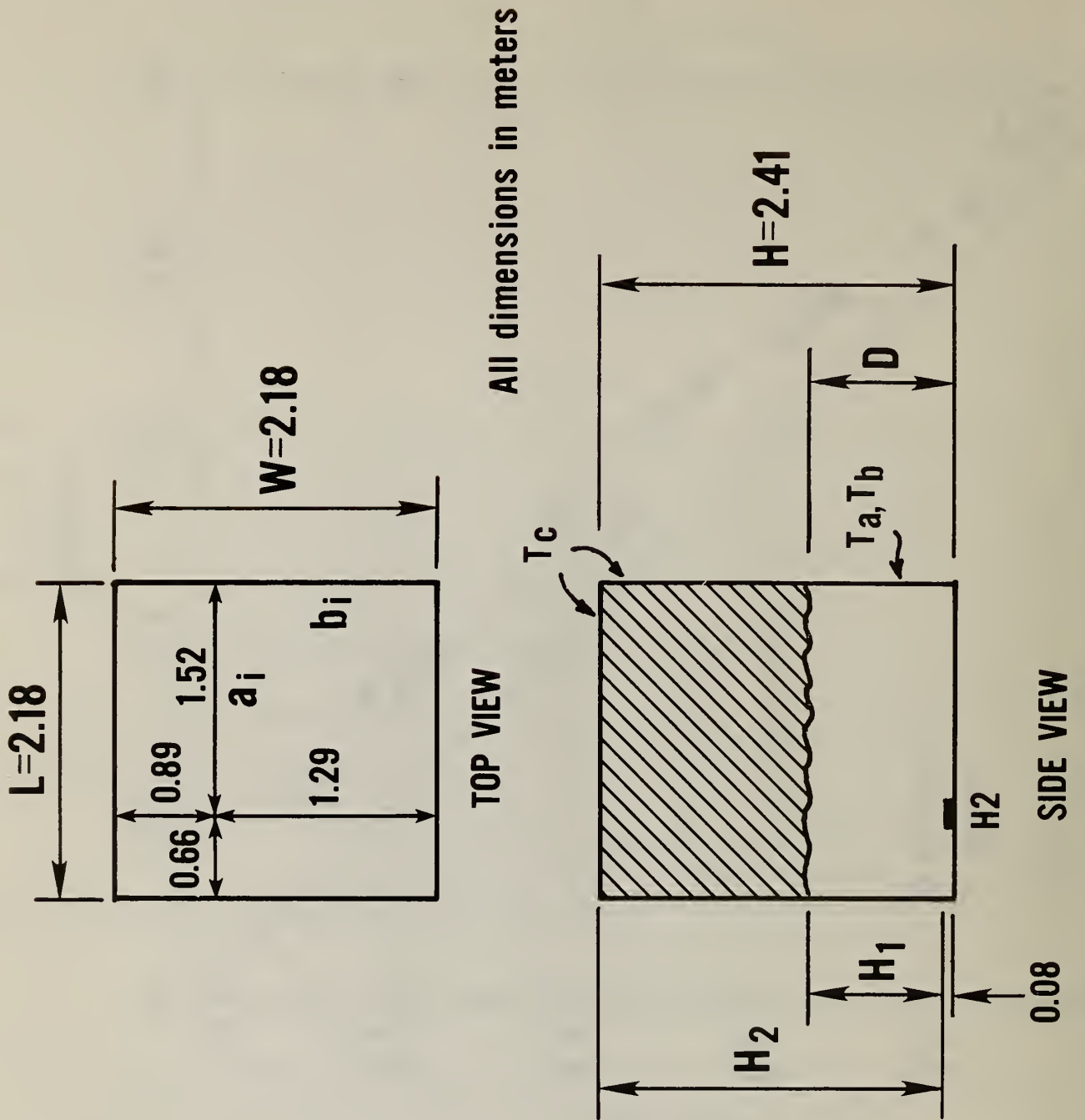
Figure 6-15. Floor target flux by Modak and Matthews [23] analysis

$$\dot{q}_i'' = \frac{1}{2\pi} \left[\left(\frac{a}{L_a} \right) \tan^{-1} \left(\frac{b}{L_a} \right) + \left(\frac{b}{L_b} \right) \tan^{-1} \left(\frac{a}{L_b} \right) \right] \left[\left(1 - e^{-k_g L_m} \right) \sigma T_g^4 + e^{-k_g L_m} \sigma T_c^4 \right]$$

$$+ \frac{\sigma T_a^4}{2\pi} \left[\tan^{-1} \left(\frac{a}{b} \right) - \left(\frac{b}{L_b} \right) \tan^{-1} \left(\frac{a}{L_b} \right) \right] + \frac{\sigma T_b^4}{2\pi} \left[\tan^{-1} \left(\frac{b}{a} \right) - \left(\frac{a}{L_a} \right) \tan^{-1} \left(\frac{b}{L_a} \right) \right] \quad (6\text{-}45b)$$

where

$$L_a = \sqrt{H_1^2 + a^2}$$

$$L_b = \sqrt{H_1^2 + b^2}$$

$$L_m = \frac{2ab \, (H_2 - H_1)}{(H_2 - H_1) \, (a + b) + ab}$$

T_g is the upper layer gas temperature

T_c is the upper layer surface temperature

and T_a and T_b are the lower layer surface temperatures. This model assumes a non-absorbing, non-emitting lower layer gas.

Values from table 3-1 were used as input data to evaluate $\dot{q}_{r,2}''$. These results were then compared to the measured values from sensor H2. The thermal height D was used, $T_g = \overline{T}_1$, $T_c = (T8 + T25)/2$, and $T_a = T_b = 22°C$. Figure 6-16 shows the computed flux, $\dot{q}_{r,z}''$ (Q2) plotted against the experimental values (QEXP). Also tabulated on the figure are the flame flux, $\dot{q}_{r,f}''$ (QF), and the layer flux, $\dot{q}_{r,\,layer}''$, (QR). The computed flux overestimates the measured values at high flux which corresponds to the hot, smoky fires. The reason for this is that the floor sensor is responding to the flux emitted from the lower portion of the layer which is at a lower temperature than $\overline{T}$. The thermocouples near the ceiling representative of $\overline{T}$ cannot be "seen" through the smoke by the sensor. This is a deficiency of the model and may necessitate the inclusion of a stratified temperature to cope with radiation transfer. The level of improvement required here will depend on the application.
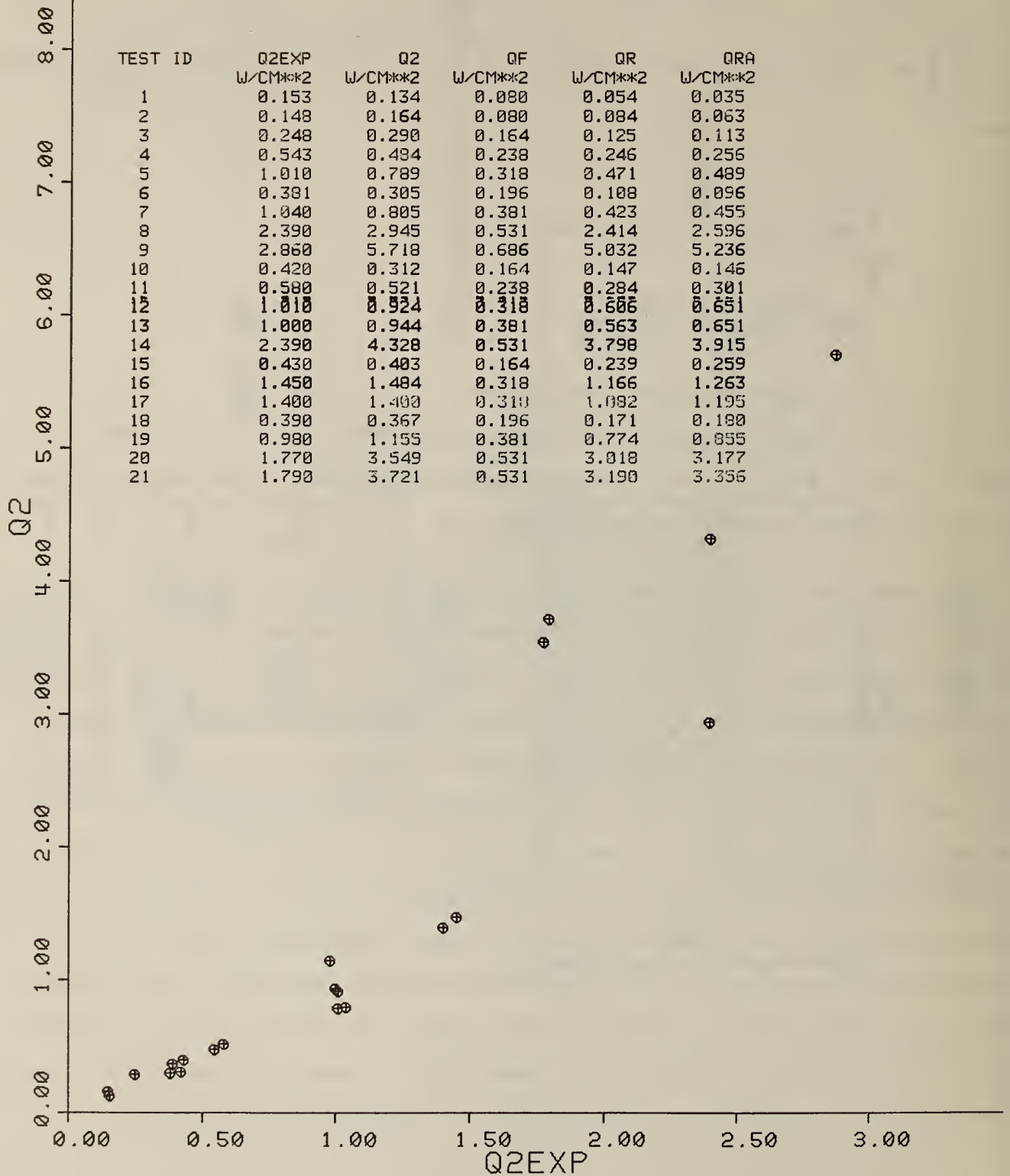
Figure 6-16. Comparison of calculated and measured incident flux by
sensor H2

124

6.3.5.3 Total Incident Heat Flux to a Ceiling Target

The heat flux to ceiling sensor H1 has two components: a convective flux, $\dot{q}_c''$; and a radiative flux $\dot{q}_r$.

$$\dot{q}_1'' = \dot{q}_c'' + \dot{q}_r'' \tag{6-45}$$

The radiative component will be derived using the methodology described by Seigel and Howell [24]. H1 is located as shown in figure 6-17 as a surface element dA, at T_s, the cooling water temperature. The surfaces bounding the upper layer, labeled 2, are the walls at a uniform temperature measured by thermocouple T25. The interfacial plane of the thermal discontinuity, labeled 3, is considered to be at a temperature T_a = 22°C which approximates the global temperature of the lower region. The absorbed radiative flux by sensor H1 is then given as

$$\dot{q}_1'' = \left(F_{12} + F_{13}\right) \varepsilon_g \, \sigma \, T_g^{\,4} + F_{12} \left(1 - \varepsilon_g\right) \sigma T_2^{\,4}$$

$$+ F_{13} \left(1 - \varepsilon_g\right) \sigma \, T_3^{\,4} - \sigma \, T_1^{\,4} \tag{6-46}$$

The configuration factors are

$$F_{12} + F_{13} = 1 \tag{6-47}$$

and

$$F_{13} = \sum_{i=1}^{4} F_i \, (a_i, b_i) \tag{6-48a}$$

$$F_i = \frac{1}{2\pi}\left[\left(\frac{a}{L_a}\right) \tan^{-1}\left(\frac{b}{L_a}\right) + \left(\frac{b}{L_b}\right)\tan^{-1}\left(\frac{a}{L_b}\right)\right] \tag{6-48b}$$

$$L_a = \sqrt{a^2 + (H-D)^2} \tag{6-48c}$$

$$L_b = \sqrt{b^2 + (H-D)^2} \tag{6-48d}$$

Thus,

$$\dot{q}_{r,1}'' = \varepsilon_g \sigma T_g^4 + \left(1 - F_{13}\right)\left(1 - \varepsilon_g\right) \sigma \; T_w^{\,4} \tag{6-49a}$$

$$+ F_{13} \left(1 - \varepsilon_g\right) \sigma T_a^{\,4} - \sigma T_s^4$$

125
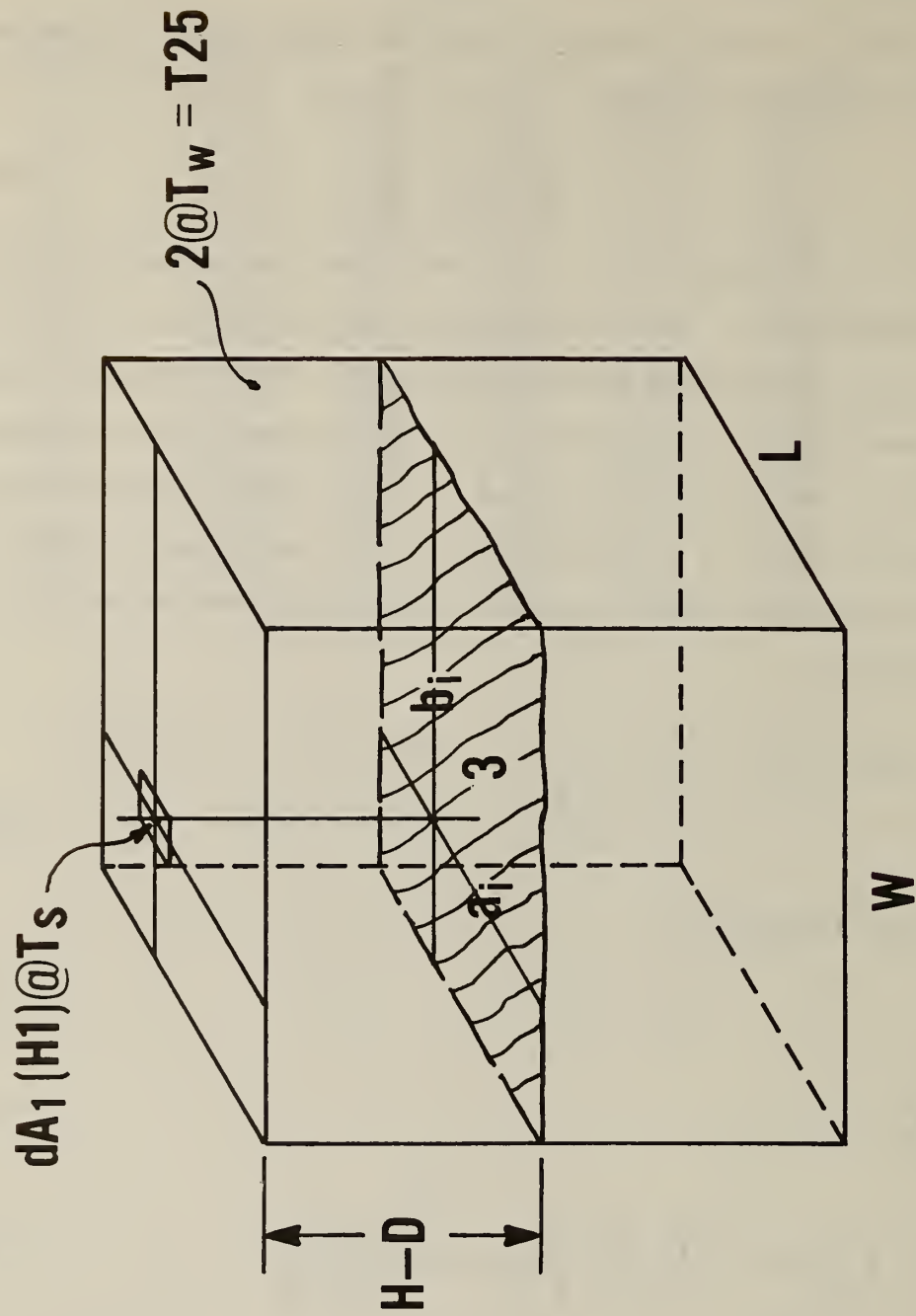
Figure 6-17.   Derivation of radiative flux from the upper layer to the ceiling element, dA

126
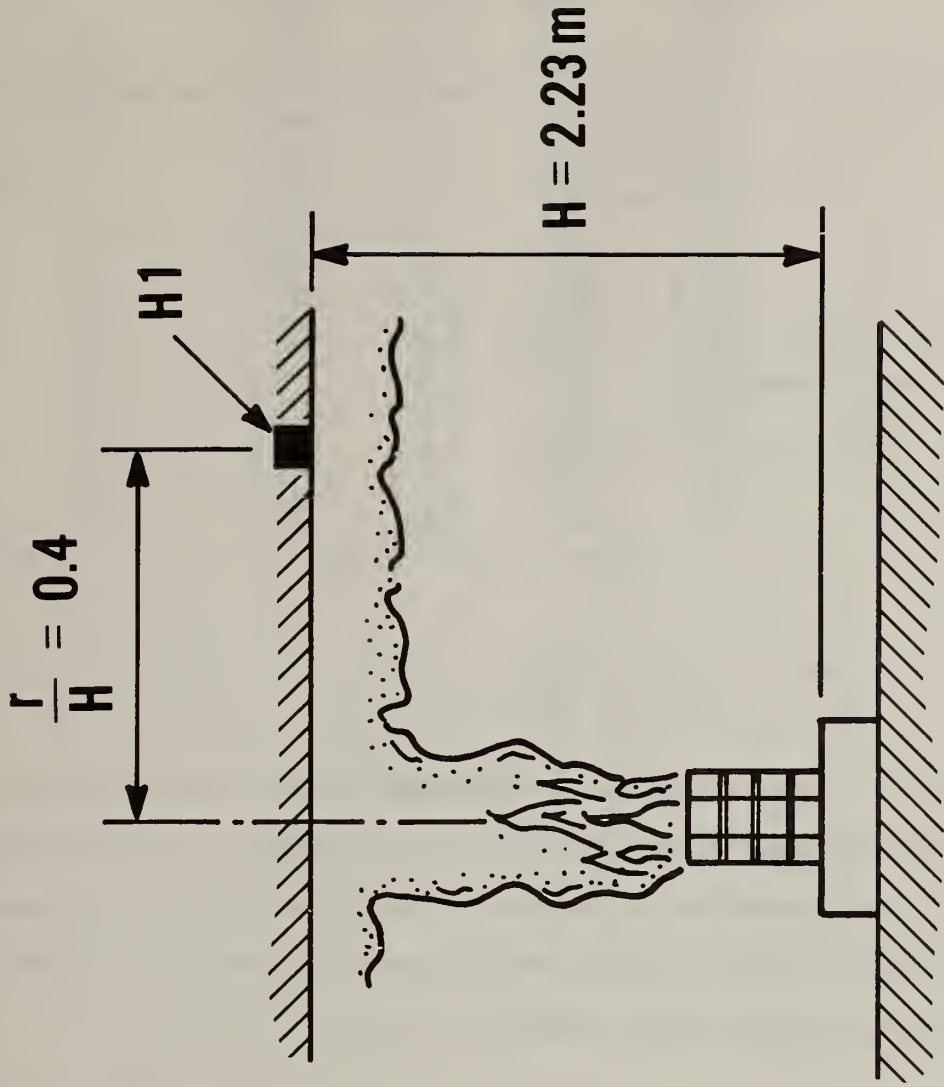
Figure 6-18. Ceiling convective heat flux analysis

with

$$\varepsilon_g = 1 - e^{-k_g L_m} \qquad (6\text{-}49b)$$

and

$$L_m = \frac{4 \times \text{Volume}}{\text{Area}} = \frac{(2WL \ (H\text{-}D)}{(H\text{-}D) \ (W+L) \ + \ WL} \qquad (6\text{-}49c)$$

The convective flux to Hl is given by Zukoski and Kubota [23] as

$$\dot{q}_C'' = h_c \ (T_{ad} - T_w) \qquad (6\text{-}50a)$$

where

T_{ad} is the adiabatic wall temperature

T_w is the wall temperature

and h_c is the convective coefficient

which

$$h_c = \rho_a \ c_p \ \sqrt{gH} \quad Q*^{1/3} \ C(r/H) \qquad (6\text{-}50b)$$

$$Q* = \frac{(1\text{-}f) \ \dot{m}_b \Delta H}{\rho_a \ c_p \ T_a \ \sqrt{gH} \ H^2} \qquad (6\text{-}50c)$$

(see figure 6-18). The convective coefficient falls off as the radial position r increases from the stagnation point where the plume strikes the ceiling. The parameter C corresponding to the sensor location (r/H) = 0.4 was taken as 0.025. Also the adiabatic wall temperature is taken to be $\overline{T}$ here (from table 3-1), and T_w is the sensor temperature, T_s.

Unfortunately, the ceiling radiometer did not function satisfactorily in these tests, and therefore the convective and radiative components could not be resolved separately. However, the theoretical components (QR and QC) are computed and the total measured flux (Q1EXP) is compared to the computed flux $\dot{q}_1''$ (Q1 in figure 6-19). Overall the computed flux is slightly higher than the measured values. It is significant to observe that for the cases of poor agreement in figure 6-16, the computed ceiling flux is in good agreement with Hl values. The same radiative error does not occur here because the gas temperature used ($\overline{T}$) is the primary source of the radiative ceiling flux in

128

TEST ID	Q1EXP W/MC**2	Q1 W/CM**2	QC W/CM**2	QR W/CM**2
1	0.000	0.363	0.357	0.006
2	0.336	0.390	0.341	0.048
3	0.774	0.833	0.723	0.111
4	1.210	1.608	1.291	0.317
5	2.540	2.497	1.829	0.668
6	0.655	0.745	0.632	0.114
7	2.060	2.245	1.637	0.607
8	7.780	7.376	3.644	3.732
9	10.400	10.927	4.406	6.521
10	0.810	1.137	0.942	0.195
11	1.300	1.649	1.289	0.360
12	2.250	2.598	1.798	0.801
13	1.900	2.241	1.532	0.709
14	6.650	7.509	3.276	4.233
15	0.900	1.275	0.973	0.303
16	3.120	3.324	2.003	1.321
17	1.950	3.057	1.855	1.202
18	0.710	0.807	0.629	0.178
19	2.110	2.489	1.567	0.922
20	5.700	6.348	2.886	3.463
21	5.940	6.747	3.087	3.660

Figure 6-19. Comparison of calculated and measured incident flux to ceiling sensor H1

129

these hot smoky fires. Although the comparison in figure 6-19 does not directly confirm the accuracy of either the convective or the radiant model, the agreement over the range of flux levels recorded does imply good accuracy for both models.

6.3.5.4 Conductive Ceiling Heat Flux

A model is needed to calculate the conductive heat flux into the heated enclosure surfaces. Since a quasi-steady simulation model is being considered for the average peak burning period, an average conductive flux must be determined that reflects the past history of wall heating. This will be approximated, although the transient conduction problem can be solved exactly with probably the greatest accuracy of all the phenomena being considered. This approximation is traded against solving the full transient problem (which essentially would require a transient burning rate input along with the transient conduction model).

For a constant surface temperature T_w for a semi-infinite solid (applicable to our walls) Carslaw and Jaeger [26] gives the surface heat flux as

$$\dot{q}''_{x=0} = \frac{\sqrt{k \rho c} \ (T_w - T_a)}{\sqrt{\pi t}} \tag{6-51}$$

where k, ρ, c are the wall material conductivity, density, and specific heat, respectively. The average heat flux over the time interval t_* is

$$\dot{q}''_{x=0} = \frac{2}{\sqrt{\pi}} \frac{\sqrt{(k \rho c)}}{\sqrt{t_*}} \ (T_w - T_a) \tag{6-52a}$$

where t_* is taken as the characteristic burn time

$$t_* = \frac{(1-\omega) M_c \alpha}{\dot{m}_v} \tag{6-52b}$$

where M_c is the mass of the crib

and α is a constant selected as 0.5 such that t_* is half of the nominal burn time. This gives a t_* of roughly 300 s, comparable to the duration of the steady peak burn period.

130

The properties of Marinite XL, the lining material are given as:

$\rho_w = 696 \text{ kg/m}^3$

$c_w = (1.12 \text{ kJ/kg-K}) \, [1 + 6.7 \times 10^{-4} \, K^{-1} \, (T_w - T_a)]$

$k_w = (0.125 \times 10^3 \text{ kW/m-K}) \, [1 + 6.7 \times 10^{-4} \, K^{-1} \, (T_w - T_a)].$

The value of ρ_w and k_w [27] were measured, c_w was taken from the literature, and the temperature variation from Taminini [28].

A measure of the accuracy of this model can be assessed by considering the heat flux balance at the ceiling position where thermocouple T8 measured the surface temperature. At that position the conductive flux ($\dot{q}_K''$ or QK) must equal the sum (QIN) of the convective ($\dot{q}_C''$ or QC) and radiative ($\dot{q}_r''$ or QR) fluxes. Since these can be evaluated separately, it can be determined how well

$$\dot{q}_k'' = \dot{q}_C'' + \dot{q}_r'' \qquad (6\text{-}53)$$

(or QK = QC + QR $\equiv$ QIN as shown in figure 6-20) at T8. $\dot{q}_k''$ is determined from equation (6-52) where T_w = T8. $\dot{q}_C''$ is found from equation (6-50) and $\dot{q}_r''$ from equation (6-49) where T_w = T25 and T_s = T8. The results are shown in figure 6-20. The results are not in good agreement; and since the models for $\dot{q}_C''$ and $\dot{q}_r''$ appear good, the convective flux model is weak. It could be fixed by decreasing the parameter α to roughly, 0.1, but a lot of scatter would still remain. The accuracy of the temperature measurements could have a bearing on this result since the temperature differences are small compared to their absolute values.

6.3.6 Crib Mass Loss Rate

Perhaps the most significant variable in achieving accuracy in a mathematical fire model is the rate of energy release. This is implied by the correlation given in equation (5-6) which displays the strong dependence of upper layer temperature on energy release rate. For discrete room furnishing items the rate of energy release could be adequately determined from an apparatus similar to that shown in figure 4-3. However, that technique would yield the free burn value, which does not account for the room effects.

131

| TEST ID	QK W/CM**2	QIN W/CM**2	QC W/CM**2	QR W/CM**2
1	0.152	0.151	0.193	-0.043
2	0.031	-0.030	0.038	-0.068
3	0.203	0.272	0.303	-0.031
4	0.308	0.547	0.497	0.050
5	0.280	0.485	0.463	0.021
6	0.243	0.322	0.302	0.020
7	0.287	0.481	0.383	0.098
8	0.332	0.806	0.423	0.383
9	0.170	0.492	0.231	0.261
10	0.341	0.576	0.510	0.066
11	0.321	0.570	0.518	0.052
12	0.315	0.709	0.523	0.186
13	0.432	0.969	0.617	0.352
14	0.141	0.466	0.185	0.281
15	0.318	0.577	0.469	0.108
16	0.205	0.440	0.331	0.109
17	0.233	0.581	0.392	0.189
18	0.220	0.325	0.276	0.049
19	0.246	0.594	0.339	0.255
20	0.199	0.851	0.276	0.575
21	0.155	0.621	0.210	0.411

Figure 6-20. Comparison of convective plus radiative heat flux into the ceiling with conductive heat flux absorbed by the ceiling

132

Recently Thomas et al. [29] has shown that flashover, when viewed as a burning instability (not a remote ignition phenomenon), requires an energy release rate of no more than 50 percent above the free burn value at the onset of this instability. In any case, the free burn value could serve as a basis for describing the room burning rate.

For (wood) crib fires fundamental correlations exist (appendix A) which can predict the free burn rate for a crib structure. This approach was not adopted here because of the inability of these correlations to account for burning rate enhancement in a burning assembly of cribs. This self-enhancement discussed in section 5.1 was due to radiative interaction between cribs in an assembly. Existing correlation could predict the burning rate of a single crib, but not an assembly of cribs. Therefore an empirical analysis was developed to account for the enhancement present in an assembly of like cribs.

If one observes a burning crib it is clear that the intensity of flaming and pyrolysis is greater for the internal sticks than the outer stick surfaces. In fact at times the outer stick surfaces may have limited involvement. Consequently an internal crib surface area (A_i) was defined which could also account for the crib faces adjacent to each other. The total exposed surface area (A) of a single crib is

$$A = n\ N\ (4bP + 2b^2) - 2b^2\ (N - 1) \qquad (6\text{-}54)$$
$$= 0.897\ m^2$$

where n, N, b, and ℓ are crib configuration parameters defined in section 2. The internal area of a configuration of cribs is defined as

$$A_i = 0.897\ n_c - (Nb\ \ell)\ S(n_c) - \ell^2 n_c \qquad (6\text{-}55)$$

where $S(n_c)$ is the number of crib sides exposed to open surroundings. In fact A_i is the total area A minus the projected surface area of the sides exposed to open surroundings; so A_i includes the exposed surfaces within a crib and the adjacent surfaces between cribs. The free burn rate is then given as

133

$$\dot{m}_{v,o} = \dot{m}''_{v,o} A_i \qquad (6\text{-}56a)$$

where $\dot{m}''_{v,o}$ is the mass loss rate per unit area and is constant for each material. In general, $\dot{m}''_{v,o}$ depends on crib configuration and material, and can be readily predicted for wood materials by the analysis in appendix A. Figure 6-21 shows this relationship plotted with the free burn data. The slope for the correlation yields:

$$\dot{m}''_{v,o} = \begin{cases} 9.5 \text{ g/m}^2\text{-s, wood} \\[2ex] 14.0 \text{ g/m}^2\text{-s, polyurethane} \end{cases} \qquad (6\text{-}56b)$$

This establishes the free burn basis; the room effects remain to be considered.

Two effects of the room on the burning of an item will be the extra heat flux received and the diminished oxygen available for combustion. The following model is proposed:

$$\dot{m}_v = \dot{m}''_{v,o} A_i + \Delta\dot{m}_R + \Delta\dot{m}_{ox} \qquad (6\text{-}57a)$$

where

$$\Delta\dot{m}_R = \frac{\dot{q}''_{r,T} A_{o,T} + \dot{q}''_{r,s} A_{o,s}}{L_{vap}} \qquad (6\text{-}57b)$$

and

$$\Delta\dot{m}_{ox} = -\dot{m}''_{v,o} A_i \left(1 - \frac{Y_{ox,\ell}}{0.23}\right) \qquad (6\text{-}57c)$$

$\Delta\dot{m}_R$ represents the gasification rate due to heat flux from the room to the top surface ($A_{o,T}$) of the crib, $\dot{q}''_{r,T}$; and the exposed sides ($A_{o,s}$) of the crib, $\dot{q}''_{r,s}$.

$$A_{o,T} = n_c \ell^2 + \ell s \, G_T(n_c) \qquad (6\text{-}57d)$$

$$A_{o,s} = bN\ell \, S(n_c) + \ell s \, G_s(n_c) \qquad (6\text{-}57e)$$

where $G_T(n,c)$ is the number of top gaps between adjacent cribs and $G_s(n_c)$ is the number of side gaps between adjacent cribs. The projected areas facing the surroundings are used here.

134
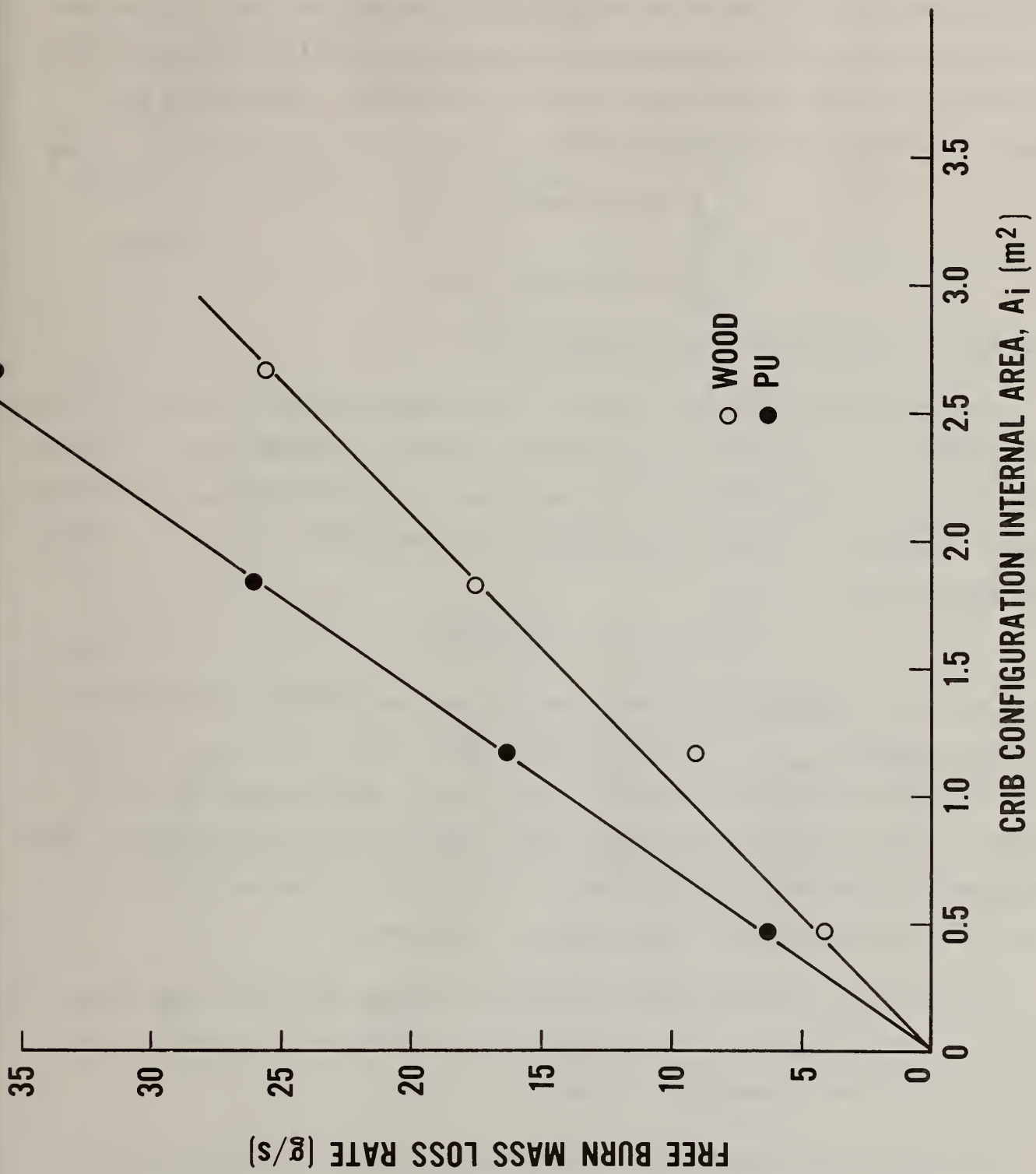
Figure 6-21. Correlation of free burn loss rate

An effective heat of vaporization was derived for each fuel material. This was done using an irradiation source to pyrolyze wood and polyurethane in air while measuring the mass loss. The rate of mass loss was surprisingly constant over a wide range of mass fraction remaining. The results are shown in table 6-9. Nominal values of

$$L_{vap} = \begin{cases} 5 \text{ kJ/g, wood} \\ \\ 8 \text{ kJ/g, polyurethane} \end{cases} \qquad (6-58)$$

were used in the computations presented here.

These values are nominal averages of the results shown in table 6-9 which neglected fuel surface heat loss effects. Neglection of the heat loss in the determination of L_{vap} was an error discovered during the preparation of this report. Assuming a linear relationship between $\dot{m}_V''$ and $\dot{q}_i''$ (as given in table 6-a) would yield

$$L_{vap} = \frac{\dot{q}_i'' - \dot{q}_o''}{\dot{m}_V''}$$

where $\dot{q}_o''$ is the surface heat loss. For the vertical samples pyrolyzed in air, the data suggest $L_{vap} = 1.9$ kJ/g for wood (sugar pine), and $L_{vap} = 2.9$ kJ/g for the rigid polyurethane (GM-37). The value $\dot{q}_o''$ was the same for both materials, and corresponds to a radiative loss from a surface at 500°C. This compares with Tewarson's [30] values of 1.82 kJ/g for Douglas fir and 4.52 kJ/g for polyurethane (GM-37) pyrolyzed in nitrogen.

Furthermore, in the analyses to follow (figures 6-22 and 6-23), these "more correct" values of L_{vap} produced changes of within 10 percent of the current calculated theoretical values.

To complete this model the radiant fluxes to the crib surfaces must be presented. The methodology of Modak and Matthews [23] were used. For simplicity the area elements were considered centered with respect to the four upper quadrants (i.e., $a_i = b_i = (2.18/2)$m for $i = 1,4$). The top element was at the crib height ($H_C + 0.18$ m) and the side element was at the mid position ($H_C/2 + 0.18$ m). The sum of the flux from the four quadrants is

Table 6-9

Pyrolysis Due to Radiation[*]

Fuel	Orientation	Incident flux $\dot{q}_i''$	$\dot{m}_v''$	$L_{vap} = \dot{q}_i''/\dot{m}_v''$ [**]
		W/cm^2	$g/cm^2\text{-}s$	J/g
Wood	vertical	3.5	0.80×10^{-3}	4387
Wood	vertical	3.0	0.527×10^{-3}	5688
Wood	horizontal	2.5	0.54×10^{-3}	4610
Wood	horizontal	2.5	0.544×10^{-3}	4595
Polyurethane	vertical	3.5	0.50×10^{-3}	7030
Polyurethane	vertical	3.0	0.343×10^{-3}	8755
Polyurethane	horizontal	2.0	(ignited after 4 minutes)	

*Data by W. Twilley [31].

** This evaluation neglected heat loss at the fuel surface.

given as

$$\dot{q}''_{r,T} = 4 \left\{ F_{uT} \left[\varepsilon_{gc} \sigma T^4_{g,u} + (1 - \varepsilon_{gc}) \sigma T^4_{w,u} \right] + F_{\ell T} \sigma T^4_{W,\ell} \right\} \qquad (6\text{-}59a)$$

where

$$F_{uT} = \frac{1}{\pi} \left(\frac{a}{L_a}\right) \tan^{-1} \left(\frac{a}{L_a}\right) \qquad (6\text{-}59b)$$

$$F_{\ell T} = \frac{1}{2\pi} \left[\frac{\pi}{2} - 2\left(\frac{a}{L_a}\right) \tan^{-1} \left(\frac{a}{L_a}\right) \right] \qquad (6\text{-}59c)$$

$$L_a = \sqrt{H_1^2 + a^2} \qquad (6\text{-}59d)$$

$$H_1 = D - (H_c + 0.18 \text{ m}) \geq 0 \qquad (6\text{-}59e)$$

$$\varepsilon_{gc} = 1 - e^{-k_g L_{mc}} \qquad (6\text{-}59f)$$

$$L_{mc} = \frac{2a \ (H-D)}{2 \ (H-D) + a} \qquad (6\text{-}59g)$$

and

$$H_2 = H - (H_c + 0.18 \text{ m}) \qquad (6\text{-}59h)$$

$$\dot{q}''_{r,s} = F_{uc} \left[\varepsilon_{gc} \sigma T^4_{g,u} + (1 - \varepsilon_{gc}) \sigma T^4_{w,u} \right] + (F_{\ell c} + 1/2) \sigma T^4_{w,\ell} \qquad (6\text{-}60a)$$

where this is the sum of the upper and lower half-space contributions, and

$$F_{uc} = \frac{1}{\pi} \left[\tan^{-1} \left(\frac{a}{H_1}\right) - \left(\frac{H_1}{L_a}\right) \tan^{-1} \left(\frac{a}{L_a}\right) \right] \qquad (6\text{-}60b)$$

$$F_{\ell c} = \frac{1}{\pi} \left[\tan^{-1} \left(\frac{H_1}{a}\right) + \left(\frac{H_1}{L_a}\right) \tan^{-1} \left(\frac{a}{L_a}\right) \right] \qquad (6\text{-}60c)$$

with L_a, H, and ε_{gc} defined as in equation (6-59).

Finally the rationale for the formulation of the oxygen effect will be discussed. In the combustion of simple systems, the burning rate due to convective effects can be described in terms of the Spalding mass transfer number B, i.e.,

$$\dot{m}''_v = \left(\frac{h}{c_g}\right) \ln (B + 1) \qquad (6\text{-}61a)$$

where h is the convective heat transfer coefficient and

c_g is the specific heat of the gases.

and

$$B = \frac{Y_{o2} \ \Delta H/r_{ox} - c_g \ (T_s - T_a)}{L_{vap}} \qquad (6\text{-}61b)$$

138

Hence, for a given fuel B is directly proportional to Y_{0_2} - in this case the oxygen concentration in the lower space, Y_{0_2}. Kanury [32] demonstrated that for charring materials, equation (6-61) is not sufficient to describe this burning phenomena unless B is defined to account for additional effects such as stick thickness and radiant intensity. Hence, it would be reaching to utilize equation (6-61) for the crib burning rate.

However, it is desirable to keep the analysis simple until a more definite approach develops. Moreover a study of crib burning in diluted atmospheres [33] indicated that, in oxygen concentrations down to 17 percent (by volume), the rate of burning was proportional to oxygen concentration. Since for small B-number, the Spalding relationship in equation (6-61) would also suggest direct proportionality to Y_{0_2}, then is assumed that

$$\Delta \dot{m}_{ox} = (\dot{m}_v) \text{ free } (\frac{Y_{ox,\ell}}{0.23} - 1) \qquad (6\text{-}62)$$

The accuracy of this model was examined by substituting experimental values of $\dot{m}_v$, $\dot{m}_a$, D, $T_{g,u} = \bar{T}$ and $T_{w,u} = (T8 + T25)/2$ (with $T_{g,\ell} = T_{w,\ell} = T_a$) for table 3-1 into formulae (6-57) through (6-62).

The results are given in table 6-10[4] and the calculated and measured values of $\dot{m}_v$ are compared in figure 6-22. The results in table 6-10 show that the enhanced radiation effect appears to be comparably counteracted by the oxygen effect. For these data however, both effects are not more than 20 percent of the mass loss rate. Hence, the room effects are not great. This is consistent with the discussion of experimental results in section 5.1.

Table 6-10. Evaluation of crib mass loss model

| TEST ID	$Y_{O_2,\ell}$ OXL G/G	$\dot{q}''_{r,s}$ QRSIDE W/M**2	$\dot{q}''_{r,T}$ QRTOP W/M**2	$\dot{m}_{v,exp}$ MVEXP G/S	$\dot{m}_{v,calc}$ MVCAL G/S	$\Delta\dot{m}_{ox}$ DOX G/S	$\Delta\dot{m}_R$ DRAD G/S
PRC 0-W-1-1	0.230	0.047	0.059	5.080	4.985	0.006	0.039
PRC 3-W-1-1	0.230	0.056	0.104	5.100	4.992	0.002	0.051
PRC 5-W-2-1	0.229	0.072	0.164	11.860	11.671	-0.043	0.119
PRC 2-W-3-1	0.227	0.123	0.333	20.140	18.335	-0.217	0.303
PRC 7-W-4-1	0.229	0.203	0.669	28.640	27.129	-0.126	0.636
PRC 1-P-1-1	0.229	0.066	0.139	6.980	6.935	-0.019	0.039
PRC 4-P-2-1	0.227	0.192	0.588	20.190	16.207	-0.246	0.221
PRC 6-P-3-1	0.228	0.972	3.443	33.020	27.016	-0.220	1.607
PRC 8-P-4-1	0.226	2.279	6.528	35.290	40.708	-0.723	4.165
PRC 9-W-2-1/2	0.230	0.080	0.197	11.940	11.723	-0.008	0.136
PRC 11-W-3-1/2	0.227	0.137	0.387	18.730	18.317	-0.277	0.345
PRC 15-W-4-1/2	0.223	0.285	0.803	28.280	26.663	-0.783	0.827
PRC 10-P-2-1/2	0.217	0.299	0.666	15.420	15.621	-0.917	0.306
PRC 18-P-3-1/2	0.216	1.948	4.305	25.020	26.783	-1.549	2.783
PRC 13-W-2-1/4	0.220	0.124	0.316	11.270	11.315	-0.492	0.213
PRC 17-W-4-1/4	0.204	0.592	1.381	24.480	25.155	-3.039	1.575
PRC 19-W-4-1/4	0.201	0.573	1.227	20.410	24.768	-3.322	1.471
PRC 12-P-1-1/4	0.218	0.098	0.215	5.900	6.621	-0.353	0.058
PRC 14-P-2-1/4	0.197	0.401	0.916	14.550	14.352	-2.295	0.415
PRC 16-P-3-1/4	0.194	1.557	3.429	21.970	23.724	-4.846	2.221
PRC 20-P-3-1/4	0.189	1.645	3.626	22.930	23.290	-4.607	2.348

140
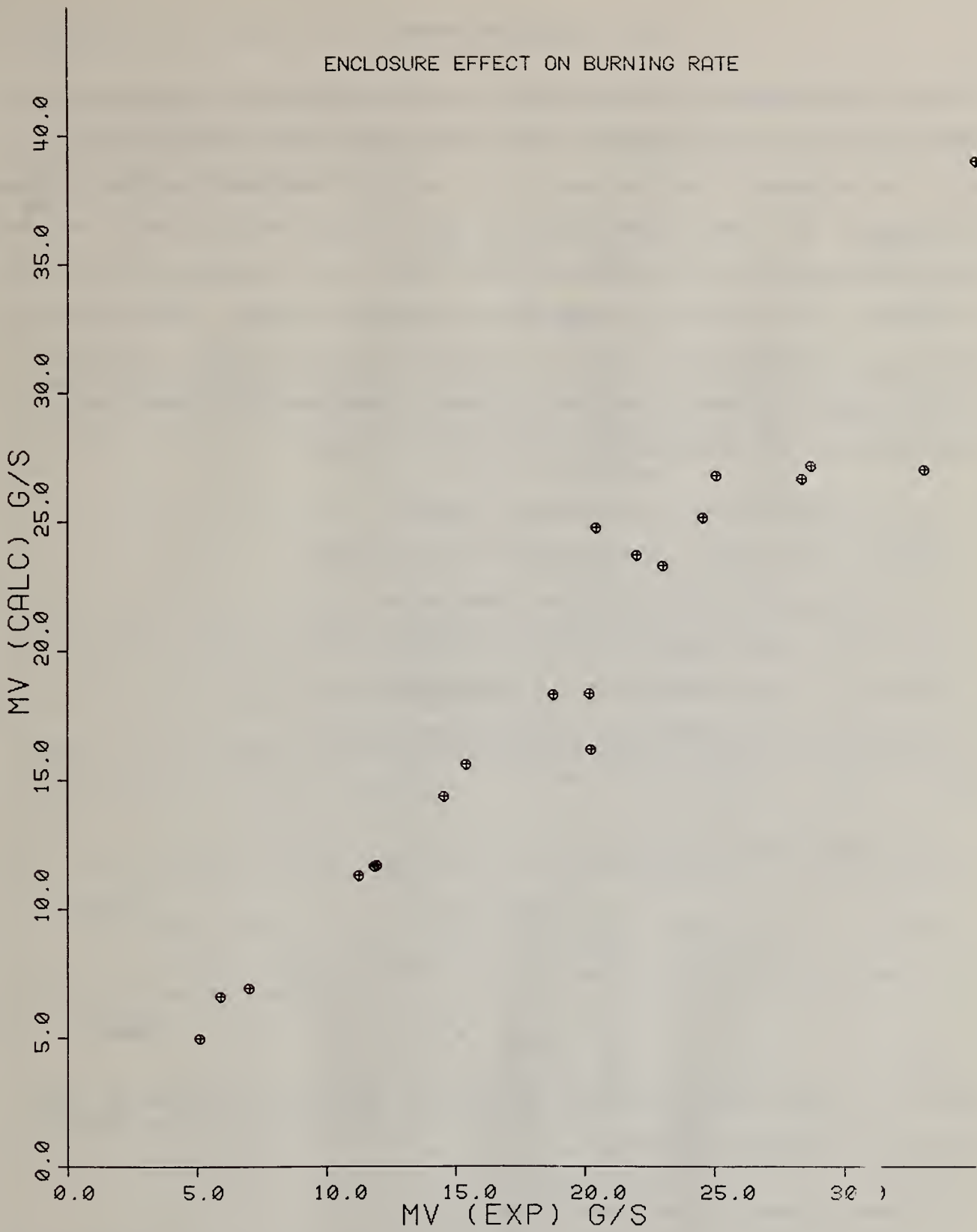
Figure 6-22.   Comparison of calculated and measured rate of mass loss in the room fire experiments

141

6.4 Simulation Model

The formulation of the governing equations essentially has been made in the previous sections. However, some modification must be made in the radiative exchanges since the analysis of section 6.3.5 dealt with an exchange with respect to a target elemental area, not a finite surface area. Following the methodology given in Siegel and Howell [24] and the approach illustrated in section 6.3.5.3 yields the necessary radiative exchange. The details of this will be omitted here; only the formulation will be listed. Basically it will consist of seven nonlinear algebraic equations with subsidiary relationships. The reduced set of unknowns (x_i) are:

x_1 = N, the height of the neutral plane

x_2 = D, the height of the thermal discontinuity

x_3 = $T_{g,u}$, the upper layer gas temperature

x_4 = $T_{w,u}$, the upper layer surface temperature

x_5 = $T_{g,\ell}$, the lower layer gas temperature

x_6 = $T_{w,\ell}$, the lower layer surface temperature

and x_7 = $\dot{m}_v$, the rate of mass loss.

The equations have the form

$$f_i(x_i) = 0 \qquad\qquad (6\text{-}63)$$

A mass balance on the plume and upper layer yields:

$$f_1 = \dot{m}_{out} - \dot{m}_a - \dot{m}_v = 0 \qquad\qquad (6\text{-}64)$$

where $\dot{m}_{out}$ (the doorway flow out) is given by equation (6-10) and $\dot{m}_a$ (the air flow) by equation (6-11b).

A mass balance on the lower layer yields:

$$f_2 = \dot{m}_p - \dot{m}_a - \dot{m}_e = 0 \qquad\qquad (6\text{-}65)$$

where $\dot{m}_p$ (the crib fire entrainment rate) is given by equation (6-25b) and $\dot{m}_e$ (the entrainment rate from the upper to the lower layer) is taken from

142

equation (6-17) with n = 1/4 and k_m = 0.5.

The energy balance on the upper layer and flame plume is the algebraic sum of the energy release $(\dot{E}_R)$, the rate of energy losses by mass transport $(\dot{E}_M)$, and heat transport $(\dot{E}_L)$.

$$f_3 = \dot{E}_R - \dot{E}_L - \dot{E}_M = 0 \tag{6-66}$$

$$\dot{E}_R = (1 - \frac{f}{2}) \, \dot{m}_b \Delta H \tag{6-67}$$

where half the energy radiated from the flame is assumed to be absorbed by the upper layer. Also, the rate of fuel reacted within the enclosure is

$$\dot{m}_b = \begin{cases} \dot{m}_v, & \dot{m}_a \geq r\dot{m}_v \\[2ex] \dot{m}_a/r, & \dot{m}_a < r\dot{m}_v \end{cases} \tag{6-68}$$

and the net rate of energy transport by fluid flow from the enclosure is

$$\dot{E}_M = (\dot{m}_a + \dot{m}_v + \dot{m}_e) \, c_p \, (T_{g,u} - T_{g,\ell}) - \dot{m}_v c_p \, (T^* - T_{g,\ell}) \tag{6-69}$$

where the last term, due to pyrolysis gases emerging from the surface at temperature T^*, will be neglected.

The net rate of heat transfer from the upper layer and flame plume is

$$\dot{E}_L = (\dot{q}''_{r,u} + \dot{q}''_{c,u}) \, A_{w,u} + \dot{q}''_{r,o} \, A_{w,u} + \dot{q}''_{o,u} + \dot{q}''_{r,D} \, A_F \tag{6-70}$$

The upper surface area is

$$A_{w,u} = WL + 2(W + L)(H - D) - A_{o,u} \tag{6-71}$$

The upper portion of the doorway opening is

$$A_{o,u} = W_o (H_o - D) \tag{6-72}$$

The floor or layer surface area is

$$A_F = WL \tag{6-73}$$

The radiative flux to the upper surface is

$$\dot{q}''_{r,u} = \epsilon_g \, \sigma \, T^4_{g,u} + \gamma_u \, (1 - \epsilon_g) \, \sigma T^4_{w,\ell} - [1 - (1-\gamma_u)(1-\epsilon_g)] \sigma T^4_{w,u} \qquad (6\text{-}74a)$$

where
$$\gamma_u = A_F/A_{w,u} \qquad (6\text{-}74b)$$

and ϵ_g is given by equation (6-49b) with k_g from equation (6-41). The radiative flux lost through the opening is

$$\dot{q}''_{r,o} = \epsilon_g \sigma T^4_{g,u} + (1-\epsilon_g) \, \epsilon \, T^4_{w,u} - \sigma T^4_a \qquad (6\text{-}75)$$

The net flux through the layer interface from the upper to the lower space is

$$\dot{q}''_{r,D} = \epsilon_g \sigma T^4_{g,u} + (1-\epsilon_g) \sigma T^4_{w,u} - T^4_{w,\ell} \qquad (6\text{-}76)$$

The convective flux to the upper surfaces is

$$\dot{q}''_{c,u} = h_{c,u} \, (T_{g,u} - T_{w,u}) \qquad (6\text{-}77)$$

where $h_{c,u}$ is given by equation (6-50) with $C = 0.01$ based on an average convective coefficient. The convective flux to the side walls has not been adequately quantified, so C is based on an "extended" ceiling. An energy balance on the lower layer is

$$F_4 = T_{g,\ell} - T_a - \left(\frac{\dot{m}_e}{\dot{m}_a + \dot{m}_e} \right) \left(T_{g,u} - T_a \right) + \frac{h_{c,\ell} \, A_{w,\ell}}{C_p (\dot{m}_a + \dot{m}_e)} \, (T_{g,\ell}) = 0 \qquad (6\text{-}78)$$

where the gas is not considered to be absorbing or emitting, and the convective (last) term was dropped in the final calculation.

Also energy balances at the upper and lower gas-surface interfaces yield two equations.

$$f_5 = \dot{q}''_{k,u} - \dot{q}''_{r,u} - \dot{q}''_{c,u} = 0 \qquad (6\text{-}79)$$

where $\dot{q}''_{k,u}$ is given by equation (6-52) with $T_w = T_w = T_{w,u}$;
and

$$f_6 = \dot{q}''_{k,\ell} - \dot{q}''_{r,\ell} - \dot{q}''_{c,\ell} = 0 \qquad (6\text{-}80a)$$

144

where $\dot{q}''_{k,\ell}$ is given by equation (6-52) with $T_w = T_{w,\ell}$

$$\dot{q}''_{c,\ell} = h_{c,\ell} \, (T_{g,\ell} - T_{w,\ell}) \text{ with } h_{c,\ell} \text{ estimated as } 0.01 \text{ KW/m}^2 - \text{K} \qquad (6\text{-}80\text{b})$$

$$\dot{q}''_{r,\ell} = \gamma_\ell \left[\epsilon_g \, \sigma \, T^4_{g,u} + (1 - \epsilon_g) \, \sigma T^4_{w,u} - \sigma T^4_{w,\ell} \right] + \frac{f}{2} \frac{\dot{m}_b \, \Delta H}{A_{w,\ell}} \qquad (6\text{-}80\text{c})$$

$$\gamma_\ell = A_F / A_{w,\ell} \qquad (6\text{-}80\text{d})$$

and $A_{w,\ell} = 2(W + L) \, D + WL \qquad (6\text{-}80\text{e})$

Finally, the seventh equation is developed from equation (6-57):

$$f_7 = \dot{m}_v - \dot{m}''_{v,o} \, A_i \left(\frac{Y_{02,\ell}}{0.23} \right) - \frac{\dot{q}''_{r,T} \, A_{o,T} + \dot{q}''_{r,s} \, A_{o,S}}{L_{vap}} = 0 \qquad (6\text{-}81)$$

The necessary subsidiary equations (6-57 through 6-60) also apply.

The resultant set of nonlinear algebraic equations to be solved are

$$f_1 \, (x_1, \, x_2, \, x_3, \, x_4, \, x_5, \, x_6, \, x_7) = 0$$

$$f_2 \, (x_1, \, x_2, \, x_3, \, x_4, \, x_7) = 0$$

$$f_3 \, (x_1, \, x_2, \, x_3, \, x_4, \, x_5, \, x_6, \, x_7) = 0 \qquad (6\text{-}82)$$

$$f_4 \, (x_1, \, x_2, \, x_3, \, x_4) = 0$$

$$f_5 \, (x_1, \, x_2, \, x_3, \, x_4, \, x_5, \, x_6, \, x_7) = 0$$

$$f_6 \, (x_1, \, x_2, \, x_3, \, x_4, \, x_5, \, x_6, \, x_7) = 0$$

$$f_7 \, (x_1, \, x_2, \, x_3, \, x_4, \, x_5, \, x_6, \, x_7) = 0$$

This set of equations was solved by a Newton-Raphson method. Problems of convergence do occur with this current algorithm so that a complete set of calculational results were not achieved for all conditions desired. A summary of the input parameters used in the basic theoretical calculations is shown in table 6-11.

Table 6-11

Input Parameters Used in the Theoretical Calculations

Parameter	Plastic	Wood
r (g air/g volatile fuel)	9.03	4.92
ΔH (kJ/g volatile fuel)	23.	15.
f (kJ radiation/kJ total energy	0.22	0.18
L_{vap} (kJ incident flux/g volatile fuel)	8.	5.
ω (g char/g solid fuel)	0.13	0.10
k_f (m^{-1})	1.3	0.80
T_f (K)	1200.	1100.
M_c (kg crib)	3.1	3.4
C_{in}		0.58-0.31 W_o (m)
C_{out}		0.68
k_m		0.5
C		0.01
x_a		1.
α		0.5
$h_{c,\ell}$ (kW/m^2-K)		0.01

6.5 Comparison of Experimental and Theoretical Results

The results of the theoretical simulation model were compared to the average peak results of the enclosure fire experiments. The theoretical results were calculated over a range of doorway widths and crib loadings of up to four or more. The combination of initial conditions for which results are available depend, at this time, on the program's ability to converge to a solution. The same symbol legend used in section 5 for the data points applies here as well. The format of the comparison will be the variable for comparison versus door width with the number of cribs as a parameter.

The rate of mass loss for both the wood and plastic cribs is presented in figure 6-23. The constancy of the theoretical results is in contrast to the actual curvature as the data points imply. This discrepancy is probably due, on one hand, to an inadequate prediction of the radiative enhancement effect for large door sizes; and, on the other hand, an inadequate treatment of the diminution of mass loss rate with oxygen depletion in the lower layer. Also calculations for small door sizes, which would lead to results with downward curvature, have not been successfully run. Despite this inability to match the curvature of the experimental results, the theoretical results are within 25 percent of the measured mass loss rates.

The results for the rate of airflow into the enclosure are shown in figures 6-24a and 6-24b for the plastic and wood respectively. Here both the inflow rate and airflow rate derived from the outflow measurement were plotted. The scatter indicates the accuracy of these data. The theoretical result gives an impression of order to the data and may indeed be more accurate. Of course, until better data is achieved a conclusion statement of the theoretical accuracy cannot be made. It should be noted that a reduction in the outflow coefficient reduced the computed rate of airflow by a proportional magnitude.
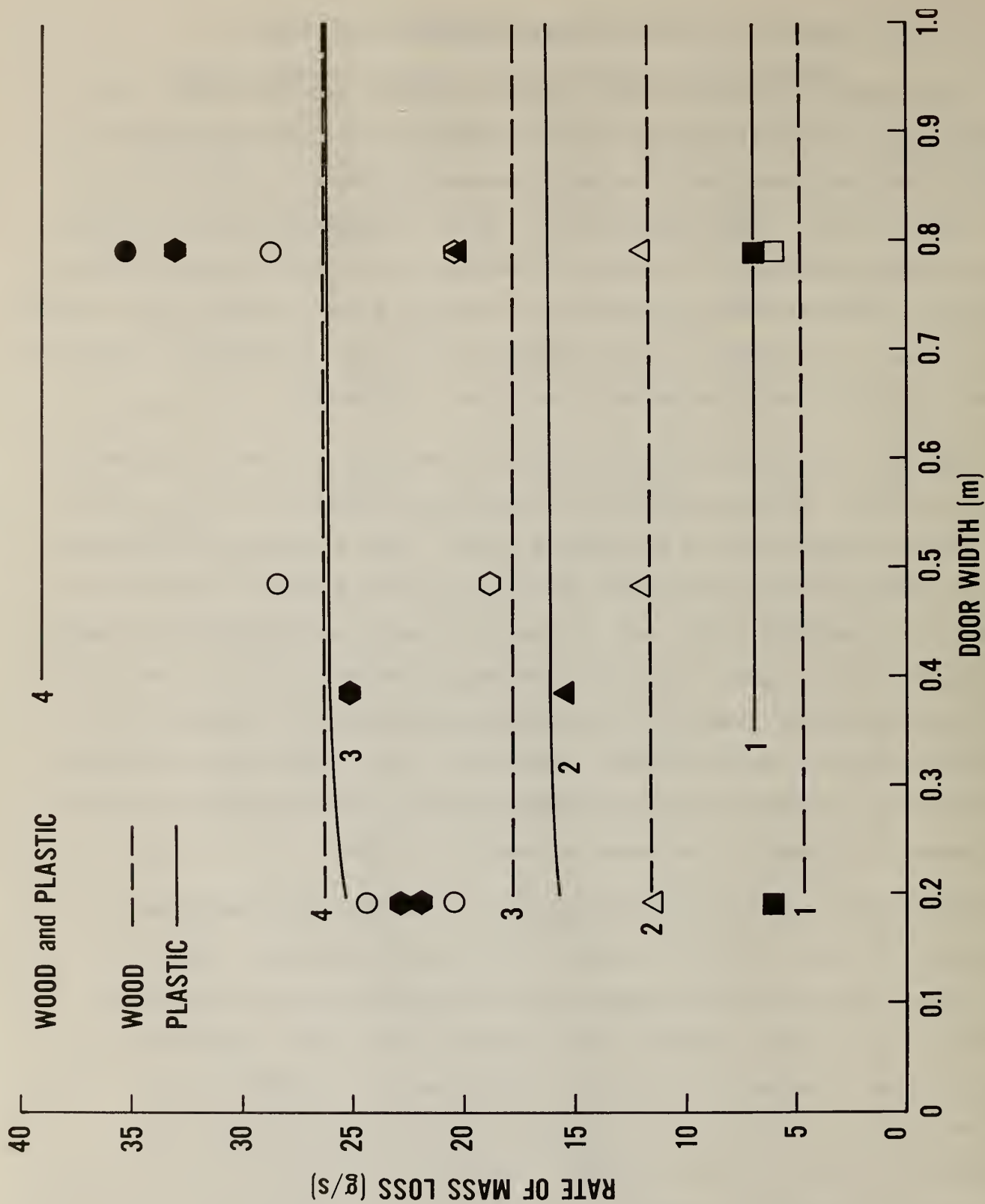
Figure 6-23. Comparison of experimental and theoretical rates of mass loss

The (velocity) neutral plane heights and thermal discontinuity heights are shown in figures (6-25a and b). Realizing, especially, that the thermal discontinuity is a nebulous quantity, the theory appears reasonably adequate.

The next two figures (6-20a and b) examine upper layer gas temperature. The lack of a unique layer temperature or an imposed procedure to derive a bulk temperature for the gases leaves a somewhat arbitrary choice of comparing experimental results to the theory. To confront this issue, the average ceiling layer temperature $\bar{T}$ from table 3-1 was plotted along with a bar tab indicating the temperature of the gases leaving at the top of the doorway. These differences are discussed in volume II and are clearly shown here. With these considerations for room temperature, the theoretical result, $T_{g,u}$, may be judged as in fair agreement with the data. It should be noted that for the polyurethane case a reduction in the wall conductive parameter α from 0.5 to 0.1 reduced the computed $T_{g,u}$ by 10 percent change in ΔH from kJ/g to 19 kJ/g, reduced $T_{g,u}$ by 15 percent, and a change in both α and ΔH yielded about 25 percent reduction in $T_{g,u}$. All of these changes would only influence the computed airflow rate by 3 percent at most.

In figures 6-27a and b the volumetric oxygen concentrations are plotted (dry basis) for the upper doorway probe. If corrected for water vapor, the data would be lower; if corrected for the vertical distribution in the doorway, the data would be higher than the average value which more correctly corresponds to the predicted value; hence, these are compensating corrections. Thus, the experimental values shown are probably close to a mixed-mean value, and are consistent with the theoretical quantity, $x_{O_2,u}$. The theoretical results appear to be in fair agreement with these data. An adjustment in the stoichiometric air-fuel ratio (r) could lead to improved results. A reduction in r of about 25 percent was suggested by analysis of the experimental results but this was not made in the simulation model computations.
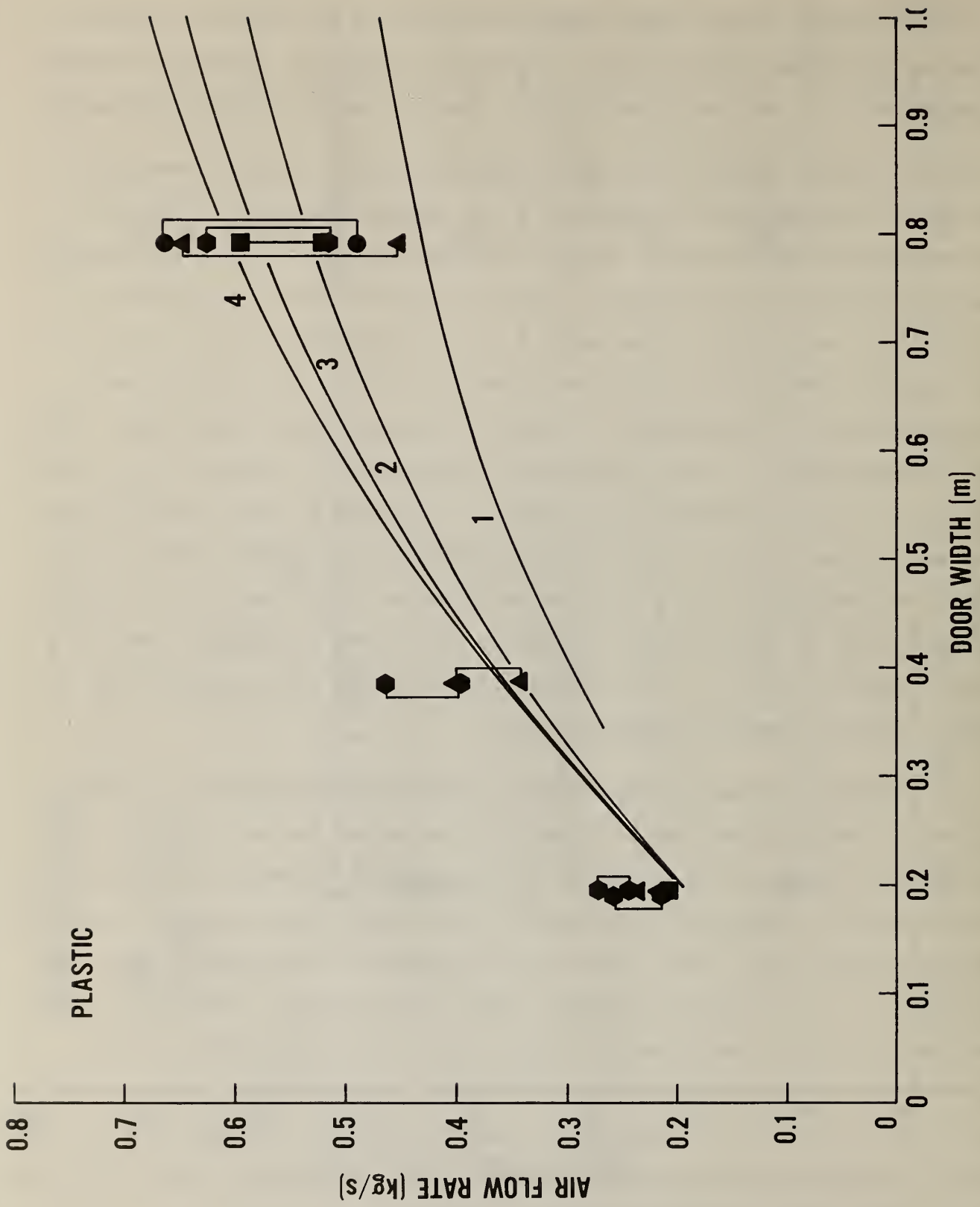
Figure 6-24a. Comparison of experimental and theoretical airflow rates - plastic fires

150
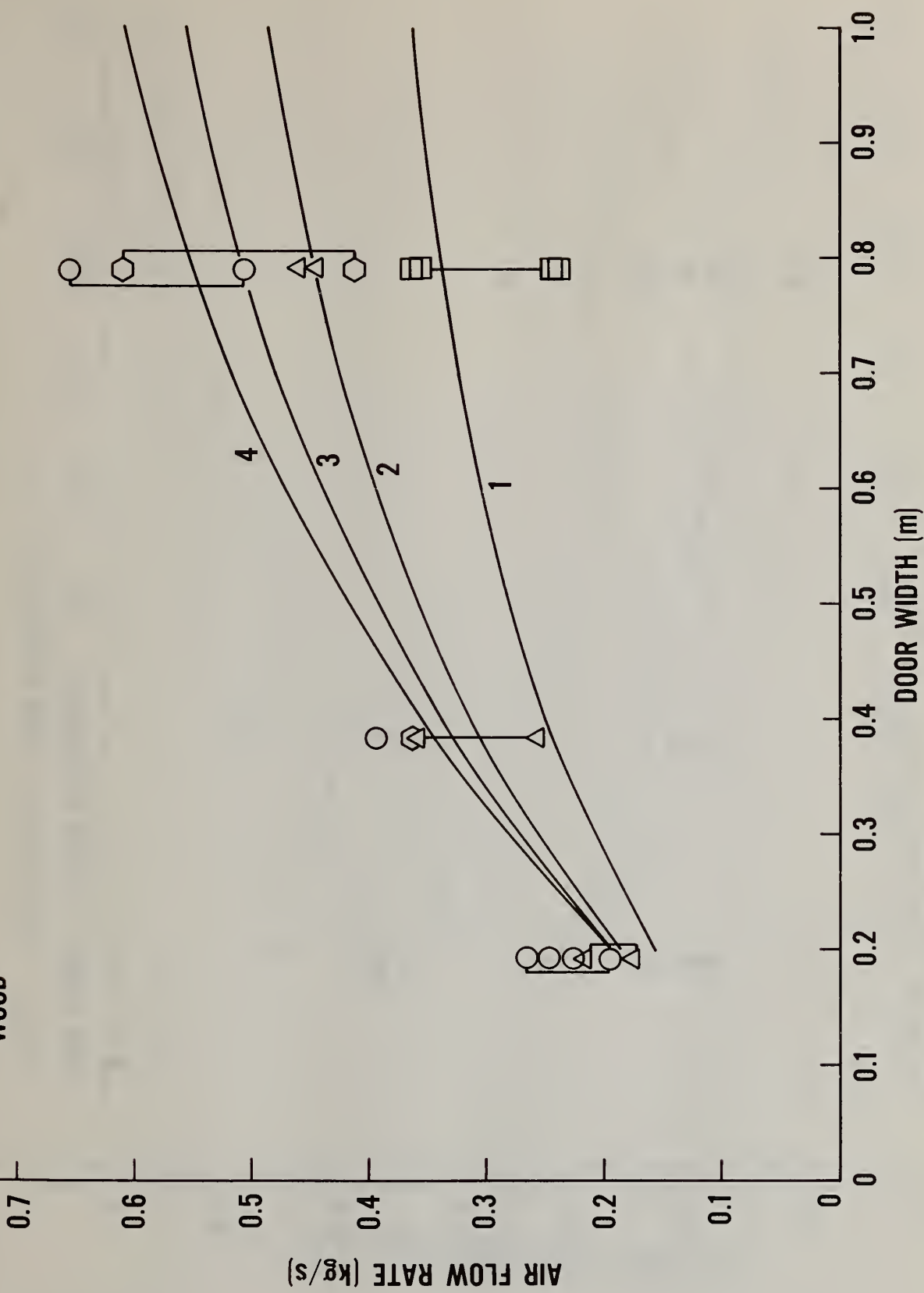
Figure 6-24b. Comparison of experimental and theoretical airflow rates - wood fires

151
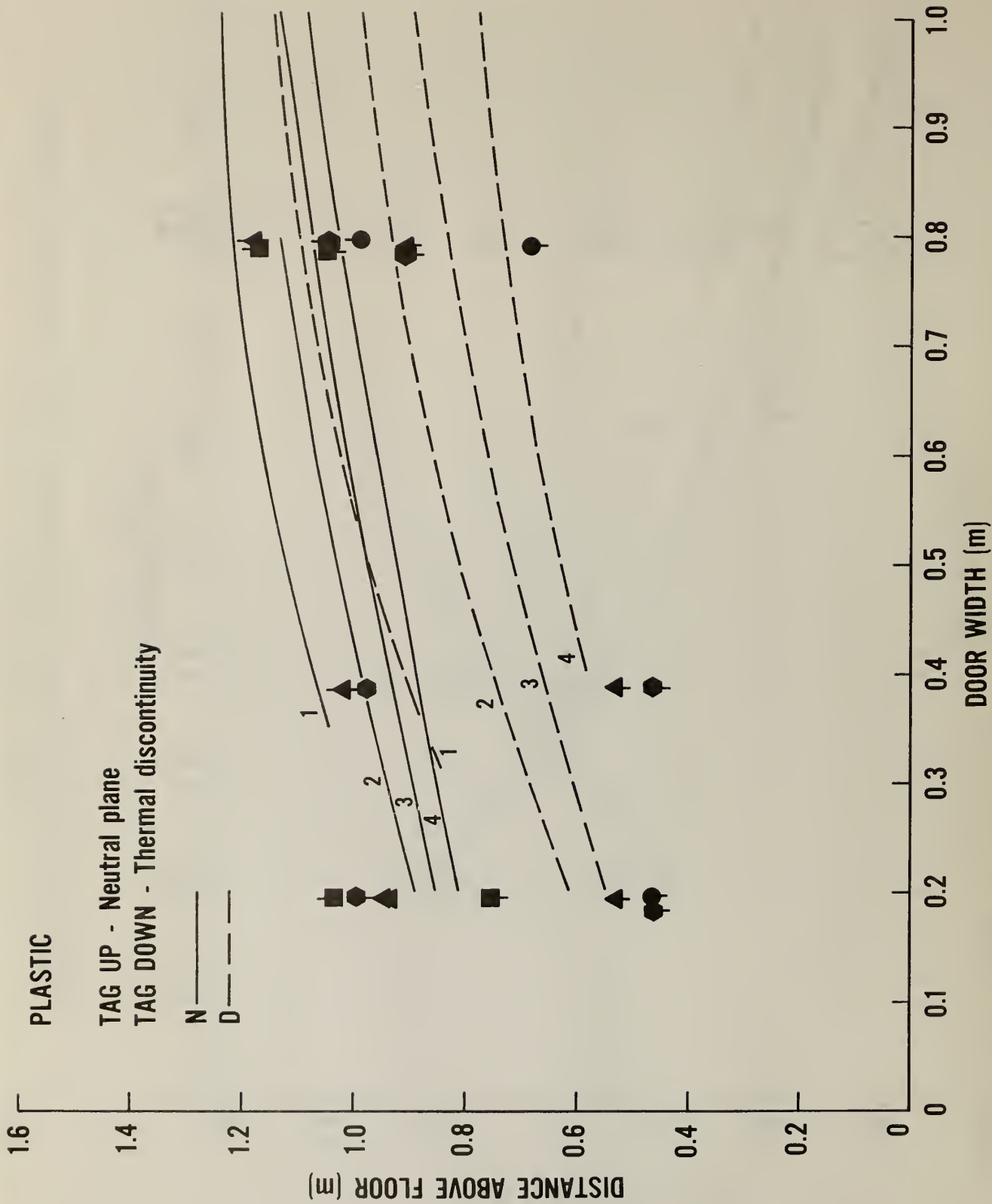
Figure 6-25a. Comparison of experimental and theoretical neutral plane and thermal layer heights – plastic fires
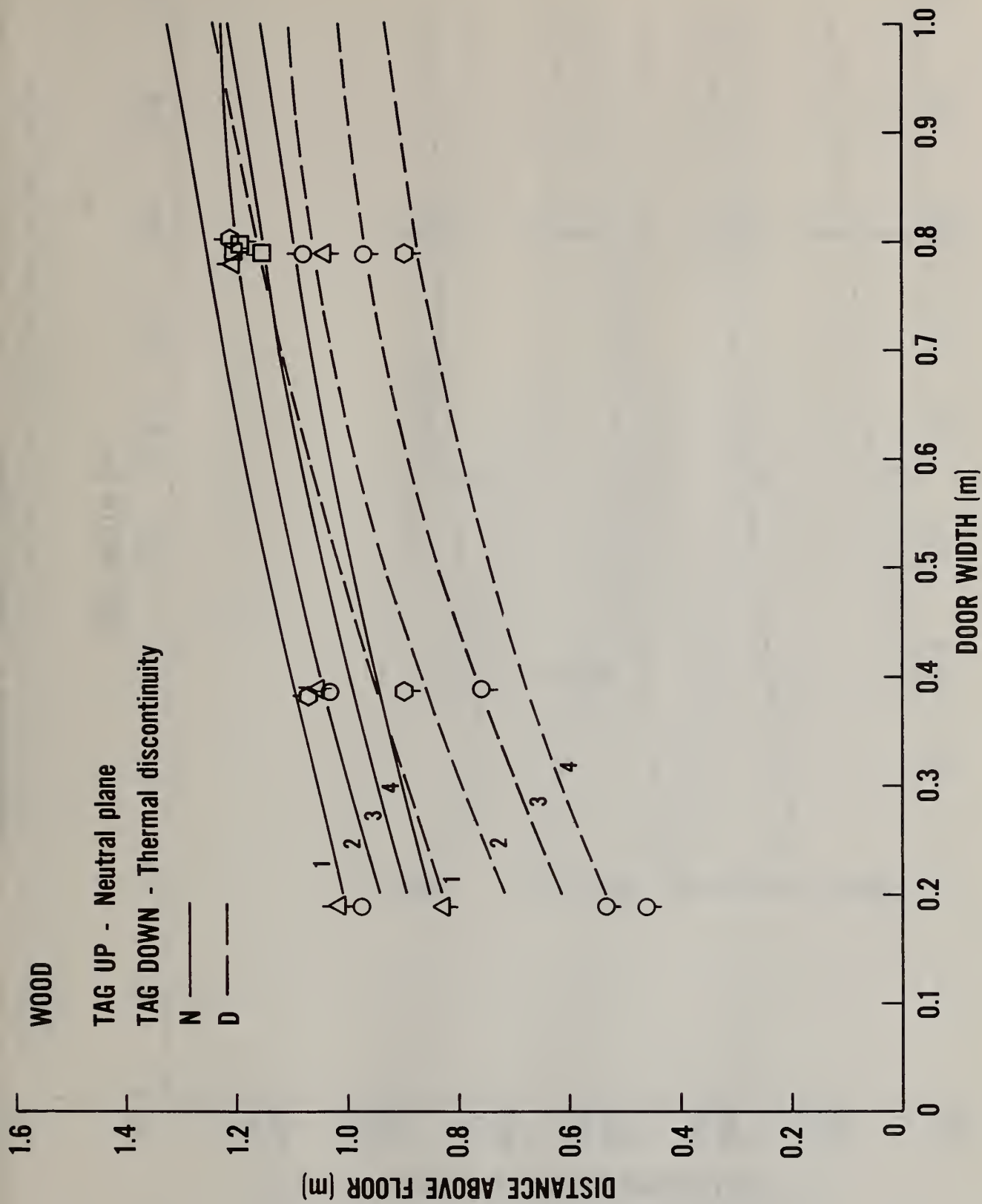
Figure 6-25b. Comparison of experimental and theoretical neutral plane and thermal layer heights – wood fires

153
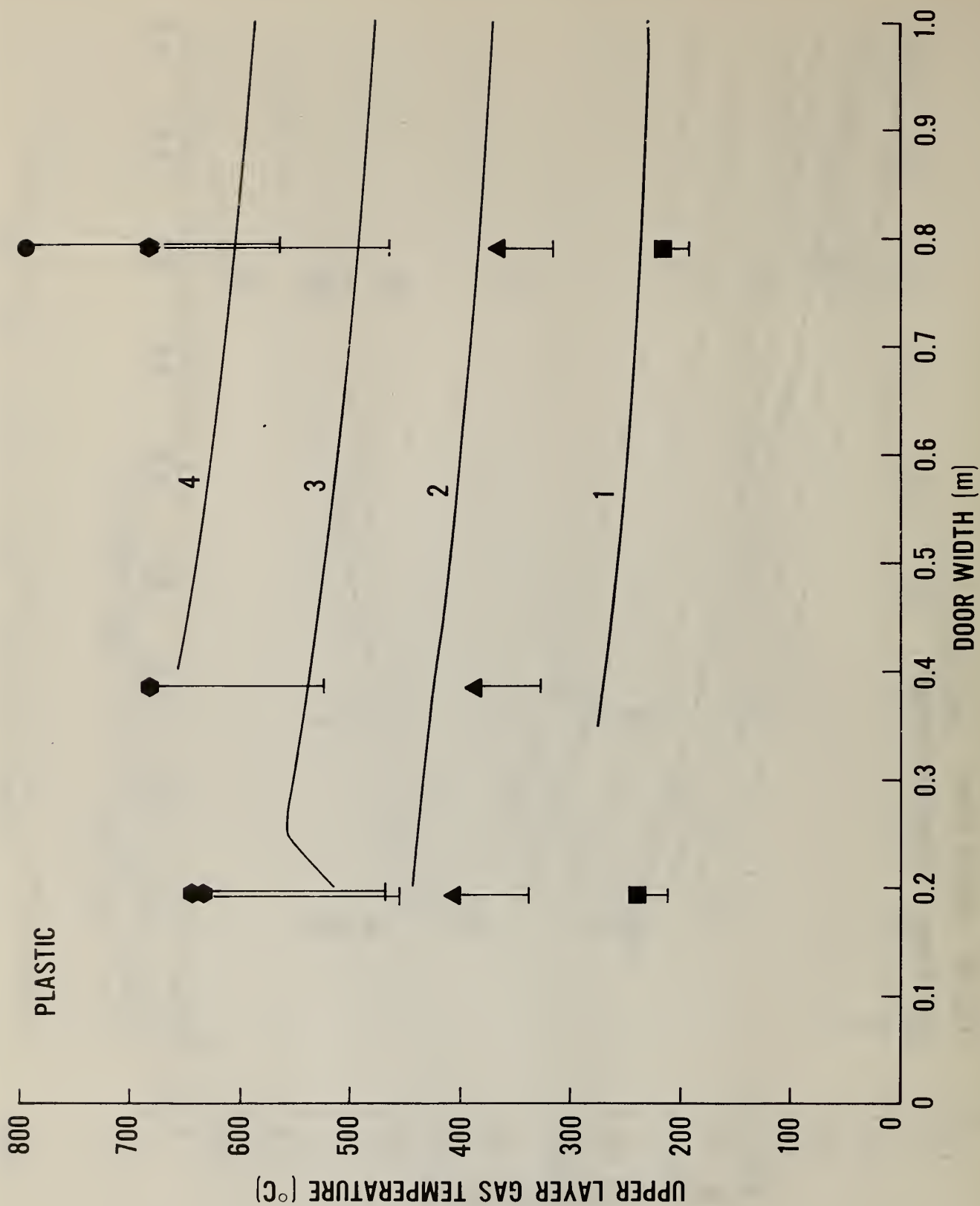
Figure 6-26a. Comparison of experimental and theoretical upper layer temperature – plastic fires

154
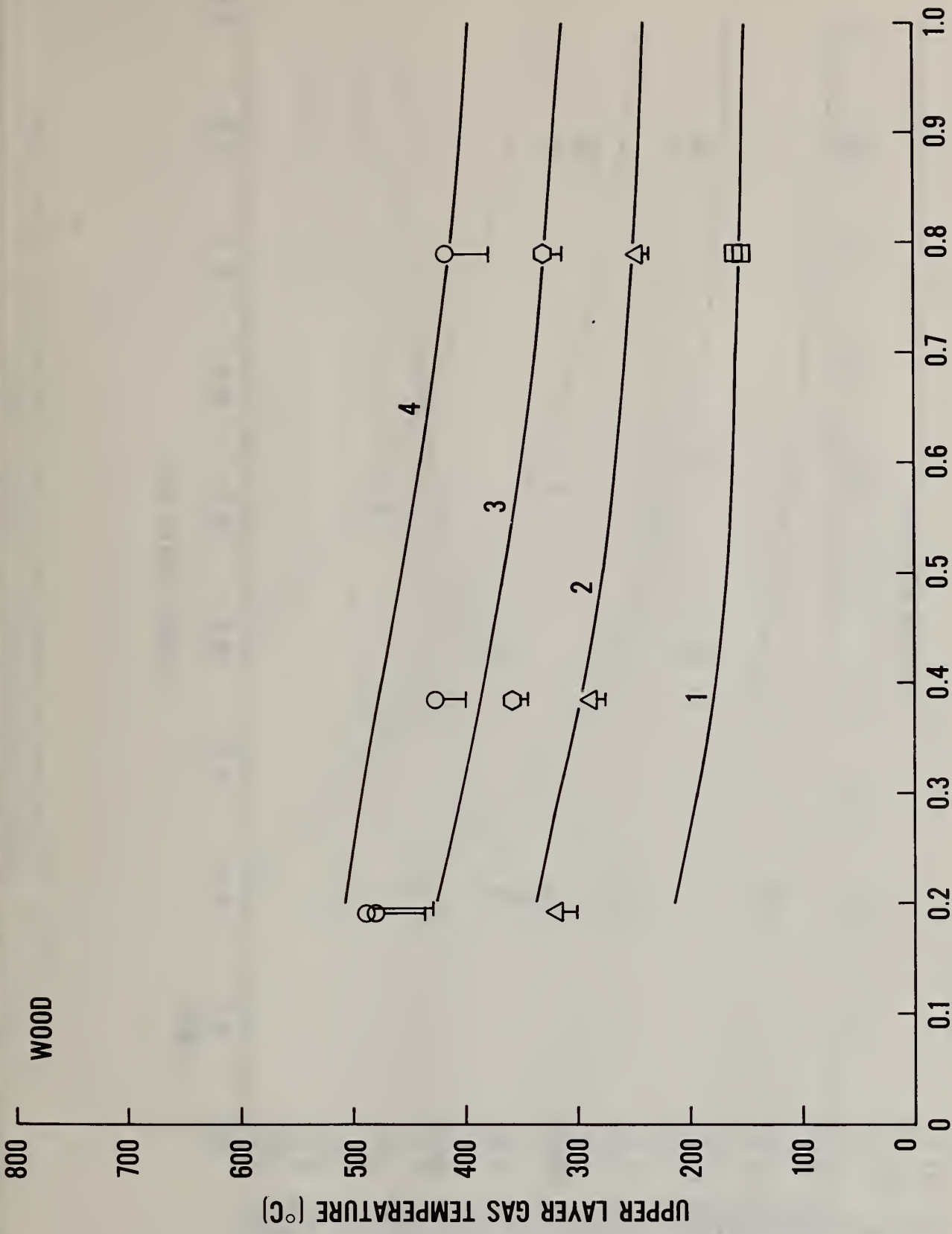
Figure 6-26b. Comparison of experimental and theoretical upper layer
temperature - wood fires
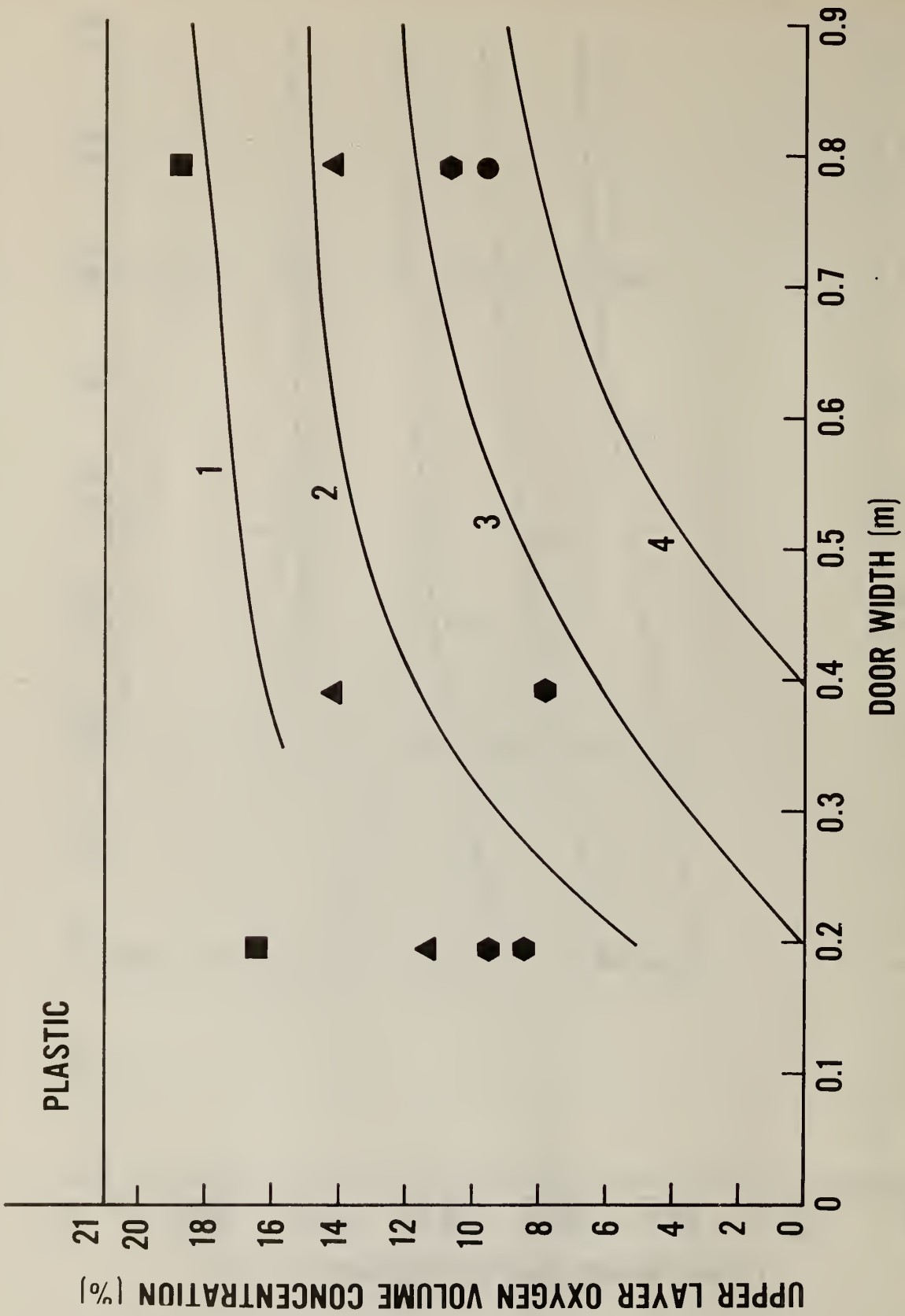
Figure 6-27a. Comparison of experimental and theoretical upper layer oxygen concentration - plastic fires

156
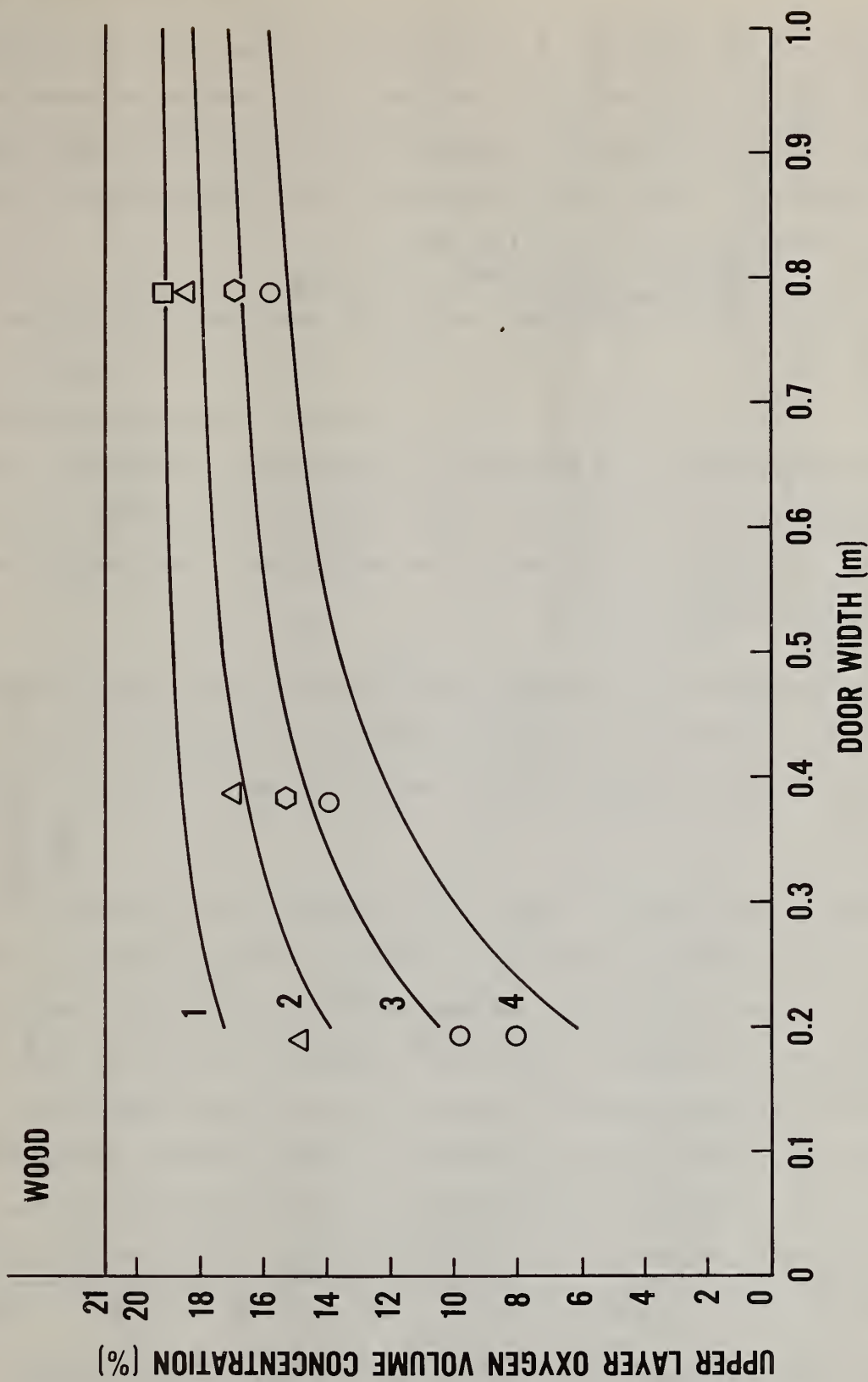
Figure 6-27b. Comparison of experimental and theoretical upper layer oxygen concentration - wood fires

157

A measure of the accuracy of the calculated lower layer gas temperature is given in figure 6-28. Again, the existence of a non-unique experimental lower layer gas temperature makes a comparison with the theoretical variable $T_{g,\ell}$ a bit tenuous. Despite some ambiguity in this interpretaion, however, the theory appears to be close to the mark.

The incident flux to the floor target (H2) was also derived from the model. For this calculation, the analysis of section 6.3.5.2 applies with $T_g = T_{g,u}$, $T_c = T_{w,u}$, and $T_a = T_b = T_{w,\ell}$. Because of the strong dependence of flux on room temperature, the variation of temperature in the room, and the smoke blockage effects in the lower layer, this prediction lacks some necessary refinements. Nevertheless its results are acceptable. The comparisons are shown in figures 6-29a and b.

Another viewpoint is to consider the incident floor target flux a function of the rate of mass loss. A comparison on this plot relaxes the burden on the theoretical model of predicting the mass loss rate. This is shown in figure 6-30.

The results presented in figure 6-30 have practical utility. They can serve to indicate whether flashover by remote ignition is likely to occur for a given fire. A nominal ignition criterion of 2 W/cm^2 will be used to make this assessment. Furthermore, additional computations were done for larger room sizes than the experimental test room. The critical mass loss rate at which a flux of 2 W/cm^2 would be reached at a floor position (given by the distance of sensor H2 from the fire source as in the experiments) was determined as a function of room size and doorway width. These results are shown in figure 6-31.

These results suggest that, with respect to the hazard of remote ignition of adjacent items in a room, the rigid polyurethane foam material is more hazardous than the sugar pine wood. Figure 6-31 indicates that for equal room and doorway sizes roughly 50 percent more wood than polyurethane must gasify to cause remote ignition in a room. Since the burning rate per unit area is
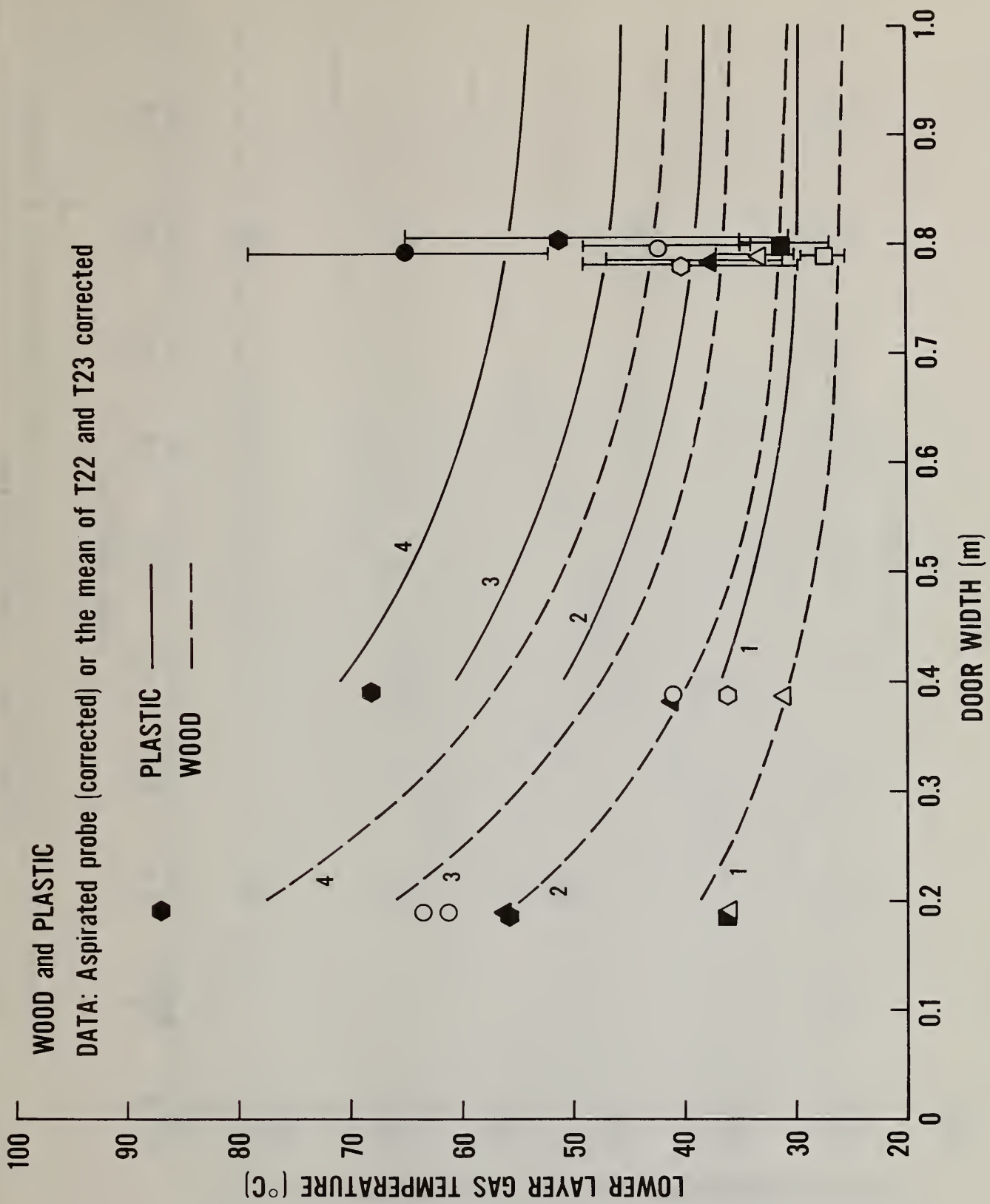
Figure 6-28. Comparison of experimental and theoretical lower layer temperature
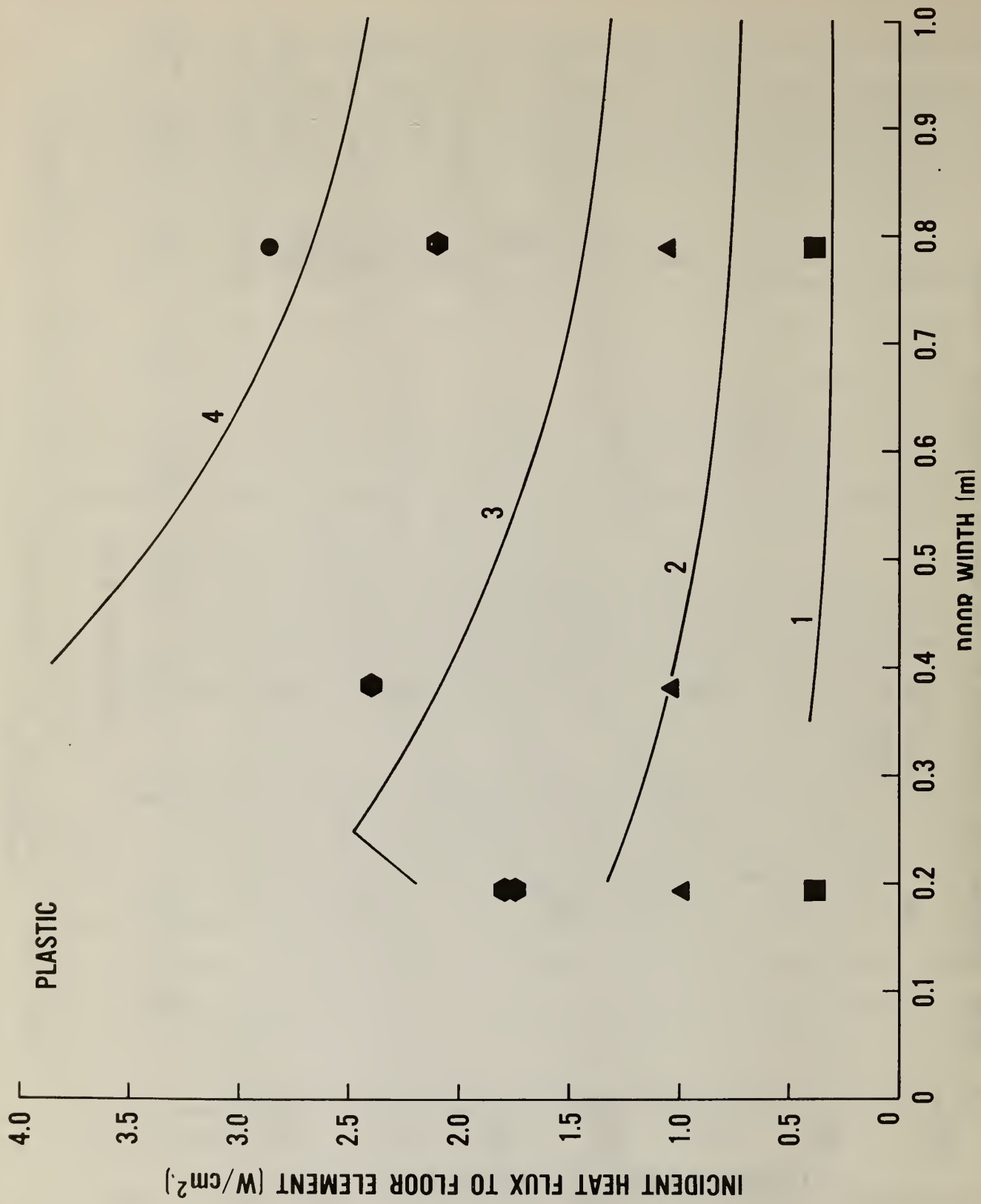
Figure 6-29a. Comparison of experimental and theoretical incident floor flux – plastic fires
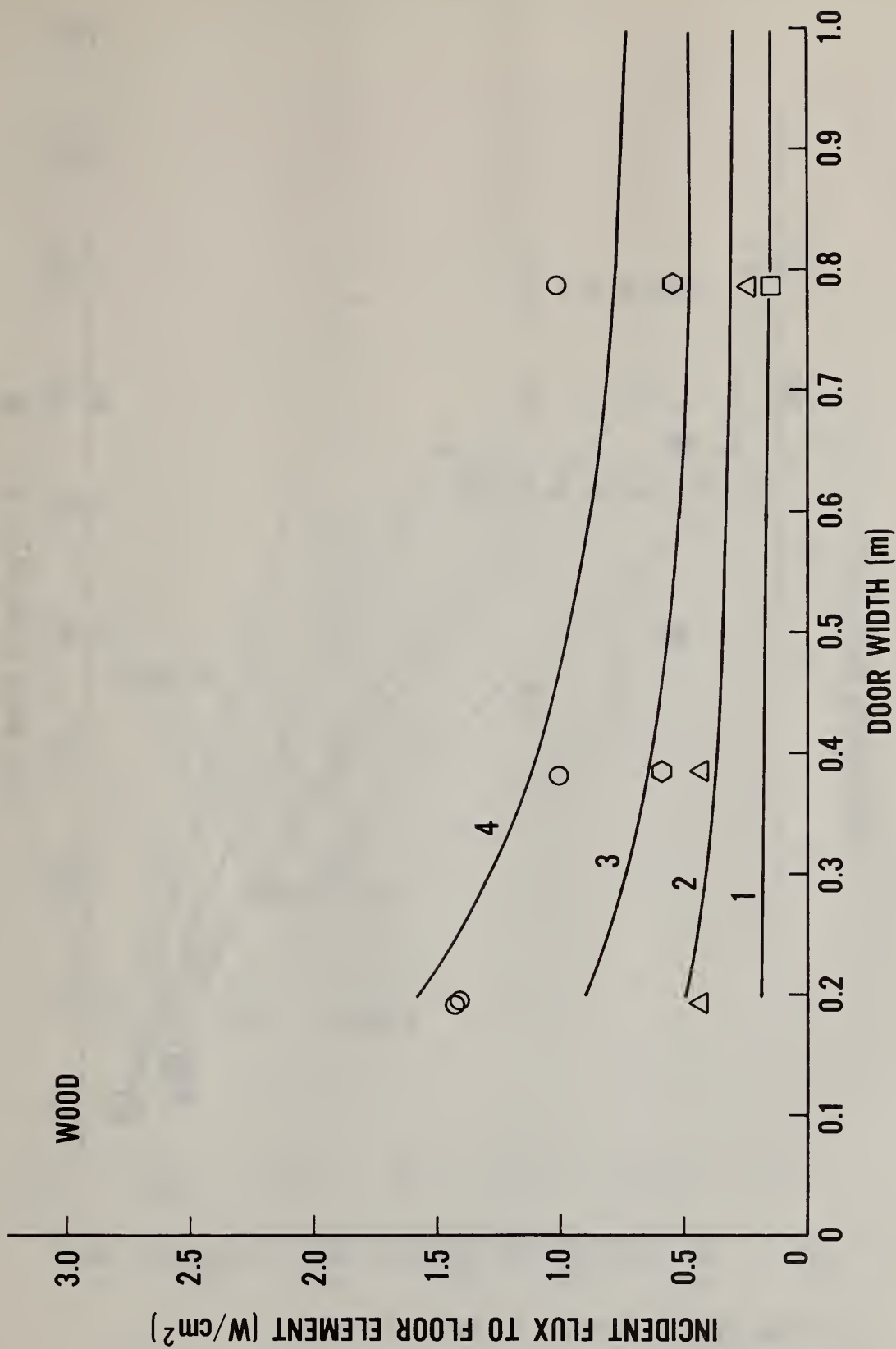
Figure 6-29b. Comparison of experimental and theoretical incident floor flux - wood fires

161
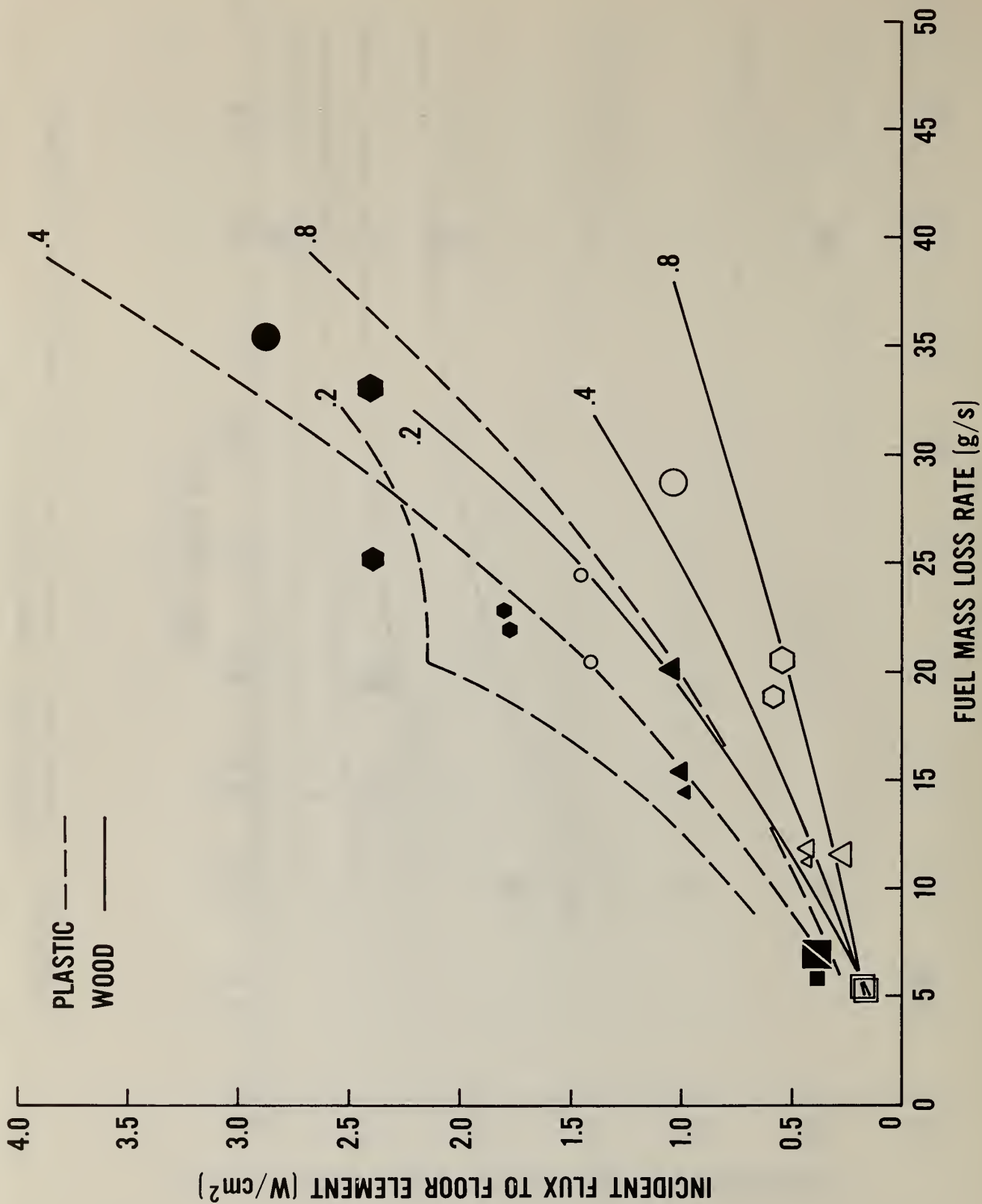
Figure 6-30. Comparison of experimental and theoretical incident floor heat flux as a function of wood and plastic rate of mass loss

162
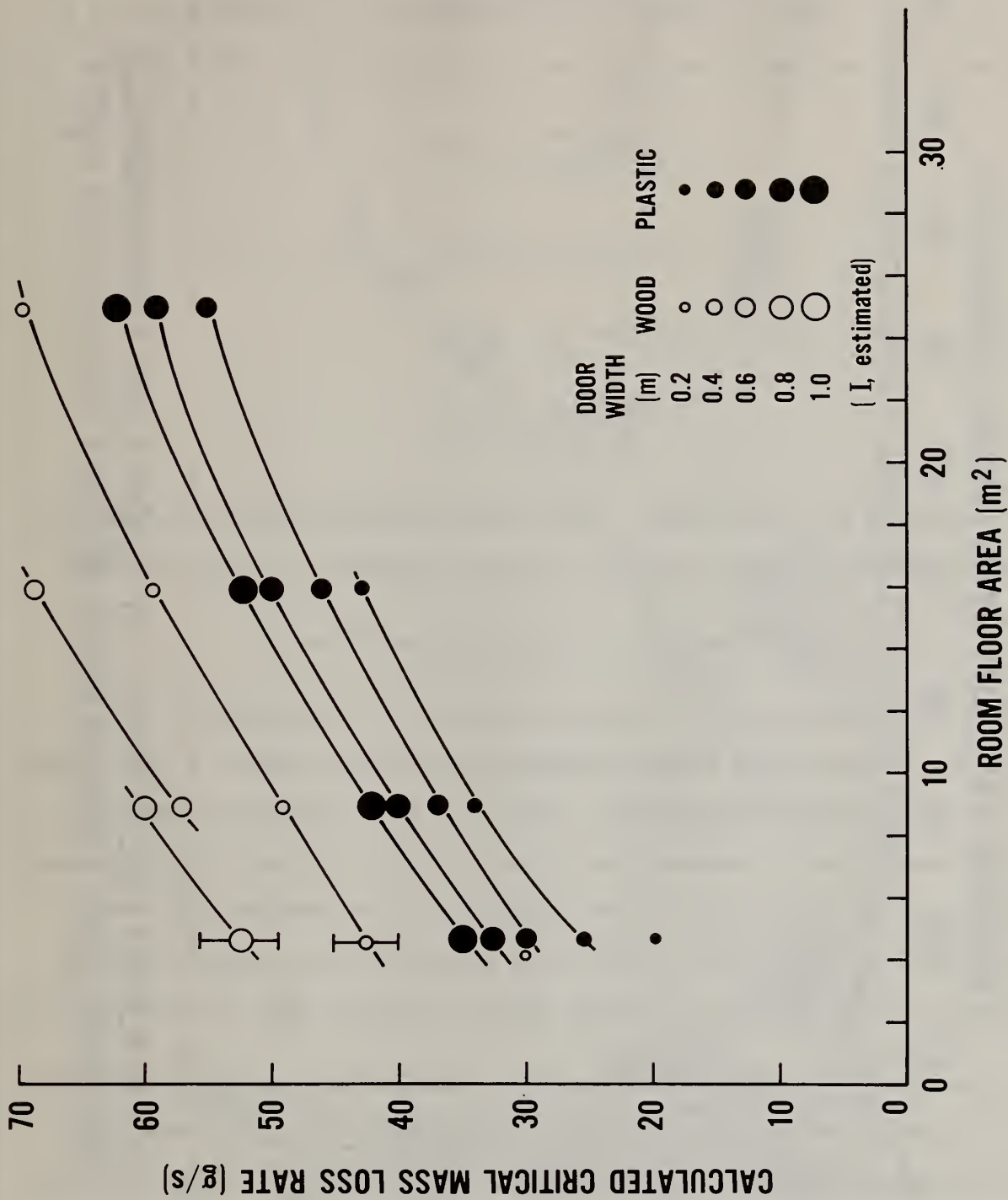
Figure 6-31. Calculated critical rates of mass loss for various size room floor areas with 2.41 m high ceiling and a door 1.83 m high and various doorway widths (also the input parameters of table 6-11 apply)

163

about 50 percent higher for the plastic cribs than the wood cribs, about twice as much wood as plastic must be burning to produce an equivalent hazard. That is, about twice the surface area of fire involvement is required by wood to cause remote ignition than is required by the polyurethane. This follows since

$$\frac{(\dot{m}''_{v,o})_{PU}}{(\dot{m}''_{v,o})_{wood}} \cong 1.5$$

and

$$(\dot{m}_{v,crit})_{wood}/(\dot{m}_{v,crit})_{PU} \cong 1.5$$

Therefore, the fire area, A_f, has the ratio

$$\frac{A_{f,wood}}{A_{f,PU}} \cong 2.25$$

to cause equivalent room heat flux. Thus more fire involvement is required for wood furnishings than for plastic to cause flashover in the same room.

6.6 Empirical Results of Room Furniture Fires

The present study applies to discrete fires in a room without the consideration of combustible lining materials and their effect on fire growth. Although the fuel element examined was cribs, it does bear some similarity to furniture assemblies. Moreover the range of burning rates considered and the extrapolation by analysis to other conditions does produce a relevant ensemble of results. This will be put into perspective by considering the results from a series of furniture fire studies found in the literature [34-41].

In a previous review of room fires [1] a tabulation was prepared of mass loss rates at the onset of perceived room flashover or the peak mass loss rates without flashover for a series of furniture items. It should be realized that those results were derived from experimental fires of rooms perhaps slightly larger than that of the present study and usually with one conventional size opening. In this tabulation no segregation due to room geometry or fuel composition was made. Moreover, since flashover did not always occur at any particular mass loss rate, a frequency of flashover was determined. These results are shown in figure 6-32.

164
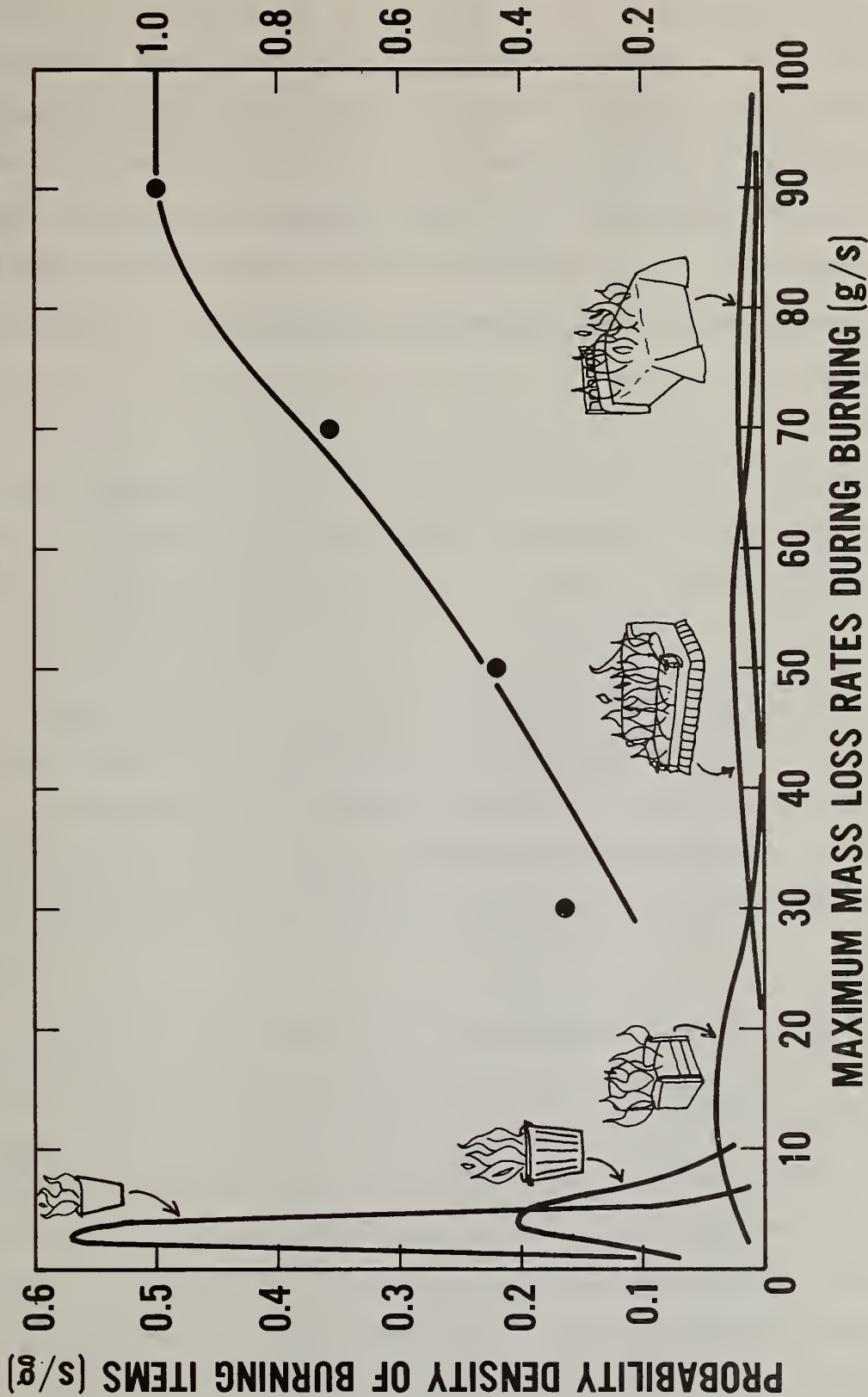
Figure 6-32. Furniture fire distribution and flashover

A careful examination and association of the theoretical results in figure 6-31 with the grossly categorized results of figure 6-32 will demonstrate a consistency of results. This comparison may provide added credibility to the theoretical results, and demonstrate the power of the theoretical solution. This is underscored when it is realized that figure 6-32 was derived from 120 experimental fires; yet these data are still not sufficient for developing continuous results and general conclusions as a theory is capable of achieving.

7. CONCLUSIONS

The primary goal of this study has been to make an assessment of the potential fire hazard of high density polyurethane foam with respect to its use in room furnishings. The study contrasted the characteristics of wood and plastic fires in a room environment. Based on these results and their analyses the following conclusions were drawn.

1. With respect to the potential for flashover by remote ignition, the plastic material (rigid polyurethane, GM37) is roughly twice as prone to cause flashover as wood (sugar pine). This is based on the critical fuel surface area burning in a given room; it does not account for the rate of spread over the fuel. By analysis this conclusion can be traced to the difference in heats of combustion and the rates of gasification of burning between the two materials.

2. For these crib experiments, the effects of the room environment on the fire were of secondary significance. Enhancement by radiation feedback and reduction in burning due to oxygen deficiency appeared to be of the order of $\pm$ 25 percent at most. This is likely to be true for some furniture items, but especially not the case in which flame spread on horizontal surfaces is a factor.

3. Although the stoichiometric air requirements are distinctly different for the two fuels, room ventilation was not a significant factor in controlling room heating over the range of doorway widths considered. The empirical correlation of equation (56) clearly shows that room temperature is a strong function of energy release rate, but a weak function of the ventilation factor. In fact, for this study, the theoretical calculations indicate a significant diminution of the mass loss rate only below doorway widths of 0.2 m. Thus, it is likely that ventilation will have a significant effect on reducing the fuel gasification rate only for very small room openings. While this ventilation controlled (small fires) fire regime may not be a hazard from a fire growth point of view, it will tend to increase the production of CO.

4. The development of the theoretical model and selective comparisons with the experimental results provide an assessment of the model's accuracy. The two-layer model is an approximation of reality and hence will never be perfectly consistent with experimental results. It is likely, however, that the imperfections of the model are becoming comparable with the uncertainty of some experimental measurements.

8. ACKNOWLEDGEMENTS

9. REFERENCES

[1] Quintiere, J. G., Growth of fire in building compartments. Fire Standards and Safety, ASTM STP 614, 131-167 (1977).

[2] Quintiere, J. G., McCaffrey, B. J. and Den Braven, K., Experimental and theoretical analysis of quasi-steady small-scale enclosure fires, Nat. Bur. Stand. (U.S.), NBSIR 78-1511 (October 1978).

[3] Emmons, H. W., Mitler, H. E. and Trefethen, L. N., Computer Fire Code III, Home Fire Project Tech. Rept. No. 25, Harvard (1978).

[4] Pape, R. and Waterman, T., Modifications to the RFIRES pre-flashover room fire computer model. IITRI Project J6400, IIT Research Institute, Chicago, Ill. (March 1977).

[5] MacArthur, C. D. and Myers, J. F., Dayton aircraft cabin fire model validation. Phase 1, Rept. No. FAA-RD-78-57, University of Dayton Research Institute, Dayton, Ohio (March 1978).

[6] Smith, E. E. and Heibel, J. T., Evaluation performance of cellular plastics in fire systems. PRC Proj. No. RP-75-1-36, Ohio State University, Columbus, Ohio (1977?).

[7] Gross, D., Experiments of the burning of cross piles of woods. Journal of Research, National Bureau of Standards, Vol. 66 C, No. 2, 99-105 (April-June 1962).

[8] Block, J. A., A theoretical and experimental study of non-propagating free-burning fires, 13th Symposium (International) on Combustion, The Combustion Institute, 971-978 (1971).

[9] Sensenig, D. L., New concept for determining rate of heat release by oxygen consumption, presented at the Fall Technical Meeting, Eastern Section of the Combustion Institute, Miami Beach, Fla. (Nov. 1978) (To be published).

[10] Croce, P. A., Modeling vented enclosure fire Part 1. Quasi-steady wood-crib source fires, FMRC J. I. 7AOR5.GU, Factory Mutual Research Corp., Norwood, MA, (July 1978).

[11] McCaffrey, B. J. and Rockett, J. A., Nat. Bur. Stand. (U.S.), J. Res., Vol. 82, No. 2, 107-117 (1977).

[12] Quintiere, J. G. and Den Braven, K., Some theoretical aspects of fire induced flows through doorways in a room-corridor scale model, NBSIR 78-1512, Nat. Bur. Stan., Washington, D.C. (Oct. 1978).

[13] Prahl, J. and Emmons, H. W., Combustion and Flame, Vol. 25, No. 3., 369-385, (Dec. 1975).

[14] Shivadev, U. K. and Emmons, H. W., Combustion and Flame, Vol. 22, 223-236 (1974).

[15] Birky, M., Private communication, 1978.

[16] Smith, R. K., Morton, B. R. and Leslie, L. M., J. Fluid Mech., Vol. 68, Part 1, 1-19 (1975).

169

[17] Quintiere, J. G., McCaffrey, B. J. and Rinkinen, W. J., Fire and Materials, Vol. 2, No. 1, 18-24 (1978).

[18] McCaffrey, B. J., Purely buoyant diffusion flames: some experimental results, Nat. Bur. Stand., (U.S.,) NBSIR 79-1910 (Oct. 1979).

[19] Dayan, A. and Tien, C. L., Combustion Science and Technology, Vol. 9. 41-47 (1974).

[20] Markstein, G., Radiative properties of plastic pool fires, FMRC J.I. 7AOR3.GU, Factory Mutual Research Corp., Norwood, Mass. (July 1978).

[21] Hagglund, B. and Persson, L. E., An experimental study of radiation from wood flames, FOA 4 Rapport, C 4589-D6 (A3), Forsvarets Forskningsanstalt, Stockholm, Sweden (June 1974).

[22] Modak, A. T., Radiation from products of combustion, FMRC J.I. OAOE6.BU-1, Factory Mutual Research Corp. Norwood, Mass. (Oct. 1978).

[23] Modak, A. T. and Matthews, M. K. Radiation augmented fires with enclosures, Tech. Rept. 22361-8, Factory Mutual Research Corp., Norwood, Mass. (Feb. 1977).

[24] Siegel, R. and Howell, J. R., Thermal radiation heat transfer, Vol. III, NASA SP-164, National Aeronautics and Space Administration, Washington, D.C. (1971).

[25] Zukoski, E. E. and Kubota, T., An experimental investigation of the heat transfer from a buoyant gas plume to a horizontal ceiling - part 2. Effects of ceiling layer, Nat. Bur. Stand. (U.S.), NBS-GCR-77-98, NBS Grant No. 5-9004 (1975).

[26] Carslaw, H. S. and Jaeger, J. C., Conduction of heat in solids, 2nd Ed. Oxford University Press, London (1959).

[27] Siu, C. I., Personal communication (1978).

[28] Tamanini, F., Personal communication (1977).

[29] Thomas, P. H., Bullen, M. L., Quintiere, J. G. and McCaffrey, B. J., Flashover and instabilities in fire behavior, Combustion and Flame, Vol. 38, 159-171 (1980).

[30] Tewarson, A., Experimental evaluation of flammabilty parameters of polymeric materials, FMRC J.I. 1A6R1. PRC Grant No. RP-75-1-33A, Factory Mutual Research Corp., Norwood, Mass. (Feb. 1979).

[31] Twilley, W., Personal communications (1978).

[32] Kanury, A. M., Rate of charring combustion in a fire, 14th Symposium (International) on Combustion, The Combustion Institute, 1131-1142 (1973).

[33] Durak, O. T., Combustion of wood cribs in diluted atmosphere, NBS Grant No. G5-9009, Northwestern University, Evanston, Ill. (June 1976).

[34] Waterman, T. E., Determination of fire conditions supporting room flashover, Final Rept. IITRI Project M6131, DASA 1886, Defense Atomic Support Agency, Washington, D.C. (Sept. 1966).

[35] Croce, P. A. and Emmons, H. W., The large-scale bedroom fire test, July 11, 1973, FMRC Ser. No. 21011.4, Factory Mutual Research Corp., Norwood, Mass. (July 1974).

[36] Croce, P. A., A study of room fire development: the second full-scale
      bedroom fire test of the home fire project (July 24, 1974), Factory
      Mutual Research Corp., Norwood, Mass. (June 1975).

[37] Hagglund, B., Jansson, R. and Onnermark, B., Fire development in resi-
      dential rooms after ignition from nuclear explosions, FOA Rep. C 20016-D6
      (A3), Forsvarets Forskningsanstalt, Stockholm, Sweden (Nov. 1974).

[38] Gross, D. and Fang, J. B., The definition of a low intensity fire,
      Nat. Bur. Stand. (U.S.), Spec. Publ. 361, Vol. 1 (March 1972).

[39] Fang, J. B., Measurement of the behavior of incidental fires in a
      compartment, Nat. Bur. Stand. (U.S.), NBSIR 75-679 (March 1975).

[40] Theobald, C. R., The critical distance for ignition from some items
      of furniture, FR Note 736, Fire Research Station, Borehamwood, England
      (Dec. 1968).

[41] Christian, W. J. and Waterman, T. E., Fire Technology, Vol. 7, No. 3,
      205-217, (Aug. 1971).

APPENDIX A.   GASIFICATION RATE OF FREE BURNING CRIB FIRES

A series of wood and plastic crib fire experiments were conducted in order to design a crib for the room fire experiments. The burning rate of wood crib fires has been studied by Gross [7] and Block [8], and the theory of Block was used as a basis for correlating our experimental results.

Basically crib fires burn in two regimes. The porosity controlled regime is where the airflow through the crib controls its rate of mass loss. Cribs with close stick spacing fall into this regime. For the porosity controlled regime, Block derived the mass loss rate per exposed surface area to be

$$\dot{m}_v'' = 1/2 \ f \ \rho \ \left\{ \left[(\rho_o - \rho)/\rho \right] \ gh \right\}^{1/2} \ \left[(\lambda - 1)/\lambda \right] \ G/\phi \qquad \text{(A-1)}$$

where $G = \left\{ \phi^{-1} \left[\dfrac{1 - e^{-\phi}}{1 - (\rho/\rho_o)^2 \ \lambda \ e^{-\phi}} \right] \right\}^{1/2}$

and $\phi = \dfrac{P_s hf}{2 \ A_{vs}}$ is a dimensionless drag coefficient

Also $\dfrac{\lambda - 1}{\lambda} = \dfrac{B}{(B + 1) + \phi^{-1} \{2/[1 + \rho/\rho_o) \lambda^{-1}]\}}$

and $B = [E\gamma - c_p \ (T_s - T_o)]/\epsilon$.

The symbols conform to those used by Block [8] and are listed below:

f = friction factor = 0.13

g = gravitational acceleration

h = height of crib

ρ = density of fluid in a crib shaft

ρ_o = density of ambient air

P_s = perimeter of a shaft

A_{vs} = cross-sectional area of a shaft

E = heat of combustion

ϵ = heat of volatilization

c_p = specific heat of solid fuel

172

T_s = surface temperature of burning solid

T_o = ambient air temperature

Furthermore, Block showed that for densely packed cribs and most cribs in general, most of the air flow enters from the bottom of crib rather than from the sides. This vertical flow rate per unit shaft area A_{vs} can be estimated as

$$\frac{\dot{m}_{air}}{A_{vs}} = \rho_o \left[\frac{\left(\frac{\rho_o}{\rho} - 1\right) \frac{gh}{\phi} (1 - e^{-\phi})}{\left(\frac{\rho_o}{\rho}\right)^2 - e^{-\phi}} \right]^{1/2} \qquad (A-2a)$$

or for $\phi \geq 1$

$$\frac{\dot{m}_{air}}{A_{vs}} \cong \rho_o \sqrt{\frac{\rho}{\rho_o} \left(1 - \frac{\rho}{\rho_o}\right) gh/\phi} \qquad (A-2b)$$

For our design crib $\dot{m}_{air}/A_{vs}$ was calculated as 0.89 kg/m^2-s or 17.5 g/s per crib.

In the open or surface area controlled regime the mass loss rate per unit exposed area is given as

$$\dot{m}_v'' = Cb^{-n} \qquad (A-3)$$

where n = 1/2 according to Block, and C is an empirical constant, determined for the polyurethane and taken from Block [8] for wood specie.

Table A-1. Crib open burn results: rate of mass loss correlation

Material	Density ρ g/cm^3	b cm	s cm	n	N	ϕ	C mg/cm$^{1.5}$-s	Ψ	$\dot{m}_v$ g/s	$\dot{m}_v/Cb^{-1/2}$
PINE, Ponderosa	0.54	1	5	3	10	0.520	1.03[+]	1.89	1.70	1.14
PINE, Ponderosa	0.42	4	6	3	10	1.73	1.03[+]	2.84	6.5	1.26
PINE, Eastern	0.36	1	5	3	10	0.520	1.	1.94	1.6	1.10
PINE, Eastern	0.36	4	6	3	10	1.73	1.	2.94	4.0	0.81
PINE, Sugar + Ponderosa	0.39 – 0.43	3.5	7	3	10	1.30	1.	3.25	5.0	1.04
PINE, Sugar	0.37	3.5	7	3	10	1.30	0.88[+]	3.69	4.4	1.04
PINE, Sugar	0.37	3.5	7	3	10	1.30	0.88[+]	3.69	5.2	1.21
Rigid Polyurethane	0.46	1	5	3	10	0.520	1.2	1.22	1.60	0.92
Rigid Polyurethane	0.46	1.5	7	2	4	0.223	1.2	1.78	0.36	0.86
Rigid Polyurethane GM-37	0.34	1	5	3	10	0.52	1.2	1.23	1.78	1.02
Rigid Polyurethane GM-37	0.34	4	6	3	10	1.73	1.2	1.85	4.0	0.66
Rigid Polyurethane GM-37	0.34	1	2	3	10	1.30	1.2	0.62	0.38	0.43
Rigid Polyurethane GM-37	0.34	3.5	7	3	10	1.30	1.2	2.18	7.2	1.24
Rigid Polyurethane GM-37	0.34	3.5	7	3	10	1.30	1.2	2.18	8.0	1.39
Rigid Polyurethane GM-37	0.34	3.5	7	3	10	1.30	1.2	2.18	6.05	0.94

[+]from Block

Table A-2

Estimated property values for crib material

Material	Stoichiometric fuel to air ratio λ g/g	Specific heat c_p J/g-°c	Heat of combustion E kJ/g	Effective surface temp. T_s °C	Heat of volatilization ε kJ/g	B
Wood*	0.27	1.26	18.6	370	1.78	2.56
Poly-urethane†	0.13	1.26	23.4	325	1.52	1.80

*from Block [8]

†from literature

The data are tabulated in table A-1. The correlation by Block [8] is based on Ψ defined as the ratio of equation (A-1) to equation (A-3). The predicted specific mass loss rate $\dot{m}_v''$ is the smaller of the values calculated from equation (A-1) or equation (A-3). The parameters required in equation (A-1) are listed in table A-2. They represent available values determined at the time this analysis was made, and are not necessarily the same as the values used in section 6. A thorough analysis of the polyurethane cribs has not been made, so those may not be the "best" values listed in table A-2. Also in the calculations, the density ratio, ρ/ρ_o, was estimated as 0.2. The experimental results are plotted in figure A-1. The plastic and wood crib designs are identical in geometry but differ in Ψ values as shown. The design crib has $\Psi = 2.18$ for the polyurethane, and $\Psi = 3.69$ for the sugar pine. Clearly there is uncertainty in selecting the "best" property values for the polyurethane from limited data, and since its sticks swell on burning. The swelling effect could cause the design value for Ψ to decrease shifting toward the porosity controlled burning regime. For the plastic crib design value of $\Psi = 2.18$, an anticipated maximum swelling of 50 percent in stick thickness reduced Ψ to 1.09--still in the surface area regime of burning.
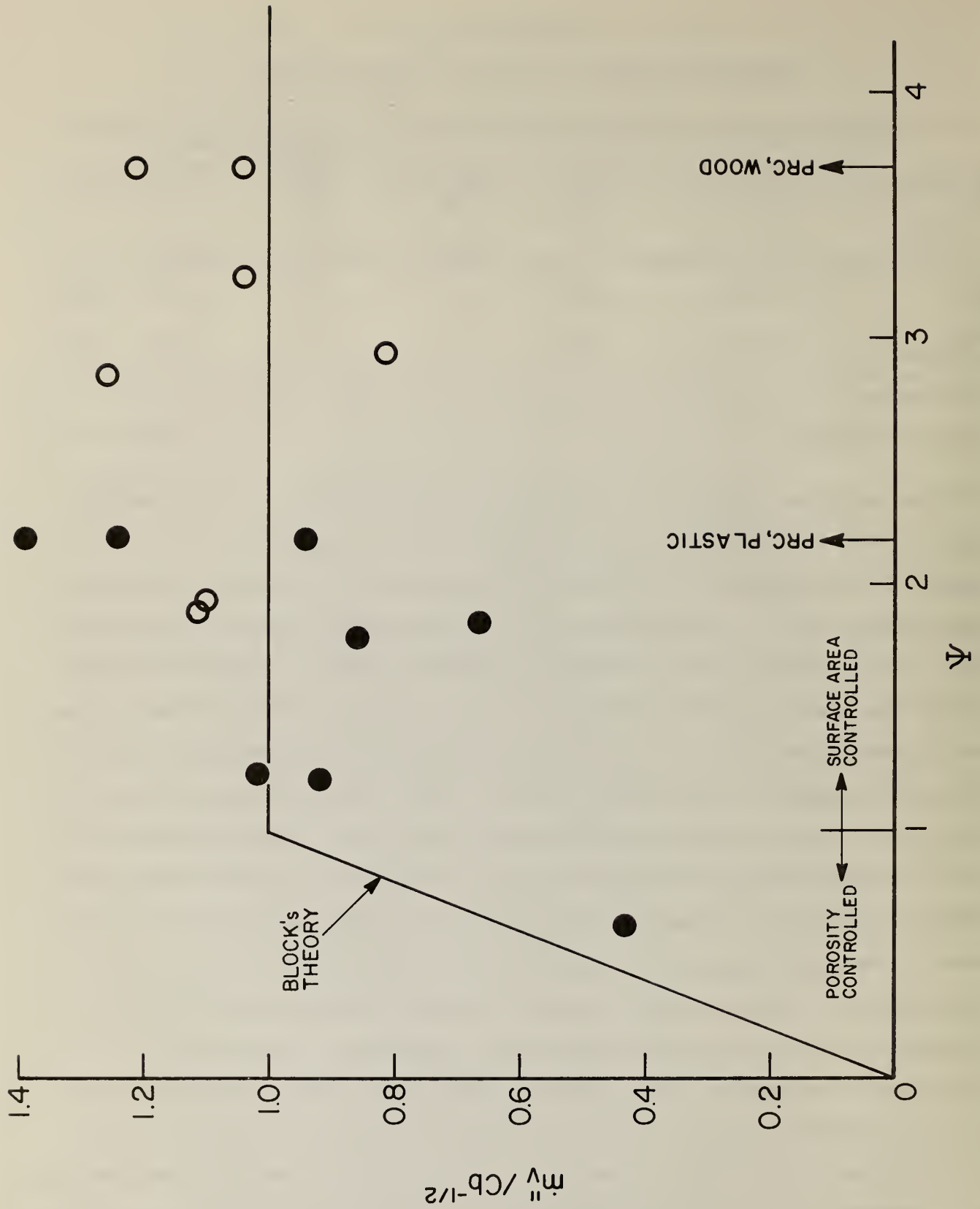
Figure A-1.   Correlation of crib burning rate data used for design

## APPENDIX B. RADIATION EFFECT ON LOWER LAYER THERMOCOUPLES

It was observed early in the experimental results that the gas temperatures in the lower portion of the room were significantly above the incoming air temperature. The lowest thermocouple (T23) read as high as 118°C (PRC 8-P-4-1). It was unclear whether this was due to radiation or heated gas in the lower space due to mixing. To resolve these results, thermocouple bead sizes were recorded for experiments subsequent to PRC 8, and small wire thermocouples and an aspirated probe were used (see figure 2-5).

In order to assess the radiation effect on a thermocouple under normal atmosphere temperature, thermocouples were irradiated with a known radiant flux from a quartz lamp. The irradiated thermocouple was in "still" air but probably was subjected to a low natural convection induced flow. The schematic of this experiment and its results are shown in figure B-1. (Data points have been omitted for the aspirated probe.) The results yield about a $-5°$ $C/W/cm^2$ correction for the aspirated probe and a $-20°$ $C/W/cm^2$ correction for the normal size thermocouples used (0.5 mm bead diameter). Figure B-2 is a plot of the same results for the "backed" beads (the reflective metal backing shown in the schematic of figure B-1) in terms of bead diameter. These results can be used to correct thermocouples due to thermal radiation effects for the case of irradiation over one bead hemisphere and thermocouple temperature above the true surrounding gas temperature.

A comparison was made between the bare thermocouple T23 and the aspirated probe T28 for the average peak burning periods. Also, the radiation corrections applied to both are also shown in figure B-3. In all but one case, the corrected data appear to be in general agreement. Also, a heated lower layer was clearly occurring in these fires.
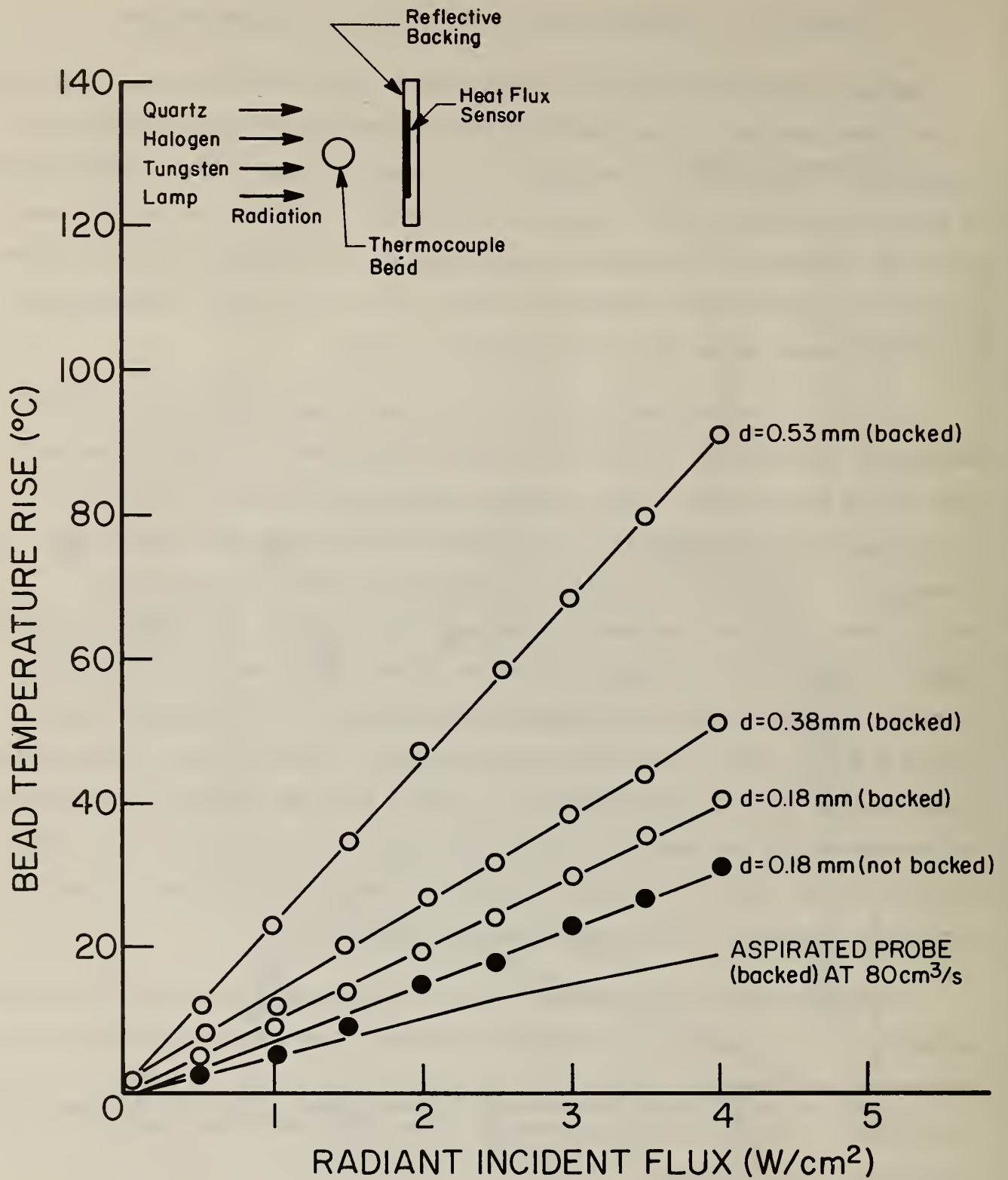
Figure B-1.   Temperature correction versus incident radiant flux
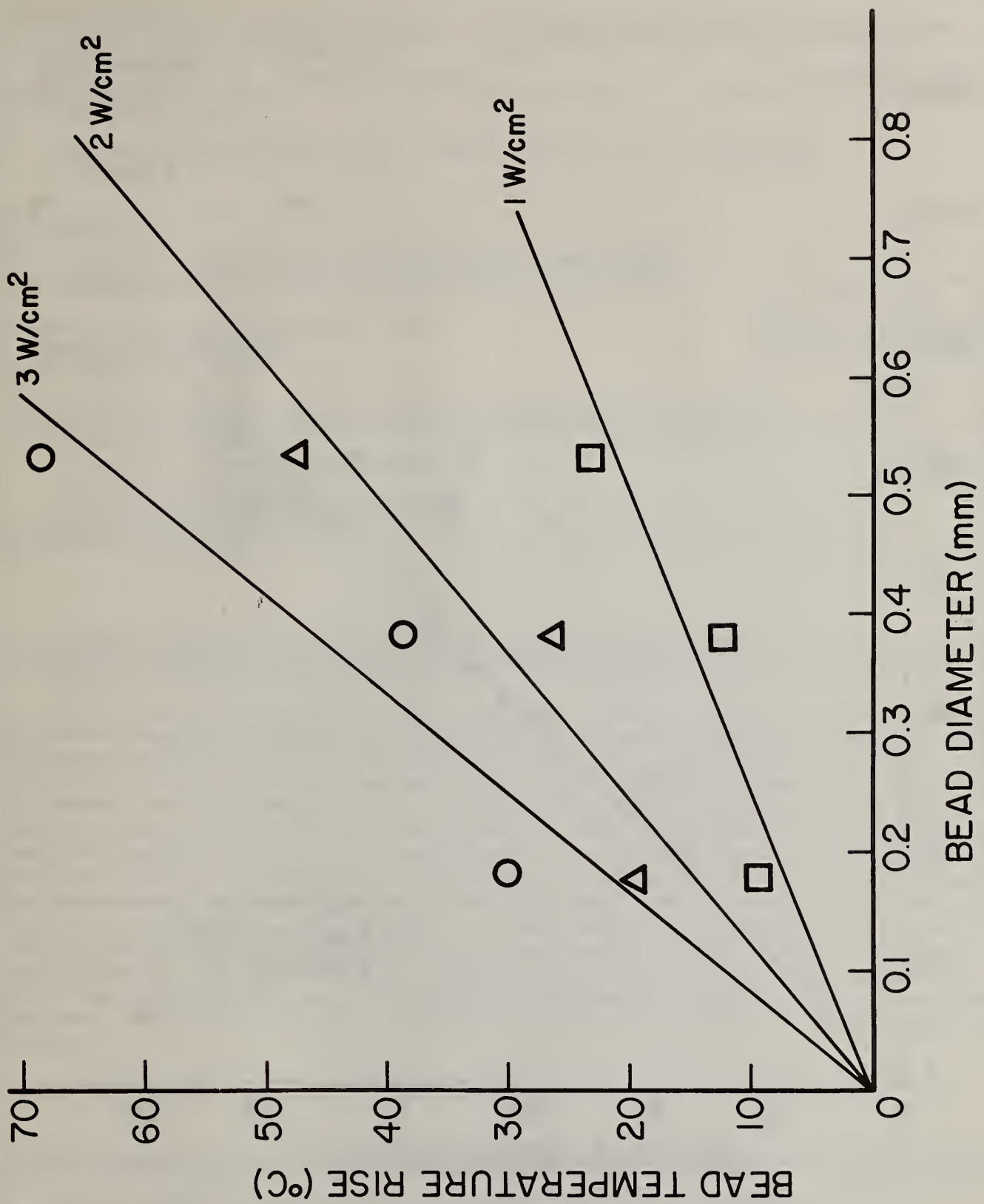
Figure B-2.   Temperature correction versus thermocouple bead diameter

179
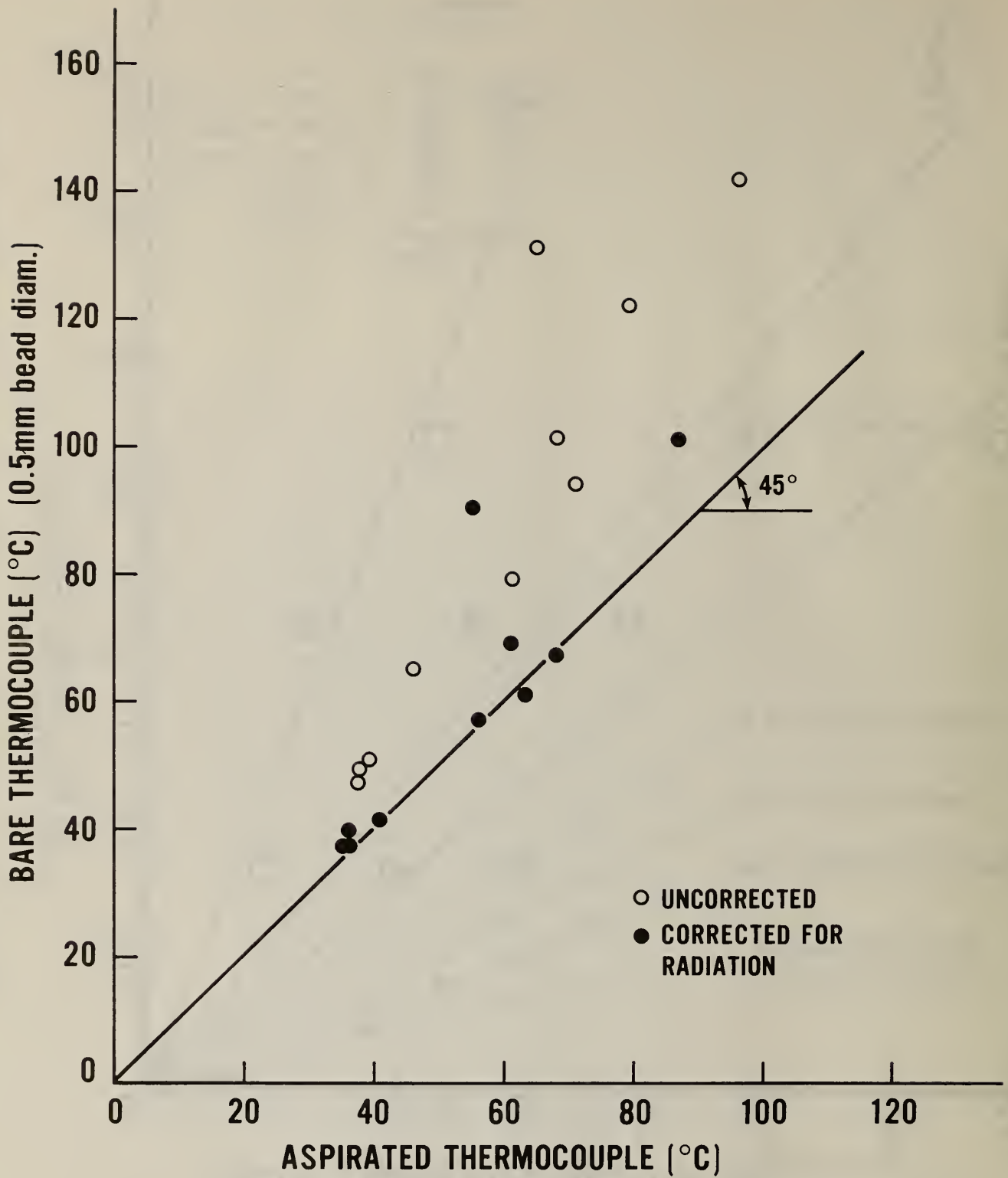
Figure B-3.   Comparison of gas temperatures measured by two
               techniques

180

U.S. DEPT. OF COMM. BIBLIOGRAPHIC DATA SHEET (See instructions)	1. PUBLICATION OR REPORT NO. NBSIR 80-2054	2. Performing Organ. Report No.	3. Publication Date November 1980

4. TITLE AND SUBTITLE

THE BURNING OF WOOD AND PLASTIC CRIBS IN AN ENCLOSURE
VOLUME I

5. AUTHOR(S)

James G. Quintiere and Bernard J. McCaffrey

6. PERFORMING ORGANIZATION (If joint or other than NBS, see instructions)	7. Contract/Grant No. Grant No. RP-76-U-2
NATIONAL BUREAU OF STANDARDS DEPARTMENT OF COMMERCE WASHINGTON, D.C. 20234	8. Type of Report & Period Covered Final

9. SPONSORING ORGANIZATION NAME AND COMPLETE ADDRESS (Street, City, State, ZIP)

Prepared for:
Products Research Committee
c/o Dr. John Lyons
National Bureau of Standards
Washington, D.C. 20234

10. SUPPLEMENTARY NOTES

☐ Document describes a computer program; SF-185, FIPS Software Summary, is attached.

11. ABSTRACT (A 200-word or less factual summary of most significant information. If document includes a significant bibliography or literature survey, mention it here)

This study was designed to assess the fire hazard of a cellular plastic material which has comparable structural characteristics to wood. The study attempts to determine the relative fire risk of such materials in furniture. Rigid (high density) structural polyurethane foam and supar pine were selected for fuels and burned in the form of cribs in a room. The crib loading and door width were parameters experimentally varied. Twenty-one room fire experiments and eight free burn experiments were conducted. Measurements of mass loss, temperature, heat flux, CO_2 and O_2 concentration were recorded. These data were analyzed and empirical correlations were developed for air flow rate and upper gas temperature. A theoretical fire simulation model was developed and yielded results in fair to good agreement with the data. An extrapolation with the theoretical model was used to predict the critical (or minimum) fuel pyrolysis rate to cause flashover (as implied by 2 W/cm^2 of incident radiation to the room floor). This was done for various size rooms and door openings. It appears that to cause flashover, for a given room and door size, about twice as much wood must be involved in fire as the rigid polyurethane material.

12. KEY WORDS (Six to twelve entries; alphabetical order; capitalize only proper names; and separate key words by semicolons)

Crib fires; experiments; mathematical model; plastic; polyurethane; room fires; wood.

13. AVAILABILITY

☒ Unlimited

☐ For Official Distribution. Do Not Release to NTIS

☐ Order From Superintendent of Documents, U.S. Government Printing Office, Washington, D.C. 20402.

☒ Order From National Technical Information Service (NTIS), Springfield, VA. 22161

14. NO. OF PRINTED PAGES

202

15. Price

$17.00